The Role of Extra-Ovarian Estrogen in Regulating Metabolism in Female Non-Human Primates

By

Molly Willging

A dissertation submitted in partial fulfillment of

the requirements for the degree of

Doctor of Philosophy

(Endocrinology and Reproductive Physiology)

at the

UNIVERSITY OF WISCONSIN- MADISON

2023

Date of final oral examination: Thursday, May 11th, 2023, at 10 AM

This dissertation is approved by the following members of the Final Oral Committee:

David H. Abbott, Professor, Obstetrics and Gynecology
Pelin Cengiz, Professor, Pediatrics
Jon E. Levine, Professor, Neuroscience
Matthew J. Merrins, Professor, Biomolecular Chemistry
Judith Simcox, Professor, Biochemistry

ACKNOWLEDGEMENTS

I had the pleasure of collaborating with so many amazing people throughout my PhD. This dissertation would not have been possible without the support of each of my mentors, peers, undergraduate students, friends, and family members.

I would like to extend my sincere thanks to Dr. Laura Hernandez, Dr. Ian Bird, Dr. Manish Patankar, Grace Jensen, Bootsy Harden, Sharon Topp, Vicki Leatherberry and Dr. Molly Carnes from ERP and TEAM-Science for their support throughout my PhD. I would also like to thank everyone at the WNPRC for your help and guidance throughout this research. To animal care, surgery, veterinarians, pathology, assay services. colony records, and compliance staff, I sincerely appreciate your willingness to provide guidance on experiments. Specifically, to Marilina and Theresa, your help was instrumental in completing this research. And to Lisa and Janet, thank you for your constant support and compassion. To Dr. Ricki Colman, Scott and Julie for their expertise and performance of the DXA scans and generating body composition data. In the Department of Nutritional Sciences, thank you Dr. Dale Schoeller, Dr. Michele Ravelli and Tim Shriver for performing the D_2H_20 estimating monkey energy expenditure.

I was incredibly lucky to have so many mentors throughout my PhD. I could not have undertaken this journey without my defense committee, Dr. Pelin Cengiz, Dr. Judith Simcox and Dr. Matthew Merrins. Thank you for your invaluable guidance and feedback. To my mentors, Dr. David Abbott and Dr. Jon Levine, thank you for encouraging me to pursue a career in research and empowering me to succeed in teaching and professional development opportunities. I would like to express my

deepest gratitude to Dave, for almost a decade of thoughtful mentorship and scientific quips. Thank you for always believing in me. To my other mentors, Dr. Joseph Kemnitz and Dr. Amita Kapoor, I am extremely grateful for your considerate guidance and scientific insight- without you this PhD would not have been possible.

I would like to thank all of the students and lab members in our lab. To the Lipid Division undergraduate scientists and honorary members, Sam, Sindhu, Lexi, Ben, Siti, Andrew, Annette, Sona, Ava, and Danielle, thank you for volunteering for early morning experiments, for your optimistic energy and your thoughtful scientific insights. Thank you to all of the other undergraduate scientists in our lab. Without all of your meaningful contributions, the experiments in this thesis would not have been possible. To Aiden and Nicole, words cannot express my gratitude for your willingness to help, your impeccable organization and your sincerity and compassion for others. To the rest of our lab, Siri, Emily, Jesi, Bob, Jake, and Elise, thank you for your vast contributions to this thesis.

To my parents, thank you for all your sacrifices that allowed me to pursue an undergraduate degree at UW-Madison, an experience that prompted my goal to pursue graduate school. From the beginning, you both fostered an environment where I felt empowered and confident to succeed in STEM. As a child, learning about Dolly and the genetic revolution, you always encouraged me to ask questions, learn more, read more, and ultimately, be a part of the investigation.

To all my amazing friends, thank you for bringing so much joy and entertainment into my life. I truly cannot express how grateful I am to each one of you for the impact you have made on my life. I would not be who I am without any of you.

I would finally like to thank my fiancé, Jack. Without your unwavering support and constant optimism, this endeavor would not have been possible. And to my incredible daughter, Aurora, the future of science, you have motivated me to complete this dissertation and never rest until science is accessible and inclusive for all folks to succeed.

ABSTRACT

Estradiol supports female metabolic function in multiple animal research models, including, mice, rats, and sheep. Estradiol action is mediated through estrogen receptors, predominately, estrogen receptor alpha (ERα) and estrogen receptor beta (ERβ). ERα has been shown extensively to be the predominant estrogen receptor regulating estradiol action in rodents by way of ovarian synthesized estradiol. While ovariectomy (OVX) in rodents enables obesity, OVX in nonhuman primates inconsistently alters weight gain, highlighting the possibility of estradiol produced outside the ovaries as an important site of estradiol synthesis signaling through ERα in nonhuman primates. We hypothesized that extra-ovarian estradiol provides key support through hypothalamic ERα for female metabolic function. We employed aromatase inhibition to eliminate extra-ovarian estradiol biosynthesis and elucidate the role of extra-ovarian estradiol in regulating energy balance in OVX adult female marmosets and rhesus macaques. Next, we employed RNAi technology to silence ERα in the mediobasal hypothalamus (MBH) of adult female OVX marmosets and ovary-intact rhesus macaques to assess the role of ERα in energy balance. Our findings provided the first evidence for estradiol's action through ERα contributing to energy homeostasis in a female nonhuman primate, and prompted speculation that extraovarian estradiol, and potentially, neuro-synthesized estrogens, may similarly regulate energy balance in other female primates, including humans.

TABLE OF CONTENTS

1. CHAPTER ONE: Literature Review: Estradiol Regulation of Metabolism

1.1 Implications for Metabolic Dysfunction in Post-Menopausal Individuals

Menopause, defined by menstruation cessation and a depletion of ovarian sex steroid hormones, increases the risk of metabolic dysfunction associated with reduced steroid actions in female adipose tissue, bone, cardiovascular tissues, pancreas, liver, and brain. Studies have shown, for example, an increased risk of metabolic syndrome by 60% in postmenopausal women[1,2]. Multiple investigations have attempted to dissociate effects of aging versus declining estradiol levels on adiposity, energy balance, cardiometabolic and brain health in menopausal women[3,4,5]. In general, these studies suggest that menopause per se is associated with increasing abdominal obesity and accompanying co-morbidities[6]. While findings on menopause-associated obesity parallel observations made in estrogen-depleted, ovariectomized (OVX) female rodents[7], causal relationships between declining ovarian estradiol during menopause, and altered body composition and energy balance, have been difficult to confirm in women. Current clinical recommendations place hormonal replacement therapy (HRT), commonly a form of estrogen combined with a synthetic progestin, as the gold standard for treating symptoms associated with menopause[8]. There is conflicting evidence on the effectiveness of HRT in mitigating the adverse metabolic symptoms associated with the menopausal transition. Studies have demonstrated that both oral and transdermal estradiol therapy in postmenopausal women are associated with a reduction in central adiposity and an increase in lean body mass[9,10], as well as reductions in insulin resistance and fasting glucose. More studies focused on glucoregulation have suggested estradiol-mediated increases in insulin sensitivity[11], while others find no

improvement[12,13]. Studies on energy expenditure after commencing HRT have demonstrated increases and decreases in lipid oxidation and energy expenditure, respectively[14]. Selective estrogen receptor modulators (SERMs), compounds that interact with estrogen receptors in specific target tissues, have shown promise in improving osteoporosis and treatment of breast cancer[15]. Although SERMs can selectively engage target tissues, like systemically acting HRT, SERM use can cause adverse side effects, such as, increased risk for thromboembolic events[16,17]. The specific metabolic consequences of menopause and/or estrogen withdrawal in women remain unclear, due in part to the uncontrolled environmental, psychosocial, and genetic factors that predominate in most clinical studies.

1.2 Estradiol Production

The major bioactive estrogen, estradiol, is a steroid hormone synthesized throughout the body by aromatase, a cytochrome P450 enzyme, encoded by the CYP19A1 gene[18-21]. While the main source of estradiol (E_2) is the ovary, E_2 is also produced in low amounts in extra-ovarian sites including, adipose tissue, adrenal glands, skin, bone, pituitary gland, and multiple brain areas[18-21].

1.3 Mechanisms of Estradiol Signaling

E_2 can act through multiple receptors and mechanisms involving various signaling cascades to effect physiological action. E_2 crosses the plasma membrane and interacts with intracellular ERα and ERβ to exert direct genomic effects when binding to cognate DNA response element sequences, i.e., estrogen response elements (EREs) in the regulatory regions of target genes. E_2 can also exert genomic actions by complexing with other transcription factors that, in turn, bind to their own cognate response

elements. Alternatively, E_2 can exert non-genomic actions via interaction with the G-protein coupled estrogen receptor (GPER1) and/or ERα and ERβ complexed with anchoring proteins at the plasma membrane, thereby activating intracellular signaling cascades.

The classical mechanism of estrogen signaling is direct genomic signaling where ERα and ERβ nuclear receptors are ligand-activated transcription factors[22,23]. In this mechanism, nuclear and/or cytoplasmic bound ERα and ERβ undergo a conformational change inducing release from molecular chaperones and receptor dimerization[24]. After dimerization, the complex binds to genomic targets; chromatin at estrogen response element (ERE) sequences, enhancer regions by or within promotor regions and regions of target genes[25]. Research has identified 35% of genes acted on by E_2 do not contain ERE-like sequences[26,27] In the absence of EREs, estrogen signaling can affect gene expression without binding directly to DNA, an “indirect genomic” action. In such mode of action, estrogen receptor complexes participate in protein-protein interactions with other transcriptional elements and response elements, like that of stimulating protein-1 (Sp-1), a crucial mediator of indirect genomic action that is enhanced by estrogen receptors[28,29].

In contrast to the classic E_2 action of changing gene expression of target genes, non-genomic E_2 signaling consists of rapid intracellular changes via membrane associated receptors. Non-genomic estrogen signaling involves activation of signal-transduction mechanisms with the subsequent production of intracellular second messengers, such as cAMP and PKA, or regulation and protein-kinase signaling cascades. The activation of these membrane-initiated signaling cascades can result in

non-genomic changes in a host of cellular activities, as well as ultimately convey signals to the nucleus to evoke transcriptional responses[30]. GPER1 (G protein-coupled estrogen receptor 1), binds to estrogens, promoting estrogen-dependent activation of adenylyl cyclase and epidermal growth factor receptor (EGFR).

1.4 Steroid Hormones, Female Energy Homeostasis

1.4.1 Female Rodent Models: Ovarian Hormones and Metabolism

In many experimental animal models, ovarian E_2 regulates body weight and composition, energy balance, and glucoregulation[31]. In rodent models, ovarian E_2-regulated control mechanisms are well established since OVX-mediated E_2 depletion reliably disrupts energy balance, and leads to increased body weight and visceral adiposity, reduced physical activity and energy expenditure[32,33], and diminished insulin sensitivity. All these effects of metabolic dysfunction can be diminished or reversed by E_2 replacement[34,35]. Further, these E_2 actions are mostly mediated by estrogen receptor alpha (ERα), as complete ERα knockout mice (ERαKO) exhibit increases in body weight and adiposity, and present energy metabolism phenotypes that largely mimic those observed in long-term OVX mice[36]. A similar marked degree of metabolic dysfunction is not found in ERβKO or GPR30KO female mice[37]. Due to the vast research on the metabolic impact of ovarian E_2 via ERα in rodents, multiple avenues of E_2 regulated energy balance have been established. These include the direct actions of E_2 on metabolically active tissues such as adipose depots, liver, muscle, and pancreas[38], E_2 activation of brown adipose tissue (BAT) via the sympathetic nervous system[39], as well as E_2 -induced alterations in neural and peripheral control of food intake and energy expenditure.

1.4.2. E_2-mediated Neural Regulation of Metabolic Function

Rodent models of ovarian estradiol regulation have also highlighted the critical role of neural ERα signaling in mediobasal hypothalamic nuclei, the ventromedial nucleus (VMN) and the arcuate nucleus (ARC), to maintain energy homeostasis via the leptin-melanocortin system[40,41]. The leptin-melanocortin system is the predominant pathway regulating energy balance in mammals[42]. The central melanocortin system includes two distinct populations of neurons in the ARC—the proopiomelanocortin (POMC) and cocaine- and amphetamine-related transcript prepropeptide (CARTPT) expressing neurons and the agouti-related peptide (AgRP) and neuropeptide Y (NPY) expressing neurons[43]. Both populations of neurons have projections into the paraventricular nucleus (PVN) of the hypothalamus and facilitate downstream mechanisms to modulate energy balance. Leptin, an adipokine secreted by adipose tissue, conveys messages to the brain regarding the body's energy stores by binding to its receptors on the orexigenic neuronal populations, AgRP and NPY and the anorexigenic neuronal populations, POMC and CART[44]. Upon binding to POMC neurons, a cleavage product of the POMC transcript, alpha-MSH (alpha melanocyte stimulating hormone) is released and subsequently, activates MC4R, melanocortin 4 receptor, in the PVN (Figure 1). This reaction results in a satiety signal and reduces food intake. In opposition, AgRP competes with alpha-MSH to bind MC4R to increase food intake. Neuropeptide Y exerts its orexigenic effects via activation of NPY Y1 and Y5 receptors.

In addition to satiety signals, leptin activation of AgRP and POMC neurons through brain-derived neurotropic factor (BDNF)-expressing neurons in the PVN, influences sympathetic innervation of white adipose tissue (WAT) and brown adipose tissue

(BAT)[45]. Leptin's ability to modify the sympathetic architecture of WAT and BAT and promote adipose thermogenesis when energy stores are in excess is an important downstream neuronal signaling mechanism for energy balance. Adipose depots, mainly BAT, are activated by sympathetic signals, such as, norepinephrine (NE) and epinephrine (E)- most notably, after cold exposure. NE and E signal through three G-protein coupled beta-adrenergic receptors located on brown adipocytes, termed 1 (ADRB1), 2 (ADRB2) and 3 (ADRB3). Upon stimulation by NE, in classical cold-induced thermogenesis in female rodents, beta-adrenergic receptors signal synthesis of cyclic AMP (cAMP), promoting cAMP driven protein kinase A (PKA) activation, stimulating lipolysis[46] (Figure 2). Lipolysis results in free fatty acid and glycerol release from the triglyceride lipid droplet and enhanced expression of uncoupling protein 1 (UCP1) mRNA. Increased UCP1 takes the energy stored in the mitochondrial electrochemical gradient and dissipates it as heat, independent of ATP synthesis, termed non-shivering thermogenesis.

E_2 modulates these neural MBH metabolic circuits in many ways; its actions can be dependent on the leptin-melanocortin system or act independently of leptin's actions altogether[47]. Like leptin, E_2 is a strong anorexigenic signal regulating energy balance by stimulating POMC and CART neurons and inhibiting NPY and AgRP neurons. It had been assumed that E_2's effect on energy balance acts in tandem with leptin's role via co-expression of leptin receptor (LepRb) and ERα in the mediobasal hypothalamus[48], but recent research in rodents has shown co-expression is more pronounced in the preoptic area (POA) and is limited in the mediobasal hypothalamus. Quantification of LepRb and ERα colocalization throughout the murine hypothalamus has shown strong

colocalization absent in all areas aside from the POA and one month after OVX, co-expression tended to decline[49]. Further, STAT3 or ERα deletion from LepRb cells does not inhibit E_2's ability to manage body weight[50]. It has been shown that circulating levels of E_2 may enhance the anti-obesity effects of leptin and specifically modulate leptin sensitivity in certain metabolic tissues like adipose and skeletal muscle[51]. Taken together, E_2 mediation of energy homeostasis via ERα is not dependent on activation of LepRb on co-expressing cells and circulating levels of E_2 may act indirectly on the leptin-melanocortin pathway.

In addition to estrogenic effects on the leptin-melanocortin pathway of energy balance, E_2 and hypothalamic ERα have been well characterized as modulators of metabolism. It has been demonstrated that viral vector mediated *ESR1* gene silencing in the VMN of both female mice and rats largely recapitulates a metabolic phenotype observed in complete ESR1KO mice, including obesity, hyperphagia, impaired glucose tolerance and reduced energy expenditure[52,53] (Figure 2). It has also been demonstrated that ERα gene deletion in specific neuronal populations of the mediobasal hypothalamus have differing impacts on metabolism. Deletion of ERα in hypothalamic steroidogenic factor-1 (SF1) expressing neurons results in abdominal obesity and hypometabolism, not hyperphagia, while ERalpha deletion in POMC neurons leads to hyperphagia[53].

Downstream of SF1 and POMC action, E_2 acts on more targets for metabolic regulation. Recent research has shown MC4R is a transcriptional target of ERα action[54]. Identification of a subset of E_2 -sensitive neurons in the ventrolateral ventromedial hypothalamic nucleus (VMHvl) with projections to the hippocampus and hindbrain

enables E_2 to modulate energy allocation. Upon E_2 influx, VMHvl neuronal MC4R signaling increases via recruitment of ERα to *MC4R*[54].

The leptin-melanocortin system by nature is sensitive to changing caloric environments. Diet induced obesity (DIO) is a feeding regime commonly used in research to mimic human obesity. DIO can assert stress on energy balance mechanisms that can help elucidate signaling pathways. DIO rodents present with normal levels of leptin receptor but despite high levels of leptin, leptin fails to stimulate the leptin signaling cascade[55]. After switching to a reduced fat diet, leptin responsiveness of NPY/AgRP and POMC neurons could now be demonstrated, with mice regaining normal leptin sensitivity and glycemic control[55], highlighting the importance of nutrient sensing in the leptin-melanocortin pathway. In the absence of obesity and diabetes, rodents fed a high fat/high calorie diet during pregnancy exhibited increased cytokine production in the hypothalamus and abnormal development of melanocortin pathways in fetal offspring[56-60]. Further, the fetal offspring, regardless of maternal obesity status, exhibit accelerated weight gain and adiposity paired with glucose intolerance[56-60]. Taken together, independent of maternal obesity, maternal diet can alter fetal develop of melanocortin signaling, induce lipotoxicity and predispose female fetal offspring to adult metabolic dysfunction similar to the effects of obesity and glucose intolerance[61].

DIO is critical in demonstrating the protective effects of E_2 against weight gain and disruption of energy homeostasis in rodents. OVX mice fed a high fat diet (HFD) and treated cyclicly with E_2, displayed insulin sensitivity and no white adipose tissue (WAT) inflammation[62]. In contrast, OVX mice fed HFD and no E_2 replacement, presented with

insulin signaling dysfunction and low-grade inflammation in WAT. Importantly. Both animal groups attained similar body weights and demonstrated equivalent fat masses[62]. These results demonstrate that E_2 regulates glucose homeostasis independently of body weight and adiposity, highlighting the protective effect of E_2 against increased cardiovascular morbidities diabetic conversion associated with high fat/high caloric environments[63].

In rodents, OVX induces rapid body weight gain and metabolic dysfunction, yet, in non-human primate models, OVX inconsistently alters body weight[64-66]. Additionally, while E_2 action via ERα and its regulation of energy balance is well characterized in rodent models, research is lacking in non-human primate (NHP) models. It remains crucial to identify whether similar mechanisms of E_2 signaling, and metabolic regulation apply to female NHPs and women.

1.4.3 Female Primate Models: Ovarian Hormones and Metabolic Regulation

Aspects of metabolism can fluctuate due to cyclic hormone secretions associated with female reproductive cycles. The degree and timing of hormonal regulation of metabolism is dependent on the type of reproductive cycle, thus eliciting species specific differences of hormonal control. Similar to rodents, some NHP species like lemurs, lorises and tarsiers, have an estrous cycle. New World Primates like marmosets (one model used in this thesis) and tamarins exhibit an ovarian cycle, while Old World Primates (i.e., rhesus macaques, model used in this thesis), great apes and humans share a menstrual cycle. It has been well established that food intake is reduced at the time of ovulation and increases during pregnancy in female animal models. Specifically, in a NHP model, decreased food intake has been observed in the peri-ovulatory phase

of the menstrual cycle in female rhesus macaques[67,68]. Such reduction of food intake during the peri-ovulatory period has also been observed in humans[69-72]. A well-supported hypothesis is the rise of E_2 in the circulation during this periovulatory period elicits alterations to hypothalamic signaling cascades involved in energy intake[73].

As described in a previous section, OVX in rodents induces weight gain, adiposity, reduced energy expenditure and glucose intolerance. In NHP models, however, OVX-mediated E_2 depletion inconsistently increases body weight[74-76]. Despite the lack of a robust metabolic phenotype following OVX in NHPs, selective estrogen receptor modifiers (SERMs) can induce modest weight loss in OVX rhesus monkeys[77]. Interestingly, in OVX cynomolgus macaques, E_2 replacement therapy has no effect on body weight or insulin sensitivity in OVX cynomolgus macaques[78]. In addition to ovarian E_2, E_2 synthesized in the brain can stimulate top-down neuronal signaling cascades and such neuro-E_2 is proposed to act as a neurotransmitter and neuromodulator[79,80]. Aromatase, the enzyme responsible for converting testosterone to E_2 has been documented to be present in rhesus macaque brain regions, including the hypothalamus[81]. We hypothesize that the failure for OVX to increase female NHP body weight is due to the residual actions of neuro-E_2 orchestrating energy balance in the hypothalamus of OVX primates. Rodent research models have provided comprehensive evidence supporting roles played by ovarian E_2 in female energy balance and body composition, yet there are few studies in female NHPs assessing ovarian and extra-ovarian E_2, possibly neuro-E_2, in regulating aspects of energy balance.

In addition to the hypoestrogenic environments induced by aromatase inhibiting drugs, like letrozole, hyperandrogenism is usually induced. In female rodent studies

treated with letrozole, animals present with hyperandrogenism and later metabolic phenotypes of dyslipidemia and insulin resistance by 5-weeks post-treatment start[133]. Further, in young female rhesus macaques, the combined treatments of hyperandrogenism and western-style diet contribute to a greater, more severe metabolic phenotype of weight gain and body fat than each treatment alone[134]. Moreover, the distribution of fat has been strongly correlated with androgen and estrogen hormonal ratios. Hyperandrogenism accompanies greater intra-abdominal fat mass in normal weight women with polycystic ovary syndrome (PCOS)[135]. Taken together, the balance between estrogens and androgens is crucial in maintaining energy balance in female rodents and primates.

1.5 Genetic and Hormonal Differences in NHP Research Models

1.5.1. Obesity risk genes in rodent and human studies

The etiology of obesity is complex and likely has many genetic, psychological, and environmental determinants. The traditional mechanism from which obesity arises involves a positive imbalance between food intake (energy consumption) and energy expenditure in favor. While caloric composition and intake, activity level and environmental alterations do contribute largely to the onset of obesity, genetic factors of obesity can contribute 40-70% of obesity variation in humans[82]. Although, genome-wide association scans (GWAS) have identified over 400 genes associated with type 2 diabetes, these genes have a low rate of predicting obesity. This may be due to the difficulty of discerning the effects of a gene or multiple gene mutations from other environmental or epigenetic factors in humans. Generally, genetic causes of obesity can be grouped into three categories[83-86]:

1) Monogenic obesity, a single gene mutation
2) Polygenic obesity, contribution of multiple genetic mutations or interactions
3) Syndromic obesity, neurodevelopmental and organ/system abnormalities

Rodent studies offer intricate, highly controlled investigations into how specific genetic modifications can contribute to the onset of obesity. Prior to the technological advancements that enable quick genetic investigation today, there had long been suspicion of genetic mutations of obesity. The parabiosis work of D.L. Coleman was the first to introduce a possible hormonal factor impacting satiety with a suspected genetic cause[87], in which an obese mouse parabiosis paired with a normal partner was found to improve weight and satiety while a diabetic obese mouse parabiosis paired with a normal partner increased body weight and fat mass. Coleman concluded the obese mouse might not produce enough “satiety factor” while the diabetic mouse had sufficient satiety factor but could not respond to it due to a defective “satiety center”[87]. This led to the identification and genetic mapping of the mouse obese (*ob*) gene and the subsequent protein it encodes, leptin, which propelled research into identifying the role of leptin and the hereditary effects of obesity[88]. Rodent research confirmed the “satiety factor” and “satiety center” lacking in the parabiosis experiments were leptin and the leptin receptor, respectively[89], leading to well established leptin deficient (ob/ob) and leptin receptor deficient (db/db) rodent models. Rodents with the genetic profile of ob/ob and db/db present with obesity, hyperphagia, reduced energy expenditure and insulin resistance[90], and while these mutations in humans cause similar phenotypes, predominately, hyperphagia, the occurrence of such monogenic mutations are rare and only found in about 1%-5% of people with severe obesity[91]. A more common occurrence

of disrupted leptin action is via leptin resistance. The levels of leptin-receptor mRNA and protein are important, given that the basic metabolic effects of leptin depend primarily upon the number of available receptors, and it has been shown that circulating leptin levels correlated with leptin receptor levels[136]. Obesity leads to a decrease in the expression of both short and long isoforms of leptin receptors in the hypothalamus, fat, and muscles[136].

The exploration into the ob/ob and db/db mouse phenotypes led to other discoveries of monogenic causes of obesity that can be generally categorized into three energy balance systems that become dysfunctional:

1) obesity via hypothalamic leptin-melanocortin system.
2) obesity via altered hypothalamic development and functions.
3) obesity via complex syndromes with unclear relationships to obesity.

The most characterized monogenic causes of obesity affect the hypothalamic leptin-melanocortin signaling pathway. As mentioned above, deleterious leptin and leptin receptor mutations have pronounced impacts on energy homeostasis. Additionally, genetic mutations of the associated genes, proopiomelanocortin (*POMC*), melanocortin receptor 4 (*MC4R*) and prohormone convertase 1/3 (*PC1/3*) in the leptin-melanocortin pathway result in disturbed energy intake and basal energy expenditure[92]. Obesity can also be a consequence of monogenic mutations associated with neurodevelopment. Three genes*, SIM1*, *BDNF* and *NTRK2* have been identified as having a critical role in hypothalamic development and compromising specific nucleotide variants induce hyperphagia and obesity. Although the etiology of obesity in these gene variant cases is not exactly known, it is posited that missing one copy of *Sim1* reduces paraventricular

nucleus (PVN) neuronal number. Since the PVN is the site of MC4R-expressing neurons, the impaired neuronal development within the PVN could result in a dysfunctional energy balance[93,94]. Acting downstream of MC4R are BDNF (brain-derived neurotrophic factor) and its receptor TRKB (tropomyosin-related kinase B) that are involved in proliferation, survival, and differentiation of neurons in neurodevelopment and plasticity, at least in adults. Haploinsufficiency of *BDNF* or *NTRK*, the gene that encodes for TRKB, also induce hyperphagia and obesity[94-96]. These single gene mutations in rodent models present with obesity, reduced energy expenditure and insulin resistance, and while they enable discovery of a gene's direct involvement in pathophysiology and are critical to identify therapies for monogenic causes of obesity in humans, the homogeneity of the inbred mouse lines are not representative of the genetic variation in humans and general obesity and may result in highly varied phenotypic outcomes.

More common are polygenic determinants of obesity in humans. Rodent models of DIO more closely mimic human obesity over monogenic models of obesity. Rodent models of polygenic obesity can therefore offer more clarity into gene-gene and gene-environment interactions due to the ability to control environmental contributions, like caloric content and consumption.

1.5.2. Important differences in regulation of estradiol production and activity between female rodents, sheep and NHPs.

Female reproductive cycles and their hormonal regulation differ among mammalian species. Rodents exhibit estrous cycles comprising four distinct phases, proestrus, estrus, metestrus, and diestrus. E_2 levels rise and eventually peak in the

proestrus phase. The estrus phase (ovulation) denotes day 1 of each estrous cycle. In contrast, certain New World Primates (NWPs), such as marmoset and tamarin monkeys, exhibit ovarian cycles with two distinct phases, follicular and luteal. Cycle day 1 of each ovarian cycle denotes the onset of each follicular phase and is temporally distinct from ovulation that occurs on the last day of the follicular phase. Old World Primates (OWPs), such as rhesus macaques, great apes, and humans, however, exhibit menstrual cycles that have primate-typical follicular and luteal phases. The first day of menses denotes day 1 of each menstrual cycle and the first day of the follicular phase. Ovulation again occurs on the last day of the follicular phase. Both ovarian and menstrual cycles share similar endocrine dynamics with follicular and luteal phases separated by ovulation. The follicular phase involves rapid ovarian follicle growth stimulated by gonadotropins, FSH and LH (or analogous, chorionic gonadotropin, CG, in New World primates), that promote ovarian follicle growth resulting in a slow rise in circulating levels of E_2. Toward the end of the follicular phase, circulating E_2 levels peak, inducing an LH (CG) surge, that ultimately triggers ovulation of a single dominant follicle (Old World and most New World primates) or 2-4 dominant follicles (certain New World primates, including marmoset and tamarin monkeys). Following ovulation, the single (or multiple) corpus luteum (lutea) produce(s) and release(s) progesterone and E_2, thus sustaining the luteal phase and implantation-receptive uterine endometrium.

The timing of pre-ovulatory E_2 surges throughout mammalian reproductive cycles has been associated with aspects of energy balance such as body weight and food intake. In rodent estrous cycles, food intake increases during the metestrus-diestrus when E_2 levels are lowest and decreases during the proestrus-estrus phase when E_2

levels are the highest[97]. During hamster estrous cycles, body weight is lowest when circulating E_2 levels are the highest, body weight is the lowest[98]. Similar to rodents, NHPs and humans exhibit reduced food intake when high midcycle (pre-ovulatory) E_2 levels occur during ovarian and menstrual cycles[99].

1.5.3. Important differences in regulation of energy homeostasis between rodents, sheep and NHPs.

There are many components that contribute to the regulation of energy homeostasis in mammals, including sleep cycles. Metabolic syndrome is a major complication of sleep disorders, prompting the importance of the circadian rhythm in regulating metabolism[100]. In humans, this has been observed in the increased incidence of diabetes and obesity in shift workers as shift work interferes with the normal pattern of sleep[101]. Specifically, disruptions to sleep cycles have demonstrated increased postprandial circulating glucose, triglyceride, and insulin concentrations[102-104]. Adiposity and glucoregulatory dysfunction have also been observed in rodent models of circadian disruption[105]. An important component of metabolic regulation via the circadian rhythm is the hormone, melatonin. In contrast to rodents, sheep and humans produce melatonin in the rest phase, even during constant darkness[106-108]. Despite a similarity in circadian rhythm and melatonin regulation, sheep differ from humans in terms of alimentary organization, as they are ruminants. Their main source of energy is acquired by metabolizing cellulose to volatile fatty acid[109] and demonstrate lower basal glucose levels, reduced post-prandial fluctuations and lower insulin sensitivity compared to humans[110,111]. Moreover, disruption to circadian rhythms in sheep disrupted plasma glucose levels but without concomitant glucose tolerance or glucose-stimulated insulin

secretion dysfunction[100]. Taken together, although circadian rhythms are consistently important for metabolic balance across mammalian species, the specific mechanisms of regulations are different.

BAT thermogenesis is an additional regulator of energy homeostasis. BAT content is critical to the energy expenditure component adaptive thermogenesis. In rodents, there are defined depots of BAT that maintain throughout adulthood[112]. In large mammals, such as sheep, NHPs, and humans, brown adipocytes are mostly interspersed within WAT. Additionally, there are characteristically distinct beige adipocytes, that are interspersed in WAT depots[112]. Small BAT depots have also been identified in neck and supraclavicular region of adult humans and NHPs[113-115,132] and adult rhesus macaques[131]. In addition to BAT, skeletal muscle is an important tissue contributing to adaptive thermogenesis potential. While in rodents, the UCP1 independent pathways promoting mitochondrial uncoupling and futile calcium signaling are well researched, more investigation is needed in large mammals to elucidate these heat producing mechanisms[112]. It is speculated that subtle changes in skeletal muscle thermogenesis can produce large energy balance consequences due to the volume of skeletal muscle in large mammals, accounting for about 40% of body mass[112].

1.6 Clinical Treatments for Estrogen-mediated Metabolic Dysfunction in Women

Individuals experiencing symptoms of menopause, like hot flashes and night sweats, are typically prescribed hormonal replacement therapy (HRT) to alleviate symptoms and help reduce osteoporosis induced by declining circulating E_2 levels. There are two main types of systemic HRT, estrogen only therapies and combinations of estrogens and progestins, including synthetic forms of progesterone. Additionally,

there are varying delivery methods for HRT, such as oral formulations, transdermal creams, patches and gels, and vaginal preparations[116]. Although protection of bone integrity is a clear benefit of HRT[117], increased risks of cancer of the breast and endometrium (if uterus is still present), blood clots, stroke, heart disease and dementia are consequences of considerable concern[118]. The literature investigating how HRT contributes to the risk of these diseases is not without inconsistencies. Many of these risks can be attributed to the timing of when HRT is started. There is an increased risk of dementia when HRT is started after mid-life, but a reduced risk if started before mid-life. In the same context, long-term HRT use[119] and chronic estrogen exposure are both associated with increased risk of breast cancer[118]. Considering the critical timing of starting HRT, new guidelines have recommended that HRT starts within 10 years of menopause should not exceed five years in duration and should not continue beyond the age of 60, unless with specific considerations[120]. Hot flashes and other symptoms associated with menopause may persist for 10-20 years from the start of menopause, but the risks associated with HRT greatly increase post-60 years of age[120]. Prior to the age of 60, hormonal combinations and doses for HRT are dependent on physiological condition and individualized risks for each patient.

Individuals who have breast cancer or a history of breast, ovarian, endometrial, or cervical cancer are not good candidates for HRT. Increased exposure to high levels of endogenous estrogens have been shown to increase breast cancer risk. Safe therapeutic interventions for breast cancer patients are incredibly important as many individuals prematurely enter menopause and experience menopausal symptoms due to cancer treatment[121]. Tamoxifen, a SERM, is a successful anti-cancer medication[122]

that blocks estrogen action by competitively binding to ERα, ERβ and GPER1. In contrast, letrozole, a non-steroidal aromatase inhibitor, blocks the conversion of testosterone to E_2 (as well as the conversion of androstenedione to E_2) and reduces circulating E_2 (and E_1) levels[123]. Both treatments have high efficacy in treating hormone-receptor-positive breast cancer in pre- and post-menopausal individuals, especially letrozole as adjuvant treatment, but both treatments present with varying safety profiles[123]. Compared to tamoxifen, letrozole use increased the chance of bone fracture, low-grade hypercholesterolemia, and cardiac events[123]. Additionally, there is evidence that both treatments can lead to weight gain and subsequent metabolic consequences[124-129].

To treat estrogen-mediated metabolic dysfunction while reducing peripheral side effects, selective and accurate hormone therapies are necessary. One potential solution is a small-molecule bio precursor prodrug, 10β,17β-dihydroxyestra-1,4-dien-3-one (DHED). The promise of this drug is immense as it converts to 17β-E_2 (or E_2) in the brain but remains inert in the rest of the body and can thus be administered systemically. DHED was shown to have neuroprotective effects and to not induce proliferation of cancerous tissues in rodents[130]. DHED has the potential to mitigate metabolic consequences associated with disorders from depleted brain E_2 levels[130], such as menopause related metabolic disorders.

1.7 Objectives and Importance

Activation of neural ERα orchestrates responses in multiple pathways that regulate metabolism in female rodents and sheep, yet we still do not fully understand ERα neuro-metabolic signaling in female NHPs and women. Understanding the mechanisms

through which E_2 mediates metabolic homeostasis via ERα will enable targeted therapeutic solutions to those experiencing menopausal- and cancer therapy-associated metabolic dysfunction.

The objectives of this thesis were therefore to test the hypotheses that, 1) in a New World Primate model, the female common marmoset, extra-ovarian E_2 signaling through hypothalamic ERα regulates body weight, body composition, energy homeostasis and glucose homeostasis **(Chapter 2),** 2) in the absence of DIO, hypothalamic ERα signaling is critically important in regulating female energy homeostasis in rhesus macaques **(Chapter 3)**, 3) extra-ovarian E_2 contributes to regulation of body weight, body composition, energy homeostasis and glucose homeostasis in female rhesus macaques **(Chapter 4)**, and 4) concluding discussion revising consideration of E_2 regulation of female energy homeostasis in NHPs and likely women **(Chapter 5)**.

This thesis is of clinical and biological importance because current modes of treating metabolic syndrome in menopausal women vary in effectiveness and possess co-morbidities. Moreover, extra-ovarian E_2 as a contributing source of estradiol maintaining energy homeostasis after the menopausal transition has never been investigated before in an NHP model. Identifying the source of E_2, and the molecular pathways through which it regulates energy balance in female NHPs, will prompt a major reconceptualization of the fundamental control systems that govern metabolic function female NHPs and likely, women. Additionally, this understanding will provide novel therapeutic opportunities to target specific neural sites of action to combat menopausal associated metabolic syndromes.

1.8 Tables & Figures

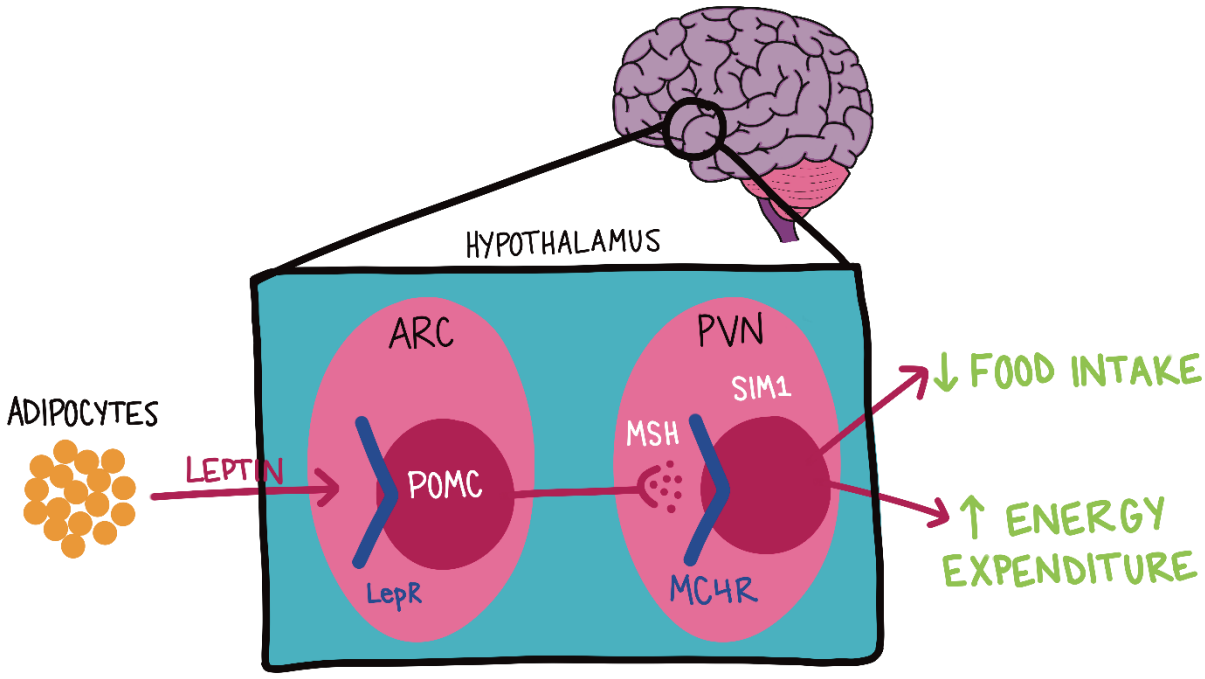

Figure 1: Depiction of leptin-melanocortin pathway. Leptin synthesized by adipose tissue activates leptin receptors (LepR) on POMC neurons in the arcuate nucleus (ARC) of the hypothalamus. This stimulates downstream activation of melanocortin 4 receptors (MC4R) in the paraventricular nucleus (PVN). Ultimately, influencing metabolic processes by decreased food intake and increased energy expenditure.

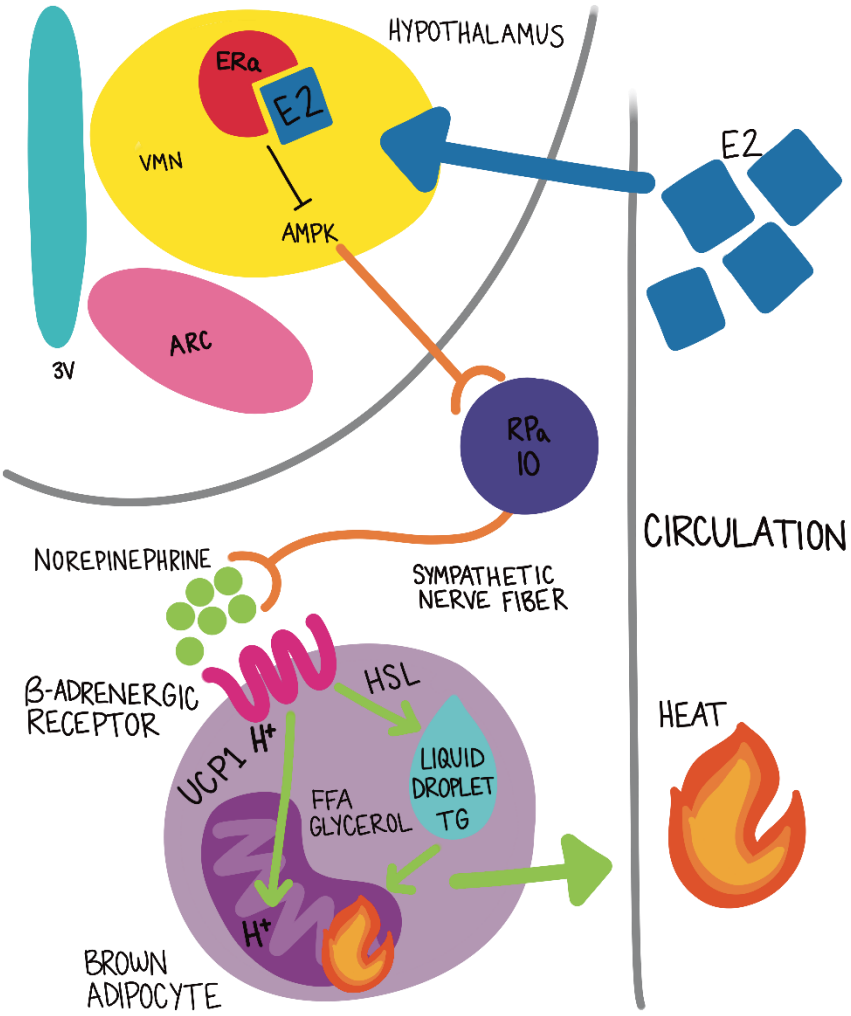

Figure 2: Depiction of estrogen receptor alpha (ERα) action via estradiol (E_2) in the ventromedial nucleus (VMN) of the hypothalamus and downstream initiation of brown adipose tissue (BAT) thermogenesis.

1.9 References

1. Park YW, Zhu S, Palaniappan L, Heshka S, Carnethon MR, Heymsfield SB. The metabolic syndrome: prevalence and associated risk factor findings in the US population from the Third National Health and Nutrition Examination Survey, 1988-1994. *Arch Intern Med*. 2003 Feb 24;163(4):427-36. doi: 10.1001/archinte.163.4.427. PMID: 12588201; PMCID: PMC3146257.
2. Molly C. Carr, The Emergence of the Metabolic Syndrome with Menopause, *The Journal of Clinical Endocrinology & Metabolism*, Volume 88, Issue 6, 1 June 2003, Pages 2404– 2411, https://doi.org/10.1210/jc.2003-030242
3. Clegg D, Hevener AL, Moreau KL, Morselli E, Criollo A, Van Pelt RE, et al. Sex Hormones and Cardiometabolic Health: Role of Estrogen and Estrogen Receptors. *Endocrinology*. 2017;158(5):1095– 105.
4. Al-Safi ZA, Polotsky AJ. Obesity and menopause. *Best Pract Res Clin Obstet Gynaecol.* 2015;29(4):548– 53.
5. Davis SR, Castelo-Branco C, Chedraui P, Lumsden MA, Nappi RE, Shah D, et al. Understanding weight gain at menopause. *Climacteric*. 2012;15(5):419–29.
6. Lovejoy, J. C., Champagne, C. M., de Jonge, L., Xie, H. & Smith, S. R. Increased visceral fat and decreased energy expenditure during the menopausal transition. *Int J Obes* (Lond) 32, 949-958, doi:10.1038/ijo.2008.25 (2008).
7. Wegorzewska IN, Walters K, Weiser MJ, Cruthirds DF, Ewell E, Larco DO, et al. Postovariectomy weight gain in female rats is reversed by estrogen receptor alpha agonist, propylpyrazoletriol. *Am J Obstet Gynecol*. 2008;199(1):67 e1–5.
8. Hong, J., Stubbins, R. E., Smith, R. R., Harvey, A. E. & Nunez, N. P. Differential susceptibility to obesity between male, female and ovariectomized female mice. *Nutr J* 8, 11, doi:10.1186/1475-2891-8-11 (2009)
9. Chmouliovsky L, Habicht F, James RW, Lehmann T, Campana A, Golay A. Beneficial effect of hormone replacement therapy on weight loss in obese menopausal women. *Maturitas*. 1999;32(3):147–53.
10. dos Reis CM, de Melo NR, Meirelles ES, Vezozzo DP, Halpern A. Body composition, visceral fat distribution and fat oxidation in postmenopausal women using oral or transdermal oestrogen. *Maturitas.* 2003;46(1):59–68.
11. Salpeter SR, Walsh JM, Ormiston TM, Greyber E, Buckley NS, Salpeter EE. Meta-analysis: effect of hormone-replacement therapy on components of the metabolic syndrome in postmenopausal women. *Diabetes Obes Metab*. 2006;8(5):538–54.
12. Duncan AC, Lyall H, Roberts RN, Petrie JR, Perera MJ, Monaghan S, Hart DM, Connell JM, Lumsden MA. The effect of estradiol and a combined estradiol/progestagen preparation on insulin sensitivity in healthy postmenopausal women. *J Clin Endocrinol Metab*. 1999 Jul;84(7):2402-7. doi: 10.1210/jcem.84.7.5836. PMID: 10404811.
13. Sites CK, L'Hommedieu GD, Toth MJ, Brochu M, Cooper BC, Fairhurst PA. The effect of hormone replacement therapy on body composition, body fat

distribution, and insulin sensitivity in menopausal women: a randomized, double-blind, placebo-controlled trial. *J Clin Endocrinol Metab.* 2005;90(5):2701–7.

14. O'Sullivan AJ, Hoffman DM, Ho KK. Estrogen, lipid oxidation, and body fat. *N Engl J Med*. 1995;333(10):669–70.
15. Haskell SG. Selective estrogen receptor modulators. *South Med J*. 2003 May;96(5):469-76. doi: 10.1097/01.SMJ.0000051146.93190.4A. PMID: 12911186.
16. Cummings SR, Eckert S, Krueger KA, et al. The effect of raloxifene on risk of breast cancer in postmenopausal women: results from the MORE randomized trial. Multiple Outcomes of Raloxifene Evaluation. *JAMA.* 1999;281:2189–2197.
17. Saphner T, Tormey DC, Gray R. Venous and arterial thrombosis in patients who received adjuvant therapy for breast cancer. *J Clin Oncol.* 1991;9:286–294.
18. Killinger DW, Perel E, Daniilescu D, Kharlip L, Blackstein ME. Aromatase activity in the breast and other peripheral tissues and its therapeutic regulation. *Steroids.* 1987 Oct-Dec;50(4-6):523-36. doi: 10.1016/0039-128x(87)90036-5. PMID: 3332939.
19. Kadioglu P, Oral G, Sayitoglu M, Erensoy N, Senel B, Gazioglu N, Sav A, Cetin G, Ozbek U. Aromatase cytochrome P450 enzyme expression in human pituitary. *Pituitary.* 2008;11(1):29-35. doi: 10.1007/s11102- 007-0065-3. PMID: 1770336
20. Weisz J. In vitro assays of aromatase and their role in studies of estrogen formation in target tissues. *Cancer Res*.1982;42(8Suppl):3295s-3298s
21. Amanatullah DF, Tamaresis JS, Chu P, Bachmann MH, Hoang NM, Collyar D, Mayer AT, West RB, Maloney WJ, Contag CH, King BL. Local estrogen axis in the human bone microenvironment regulates estrogen receptor-positive breast cancer cells. *Breast Cancer Res.* 2017 Nov 15;19(1):121. doi: 10.1186/s13058-017-0910-x. PMID: 29141657; PMCID: PMC5688761
22. Marino M, Galluzzo P, Ascenzi P. Estrogen signaling multiple pathways to impact gene transcription. *Curr Genomics*. 2006;7(8):497-508. doi: 10.2174/138920206779315737. PMID: 18369406; PMCID: PMC2269003.
23. Auboeuf D, Dowhan DH, Dutertre M, Martin N, Berget SM, O'Malley BW. A subset of nuclear receptor coregulators act as coupling proteins during synthesis and maturation of RNA transcripts. *Mol Cell Biol.* 2005 Jul;25(13):5307-16. doi: 10.1128/MCB.25.13.5307-5316.2005. PMID: 15964789; PMCID: PMC1156981.
24. Le Dily F, Beato M. Signaling by Steroid Hormones in the 3D Nuclear Space. *Int J Mol Sci*. 2018 Jan 23;19(2):306. doi: 10.3390/ijms19020306. PMID: 29360755; PMCID: PMC5855546.
25. Klinge CM. Estrogen receptor interaction with estrogen response elements. Nucleic Acids Res. 2001 Jul 15;29(14):2905-19. doi: 10.1093/nar/29.14.2905. PMID: 11452016; PMCID: PMC55815.
26. Carleton JB, Ginley-Hidinger M, Berrett KC, Layer RM, Quinlan AR, Gertz J. Regulatory sharing between estrogen receptor α bound enhancers. Nucleic Acids Res. 2020 Jul 9;48(12):6597-6610. doi: 10.1093/nar/gkaa454. PMID: 32479598; PMCID: PMC7337896.

27. Vrtačnik P, Ostanek B, Mencej-Bedrač S, Marc J. The many faces of estrogen signaling. *Biochem Med (Zagreb).* 2014 Oct 15;24(3):329-42. doi: 10.11613/BM.2014.035. PMID: 25351351; PMCID: PMC4210253.
28. Bajic VB, Tan SL, Chong A, Tang S, Ström A, Gustafsson JA, Lin CY, Liu ET. Dragon ERE Finder version 2: A tool for accurate detection and analysis of estrogen response elements in vertebrate genomes. *Nucleic Acids Res*. 2003 Jul 1;31(13):3605-7. doi: 10.1093/nar/gkg517. PMID: 12824376; PMCID: PMC168924.
29. O'Lone R, Frith MC, Karlsson EK, Hansen U. Genomic targets of nuclear estrogen receptors. *Mol Endocrinol.* 2004 Aug;18(8):1859-75. doi: 10.1210/me.2003-0044. Epub 2004 Mar 18. PMID: 15031323.
30. Lösel R, Wehling M. Nongenomic actions of steroid hormones. *Nat Rev Mol Cell Biol.* 2003 Jan;4(1):46-56. doi: 10.1038/nrm1009. PMID: 12511868.
31. Roberta Diaz Brinton, Minireview: Translational Animal Models of Human Menopause: Challenges and Emerging Opportunities, *Endocrinology*, Volume 153, Issue 8, 1 August 2012, Pages 3571– 3578, https://doi.org/10.1210/en.2012-1340
32. Yonezawa R, Wada T, Matsumoto N, Morita M, Sawakawa K, Ishii Y, Sasahara M, Tsuneki H, Saito S, Sasaoka T. Central versus peripheral impact of estradiol on the impaired glucose metabolism in ovariectomized mice on a high-fat diet. *Am J Physiol Endocrinol Metab*. 2012 Aug 15;303(4):E445-56. doi: 10.1152/ajpendo.00638.2011. Epub 2012 May 1. PMID: 22550066
33. Hong, J., Stubbins, R. E., Smith, R. R., Harvey, A. E. & Nunez, N. P. Differential susceptibility to obesity between male, female and ovariectomized female mice. *Nutr J* 8, 11, doi:10.1186/1475-2891-8-11 (2009).
34. Gambacciani, M., Ciaponi, M., Cappagli, B. & Genazzani, A. R. Effects of low-dose continuous combined conjugated estrogens and medroxyprogesterone acetate on menopausal symptoms, body weight, bone density, and metabolism in postmenopausal women. *Am J Obstet Gynecol* 185, 1180-1185, doi:10.1067/mob.2001.117669 (2001)
35. Mattiasson, I., Rendell, M., Tornquist, C., Jeppsson, S. & Hulthen, U. L. Effects of estrogen replacement therapy on abdominal fat compartments as related to glucose and lipid metabolism in early postmenopausal women. *Horm Metab Res* 34, 583-588, doi:10.1055/s-2002-35420 (2002).
36. Park CJ, Zhao Z, Glidewell-Kenney C, Lazic M, Chambon P, Krust A, Weiss J, Clegg DJ, Dunaif A, Jameson JL, Levine JE. Genetic rescue of nonclassical ERα signaling normalizes energy balance in obese Erα-null mutant mice. J Clin Invest. 2011 Feb;121(2):604-12. doi: 10.1172/JCI41702. *Epub* 2011 Jan 18. PMID: 21245576; PMCID: PMC3026715.
37. Roepke TA, Bosch MA, Rick EA, Lee B, Wagner EJ, Seidlova-Wuttke D, Wuttke W, Scanlan TS, Rønnekleiv OK, Kelly MJ. Contribution of a membrane estrogen receptor to the estrogenic regulation of body temperature and energy

homeostasis. *Endocrinology.* 2010 Oct;151(10):4926-37. doi: 10.1210/en.2010-0573. Epub 2010 Aug 4. PMID: 20685867; PMCID: PMC2946146.

38. Mauvais-Jarvis F, Clegg DJ, Hevener AL. The role of estrogens in control of energy balance and glucose homeostasis. Endocr Rev. 2013 Jun;34(3):309-38. doi: 10.1210/er.2012-1055. *Epub* 2013 Mar 4. PMID: 23460719; PMCID: PMC3660717.
39. Martínez de Morentin PB, González-García I, Martins L, Lage R, Fernández-Mallo D, Martínez-Sánchez N, Ruíz-Pino F, Liu J, Morgan DA, Pinilla L, Gallego R, Saha AK, Kalsbeek A, Fliers E, Bisschop PH, Diéguez C, Nogueiras R, Rahmouni K, Tena-Sempere M, López M. Estradiol regulates brown adipose tissue thermogenesis via hypothalamic AMPK. *Cell Metab*. 2014 Jul 1;20(1):41-53. doi: 10.1016/j.cmet.2014.03.031. Epub 2014 May 22. PMID: 24856932; PMCID: PMC4082097.
40. Musatov S, Chen W, Pfaff DW, Mobbs CV, Yang XJ, Clegg DJ, Kaplitt MG, Ogawa S. Silencing of estrogen receptor alpha in the ventromedial nucleus of hypothalamus leads to metabolic syndrome. *Proc Natl Acad Sci U S A*. 2007 Feb 13;104(7):2501-6. doi: 10.1073/pnas.0610787104. Epub 2007 Feb 6. PMID: 17284595; PMCID: PMC1892990
41. van Veen JE, Kammel LG, Bunda PC, Shum M, Reid MS, Massa MG, Arneson D, Park JW, Zhang Z, Joseph AM, Hrncir H, Liesa M, Arnold AP, Yang X, Correa SM. Hypothalamic estrogen receptor alpha establishes a sexually dimorphic regulatory node of energy expenditure. *Nat Metab.* 2020 Apr;2(4):351- 363. doi: 10.1038/s42255-020-0189-6. Epub 2020 Apr 13. PMID: 32377634; PMCID: PMC7202561.
42. Baldini G, Phelan KD. The melanocortin pathway and control of appetite-progress and therapeutic implications. *J Endocrinol*. 2019 Apr 1;241(1):R1-R33. doi: 10.1530/JOE-18-0596. PMID: 30812013; PMCID: PMC6500576.
43. Ellacott KL, Cone RD. The central melanocortin system and the integration of short- and long-term regulators of energy homeostasis. *Recent Prog Horm Res*. 2004;59:395-408. doi: 10.1210/rp.59.1.395. PMID: 14749511.
44. Ranadive SA, Vaisse C. Lessons from extreme human obesity: monogenic disorders. *Endocrinol Metab Clin North Am*. 2008 Sep;37(3):733-51, x. doi: 10.1016/j.ecl.2008.07.003. PMID: 18775361; PMCID: PMC5877402.
45. Wang P, Loh KH, Wu M, Morgan DA, Schneeberger M, Yu X, Chi J, Kosse C, Kim D, Rahmouni K, Cohen P, Friedman J. A leptin-BDNF pathway regulating sympathetic innervation of adipose tissue. Nature. 2020 Jul;583(7818):839-844. doi: 10.1038/s41586-020-2527-y. Epub 2020 Jul 22. PMID: 32699414.
46. Jung SM, Sanchez-Gurmaches J, Guertin DA. Brown Adipose Tissue Development and Metabolism. *Handb Exp Pharmacol*. 2019;251:3-36. doi: 10.1007/164_2018_168. PMID: 30203328; PMCID: PMC7330484.
47. Joon S. Kim, Mohammed Z. Rizwan, Deborah J. Clegg, Greg M. Anderson, Leptin Signaling Is Not Required for Anorexigenic Estradiol Effects in

Female Mice, *Endocrinology,* Volume 157, Issue 5, 1 May 2016, Pages 1991–2001, https://doi.org/10.1210/en.2015-1594

48. Diano S, Kalra SP, Sakamoto H, Horvath TL. Leptin receptors in estrogen receptor-containing neurons of the female rat hypothalamus. *Brain Res.* 1998 Nov 23;812(1-2):256-9. doi: 10.1016/s0006-8993(98)00936-6. PMID: 9813356.
49. 1S1S. Del Bianco-Borges B, Cabral FJ, Franci CR. Co-expression of leptin and oestrogen receptors in the preoptic-hypothalamic area. *J Neuroendocrinol.* 2010 Sep;22(9):996-1003. doi: 10.1111/j.1365-2826.2010.02046.x. Epub 2010 Jun 24. PMID: 20584107.
50. Clegg DJ, Brown LM, Woods SC, Benoit SC. Gonadal hormones determine sensitivity to central leptin and insulin. *Diabetes.* 2006 Apr;55(4):978-87. doi: 10.2337/diabetes.55.04.06.db05-1339. Erratum in: Diabetes. 2007 Oct;56(10):2649.
51. Alonso A, Fernández R, Moreno M, Ordóñez P, Díaz F, González C. Leptin and its receptor are controlled by 17beta-estradiol in peripheral tissues of ovariectomized rats. *Exp Biol Med (Maywood).* 2007 Apr;232(4):542-9. PMID: 17392490.
52. Musatov S, Chen W, Pfaff DW, Mobbs CV, Yang XJ, Clegg DJ, Kaplitt MG, Ogawa S. Silencing of estrogen receptor alpha in the ventromedial nucleus of hypothalamus leads to metabolic syndrome. *Proc Natl Acad Sci U S A.* 2007 Feb 13;104(7):2501-6. doi: 10.1073/pnas.0610787104. Epub 2007 Feb 6. PMID: 17284595; PMCID: PMC1892990.
53. Xu Y, Nedungadi TP, Zhu L, Sobhani N, Irani BG, Davis KE, Zhang X, Zou F, Gent LM, Hahner LD, Khan SA, Elias CF, Elmquist JK, Clegg DJ. Distinct hypothalamic neurons mediate estrogenic effects on energy homeostasis and reproduction. *Cell Metab.* 2011 Oct 5;14(4):453-65. doi: 10.1016/j.cmet.2011.08.009. Erratum in: Cell Metab. 2019 May 7;29(5):1232. PMID: 21982706; PMCID: PMC3235745.
54. Krause WC, Rodriguez R, Gegenhuber B, Matharu N, Rodriguez AN, Padilla-Roger AM, Toma K, Herber CB, Correa SM, Duan X, Ahituv N, Tollkuhn J, Ingraham HA. Oestrogen engages brain MC4R signalling to drive physical activity in female mice. *Nature.* 2021 Nov;599(7883):131-135. doi: 10.1038/s41586-021-04010-3. Epub 2021 Oct 13. PMID: 34646010; PMCID: PMC9113400.
55. Enriori PJ, Evans AE, Sinnayah P, Jobst EE, Tonelli-Lemos L, Billes SK, Glavas MM, Grayson BE, Perello M, Nillni EA, Grove KL, Cowley MA. Diet-induced obesity causes severe but reversible leptin resistance in arcuate melanocortin neurons. *Cell Metab.* 2007 Mar;5(3):181-94. doi: 10.1016/j.cmet.2007.02.004. PMID: 17339026.
56. McCurdyCE, Bishop JM, Williams SM, et al. Maternal high-fat diet triggers lipotoxicity in the fetal livers of nonhuman primates.*JClin Invest* 2009;119(2):323–335

57. Frias AE, Morgan TK, Evans AF, et al Maternal high-fat diet disturbs uteroplacental hemodynamics and increases the frequency of Seminars in stillbirth in a nonhuman primate model of excess nutrition. *Endocrinology* 2011;152(6):2456–2464
58. Grant WF, Gillingham MB, Batra AK,et al. Maternal high fat diet is associated with decreased plasma n-3 fatty acids and fetal hepatic apoptosis in nonhuman primates. *PLoS ONE* 2011; 6(2):e17261
59. Grayson BE, Levasseur PR, Williams SM, Smith MS, Marks DL, Grove KL. Changes in melanocortin expression and inflammatory pathways in fetal offspring of nonhuman primates fed a high-fat diet. *Endocrinology* 2010;151(4):1622–1632
60. Sullivan EL, Grayson B,Takahashi D, etal. Chronic consumption of a high-fat diet during pregnancy causes perturbations in the serotonergic system and increased anxiety-like behavior in nonhuman primate offspring. *J Neurosci* 2010;30(10):3826–3830
61. Frias AE, Grove KL. Obesity: a transgenerational problem linked to nutrition during pregnancy. *Semin Reprod Med.* 2012 Dec;30(6):472-8. doi: 10.1055/s-0032-1328875. *Epub* 2012 Oct 16. PMID: 23074005; PMCID: PMC3615704.
62. Shen M, Kumar SP, Shi H. Estradiol regulates insulin signaling and inflammation in adipose tissue. *Horm Mol Biol Clin Investig*. 2014 Feb;17(2):99-107. doi: 10.1515/hmbci-2014-0007. PMID: 25372734; PMCID: PMC4221806.
63. Mauvais-Jarvis F, Clegg DJ, Hevener AL. The role of estrogens in control of energy balance and glucose homeostasis. *Endocr Rev.* 2013 Jun;34(3):309-38. doi: 10.1210/er.2012-1055. Epub 2013 Mar 4. PMID: 23460719; PMCID: PMC3660717.
64. Sullivan EL, Daniels AJ, Koegler FH, Cameron JL. Evidence in female rhesus monkeys (Macaca mulatta) that nighttime caloric intake is not associated with weight gain. *Obes Res*. 2005 Dec;13(12):2072-80. doi: 10.1038/oby.2005.257. PMID: 16421340.
65. Sandoval-Guzmán T, Stalcup ST, Krajewski SJ, Voytko ML, Rance NE. Effects of ovariectomy on the neuroendocrine axes regulating reproduction and energy balance in young cynomolgus macaques. *J Neuroendocrinol*. 2004 Feb;16(2):146-53. doi: 10.1111/j.0953-8194.2004.01143.x. PMID: 14764001.
66. Wagner JD, Clarkson TB, St Clair RW, Schwenke DC, Shively CA, Adams MR. Estrogen and progesterone replacement therapy reduces low density lipoprotein accumulation in the coronary arteries of surgically postmenopausal cynomolgus monkeys. *J Clin Invest.* 1991 Dec;88(6):1995-2002. doi: 10.1172/JCI115526. PMID: 1752958; PMCID: PMC295786.
67. Kemnitz JW, Eisele SG, Lindsay KA, Engle MJ, Perelman RH, Farrell PM. Changes in food intake during menstrual cycles and pregnancy of normal and diabetic rhesus monkeys. *Diabetologia*. 1984 Jan;26(1):60-4. doi: 10.1007/BF00252265. PMID: 6706046.

68. Czaja JA. Ovarian influences on primate food intake: assessment of progesterone actions. *Physiol Behav*. 1978 Dec;21(6):923-8. doi: 10.1016/0031-9384(78)90167-1. PMID: 552083.
69. Lissner L, Stevens J, Levitsky DA, Rasmussen KM, Strupp BJ. Variation in energy intake during the menstrual cycle: implications for food-intake research. *Am J Clin Nutr.* 1988 Oct;48(4):956-62. doi: 10.1093/ajcn/48.4.956. PMID: 3421205.
70. Gong EJ, Garrel D, Calloway DH. Menstrual cycle and voluntary food intake. *Am J Clin Nutr.* 1989 Feb;49(2):252-8. doi: 10.1093/ajcn/49.2.252. PMID: 2916445.
71. Fong AK, Kretsch MJ. Changes in dietary intake, urinary nitrogen, and urinary volume across the menstrual cycle. *Am J Clin Nutr*. 1993 Jan;57(1):43-6. doi: 10.1093/ajcn/57.1.43. PMID: 8416663.
72. Johnson WG, Corrigan SA, Lemmon CR, Bergeron KB, Crusco AH. Energy regulation over the menstrual cycle. *Physiol Behav.* 1994 Sep;56(3):523-7. doi: 10.1016/0031-9384(94)90296-8. PMID: 7972403.
73. Fong AK, Kretsch MJ. Changes in dietary intake, urinary nitrogen, and urinary volume across the menstrual cycle. *Am J Clin Nutr.* 1993 Jan;57(1):43-6. doi: 10.1093/ajcn/57.1.43. PMID: 8416663.
74. Sandoval-Guzman, T., Stalcup, S. T., Krajewski, S. J., Voytko, M. L. & Rance, N. E. Effects of ovariectomy on the neuroendocrine axes regulating reproduction and energy balance in young cynomolgus macaques. *J Neuroendocrinol* 16, 146-153 (2004).
75. Cefalu WT, Wagner JD, Bell-Farrow AD, Wang ZQ, Adams MR, Toffolo G, Cobelli C. The effects of hormonal replacement therapy on insulin sensitivity in surgically postmenopausal cynomolgus monkeys (Macaca fascicularis). *Am J Obstet Gynecol.* 1994 Aug;171(2):440-5. doi: 10.1016/0002-9378(94)90280-1. PMID: 8059824.
76. Kraynak M, Willging MM, Kuehlmann AL, Kapoor AA, Flowers MT, Colman RJ, Levine JE, Abbott DH. Aromatase Inhibition Eliminates Sexual Receptivity Without Enhancing Weight Gain in Ovariectomized Marmoset Monkeys. *J Endocr Soc.* 2022 Apr 22;6(6):bvac063. doi: 10.1210/jendso/bvac063. PMID: 35592515; PMCID: PMC9113444.
77. Sullivan EL, Shearin J, Koegler FH, Cameron JL. Selective estrogen receptor modulator promotes weight loss in ovariectomized female rhesus monkeys (Macaca mulatta) by decreasing food intake and increasing activity. *Am J Physiol Endocrinol Metab.* 2012 Apr 1;302(7):E759-67. doi: 10.1152/ajpendo.00327.2011. Epub 2012 Jan 17. PMID: 22252940.
78. Cefalu WT, Wagner JD, Bell-Farrow AD, Wang ZQ, Adams MR, Toffolo G, Cobelli C. The effects of hormonal replacement therapy on insulin sensitivity in surgically postmenopausal cynomolgus monkeys (Macaca fascicularis). *Am J Obstet Gynecol*. 1994 Aug;171(2):440-5. doi: 10.1016/0002-9378(94)90280-1. PMID: 8059824.

79. Ellinwood WE, Hess DL, Roselli CE, Spies HG, Resko JA, 1984. Inhibition of aromatization stimulates luteinizing hormone and testosterone secretion in adult male rhesus monkeys. *J. Clin. Endocrinol. Metab* 59, 1088–1096
80. Terasawa E. Neuroestradiol in regulation of GnRH release. *Horm Behav.* 2018 Aug;104:138-145. doi: 10.1016/j.yhbeh.2018.04.003. Epub 2018 Apr 19. PMID: 29626484; PMCID: PMC6941749.
81. Roselli CE, Klosterman S, Resko JA, 2001. Anatomic relationships between aromatase and androgen receptor mRNA expression in the hypothalamus and amygdala of adult male cynomolgus monkeys. *J. Comp. Neurol* 439, 208–223.
82. Davis SR, Castelo-Branco C, Chedraui P, Lumsden MA, Nappi RE, Shah D, Villaseca P; Writing Group of the International Menopause Society for World Menopause Day 2012. Understanding weight gain at menopause. *Climacteric.* 2012 Oct;15(5):419-29. doi: 10.3109/13697137.2012.707385. PMID: 22978257.
83. Ranadive SA, Vaisse C. Lessons from extreme human obesity: monogenic disorders. *Endocrinol Metab Clin North Am.* 2008 Sep;37(3):733-51, x. doi: 10.1016/j.ecl.2008.07.003. PMID: 18775361; PMCID: PMC5877402.
84. Thaker VV. GENETIC AND EPIGENETIC CAUSES OF OBESITY. *Adolesc Med State Art Rev.* 2017 Fall;28(2):379-405. PMID: 30416642; PMCID: PMC6226269.
85. Huvenne H, Dubern B, Clément K, Poitou C. Rare Genetic Forms of Obesity: Clinical Approach and Current Treatments in 2016. *Obes Facts*. 2016;9(3):158-73. doi: 10.1159/000445061. Epub 2016 Jun 1. PMID: 27241181; PMCID: PMC5644891.
86. Czajkowski P, Adamska-Patruno E, Bauer W, Fiedorczuk J, Krasowska U, Moroz M, Gorska M, Kretowski A. The Impact of FTO Genetic Variants on Obesity and Its Metabolic Consequences is Dependent on Daily Macronutrient Intake. *Nutrients*. 2020 Oct 23;12(11):3255. doi: 10.3390/nu12113255. PMID: 33114268; PMCID: PMC7690875.
87. Coleman DL. Effects of parabiosis of obese with diabetes and normal mice. *Diabetologia.* 1973 Aug;9(4):294-8. doi: 10.1007/BF01221857. PMID: 4767369.
88. Green ED, Maffei M, Braden VV, Proenca R, DeSilva U, Zhang Y, Chua SC Jr, Leibel RL, Weissenbach J, Friedman JM. The human obese (OB) gene: RNA expression pattern and mapping on the physical, cytogenetic, and genetic maps of chromosome 7. *Genome Res*. 1995 Aug;5(1):5-12. doi: 10.1101/gr.5.1.5. PMID: 8717050.
89. Ahima RS, Antwi DA. Brain regulation of appetite and satiety. *Endocrinol Metab Clin North Am*. 2008 Dec;37(4):811-23. doi: 10.1016/j.ecl.2008.08.005. PMID: 19026933; PMCID: PMC2710609.
90. Clément K, Vaisse C, Lahlou N, Cabrol S, Pelloux V, Cassuto D, Gourmelen M, Dina C, Chambaz J, Lacorte JM, Basdevant A, Bougnères P, Lebouc Y, Froguel P, Guy-Grand B. A mutation in the human leptin receptor gene causes obesity and pituitary dysfunction. *Nature.* 1998 Mar 26;392(6674):398-401. doi: 10.1038/32911. PMID: 9537324.

91. Grill HJ, Skibicka KP, Hayes MR. Imaging obesity: fMRI, food reward, and feeding. *Cell Metab*. 2007 Dec;6(6):423-5. doi: 10.1016/j.cmet.2007.11.007. PMID: 18054310.
92. Santini F, Maffei M, Pelosini C, Salvetti G, Scartabelli G, Pinchera A. Melanocortin-4 receptor mutations in obesity. *Adv Clin Chem*. 2009;48:95-109. PMID: 19803416.
93. Michaud JL, Boucher F, Melnyk A, Gauthier F, Goshu E, Lévy E, Mitchell GA, Himms-Hagen J, Fan CM. Sim1 haploinsufficiency causes hyperphagia, obesity and reduction of the paraventricular nucleus of the hypothalamus*. Hum Mol Genet.* 2001 Jul 1;10(14):1465-73. doi: 10.1093/hmg/10.14.1465. PMID: 11448938.
94. Xu B, Goulding EH, Zang K, Cepoi D, Cone RD, Jones KR, Tecott LH, Reichardt LF. Brain-derived neurotrophic factor regulates energy balance downstream of melanocortin-4 receptor. *Nat Neurosci*. 2003 Jul;6(7):736-42. doi: 10.1038/nn1073. PMID: 12796784; PMCID: PMC2710100.
95. Lyons WE, Mamounas LA, Ricaurte GA, Coppola V, Reid SW, Bora SH, Wihler C, Koliatsos VE, Tessarollo L. Brain-derived neurotrophic factor-deficient mice develop aggressiveness and hyperphagia in conjunction with brain serotonergic abnormalities. *Proc Natl Acad Sci U S A*. 1999 Dec 21;96(26):15239-44. doi: 10.1073/pnas.96.26.15239. PMID: 10611369; PMCID: PMC24804.
96. Gray J, Yeo GS, Cox JJ, Morton J, Adlam AL, Keogh JM, Yanovski JA, El Gharbawy A, Han JC, Tung YC, Hodges JR, Raymond FL, O'rahilly S, Farooqi IS. Hyperphagia, severe obesity, impaired cognitive function, and hyperactivity associated with functional loss of one copy of the brain-derived neurotrophic factor (BDNF) gene. *Diabetes*. 2006 Dec;55(12):3366-71. doi: 10.2337/db06-0550. PMID: 17130481; PMCID: PMC2413291.
97. Olofsson LE, Pierce AA, Xu AW. Functional requirement of AgRP and NPY neurons in ovarian cycle-dependent regulation of food intake. *Proc Natl Acad Sci U S A*. 2009 Sep 15;106(37):15932-7. doi: 10.1073/pnas.0904747106. Epub 2009 Sep 2. PMID: 19805233; PMCID: PMC2747221.
98. Morin LP, Fleming AS. Variation of food intake and body weight with estrous cycle, ovariectomy, and estradiol benzoate treatment in hamsters (Mesocricetus auratus). *J Comp Physiol Psychol.* 1978 Feb;92(1):1-6. doi: 10.1037/h0077435. PMID: 564357.
99. Rosenblatt H, Dyrenfurth I, Ferin M, vande Wiele RL. Food intake and the menstrual cycle in rhesus monkeys. *Physiol Behav.* 1980 Mar;24(3):447-9. doi: 10.1016/0031-9384(80)90234-6. PMID: 6769135.
100. Pan X, Mota S, Zhang B. Circadian Clock Regulation on Lipid Metabolism and Metabolic Diseases. *Adv Exp Med Biol*. 2020;1276:53-66. doi: 10.1007/978-981-15-6082-8_5. PMID: 32705594; PMCID: PMC8593891.
101. Varcoe TJ, Gatford KL, Voultsios A, Salkeld MD, Boden MJ, Rattanatray L, Kennaway DJ. Rapidly alternating photoperiods disrupt central and peripheral rhythmicity and decrease plasma glucose, but do not affect glucose tolerance or

insulin secretion in sheep. *Exp Physiol.* 2014 Sep;99(9):1214-28. doi: 10.1113/expphysiol.2014.080630. Epub 2014 Jun 20. PMID: 24951500.

102. Hampton SM, Morgan LM, Lawrence N, Anastasiadou T, Norris F, Deacon S, Ribeiro D & Arendt J (1996). Postprandial hormone and metabolic responses in simulated shift work. *J Endocrinol* 151, 259–267.
103. Scheer FA, Hilton MF, Mantzoros CS & Shea SA (2009). Adverse metabolic and cardiovascular consequences of circadian misalignment. *Proc Natl Acad Sci U S A* 106, 4453–4458.
104. Kennaway DJ, Gilmore TA & Seamark RF (1982). Effects of melatonin implants on the circadian rhythm of plasma melatonin and prolactin in sheep. *Endocrinology* 110, 2186–2188.
105. Earl CR, D'Occhio MJ, Kennaway DJ & Seamark RF (1990). Temporal changes in the pattern of melatonin secretion in sheep held in constant darkness. *J Pineal Res* 8, 115–121
106. Piccione G, Caola G & Refinetti R (2005). Temporal relationships of 21 physiological variables in horse and sheep. *Comp Biochem Physiol A Mol Integr Physiol* 142, 389–396.
107. Bergman EN (1990). Energy contributions of volatile fatty acids from the gastrointestinal tract in various species. Physiol Rev 70, 567–590.
108. Elmahdi B, Sallmann HP, Fuhrmann H, von Engelhardt W & Kaske M (1997). Comparative aspects of glucose tolerance in camels, sheep, and ponies. *Comp Biochem Physiol A Physiol* 118, 147–151.
109. Kaske M, Elmahdi B, von Engelhardt W & Sallmann HP (2001). Insulin responsiveness of sheep, ponies, miniature pigs and camels: results of hyperinsulinemic clamps using porcine insulin. *J Comp Physiol B* 171, 549–556.
110. Bergman EN, Reulein SS, Corlett RE. Effects of obesity on insulin sensitivity and responsiveness in sheep. *Am J Physiol*. 1989 Nov;257(5 Pt 1):E772-81. doi: 10.1152/ajpendo.1989.257.5.E772. PMID: 2688439.
111. Trenkle A. Postprandial changes in insulin secretion rates in sheep. *J Nutr.* 1971 Aug;101(8):1099-103. doi: 10.1093/jn/101.8.1099. PMID: 5565097.
112. Fuller-Jackson JP, Henry BA. Adipose and skeletal muscle thermogenesis: studies from large animals. *J Endocrinol.* 2018 Jun;237(3):R99-R115. doi: 10.1530/JOE-18-0090. PMID: 29703782.
113. Nedergaard J, Bengtsson T & Cannon B 2007 Unexpected evidence for active brown adipose tissue in adult humans. *American Journal of Physiology: Endocrinology and Metabolism* 293 E444–E452. (https://doi.org/10.1152/ajpendo.00691.2006)
114. Cypess AM, White AP, Vernochet C, Schulz TJ, Xue R, Sass CA, Huang TL, Roberts-Toler C, Weiner LS & Sze C 2013 Anatomical localization, gene expression profiling and functional characterization of adult human neck brown fat. *Nature Medicine* 19 635–639. (https://doi.org/10.1038/nm.3112)
115. van Marken Lichtenbelt WD, Vanhommerig JW, Smulders NM, Drossaerts JMAFL, Kemerink GJ, Bouvy ND, Schrauwen P & Jaap Teule GJ 2009 Cold

activated brown adipose tissue in healthy men. *New England Journal of Medicine* 360 1500–1508. (https://doi.org/10.1056/NEJMoa0808718)

116. Mehta J, Kling JM, Manson JE. Risks, Benefits, and Treatment Modalities of Menopausal Hormone Therapy: Current Concepts. *Front Endocrinol (Lausanne).* 2021 Mar 26;12:564781. doi: 10.3389/fendo.2021.564781. PMID: 33841322; PMCID: PMC8034540.
117. Gambacciani M, Levancini M. Management of postmenopausal osteoporosis and the prevention of fractures. *Panminerva Med*. 2014 Jun;56(2):115-31. Epub 2014 Jun 19. PMID: 24942322.
118. Vinogradova Y, Coupland C, Hippisley-Cox J. Use of hormone replacement therapy and risk of breast cancer: nested case-control studies using the QResearch and CPRD databases. *BMJ*. 2020 Oct 28;371:m3873. doi: 10.1136/bmj.m3873. PMID: 33115755; PMCID: PMC7592147.
119. Skoog I, Gustafson D. HRT and dementia. *J Epidemiol Biostat*. 1999;4(3):227-51; discussion 252. PMID: 10695961.
120. Martin KA, Manson JE. Approach to the patient with menopausal symptoms. *J Clin Endocrinol Metab.* 2008 Dec;93(12):4567-75. doi: 10.1210/jc.2008-1272. PMID: 19056840.
121. Brennan A, Hickey M. Management of Early Menopause/Premature Ovarian Insufficiency in Women with or at High Risk of Breast Cancer. *Semin Reprod Med.* 2020 Sep;38(4-05):309-314. doi: 10.1055/s-0041-1726467. Epub 2021 Mar 31. PMID: 33791998.
122. Quirke VM. Tamoxifen from Failed Contraceptive Pill to Best-Selling Breast Cancer Medicine: A Case-Study in Pharmaceutical Innovation. *Front Pharmacol.* 2017;8:620.
123. Breast International Group (BIG) 1-98 Collaborative Group; Thürlimann B, Keshaviah A, Coates AS, Mouridsen H, Mauriac L, Forbes JF, Paridaens R, Castiglione-Gertsch M, Gelber RD, Rabaglio M, Smith I, Wardley A, Price KN, Goldhirsch A. A comparison of letrozole and tamoxifen in postmenopausal women with early breast cancer. *N Engl J Med*. 2005 Dec 29;353(26):2747-57. doi: 10.1056/NEJMoa052258. Erratum in: *N Engl J Med*. 2006 May 18;354(20):2200. Wardly, Andrew [corrected to Wardley, Andrew]. PMID: 16382061.
124. Elisaf MS, Bairaktari ET, Nicolaides C, et al. Effect of letrozole on the lipid profile in postmenopausal women with breast cancer. *Eur J Cancer* 2001;37:1510-1513
125. Saquib N, Flatt SW, Natarajan L, Thomson CA, Bardwell WA, Caan B, Rock CL, Pierce JP. Weight gain and recovery of pre-cancer weight after breast cancer treatments: evidence from the women's healthy eating and living (WHEL) study. *Breast Cancer Res Treat*. 2007 Oct;105(2):177-86. doi: 10.1007/s10549-006-9442-2. Epub 2006 Nov 23. PMID: 17123151.
126. Makari-Judson G, Braun B, Jerry DJ, Mertens WC. Weight gain following breast cancer diagnosis: Implication and proposed mechanisms. *World J Clin Oncol*.

2014 Aug 10;5(3):272-82. doi: 10.5306/wjco.v5.i3.272. PMID: 25114844; PMCID: PMC4127600.

127. Raghavendra A, Sinha AK, Valle-Goffin J, Shen Y, Tripathy D, Barcenas CH. Determinants of Weight Gain During Adjuvant Endocrine Therapy and Association of Such Weight Gain With Recurrence in Long-term Breast Cancer Survivors. *Clin Breast Cancer*. 2018 Feb;18(1):e7-e13. doi: 10.1016/j.clbc.2017.11.006. Epub 2017 Nov 9. PMID: 29239836; PMCID: PMC5937690.
128. Battisti S, Guida FM, Coppa F, Vaccaro DM, Santini D, Tonini G, Zobel BB, Semelka RC. Modification of abdominal fat distribution after aromatase inhibitor therapy in breast cancer patients visualized using 3-D computed tomography volumetry. *Clin Breast Cancer*. 2014 Oct;14(5):365-70. doi: 10.1016/j.clbc.2014.02.003. Epub 2014 Mar 6. PMID: 24850544.
129. Pfeiler G, Königsberg R, Fesl C, Mlineritsch B, Stoeger H, Singer CF, Pöstlberger S, Steger GG, Seifert M, Dubsky P, Taucher S, Samonigg H, Bjelic-Radisic V, Greil R, Marth C, Gnant M. Impact of body mass index on the efficacy of endocrine therapy in premenopausal patients with breast cancer: an analysis of the prospective ABCSG-12 trial. *J Clin Oncol*. 2011 Jul 1;29(19):2653-9. doi: 10.1200/JCO.2010.33.2585. Epub 2011 May 9. PMID: 21555684.
130. Prokai L, Nguyen V, Szarka S, Garg P, Sabnis G, Bimonte-Nelson HA, McLaughlin KJ, Talboom JS, Conrad CD, Shughrue PJ, Gould TD, Brodie A, Merchenthaler I, Koulen P, Prokai-Tatrai K. The prodrug DHED selectively delivers 17β-estradiol to the brain for treating estrogen-responsive disorders. *Sci Transl Med.* 2015 Jul 22;7(297):297ra113. doi: 10.1126/scitranslmed.aab1290. PMID: 26203081; PMCID: PMC4591937.
131. Swick AG, Kemnitz JW, Houser WD, Swick RW. Norepinephrine stimulates the activity of brown adipose tissue in rhesus monkeys. *Int J Obes.* 1986;10(3):241-4.
132. Strieleman PJ, Gribskov CL, Kemnitz JW, Schalinske KL, Claude P, Parada I, Shrago E, Swick RW. Brown adipose tissue from fetal rhesus monkey (Macaca mulatta): morphological and biochemical aspects. *Comp Biochem Physiol B.* 1985;81(2):393-9. doi: 10.1016/0305-0491(85)90331-1. PMID: 4017553.
133. Skarra DV, Hernández-Carretero A, Rivera AJ, Anvar AR, Thackray VG. Hyperandrogenemia Induced by Letrozole Treatment of Pubertal Female Mice Results in Hyperinsulinemia Prior to Weight Gain and Insulin Resistance. Endocrinology. 2017 Sep 1;158(9):2988-3003. doi: 10.1210/en.2016-1898. PMID: 28911175; PMCID: PMC5659661.
134. Dumesic DA, Akopians AL, Madrigal VK, Ramirez E, Margolis DJ, Sarma MK, Thomas AM, Grogan TR, Haykal R, Schooler TA, Okeya BL, Abbott DH, Chazenbalk GD. Hyperandrogenism Accompanies Increased Intra-Abdominal Fat Storage in Normal Weight Polycystic Ovary Syndrome Women. *J Clin Endocrinol Metab.* 2016 Nov;101(11):4178-4188. doi: 10.1210/jc.2016-2586. Epub 2016 Aug 29. PMID: 27571186; PMCID: PMC5095243.

135. True CA, Takahashi DL, Burns SE, Mishler EC, Bond KR, Wilcox MC, Calhoun AR, Bader LA, Dean TA, Ryan ND, Slayden OD, Cameron JL, Stouffer RL. Chronic combined hyperandrogenemia and western-style diet in young female rhesus macaques causes greater metabolic impairments compared to either treatment alone. *Hum Reprod*. 2017 Sep 1;32(9):1880-1891. doi: 10.1093/humrep/dex246. PMID: 28854721; PMCID: PMC5850848.
136. Gruzdeva O, Borodkina D, Uchasova E, Dyleva Y, Barbarash O. Leptin resistance: underlying mechanisms and diagnosis. *Diabetes Metab Syndr Obes.* 2019 Jan 25;12:191-198. doi: 10.2147/DMSO.S182406. PMID: 30774404; PMCID: PMC6354688.

2. CHAPTER TWO: Hypothalamic Estrogen Receptor Alpha*, but not extra-ovarian estradiol,* essential for Metabolic Regulation in Female Marmoset Monkeys

Willging, MM, Kraynak M, Kuehlmann AL, Uhlrich DJ, Shapiro RA, Flowers MT, Manning KA, Kapoor AA, Williams SM, Henjum LJ, Marrah RC, Yohnk HR, Berg CB, Colman RJ, Abbott DH, and Levine JE

[This chapter was adapted from two published manuscripts, one of which was co-first authored with M.K. and the other involved second authorship. Contribution to these manuscripts: Conducted the data analysis and prepared the manuscripts for publication.]

2.1 Abstract

Ovarian estradiol via estrogen receptor alpha (ERα) regulates metabolic function in many female animal models. While ovariectomy (OVX) in rodents enables obesity, OVX in nonhuman primates inconsistently alters weight gain. We hypothesize that extra-ovarian estradiol provides key support for metabolism through hypothalamic ERα, and to test this idea, we completed two separate experiments. First, we employed aromatase inhibition to eliminate extra-ovarian estradiol biosynthesis and diet-induced obesity to enhance weight gain. Thirteen adult female marmosets were OVX and received (1) estradiol-containing capsules and daily oral treatments of vehicle (E2; n = 5); empty capsules and daily oral treatments of either (2) vehicle (VEH, 1 mL/kg, n = 4), or (3) letrozole (LET, 1 mg/kg, n = 4). VEH and LET females demonstrated increased % body weight gain (P = 0.01). Relative estradiol levels in peripheral serum were E2 >>> VEH > LET, while those in hypothalamus ranked E2 = VEH > LET, confirming inhibition of local hypothalamic estradiol synthesis by letrozole. Next, we utilized MRI-guided viral vector infusion to knockdown hypothalamic ERα expression in target regions of hypothalamic ventromedial (VMN) and arcuate (ARC) nuclei. Eleven adult female marmosets were OVX and received (1) OVX + estradiol replacement + scrambled virus shRNA (control; n=5) or (2) OVX + estradiol replacement + ERα gene silencing shRNA (ERαKD; n=4). ERα expressing cells were less numerous in the VMN in ERαaKD compared to control females, while intensity of ERα expression in the ARC was less in ERαKD compared to control females. Our findings provide clear evidence for ovarian estradiol protecting female nonhuman primates from obesity and they also support the

notion that the majority of metabolically effective E_2 activity is mediated through ERα within the hypothalamic VMN and ARC.

2.2 Introduction

Aromatase, a cytochrome P450 enzyme, encoded by the CYP19A1 gene, converts testosterone to E_2, and androstenedione to estrone. While the ovaries are a major source of E_2, the same hormone is also produced at aromatase- expressing extra-ovarian sites, including liver, breast, skin, bone, pituitary gland, and various brain regions[1-4]. Neural production of E_2 in particular has been identified in birds[5-7], mice[8], rats[9-12], as well as in monkeys[13-16]. Brain aromatase is expressed at high levels in the medial basal hypothalamus, preoptic area, amygdala, and hippocampus, and has a higher affinity for androgen substrates than its ovarian counterpart[8,17]. A role for hypothalamic aromatase in regulating gonadotropin-releasing hormone (GnRH) in female rhesus monkeys was recently demonstrated to show that (1) E_2 is produced and released at detectable levels within OVX monkey pituitary stalk-median eminence (SME), (2) E_2 synthesis and release depends upon acute elevations in systemic E_2 initiating detectable aromatase activity in the SME, and (3) hypothalamic E_2 can rapidly stimulate GnRH release in the SME[14,15,18]. These studies, in addition to previous work in female marmoset monkeys[16,19], provide evidence for extra-ovarian E_2 production in female nonhuman primates (NHPs) engaging neural action.

In many mammalian species, including rodents (rats, mice, guinea pigs), sheep, and NHPs, E_2 is a major regulator of female body weight regulation and insulin–glucose homeodynamics[20-22], mediating most of its activity by binding to estrogen receptor alpha (ERα)[23-25]. Neural signaling by E_2 in the female hypothalamus regulates metabolic homeostasis[26,27]. Hypothalamic E_2 activity is mostly mediated by estrogen receptor alpha (ERα and its encoding gene, *ESR1*)[28,29]. ERα exerts descending control over

systemic organ systems via autonomic innervation[30-32] and intra-hypothalamic innervation[33], including E_2-induced alterations in neuroendocrine regulation of ovarian function and food intake and energy expenditure, producing secondary endocrinological and metabolic states.

E_2-regulated metabolic control mechanisms are pronounced in female rodents, exemplified by OVX-mediated E_2 depletion reliably increasing body weight and visceral adiposity, reducing physical activity and energy expenditure, as well as diminishing glucose tolerance and insulin sensitivity[34-38]. Consistent with these findings, aromatase knockout female mice develop obesity with insulin resistance in the absence of endogenous E_2 synthesis[39]. All these effects are prevented or reversed by physiological E_2 replacement[40,41]. Furthermore, while intact female mice are resistant to high- fat diet-induced obesity (DIO) and its associated sequelae, OVX-mediated E_2 depletion abolishes this protection[42,43]. Virtually all of these E_2 activities are mediated by ERα, as ERα knockout adult mice (ERαKO) bearing null mutations of *ESR1* gene exhibit body weight, adiposity, and energy metabolism phenotypes that largely mimic those observed in long-term OVX adult mice[23-25]. In addition, loss of E_2 bioactivity in bone, particularly that mediated by ERα, reliably results in skeletal bone loss[44].

Estrogen deficiency is of particular clinical relevance for women in their post-reproductive years (menopause)[45], as well as for 80% of girls and young women who survive cancer yet live with premature ovarian insufficiency (premature menopause) as a result of alkylating agent and/or radiation cancer therapy[46,47]. Women with such estrogen deficiency experience compromised cardiometabolic dysfunction, obesity, and osteoporosis[48]. Hormonal therapies, including systemically administered E_2, alleviate

clinical conditions to varying degrees[49,50]. Currently approved estrogen medications, however, increase the risk for harmful systemic side-effects[51,52], including blood clots and cancer[53,54]. Estrogen treatments will therefore never realize their full potential until, perhaps, their actions are limited to the brain. In this regard, however, the extent to which E_2 regulates neural control systems in women is largely unknown.

With regard to the hypothalamic regulation of female NHP metabolic homeostasis, the VMN has been identified as a key regulatory site following electrolytic lesions of the female macaque hypothalamus[54,55]. When lesions included portions of the VMN, female macaques demonstrate increased weight gain. Stimulatory effects of E_2 on energy expenditure are transduced in ERα-expressing neurons within the VMN[56] and by non-classical ERα signaling[57] coupled to activation of PI3-kinase[58]. E_2 also regulates gene expression associated with regulation of food intake and energy expenditure in the female hypothalamus, largely through ERα activation[59,60]. Furthermore, it has been demonstrated that viral vector-mediated ERα gene silencing in the VMN of both female mice and rats largely recapitulates a metabolic phenotype observed in whole-body ERα knockout (ERαKO) mice, including obesity, hyperphagia, impaired glucose tolerance and reduced energy expenditure[21-23]. In addition, ERα-expressing neurons within the ARC have also been demonstrated to play key roles in regulating female metabolic homeostasis[27].

In menopausal women, declining E_2 concentrations and progressive testosterone predominance are generally associated with increased abdominal fat mass and increased risk for impaired glucose metabolism[61-63]. Metabolic functions of E_2 in women have been difficult to define, however, partly due to logistical and ethical constraints in

designing definitive experiments with rigorous control. OVX-mediated E_2 depletion had small effects on female rhesus macaque body weight in one study[64], and no effects on female body weight were observed in two studies of cynomolgus macaques[65,66]. While a putative selective estrogen receptor modifier (SERM) can promote weight loss in OVX rhesus monkeys[67], E_2 replacement therapy has no effect on body weight in OVX cynomolgus macaques[66,68]. E_2 and SERM activity, however, both reliably maintain skeletal bone mass in female macaques[69-71].

To address the different contributions of ovarian and extra-ovarian E_2 in a female NHP model and to elucidate the major neural receptor mechanism of E_2 signaling and its role in regulating female metabolic function, two studies were undertaken. First, an aromatase inhibitor, letrozole, was employed to diminish E_2 production in OVX female marmosets and thereby enable an investigation into whether extra-ovarian estradiol contributes to female weight gain in addition to ovarian E_2. We hypothesize that an extra-ovarian source of E_2, likely the hypothalamus, will be diminished by aromatase inhibition and subsequently will enhance weight gain and skeletal bone loss, compared with both E_2-replaced female marmosets and those experiencing the loss of ovarian E_2 alone. Second, to investigate the role for ERα-expressing neurons in the hypothalamic VMN and ARC in regulating female metabolic homeostasis in a female NHP, we used MRI-guided, neural infusions of an adeno-associated virus, AAV8, into the adult female marmoset hypothalamic VMN and ARC in order to deliver a small hairpin RNA (shRNA) either encoding a scrambled virus control, with no known gene targets in this species, or an shRNA specifically designed to associate with *ESR1* mRNA, alone, to prevent translation of ERα protein. We hypothesize that like female rodents[5,6], *ESR1* gene

silencing in both the VMN and ARC of female marmoset monkeys will disrupt metabolic homeostasis.

2.3 Methods

EXPERIMENT 1: Diminished E_2 production: ovarian (OVX) depletion of E_2 (VEH) versus extra-ovarian and ovarian (OVX + aromatase inhibitor, letrozole) depletion of E_2 (LET) versus Peri-Ovulatory E2 Replacement (OVX + E_2, E2)

Animals

Thirteen adult female common marmosets from the Wisconsin National Primate Research Center (WNPRC) colony were OVX and assigned to 1 of 3 treatment groups that were balanced by age and body weight at the onset of the study (Table 1), systemic mid-cycle, peri-ovulatory E_2 replaced (E2; n = 5), systemic E_2 depleted, OVX plus daily vehicle (VEH; n = 4), or extra-ovarian E_2 depletion, OVX plus daily letrozole administration (LET; n = 4). Systemic (mid-cycle, peri- ovulatory) E_2 replacement was achieved through subcutaneous E_2-filled capsules that maintained a systemic level of E_2 (Table 2) mimicking mid-cycle, peri-ovulatory circulating E_2 levels. The latter were sufficient to maintain negative feedback regulation of circulating pituitary gonadotropin levels within the ovary intact female range (Table 2)[19]. To maintain constant E_2 levels, capsules were replaced every 3 months throughout the study[72]. VEH females received a daily oral 200 µL of 1 mL/ kg Ensure© as vehicle control, while LET females were given daily oral 1 mg/kg of letrozole dissolved in 200 µL of vehicle, as previously determined[19], and females in both groups received empty capsules when E_2 females received E_2-filled capsules and replacements.

All females lived with a well-established male cage mate in 0.60 m × 0.91 m × 1.83 m enclosures and were maintained with 12-hour lighting (06:00 hours to 18:00 hours), ambient temperature of ~27°C and humidity of ~50%. The protocol for this study was approved by the Animal Care and Use Committee of the Office of the Vice Chancellor for Graduate Research and Education of the University of Wisconsin–Madison, an AAALAC-accredited program. Following baseline assessments, bilateral OVX was performed. Cloprostenol (Estrumate®, 0.75-1.50 µg intramuscular injection for 2 successive days approximately 11-60 days after ovulation), an analog of prostaglandin-F2-alpha, was administered prior to OVX to facilitate scheduling of OVX during the follicular phase[19]. Treatment onset (0 months) was the day of the OVX procedure.

Hormone Assays

Plasma samples and hypothalami were analyzed for several hormones. Hypothalami were dissected at necropsy and frozen at –80°C. They were subsequently thawed, transected along the midline, and separated into hemi-hypothalami. The right hemi-hypothalamus per monkey was divided into 50- to 75-mg aliquots. For steroid hormone analyses, plasma and hemi-hypothalami aliquots underwent extraction[13] and hemi-hypothalamic aliquots were recombined after extraction. Extracted samples were subsequently submitted for analysis on a QTRAP 5500 quadruple linear ion trap mass spectrometer (AB Sciex) equipped with an atmospheric pressure chemical ionization source (liquid chromatography tandem mass spectrometry [LC-MS/MS])[19].

Diet-induced Obesity from Consumption-driven Weekly Increments in Daily Calories

Animals were fed with Mazuri Callitrichid High Fiber Diet #5MI6 (Purina Mills International, St. Louis, MO), providing 53% carbohydrate, 20% protein, 6% fat, and 10% fiber by weight, with a metabolizable energy of 3.3 kcal/g (~61%, 23%, and 16% kcal from carbohydrate, protein, and fat, respectively)[73]. Following OVX at study onset, total daily calorie consumption by each male–female study pair was recorded. To achieve DIO, diet allotment for each male–female study pair was increased weekly by ~66 kcal per day (equivalent to 20 g diet wet weight/day) if the entire daily allotment had been consumed during at least 4 out the 7 previous days. Calorie increments and total calories consumed, however, remained comparable across the pairs between treatment groups (Figure 1).

Assessment of Daily Calorie Consumption While Maintaining DIO

At 6 to 7 months post-OVX, each female was singly housed within a marmoset housing room, but outside visual contact with her male pair mate, while still maintaining vocal and auditory contact. Each female's daily calorie allotment began at 50% of those provided when housed with their male pair mate. Dietary allotment was increased weekly by ~33 kcal per day (~10 g diet wet weight) only when the entire daily allotment was consumed during at least 4 out the 7 previous days. Calorie increments and total calories consumed, however, remained comparable across females between treatment groups (Figure 1). The total kilocalories consumed daily were recorded for each female for 8 weeks.

Body Composition and Bone Mass

Animals were weighed weekly. Area under the curve (AUC) assessment of weight parameters over time, calculated by the trapezoid rule, was employed to better detect

recurring differences in weight gain, as previously employed[74]. For the first study, at baseline and 5 to 6 months post-OVX and for the second study, at baseline and 3 and 6 months post-OVX, total body com- position, as well as bone mineral content (BMC) and bone mineral density (BMD), were assessed by dual-energy X-ray absorptiometry (DXA, iDXA, GE/Lunar Corp., Madison, WI) on sedated animals. Fat, fat-free mass (FFM) (excluding bone), BMC, and BMD were determined for total body as well as previously validated body regions of interest, including abdomen, chest, thighs, lower legs, and arms[75].

Locomotor Activity

At baseline and 5 to 6 months post-OVX, a small accelerometer (Actiwatch Mini, CamNtech Ltd, Cambridge UK) was added to each female's standard collar. Activity and in- tensity of movement were recorded over a ~2-4-week period after which the accelerometers were removed. For the most part, activity recorded represented whole-body movements, and not limb or head movements, alone, as previously validated in marmosets[76]. The accelerometer sampled such activity counts every 30 seconds and these data were averaged for every hour, day (during lights on), night (during lights off), morning (06:00-12:00 hours), afternoon (12:00-18:00 hours), and 24 hours. AUC activity values were also assessed to detect recurring differences in activity over time.

Fasting Glucose and Oral Glucose Tolerance Test

Fasting glucose and glucoregulation were assessed in over- night fasted, awake animals. Fasting glucose was determined at baseline and 6 months post-OVX, while glucoregulation was assessed by oral glucose tolerance test (OGTT) at 6 months following OVX. Following a baseline blood sample, animals were given an oral dose (5

mL/kg) of 40% sucrose. Blood samples were then collected at 15, 30, 60, and 120 minutes (2 hours) following sucrose administration and assessed for glucose, as previously validated for marmosets[77]. Glucose was measured by glucometer (Accu-Check Aviva, Roche Diagnostics, Indianapolis, IN). AUC glucose values during the OGTT were also assessed to detect between group differences in accumulating high levels of glucose over time.

Statistical Analysis

Data were analyzed utilizing SPSS software (IBM, Armonk, NY). Hormone measures were analyzed with a 1-way analysis of variance (ANOVA), followed by Bonferroni multiple comparison post hoc tests. All other between group analyses were performed using a 2-way ANOVA for repeated measures. Nonparametric Spearman's correlation tests were utilized to identify relationships between hormone values and metabolic parameters. Spearman's rho coefficients are expressed as r_s. Statistical significance was determined at $P \leq .05$.

EXPERIMENT 2: Diminished hypothalamic E_2 activity: silencing RNA specific for ESR1 (shRNA-ESR1) targeted on the hypothalamic VMN and ARC

Animals, Ovariectomy and E_2 Replacement

Nine adult female common marmosets (2-6 years of age) from the WNPRC colony, and already housed in well-established male-female pairs were evenly assigned into two groups based on age, body weight and body mass index (BMI) (Table 3): OVX + E2 replacement + scrambled virus shRNA (control; n=5) and OVX + E2 replacement + ERα gene silencing shRNA (ERαKD; n=4). Monkeys were maintained in these two groups for ~9 months in 0.60m x 0.91m x 1.83m enclosures under 12-h lighting,

ambient temperature of ~27°C and humidity of ~50%. The animal care and use program at the University of Wisconsin maintains a Public Health Services Assurance. The protocol for this study was approved by the Animal Care and Use Committee of the Office of the Vice Chancellor for Graduate Research and Education of the University of Wisconsin–Madison, an AAALAC-accredited program.

Following baseline assessments, bilateral OVX was performed in all females at least one month prior to neural surgery. Cloprostenol (Estrumate., 0.75-1.50 µg intramuscular injection for two successive days approximately 11-60 days after ovulation), an analog of prostaglandin-F2-alpha, was administered prior to OVX to facilitate scheduling of OVX during the follicular phase. Such cloprostenol administration is without subsequent effect on study outcomes[19,78]. All females received subcutaneous, E2-filled silastic capsules immediately following OVX. Silastic capsules were removed and replaced at 3-month intervals post-OVX to approximate mid-cycle, peri-ovulatory systemic E2 levels and to maintain negative feedback regulation of circulating pituitary gonadotropin levels within the range of ovary intact female marmosets[19,78] (Table 2).

Neural Infusion Surgery and ERα Knockdown

OVX adult female marmosets received bilateral stereotaxic injections into the hypothalamic VMN and ARC of adeno-associated virus 8 (AAV8) expressing shRNA targeting *ESR1* for *in vivo* RNAi, and thus diminishing *ESR1* translation into ERα (ERaKD, n=4), or a control scrambled shRNA (Control, n=5). Treatment onset (0 months) was the day of neural infusion surgery.

Since accurate, within-brain placement of viral vector was essential for gene silencing efficacy and specificity, we used a single, presurgical, neuro-anatomical MRI

scan to refine the unique locations of each VMN and ARC within each marmoset, refined and adapted from previous studies[79]. To accomplish this, each female marmoset was food deprived overnight, sedated with an intramuscular (IM) injection of ketamine (10 mg), anesthesia was continued with an IM injection of meloxicam (2 mg), 2 ml isotonic saline was injected subcutaneously (SC) to provide fluid administration and atropine (0.016 mg) was administered IM, followed by placement of the marmoset into an MRI-compatible stereotaxic frame. Lateral placements of both left and right earbars, as well as vertical placements of palate and left and right eye bars, were all noted. Three-dimensional coordinate locations of both left and right VMN and ARC were subsequently obtained from a T1 MRI anatomical scan adapted for marmosets[80] in a next-generation 3T MRI system MR750 (GE Healthcare, Waukesha, WI) and performed at least 3 days prior to viral vector infusion (Figure 2).

Each presurgical scan employed a 3-inch surface coil and comprised 3D T1-weighted (T1W) images with an inversion-recovery (IR) prepped, fast gradient-echo (IR-fGRE) sequence adapted for marmosets[80]. Scanning parameters included an inversion time (TI) of 450 ms, repetition time (TR) of 6.8 ms, echo time (TE) of 2.9 ms, and receiver bandwidth of 62.5 kHz. The matrix size was 256 × 256 × 128 (X × Y × Z). The 3D T1W scans produced 248 coronal 0.3-mm-thick contiguous slices. Using coronal slices incorporating the hypothalamus from each monkey's presurgical scan, we utilized contrast-agent filled earbars in the stereotaxic frame to provide a rostral-caudal (RC) zero plane (Z coordinates), the middle of the 3rd ventricle at the level of the mediobasal hypothalamus to generate a medial zero plane (X coordinates), and the farthest lateral point of each earbar to provide a dorso-ventral zero plane for right and left sides

separately (X coordinates). Based on these 3D parameter sets, target coordinates for entry into the skull, as well as for rostral, medial-rostral, medial-caudal and caudal left and right VMN, and analogous locations for both left and right ARC, were estimated based on marmoset neuroanatomy atlas coordinates[79].

For viral vector infusion surgery, each marmoset was sedated and prepped as described for their presurgical MRI scan. In addition, each monkey was intubated, and the anesthesia was continued under isoflurane (1-2%). Each marmoset was re-positioned into similar stereotaxic frame parameters as noted during their presurgical MRI scan. Vital signs (heart rate, blood oxygen, respiration, and temperature) were regularly monitored during the procedure and the animals were wrapped for warmth. A series of small-volume, subcutaneous (SC) injections of lidocaine (total, 1 mg) were given along the anticipated incision site to provide local anesthesia. A ~30mm incision was made on the top of the animal's head. Stereotaxic coordinates, estimated from our pre-surgery anatomical MRI scan, allowed calculation for the insertion sites of a 22-gauge guide cannula housing a 28-gauge stylet to target the VMN and ARC in the hypothalamus. The estimated midline location above the medial sites for both VMN and ARC was marked on the skull to enable excision of a ~10 mm diameter portion of skull using a surgical bone drill. A micromanipulator, with cannula holder and guide cannula with screw-in solid stylet, were placed on the stereotaxic frame to confirm midline of the brain from the medial location of the superior sagittal sinus, and presurgical scan estimated target coordinates for left VMN and ARC sites were revised accordingly. A 27g needle, customized into a miniature scalpel blade, was used to open a ~5mm incision in the dura mater vertically above the anticipated locations of the VMN and ARC

infusion sites on the left side of the marmoset brain, and avoiding the left lateral extent of the superior sagittal sinus.

At a trajectory angle of 0° (vertical), a 22-gauge guide cannula housing a sterile 28-gauge stylet was lowered into the medial-rostral estimated extent of the left ARC, as modified for marmosets[82,84]. The stylet was then replaced by a 28-gauge infusion cannula attached to a Hamilton syringe controlled by a programmable infusion pump, A solution of viral vector (~2 x 10^{10} packaged genomic particles of AAV8 in 3.0 µL of sterile saline) mixed with gadolinium-containing Multihance MRI contrast agent (2 mM gadobenate dimeglumine, Bracco Diagnostics Inc.), was infused at 0.2 µL per minute. The AAV8 virus utilized in this study was shown to readily infect neurons[83] and was without notable inflammation in NHP brain[84]. To minimize dorsal tracking of viral particles and contrast agent when the infusion cannula was raised, there was a 5-min delay following cessation of infusion before infusion cannula removal alone to permit its flushing of sufficient fluid while outside the brain to confirm infusion integrity of the system. The stylet was re-positioned inside the guide cannula. Both guide cannula and stylet were then gradually removed from the brain. Superficial skin sutures were placed using 4/0 vicryl suture to temporarily close the incision site during transfer to the MRI scanning room while the marmoset remained in the stereotaxic frame.

The contrast agent remaining at the medial-rostral ARC infusion site was used to confirm accuracy of the infusion site location from a mid-surgery, an ~23-min MRI T1 scan obtained approximately 10-20 min following the first infusion on the left side. When necessary, presurgical scan estimated target coordinates for left VMN and ARC sites were revised. Guide cannula, stylet and infusion cannula insertion, infusion and removal

procedures were then repeatedly performed to enable AAV8 infusion into rostral, medial-rostral, medial-caudal, and caudal VMN and ARC target sites on the left side of the brain.

Following all left side infusions, a 27g needle customized into a miniature scalpel blade, was used to open a ~5mm incision in the dura mater vertically above the anticipated locations of the VMN and ARC infusion sites on the right side of the marmoset brain, avoiding the right lateral extent of the superior sagittal sinus. A similar series of procedures, infusions and MRI scan were performed on the right side of the brain analogous to those performed on the left. When necessary, adjustments to presurgical estimates for rostral, medial-rostral, medial-caudal, and caudal right VMN and ARC target sites were made following the 2nd within-surgery MRI scan.

Immunohistochemical processing of marmoset brain for visualizing and quantifying green fluorescent protein (GFP) and ERα protein expression

Following upper body perfusion with 4% paraformaldehyde (PFA) (pH 7.6), the brain was removed, post-fixed at 4C for an additional 12-16h and cryoprotected in graded (10-30%) sucrose/PBS (pH 7.2) solutions. Before final storage at 4C in a sodium azide-30% sucrose-4% PFA solution, each post-fixed, brain was placed in a customized plastic mold designed to accommodate the dorsal surface of an adult marmoset brain and expose the ventral surfaces landmarks, enabling placement of mold-guided, microtome blades cutting the brain into coronal plane portions. The medial rostral-caudal portion (~2-3 mm), including the hypothalamus, was separated immediately rostral to the optic chiasm to immediately caudal to the mammillary bodies. This medial rostral-caudal portion of whole-brain was cryosectioned into consecutive 40µm frozen sections in the

coronal plane to include the rostral-caudal extent of the hypothalamus from the rostral extent of the mPOA to the caudal extent of the ARC.

Immunohistochemistry (IHC) procedures for GFP and ERα were performed and adapted for the marmoset monkey[85]. Cryo-sections of 40 µm, at regular intervals, were immunostained for ERα using the mouse monoclonal antibody, 6F11 (Thermo Fisher Scientific, Hampton, NH)[20]. DAB-staining was subsequently used to reveal specific primary antibody binding. Sections close by to those selected for ERα immunostaining were stained for GFP using the rabbit polyclonal antibody, AB3080 (MilliporeSigma, Burlington, NH)[86].

Confirmation of neural targeting accuracy from immunohistochemical analyses of GFP expression in the mediobasal hypothalamus

Digital images from coronal brain sections immunostained for GFP were obtained with a Nikon Microphot-FA microscope using a QImaging Retiga 200R CCD camera and Nikon NIS Elements software. Most images for analysis were obtained using a 4X objective. Each tissue section picture was the composite of several images stitched together by the Nikon system during the photo acquisition process. This resulted in a series of coronal images through the hypothalamus from the rostral POA at the level of the optic chiasm to the mammillary bodies in the caudal hypothalamus. As illustrated by a coronal section from approximately the mid-rostral-caudal extents of VMN and ARC within the hypothalamus (Figure 3), abundant GFP-immunoreactive (ir) labeling was demonstrated in VMN and ARC, and in portions of the immediately ventral PIT and immediately lateral optic tracts (Figure 3).

Analysis of Neural Targeting of ERα Gene Silencing

ERα-immunoreactive (ir) labeling in the POA, VMN and ARC, employing measures of cell counts, cell density per unit area (number of cells/mm^2), and labeling intensity (pixel intensity of individual cells). Labeled cells were detected using the NIS Elements AR Dark Spot Detection feature. The contrast threshold in the detection algorithm was determined for each case by adjusting cell counts derived from the spot detection algorithm to match cell counts made by three observers on identical images of tissue. Observer counts differed by < 15%, and NIS-derived cell counts fell within 5% of the average counts of all observers. The NIS Elements AR software calculated the mean pixel intensity of each identified cell, and we used this to derive the intensity of ER staining. The average pixel values of the observer-derived threshold cells determined the low (lighter) end of the intensity staining range. The high (darker end) of the range was determined by the average pixel intensities of the darkest 2% of labelled cells, typically in the POA or pituitary, which were not targeted by the infusion. The staining intensity of individual cells was normalized (from 0 to 1) within the light to dark intensity range.

The number of labeled ERα cells was quantified in terms of cell density per unit area. This was determined by counting the number of immunostained neurons within regions of interest (ROIs) of 1000μm X 500μm ellipses (areas of 0.395 mm^2) positioned within POA, VMN and ARC, in addition to ROIs within ventral VMN (VMNv) and dorsal ARC (ARCd) for all nine female marmosets. For each hypothalamic ROI within each female, we used the average of the three most intensely staining areas (comprising most 'dark' or most 'dark' and 'light' cells) as the density measure for that ROI. One exception, however, involved the rostral POA, the area with typically the most ERα expression, that

was lost during processing in one control female, The POA ROI density measures from this control female were thus obtained from a typically more demure, ERα immunostained portion of the POA. Since this POA ROI density value for ERα was not an outlier in the context of the remaining eight females, it was retained for quantitative analyses.

Technical note regarding effects of focus plane on cell quantification.

Cells appear most darkly labeled when the microscope objective is focused at the tissue depth that contains the cell. When the focal plane deviates from the depth of the cell, the cell blurs, and its staining darkness declines. To minimize this confound, images were collected when the microscope objective was focused on the middle depth of the tissue. While this will lead to underestimating the darkness of label of a cell located above or below the middle of the tissue and possibly prevent its detection, we found this effect to be small when using a 4X objective with its relatively large depth of field. To determine the effect of focus on estimates of staining intensity and cell count, we systematically varied focus across the depth of a tissue section and collected images through a large group of labeled cells. We applied the NIS analysis to the images and found that an image captured with a 4X objective focused in the center depth of the tissue provides a reliable estimate of the number of cells and their staining intensity. On average, mid-depth focus captured >95% of cells that were identified at all the focal positions. The additional cells were stained lightly, near detection threshold. To examine the effects on estimates of staining intensity, we tracked the mean pixel intensity of all identified cells across the depths of focus. The average difference between the estimate of staining darkness at mid-depth focus and the maximum darkness at any depth, normalized to the full range of staining intensities, was ~ 0.021 +/- 0.027 std.

Hormone Values

Plasma samples and hypothalami were analyzed for several hormones as described above in Experiment 1.

Diet-induced Obesity from Consumption-driven Weekly Increments in Daily Calories

Animals were fed with Mazuri Callitrichid High Fiber Diet #5MI6 (Purina Mills International, St. Louis, MO), providing 53% carbohydrate, 20% protein, 6% fat, and 10% fiber by weight, with a metabolizable energy of 3.3 kcal/g (~61%, 23%, and 16% kcal from carbohydrate, protein, and fat, respectively)[73]. Following OVX at study onset, total daily calorie consumption by each male–female study pair was recorded, and DIO was achieved as described above in Experiment 1.

Assessment of Daily Calorie Consumption While Maintaining DIO

At 6 to 7 months post-OVX, each female was singly housed within a marmoset housing room, but outside visual contact with her male pair mate, while still maintaining vocal and auditory contact. Each female's daily calorie allotment began at 50% of those provided when housed with their male pair mate. Dietary allotment was increased weekly by ~33 kcal per day (~10 g diet wet weight) only when the entire daily allotment was consumed during at least 4 out the 7 previous days. Calorie increments and total calories consumed, however, remained comparable across females between treatment groups. The total kilocalories consumed daily were recorded for each female for 8 weeks.

Body Composition and Bone Mass

Animals were weighed weekly. Area under the curve (AUC) assessment of weight parameters over time, calculated by the trapezoid rule, was employed to better detect

recurring differences in weight gain, as previously employed[74]. At baseline, 3 and 6 months post-OVX, total body composition, as well as bone mineral content (BMC) and bone mineral density (BMD), were assessed by dual-energy X-ray absorptiometry (DXA, iDXA, GE/Lunar Corp., Madison, WI) on sedated animals as described in Experiment One.

Locomotor Activity

At baseline, 3 and 6 months post-OVX, a small accelerometer (Actiwatch Mini, CamNtech Ltd, Cambridge UK) was added to each female's standard collar. Activity and intensity of movement were recorded over a ~2-4-week period after which the accelerometers were removed. Activity was measured and analyzed as described in Experiment One.

Fasting Glucose and Oral Glucose Tolerance Test

Fasting glucose and glucoregulation were assessed in over- night fasted, awake animals. Fasting glucose was determined at baseline and 6 months post-OVX, while glucoregulation was assessed by oral glucose tolerance test (OGTT) at 6 months following OVX. Following a baseline blood sample, animals were given an oral dose (5 mL/kg) of 40% sucrose. Blood samples were then collected at 15, 30, 60, and 120 minutes (2 hours) following sucrose administration and assessed for glucose, as previously validated for marmosets[77]. Glucose was measured by glucometer (Accu-Check Aviva, Roche Diagnostics, Indianapolis, IN). AUC glucose values during the OGTT were also assessed to detect between group differences in accumulating high levels of glucose over time.

Statistical Analysis

Data were analyzed utilizing SPSS software (IBM, Armonk, NY). Hormone measures were analyzed with a 1-way analysis of variance (ANOVA), followed by Bonferroni multiple comparison post hoc tests. All other between group analyses were performed using a 2-way ANOVA for repeated measures. Steroid and CG hormone data were log transformed, and behavioral data were transformed to arcsin, prior to ANOVA or correlation tests. Nonparametric Spearman's correlation tests were utilized to identify relationships between hormone values and metabolic parameters. Spearman's rho coefficients are expressed as r_s. Statistical significance was determined at $P \leq 0.05$.

2.4 Results

EXPERIMENT 1

Circulating E_2 and Pituitary GC Levels Confirm Anticipated Estrogen Status

As expected, E2 females alone exhibited circulating E_2 levels approximating those of mid-cycle, ovary intact female marmosets (Table 2). Greatly diminished circulating levels of E_2 were found in both VEH and LET females, with LET females demonstrating the more extreme E_2 depletion (Table 2). It was not surprising to find elevated circulating chorionic gonadotropin (CG) levels in VEH ($P < 0.08$, trend) and LET ($P < 0.05$) compared with E_2 females, reflecting insufficient circulating E_2 for maintenance of negative feedback regulation of pituitary CG release in estradiol-depleted female groups (Table 2). CG levels in LET females, however, were ~35% greater than in VEH females.

Circulating Steroid Hormones and Hypothalamic Steroid Content

Eliminating ovarian E_2 (VEH) or both ovarian and extra-ovarian E_2 (LET) produced notable changes in hypothalamic estrogen and androgen content, as well as in circulating steroid hormone levels, when compared with females in the E2 group. Hypothalamic E_2 content was diminished in LET females, alone, when compared with both E2 ($P = 0.005$) and VEH ($P = 0.013$) female groups (Table 4). Notably, comparable hypothalamic E_2 content was maintained between E_2 and VEH groups despite the large systemic deficit in circulating E_2 levels ($P = 0.001$) exhibited by VEH females that greatly increased the ratio of hypothalamic E_2 (pg/g wet weight): systemic circulation E_2 (pg/mL) from approximately 0.5 (E2 females) to 31.2 (VEH). Circulating levels of E_2, however, tended ($P = 0.08$) to be lower in LET than in VEH females (Table 2), maintaining a high ratio of hypothalamic E_2: systemic circulation E_2 of approximately 23.3 (LET).

Hypothalamic androgen content, in contrast to that for E_2, was generally increased in the absence of ovarian E_2 levels (VEH) and was not further augmented by additional depletion of extra-ovarian E_2 (LET) (Table 4). Hypothalamic androstenedione content was elevated in both VEH ($P = 0.03$) and LET ($P = 0.05$) compared with E_2 (Table 34 females, resulting in hypothalamic: systemic ratios for androstenedione of 0.2 (E_2), 1.3 (VEH), and 1.5 (LET). Hypothalamic dehydroepiandrosterone (DHEA) content, however, was only elevated in VEH ($P = 0.04$), but not LET, females when compared with those in the E_2 group, resulting in hypothalamic: systemic ratios for DHEA of 0.3 (E_2), 0.1 (VEH) and 0.05 (LET). Despite demonstrating a similar overall pattern, hypothalamic testosterone values remained comparable across all female groups (Table 4) with relative consistency of hypothalamic vs circulating testosterone ratios between female groups of 0.2 (E_2), 0.1 (VEH), and 0.2 (LET). Changes in circulating

androgen levels (Table 2), however, did not mirror those found in hypothalamic content (Table 4). Circulating levels of DHEA, alone, increased in VEH ($P < .001$) and LET (Table 2; $P = .001$) groups compared with those in E2 females. Circulating levels of androstenedione and testosterone (Table 2) remained comparable across all female groups.

While circulating levels of progestins, progesterone, and 17OHP4, and their ratios, remained comparable across female groups (Table 2), hypothalamic content of 17OHP4 more than doubled in VEH compared with E_2 and LET female groups (Table 4), thus increasing the hypothalamic to circulating 17OHP4 ratio to 10.9 (VEH) in comparison with 2.6 (E2) and 6.4 (LET). Hypothalamic progesterone content, and its hypothalamic to circulating ratio, demonstrated more modest increases following estrogen depletion (E_2, 1.0; VEH, 2.7; LET 2.8).

With regard to ratios of hypothalamic steroid hormones, selected to quantify aspects of androgen biosynthesis (Table 4), the ratio of androstenedione: DHEA was higher in both VEH ($P = 0.05$) and LET ($P = 0.005$) than in E_2 females. There were no effects of eliminating ovarian E_2 (VEH) or both ovarian and extra-ovarian E_2 (LET) on the ratios of hypothalamic testosterone: androstenedione or 17OHP4: progesterone (Table 4), respectively. The ratio of hypothalamic E_2: testosterone, in contrast, was decreased ($P = 0.002$) in both VEH and LET compared with E2, as well as in LET compared with VEH females ($P = 0.05$).

Calorie Consumption, Body Weight, and Body Composition

Only male–female pairs from the LET female group consumed more calories ($P = 0.02$) per day than male–female pairs from the E_2 female group during weekly

increments of daily calories from months 1 to 5 following OVX (Figure 1). When females were separated from their male pair mates at 6 to 7 months following OVX for individual behavioral and calorie intake assessments, total daily calories provided to all 3 female groups were comparable, with female consuming ~80% of calories provided (Figure 1). Females from both E_2 depleted, VEH ($P < 0.001$) and LET ($P < 0.001$) groups, however, consumed more calories, corrected for FFM, than E_2 group females (Figure 1).

While female body weight increased ~5% to 10% during the DIO study regimen irrespective of treatment group ($P < 0.016$) (Figure 7) the AUC % body weight increases from baseline, with or without correction for FFM (Figure 7) was greater ($P = 0.02$) in both E_2-depleted VEH and LET females compared with those in the E_2 group. At both baseline and 6 months following OVX, all female marmosets were obese (>14% body fat), with mean fat-to-lean mass ratios in each treatment group exceeding 0.3 (Table 5). While there were no obvious differences in DXA-determined fat mass 6 months following OVX in any female group for total body or previously validated body regions of interest, including abdomen and hips/thighs, in contrast, total body ($P = 0.014$), abdominal ($P = 0.002$), and upper leg ($P = 0.025$) FFM increased ~5% to 10% during the DIO study regimen irrespective of treatment group (Table 5). Increased abdominal FFM, however, was greater ($P = 0.041$) in VEH than in both E_2 and LET female groups. FFM increases in all female groups combined were not correlated with either circulating or hypothalamic steroid hormone levels or ratios, including those for E_2.

Higher hypothalamic, but not circulating, androstenedione values and the androstenedione to DHEA ratio predicted greater AUC % body weight gain, with (androstenedione: $r^2 = 0.55$, $P = 0.006$; androstenedione to DHEA ratio: $r^2 = 0.44$, $P =$

0.019) or without (androstenedione: $r^2 = 0.53$, P = .0007; androstenedione to DHEA ratio: $r^2 = 0.41$, P = 0.025) correction for FFM, when all female groups were combined. In contrast, circulating but not hypothalamic, androstenedione to DHEA ratio predicted ($r^2 = 0.45$, P = 0.011) greater AUC calories consumed corrected for FFM. No correlations were found between measures of body weight or calories consumed and the remaining hypothalamic or circulating steroid hormone values or ratios, including those for estradiol.

Both total body BMC and BMD, and the same bone parameters in previously validated body regions of interest, were comparable across all 3 female groups. No bone parameter was diminished by depletion of either ovarian E_2 or ovarian and extra-ovarian E_2.

Locomotor Activity

Activity collar assessments of female locomotion were obtained at both baseline (while pair housed with their male cage mate) and 6 months following OVX (when singly housed) in E_2 depleted groups, alone. AUC locomotor activity was greater during the daytime in VEH than in LET females at both baseline (P = 0.001) and 6 months following OVX (P = 0.01) (Figure 8A, 8B). In contrast, during the resting hours of nighttime, there were no differences in locomotor activity between female groups. When comparing the AUC % change in locomotory activity, however, from baseline to 6 months following OVX, LET females became slightly more active than VEH during both daytime (P = 0.057) and nighttime (P = 0.01) (Figure 8C). Increased activity in LET females was notable late in the day and throughout much of the night.

Fasting Glucose

By 6 months following OVX, in all female groups combined, DIO induced a trend (P = 0.055) toward increased fasting glucose levels from baseline (Table 6) irrespective of circulating E_2 levels. OGTT 2-hour glucose, similar to fasting glucose, revealed no between group differences. Glycogenic hepatopathy was observed in 20% (1/5) of E_2 females, 50% (2/4) of VEH females, and 75% (3/4) of LET females during post-necropsy histopathological hepatic assessment.

EXPERIMENT 2

Targeted gene knockdown of ERα within VMN and ARC regions of interest (ROIs) of the mediobasal hypothalamus in ERαKD female marmosets

Quantitative assessment of ERα immunopositive cells within the mediobasal hypothalamus of OVX adult female marmosets demonstrated clear bilateral knockdown of ERα protein expression within the targeted VMN and ARC, but not POA or pituitary, in ERαKD compared to control female marmosets. Intra-hypothalamic infusion of AAV8 comprising shRNA specific for *ESR1* into ERαKD female marmosets resulted in fewer numbers of cells expressing ERα within ROIs incorporating the VMN, or portions of it, in comparison to control females (p=0.013-0.046; Figure 9). In contrast, ROIs incorporating POA, ARC or portions of ARC, exhibited comparable numbers of ERα immunopositive cells in ERαKD compared to control females (p=0.069-0.561, Figure 9). Intensity of immunopositive ERα cells, however, was diminished in ERαKD compared to control females within the entire ARC (p=0.049), as well as within its dorsal extent alone (p=0.021). Intensity of the immunohistochemical stain for ERα expression, nevertheless, remained comparable between the two female groups when POA and VMN ROIs were examined (Figure 9).

Not surprisingly, therefore, the product of ERα immunopositive cell density x ERα immunopositive intensity (D x I) was diminished in ERαKD compared to control females within the VMN and dorsal extent of the ARC (p=0.013-0.041; Figure 9), but not within the POA. The combined ROI for VMN and ARC exhibited fewer ERα expressing cells (p=0.020) and diminished immunopositive cell density x intensity for ERα expression in ERαKD compared to control females.

Positive correlations between ERα immunopositive cell numbers and intensity were identified in ERαKD, but not control females. Numbers of ERα immunopositive cells in ERαKD females positively correlated between VMN and ARC ROIs, alone, whereas intensity of ERα immunopositive expression values yielded positive correlates between VMN and ARC ROIs, as well as between POA and ARC ROIs. There were no between ROI correlations for ERα immunopositive cell density x intensity values. The finding of multiple positive correlations between ERα immunopositive values in VMN and ARC of ERαKD females, alone, highly suggests predictable degrees of ERα knockdown will be quantified in ARC from quantitation of ERα immunopositive cells in the VMN, alone. Thus, following intra-hypothalamic infusion of AAV8 comprising shRNA specific for *ESR1*, neuroanatomical locations for assignment of any change in female marmoset functionality are limited to the combined VMN-ARC and not to either VMN or ARC, separately.

Individual marmoset variation in the rostral-caudal extent from POA to ARC of ERα immunopositive cells within the mediobasal hypothalamus is illustrated by representative examples from a control (cj1) and an ERαKD (cj2) female, (Figures 5), respectively. In considering the control female, ERα immunopositive cells cluster peri-ventricularly within

the rostral POA, assuming a more dorsal and lateral position in the caudal POA. Distribution of VMN ERα immunopositive neurons in the VMN, are more dorsal to those in the ARC, and extend less caudally than those in ARC. Compared to the control female, the mediobasal hypothalamus of the ERαKD female exhibits fewer ERα immunopositive cells, almost all of which comprise 'light' immunostaining. In all female marmosets in which the pituitary remained intact during processing (ERαKD, n=3; C, n=1), the anterior pituitary exhibited a high proportion of 'dark', ERα immunopositive cells and no obvious between female group differences (Figures 5). All control females exhibited a similar pattern of ERα immunopositive cells, with highest immunopositive cell density and intensity in the POA and lowest in VMN.

Subtle changes in calorie consumption, but not in body weight and body composition, following ERα knockdown in the mediobasal hypothalamus

Male-female pairs from the ERαKD female group consumed fewer calories (p=0.02) than control male-female pairs during weekly increments of daily calories from months 1-7 following OVX (Figure 6A). When females were separated from their male pair mates after seven months following OVX for individual behavioral and calorie intake assessments, total daily calories provided to both female groups were comparable, with singly housed females from both groups consuming ~80% of calories provided (Figure 6B). ERαKD (p=0.001) females, however, consumed fewer calories (AUC kcal corrected for fat-free mass, 1004 ± 12.50 kcal/g fat free mass*56days) in comparison to control females (1161 ± 5.83 kcal/g fat free mass* 56days).

In contrast, female body weight, as well as AUC % body weight increased from baseline and AUC % body weight increase from baseline corrected for fat free mass all

demonstrated comparable increments during the study irrespective of female group (Figure 10). There were no obvious changes in DXA-determined body composition between baseline and 3- or 6-months following ERα knockdown, including fat and fat-free mass for total body or previously validated body regions of interest, including abdomen and hips/thighs. There were also no between female group differences in fat mass and fat-free mass percent change between any of the DXA timepoints (Figure 11).

Diminished locomotor activity following ERα knockdown in the mediobasal hypothalamus

Activity collar assessments of female locomotion were obtained at both 3 and 6 months post-AAV8 intra-hypothalamic infusion (while pair housed with their male cagemate). AUC locomotor activity was less during the daytime in ERαKD compared to control females at both 3 (p=0.001) and 6 months following ERα knockdown (p=0.01) (Figure 12). In contrast, during the resting hours of nighttime, there were no differences in locomotor activity between female groups. When comparing the AUC % change in locomotory activity, however, from 3 to 6 months following ERα knockdown, ERαKD females became slightly less active than controls during both daytime (p=0.057) and nighttime (p=0.01) (Figure 12). Decreased activity in ERαKD females was notable late in the day and throughout much of the night.

Fasting glucose

Fasting glucose levels remained comparable across female groups at baseline and at 6 months following ERα knockdown, as was 2h-glucose derived from an oral glucose tolerance test (OGTT) performed at 6 months following ERα knockdown (Figure

13). AUC glucose derived from the 6-month OGTT, however, revealed hyperglycemia in ERαKD females, alone (Figure 13).

2.5 Discussion

In Experiment 1, ovarian and extra-ovarian E_2 depletion of adult female marmoset monkeys, in contrast to depletion of ovarian E_2, alone, demonstrated little functional contribution provided by extra-ovarian E_2 in support of female metabolic homeostasis. Ovarian E_2 depletion, in addition to ovarian and extra-ovarian E_2 depletion, nevertheless, enhanced DIO calorie consumption and weight gain in comparison to E_2 replete females, illustrating the contribution of E_2 toward protecting female marmoset monkeys from DIO-associated metabolic dysfunction. DIO, in contrast and regardless of E_2 depletion, induced modest glucose intolerance, possibly due to impaired hepatic glucose metabolism related to glycogenic hepatopathy observed in all 3 female groups. Prior to Experiment 2, hypothalamic neuronal receptor mechanisms governing E_2 regulation of female NHP metabolic function were previously unknown. The results of Experiment 2, however, provide little evidence that ERα is a key hypothalamic receptor mechanism for E_2 regulation of female metabolic homeostasis in NHPs, and likely women. Experiment 2 was modeled after published gene silencing approaches examining ERα's role in discrete nuclei of the hypothalamus in female rats[6]. Compared with approaches employed with female rats, we employed MRI-guidance in order to refine individual targeting of the VMN and ARC, as NHPs have notable individual variations in neuroanatomical locations[80,85]. Based on IHC analysis of ERα expression in marmoset hypothalamic mPOA, VMN and ARC, ERα expression was significantly diminished in the VMN of females receiving ERα silencing shRNA. ERα expression in the ARC also appears diminished, but less so in the

mPOA. ARC and mPOA deficits in ERα expression, however, were less consistent than in the VMN. The results Experiments 2 and 2 taken together confirm hypothalamic ERα as a contributor to female marmoset metabolism and that systemic aromatase inhibition does not exaggerate the metabolic dysfunction of ovarian E_2 depletion, alone.

Endogenous estrogenic source(s) beyond the ovaries include a variety of organ systems as well as the brain[7,8,11,12,17,88]. This is of considerable importance to clinical management of women's health. For example, the oral, nonsteroidal aromatase inhibitor letrozole, employed in the current NHP study, is widely used in clinical practice, including minimizing recurrence of estrogen receptor positive breast cancer following surgical intervention[89,90].and enabling menopausal hormone therapy[91,92]. In addition, as found in this NHP study, aromatase inhibition treatment of women with breast cancer enables weight gain (including increased adiposity), perturbing female metabolic homeostasis[93,94]. In the present NHP study, however, DIO rather than aromatase inhibition, increased glucose intolerance. Women with naturally occurring gene variants in CYP19A1, while exceedingly rare, present with varying degrees of systemic estrogen depletion accompanied by overweight or obesity, impaired glucoregulation, borderline hyperlipidemia, and osteopenia/osteoporosis[95]. Unlike the present study, however, genetically determined CYP19A1 deficiency manifests E_2 depletion through all developmental stages, resulting in widespread organ system abnormalities that are absent from our adult-onset E_2 depletion.

As might be expected, systemically administered E_2 alleviates metabolic[96] dysfunction in women, but to varying degrees[97], while also increasing the risk for harmful side-effects, including cardiovascular disease and cancer[89,97]. SERMs,

nonsteroidal compounds that interact with estrogen receptors, and display distinct differences in degree of agonism vs antagonism action at estrogen receptors in target tissues, show efficacy for osteoporosis and breast cancer[98]. SERMs, however, all carry safety risks, most notably venous thromboembolic events. Treatments that avoid systemic estrogenic activity by delivering bioactive E_2 to the brain, alone, thus have tremendous potential to alleviate female metabolic dysfunction, as indicated by the findings from our current female NHP study. In this regard a synthetically derived, inactive precursor of E_2, when administered orally to female rodents, is only metabolized to a bioactive estrogen, in this case E_2, within the central nervous system following transport across the blood–brain barrier[99], providing amelioration to hypothalamically driven hot flashes without estrogenic effect on systemic estrogen-responsive organs and tissues, such as the uterus.

E_2, Body Fat, and Glucoregulation

Attempts have been made in a variety of studies to dissociate effects of normal aging vs declining E_2 levels on adiposity, energy balance, and cardiometabolic health in postmenopausal women[100-105]. In general, these studies support the idea that menopause per se is associated with increasing abdominal obesity and that visceral fat accumulation may, in part, be secondary to an acceleration of aging-related decline in fat oxidation and metabolic energy expenditure[62]. While these changes parallel those observed in OVX rodents[106], a causal relationship between declining ovarian E_2 in menopause and altered body composition and energy balance has been difficult to confirm[107,108]. Some randomized controlled studies have demonstrated that both oral and transdermal E_2 therapy in postmenopausal women are associated with a reduction

in central adiposity and an increase in lean body mass[109,110], as well as reductions in insulin resistance and fasting glucose, new-onset type 2 diabetes, blood lipids, blood pressure, adhesion molecules, and procoagulant factors[111]. Of the few studies focusing on energy expenditure during menopausal hormone replacement therapy comprising a variety of estrogenic formulations, some demonstrate increases in lipid oxidation and energy expenditure[112,113], while others reveal acute decreases in lipid oxidation and energy expenditure[114]. There are similarly conflicting data on the effects of hormone replacement therapy on insulin sensitivity, with some suggesting beneficial effects[111], while others find no consistent improvement[115-117].

In the first female marmoset monkey study completed here, mean baseline body weights in each female group (~400 g) were typical for this colony[73,118,119], while baseline total body fat exceeded 14% of body mass in all females. Body fat in excess of 14% body mass is considered obese for this laboratory NHP[120], but is typical for this colony[75]. By 9 months following OVX, however, ovarian as well as ovarian and extra-ovarian E_2 depletion resulted in DIO relative weight gain, with and without correction for FFM, as well as increased calorie consumption, in excess of the gains made by E_2-replete females. E_2, therefore, diminishes increased calorie consumption and weight gain in female marmosets in the context of DIO, as has previously been reported in mice[20,21,121]. There were, nevertheless, no changes in DXA- determined total, or depot-specific, body fat associated with either E_2 depletion. Such relatively modest fat accumulation in female marmosets may thus occur across a variety of specific depots.

Increased DXA-determined FFM, particularly in the abdomen and upper legs, unexpectedly contributed to combined E_2 depletion and DIO-induced weight gain in

female marmosets. While neither treatment has previously been associated with gain in FFM, E_2 depletion in female marmosets also induced hyperandrogenism. Induction of hyperandrogenism in female NHPs[122] and female-to-male transition[123] is associated with increased FFM, particularly in upper legs[123], and with androgen-receptor activity in NHPs[122], but in the present study no correlations between circulating or hypothalamic androgen concentrations or androgenic hormone ratios were associated with increases in FFM.

The actions of E_2 via ERα on adiposity may occur directly in white adipose tissue, liver, muscle, and/or pancreas[34,38], as well as in hypothalamic neurons expressing ERα[59,56]. The latter exert descending control over systemic organ systems via autonomic innervation[124-126], including E_2-induced alterations in food intake and energy expenditure, producing secondary metabolic states, or by a combination of these. Stimulatory effects of E_2 on energy expenditure are transduced in ERα expressing neurons of the VMN of the hypothalamus[56] by nonclassical ERα signaling[59] coupled to activation of PI3-kinase[9]. E_2 also regulates gene expression associated with regulation of food intake and energy expenditure in the hypothalamus, largely through ERα activation[21]. Furthermore, a study by Musatov et al[56] demonstrated that viral vector–mediated ERα gene silencing in the VMN of both female mice and rats largely recapitulates a metabolic phenotype observed in whole-body ERαKO mice, including obesity, hyperphagia, impaired glucose tolerance, and reduced energy expenditure[22-24]. In the current female NHP study, however, and in contrast to female rodents, we found no evidence of impaired glucoregulation at 6 months following E_2 depletion. We nevertheless identified a trend toward DIO-associated glucose intolerance in all female

groups combined, likely the result of insufficient increase in compensatory pancreatic beta cell insulin release to accommodate DIO-induced systemic insulin resistance. Such DIO-associated impairments of glucoregulatory function in the present study are reminiscent of glucoregulatory dysfunction reported in a previous female marmoset study employing a glucose-enriched DIO[127]. Therefore, while E_2 ameliorated DIO increased energy intake and relative weight gain, E_2 may have failed to ameliorate pancreatic beta cell insulin decompensation due to weight gain–mediated systemic insulin resistance[127]. It is unclear whether the 50% to 75% incidence of glycogenic hepatopathy (excessive accumulation of glycogen in hepatocytes) found in E_2-depleted female marmosets in the present study represents an increase above a previously reported incidence of 34% in laboratory housed female marmosets[128]. Glycogenic hepatopathy can indicate chronic recurrence of hyperglycemic episodes[129].

Since E_2 depletion enables maturation of the female marmoset's androgenic zona reticularis in the adrenal cortex[130], and aromatase inhibition commonly results in androgenic precursor excess[19,131], the positive correlations between hypothalamic androstenedione and androstenedione to DHEA ratio with weight gain may simply represent biomarkers for the degree and duration of E_2 depletion rather than androgenic effects per se. Long-term testosterone treatment, however, increases body weight in ovary intact pre-pubertal[29] and adolescent–young adult[30] as well as ovariectomized adult[122] female rhesus macaques, without glucoregulatory impairment. Furthermore, addition of DIO to testosterone treatment of adolescent female rhesus macaques exaggerates weight gain and induces glucoregulatory impairments accompanying insulin resistance[30]. The absence of glucoregulatory impairments in our E_2-depleted and

hyperandrogenic OVX female marmosets would be consistent with the requirement for E_2 activity, likely in the liver, to complete androgen-mediated glucoregulatory dysfunction, as found in organ-selective androgen receptor knockout female mouse models[31].

Skeletal Bone Mass Maintained Independently of E_2 in Female Marmosets

In almost all female mammals with regular, frequent ovarian cycles, a reduction in circulating estrogen concentrations, either spontaneous or experimentally induced, leads to a reduction in bone mass. This has been demonstrated in numerous primate species and occurs in as little as 3 months in rhesus macaques[32,60,134-136]. Therefore, it is surprising that we found no deficit in bone mass or bone density of either the total body or lumbar spine associated with systemic or systemic and hypothalamic E_2 deficiency, though, importantly, estrogen and aromatase activity within the bone microenvironment[4] were not assessed. There are several potential reasons for this finding.

Evidence for estrogen control of bone mass in common marmosets is controversial. In several experiments, we were unable to find any evidence of bone loss following estrogen depletion due to either social subordination or OVX in marmosets[118]. Similar to the conclusions of Kraynak and colleagues[75] that primates evolved metabolic control systems regulated by extra-ovarian E_2 or that are generally less subject to E_2 regulation, a conclusion arising from this study was that brain-derived estrogen may be enough to maintain bone mass even in the context of circulating E_2 deficiency. There have been some limited reports of bone degeneration in marmosets. For example, Seidlová-Wuttke and colleagues[137] found some evidence of bone loss in

orchidectomized male marmosets though the level of bone loss only reached WHO criteria for osteoporosis in 2 older animals (10 and 11 years of age). It is challenging, however, to separate potential hormonal causes from overall gastrointestinal health issues, nutritional deficits, and vitamin D malabsorption[138,139]. While marmosets may represent an intriguing model of estrogen deficiency bone loss, some caution must be taken particularly given their high circulating vitamin D levels and associated end organ resistance related to the overexpression of vitamin D response element binding proteins[140,141]. In addition, such end organ resistance may be evidence of a broader resistance to select actions of steroid hormones. Bone in marmosets may therefore have evolved to be less subject to estrogen regulation.

Applications to Understanding Metabolic Dysfunction in Women

Our experiments are the first to investigate the metabolic consequence of knocking down hypothalamic ERα expression in a nonhuman primate model and subsequently, investigate the main source of E_2 synthesis in regulating female metabolism via ERα. Our investigations provided evidence that in adult female marmoset monkeys, mediobasal hypothalamic ERα is an important receptor in maintaining female energy balance and extra-ovarian E_2 is not crucial to maintain ERα metabolic signaling cascades. It is important to note that marmoset monkeys are not the most similar NHP research model to humans, in contrast to say the rhesus monkey, a more physiological, neuroendocrinological, and genetically similar NHP to humans. To further determine how ERα dictates energy balance via ovarian and extra-ovarian sources of E_2, it would be of great benefit to perform hypothalamic ERα knockdown and use aromatase inhibition in adult female rhesus monkeys to elucidate possible neuro-E_2 mechanisms

likely relevant in human metabolic function. Identifying the predominate estrogen receptor and tissue from which E_2, is synthesized, potentially, the brain, and their roles in regulating female metabolism is critical understanding to create therapeutic targets that discretely act on a site while reducing peripheral side effects.

2.6 Tables & Figures

Parameter	E2 (n = 5)	VEH (n = 4)	LET (n = 4)	*P* value
Age at baseline (years)	3.1 ± 0.5	3.2 ± 0.3	2.9 ± 0.1	.854
Body weight at baseline (g)	402 ± 26	396 ± 35	382 ± 12	.863

Table 1: Age, body weight and uterine characteristics (mean ± SEM) of E2, VEH, and LET ovariectomized adult female marmoset monkeys.

Circulating hormone	E2 (n = 5)	VEH (n = 4)	LET (n = 4)	*P* value
Estradiol (pg/mL)	1174.8 ± 214.0	24.7 ± 11.9[a]	3.0 ± 0.1[a,b]	.001
Estrone (pg/mL)	ND	ND	ND	ND
Progesterone (ng/mL)	1.32 ± 0.40	0.94 ± 0.33	0.47 ± 0.30	.118
17-OHP_4 (ng/mL)	3.37 ± 1.89	2.19 ± 0.36	2.00 ± 0.36	.743
DHEA (ng/mL)	0.15 ± 0.02	1.93 ± 0.76 [a]	1.80 ± 0.79[a]	.001
Androstenedione (ng/mL)	3.22 ± 0.37	7.16 ± 3.49	3.23 ± 2.13	.468
Testosterone (ng/mL)	0.18 ± 0.03	1.11 ± 0.62	0.42 ± 0.24	.518
CG (ng/mL)	2.70 ± 0.40	6.31 ± 2.22[c]	8.50 ± 1.52[d]	.014
Hormone ratio				
Estradiol:Testosterone	8.3 ± 1.9	0.3 ± 0.3[a]	0.02 ± 0.01[a]	.001
17OHP_4:Progesterone	3.3 ± 1.8	2.8 ± 1.5	6.0 ± 2.1	.482
Androstenedione:DHEA	24.2 ± 4.6	4.1 ± 2.4 [a]	5.2 ± 2.0 [d]	.004
Testosterone:Androstenedione	0.06 ± 0.01	3.87 ± 2.15	3.32 ± 2.19	.225

Table 2: Circulating levels (mean± SEM) of sex steroid and gonadotropic hormones in ovariectomized female marmosets receiving E_2 replacement (E2), empty capsules (VEH) or the aromatase inhibitor, letrozole (LET) at 6 months following OVX at 09:00 hours, immediately prior to necropsy.

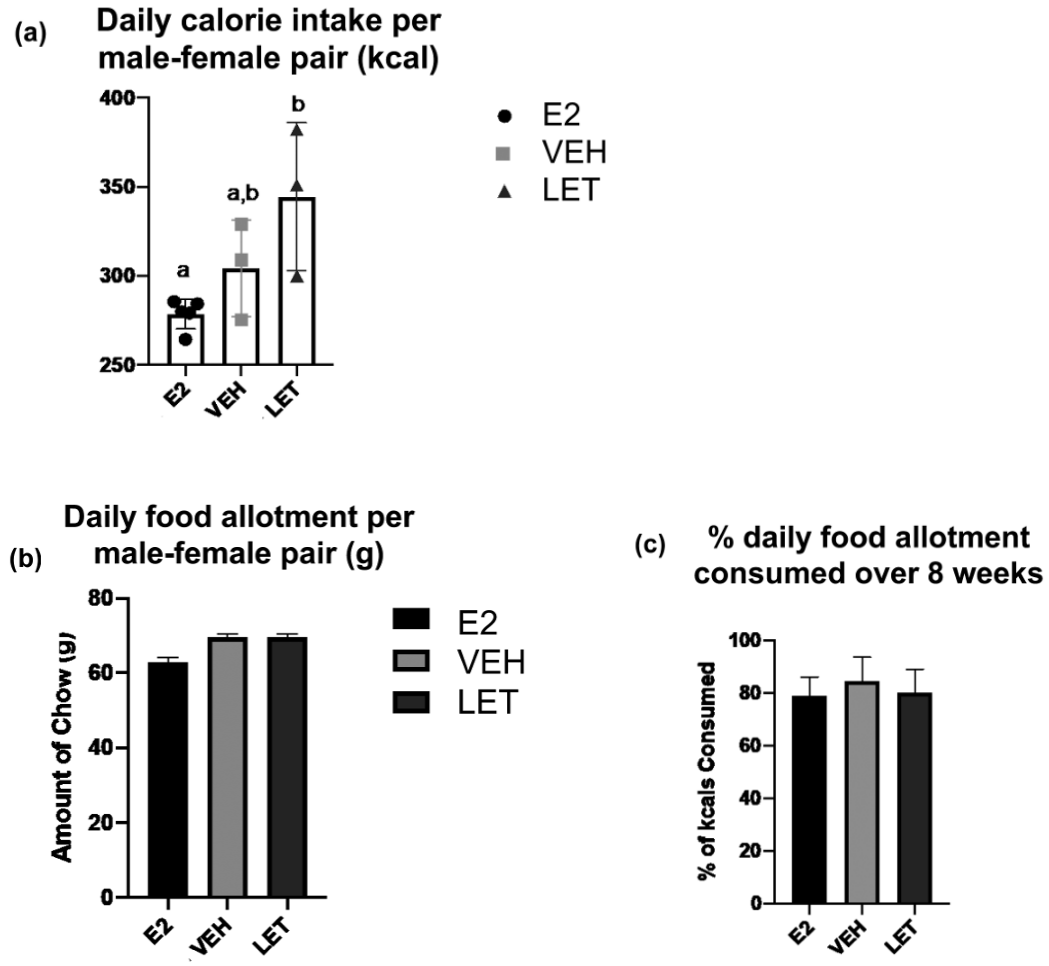

Figure 1. (A) Calories consumed (mean ± SEM) by both males and females combined in the male–female pairs (symbols illustrate individual male–female pair consumption) comprising the treatment groups E2 (black circles), VEH (light gray squares), and LET (dark gray triangles) from ovariectomy (OVX) until 5 months (months) after OVX, (B) amount of chow (mean ± SEM wet weight) provided to singly housed females during months 6 to 7 following OVX (E2 black bar, VEH light gray bar, LET dark gray bar), and (C) % calories consumed (mean ± SEM) by singly housed females during months 6 to 7 following OVX (E2 black bar, VEH light gray bar, LET dark gray bar).

	Age (years)	Body Weight (g)
Scrambled Controls	3.44 ± 0.55	440.5 ± 24.3
ERα Gene Silenced	3.32 ± 0.31	412.4 ± 32.9

Table 3: Comparable ages and body weights among all female marmoset groups (Scrambled controls, n=4; ERαKD, n=4) at study baseline.

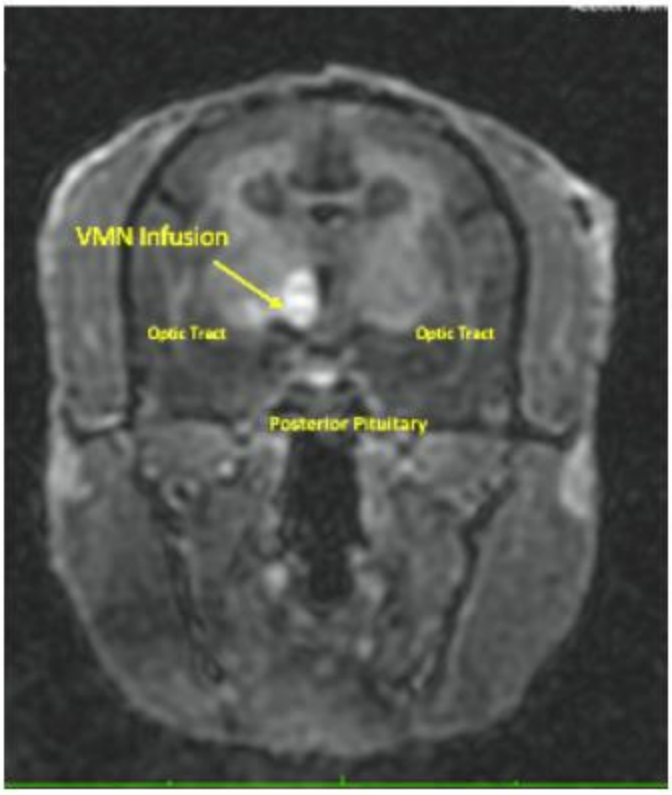

Figure 2: Use of MRI and Multihance, a contrast agent, allows successful targeting of the neural infusion of the viral vector encapsulated shRNA to the VMN and ARC of the hypothalamus. MRI images are taken prior to surgery to generate approximate targeting coordinates and following infusions (shown here) to confirm accurate targeting of the VMN.

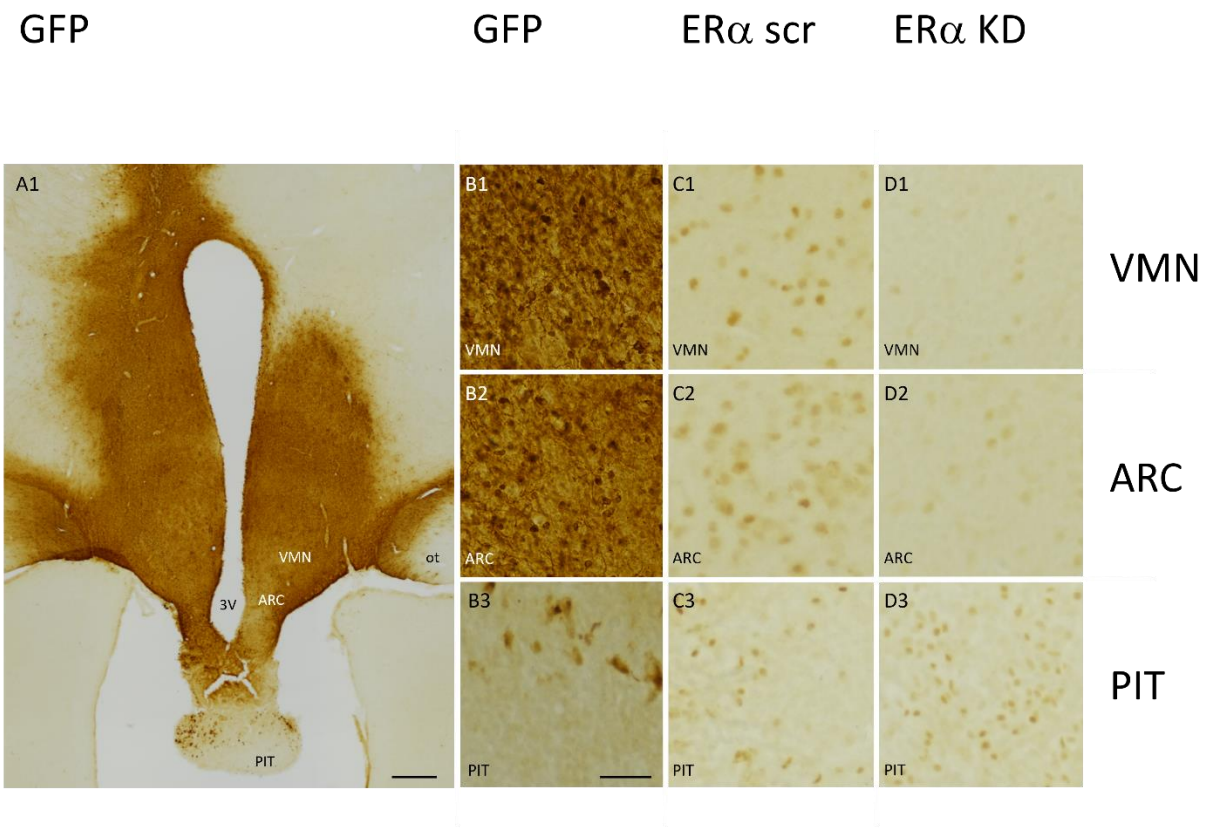

Figure 3: ERα gene silencing shRNA effectively ablates ERα in the VMN and ARC of female marmoset monkeys. 40x image of GFP in left most panel (A); panel (B) demonstrates expression of GFP (a/b: MAB3580) in an animal receiving the ERα gene silencing viral vector in the VMN, ARC and PIT, demonstrating infection of cells throughout the VMN and ARC, while the panel (C) illustrates 6F11 staining in a scrambled control animal and panel (D) illustrates an absence of ERα immunoreactivity in the VMN and ARC, with robust staining in the pituitary gland (D3).

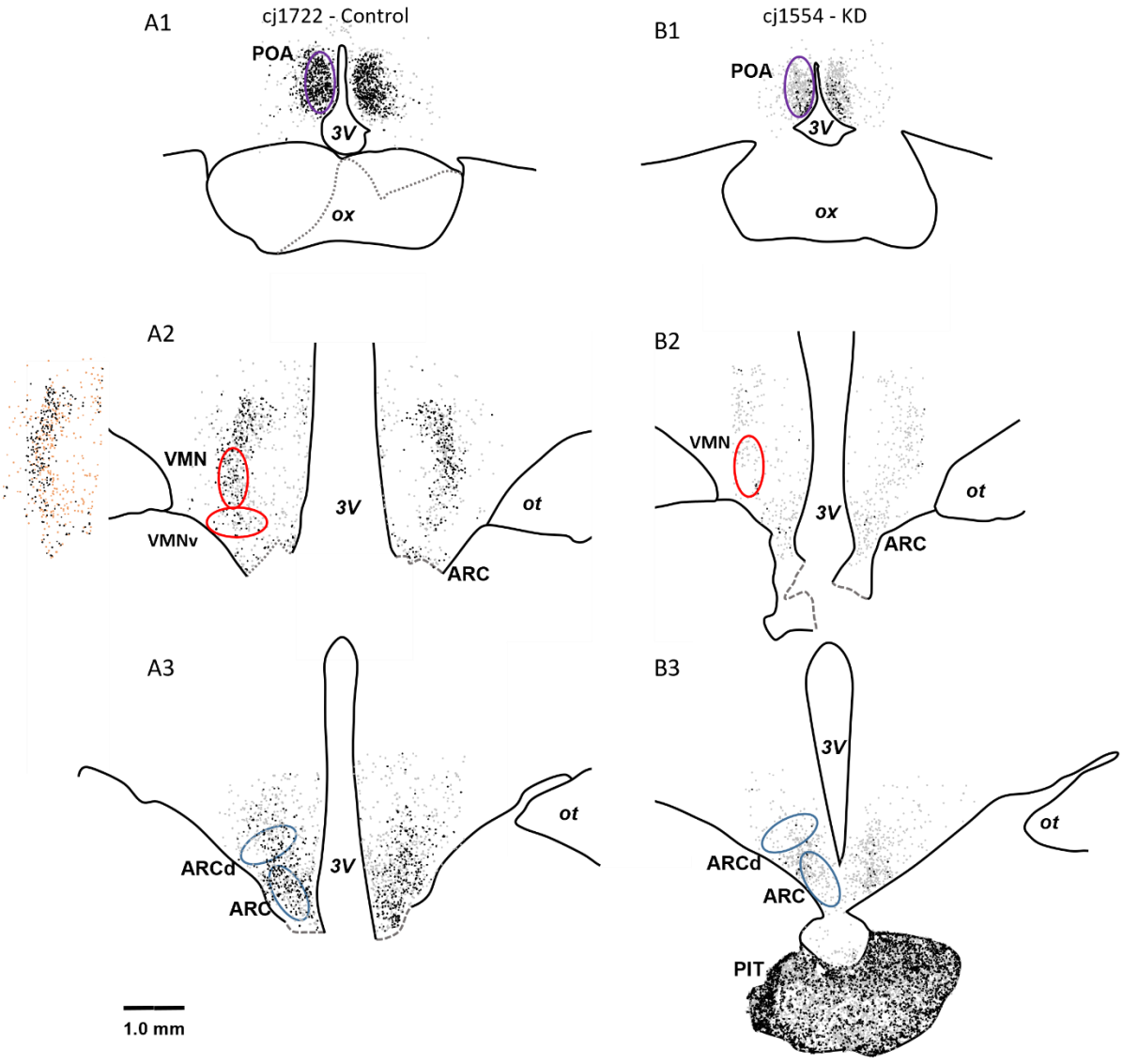

Figure 4: Distribution of ERα labeled cells in the hypothalamus. Representative sections are shown from the rostral (top) to caudal (bottom) hypothalamus for an ERαKD (right) and scrambled control (left) monkey. Black dots indicate the location of darkly stained cells. Dotted lines indicate damaged tissue. Black dots indicate the location of darkly stained cells (upper half of the ERα staining intensity range for that animal). Gray dots indicate the location of the lightly stained cells (lower half of the

intensity range). Abbreviations: ox: optic chiasm; ac: anterior commissure; opt: optic tract; 3V: third ventricle

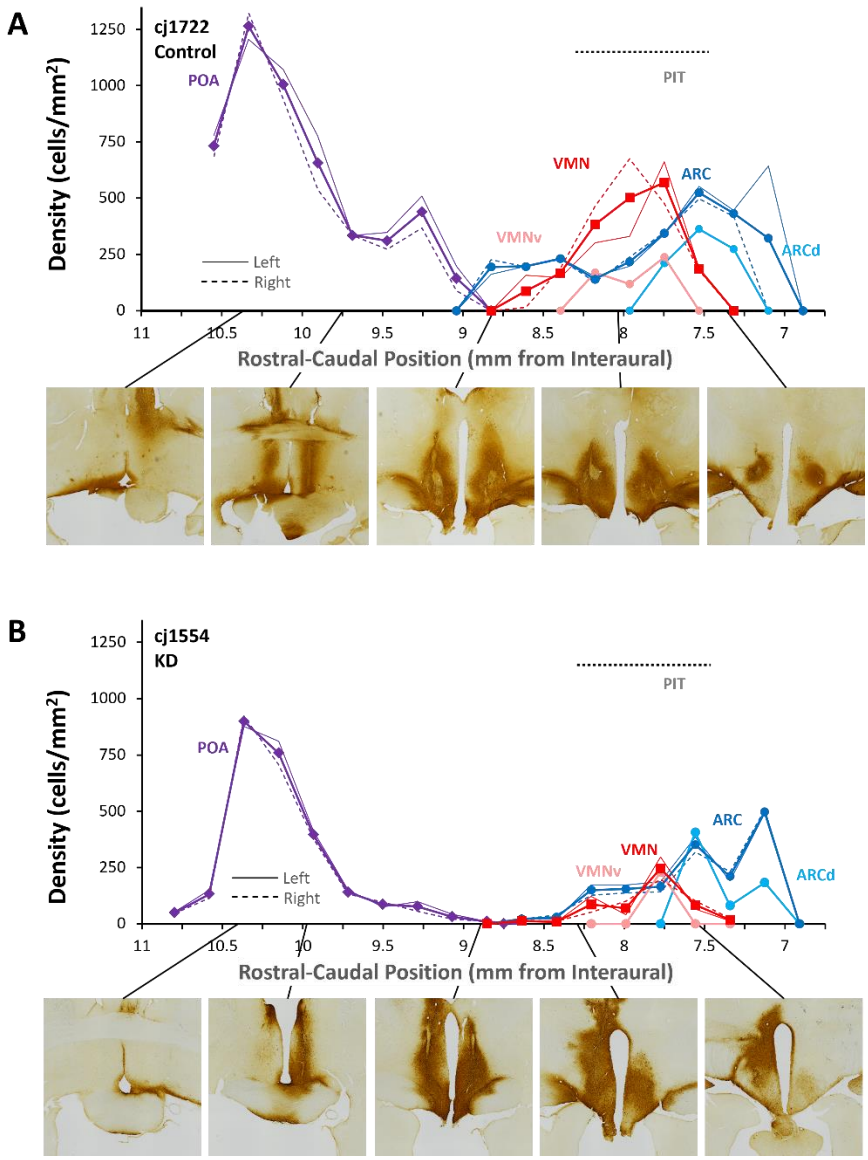

Figure 5: ERα positive cells were quantified in coronal brain sections from the most rostral extent of quantification (mid-optic chiasm) through the most caudal extend (causal sections of the ARC including portions of the mammillary bodies). Thick, solid, purple lines denote numbers of ERα positive cells in the POA, red lines=VMN, and blue lines=ARC, and denote the summation of the right and left side of each nuclei. Thin lines represent the left (solid) and the right (dotted) cell counts at each location. Each plot represents one female (Scrambled control (A), ERα knockdown (B).

Hypothalamic hormone	E2 (n = 5)	VEH (n = 4)	LET (n = 4)	*P* value
Estradiol (pg/mg)	0.56 ± 0.16	0.77 ± 0.33	0.07 ± 0.04[a,b]	.004
Estrone (pg/mg)	0.26 ± 0.10	0.32 ± 0.15	0.10 ± 0.04	.154
Progesterone (pg/mg)	1.30 ± 0.25	2.55 ± 0.76	1.32 ± 0.40	.266
17-OHP_4 (pg/mg)	8.80 ± 1.46	23.83 ± 5.17[a]	12.75 ± 2.11	.042
DHEA (pg/mg)	0.04 ± 0.01	0.20 ± 0.06[a]	0.09 ± 0.02	.010
Androstenedione (pg/mg)	0.75 ± 0.04	9.34 ± 5.32[a]	4.88 ± 1.75[c]	.008
Testosterone (pg/mg)	0.04 ± 0.01	0.15 ± 0.03[a]	0.08 ± 0.03	.019
Hypothalamic hormone ratio				
Estradiol:Testosterone	127.4 ± 63.2	62.9 ± 0.3[a]	0.02 ± 0.01[a,b]	.002
17OHP_4:Progesterone	6.7 ± 0.8	9.8 ± 1.9	10.9 ± 2.0	.215
Androstenedione:DHEA	17.7 ± 1.2	38.9 ± 11.3	53.3 ± 9.9 [a]	.009
Testosterone:Androstenedione	0.06 ± 0.01	0.03 ± 0.01 [a]	0.02 ± 0.01 [a]	.003

Table 4: Hypothalamic levels (mean ± SEM) of sex steroid hormones in OVX female marmosets receiving E_2 replacement (E2), empty capsules (VEH), or the aromatase inhibitor letrozole (LET) at 6 months following OVX.

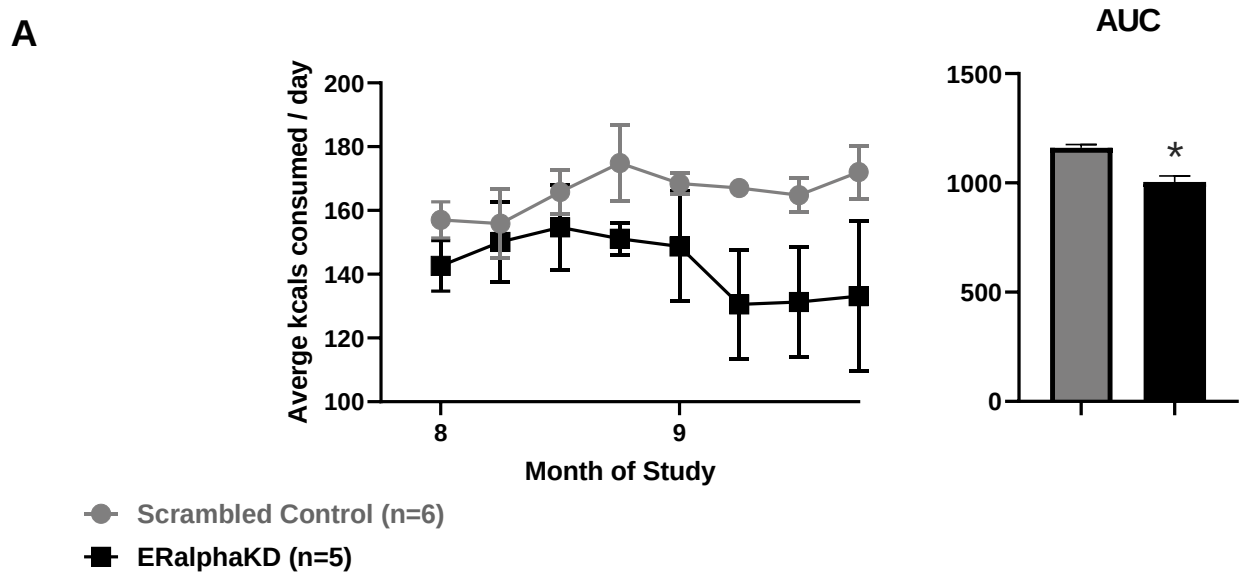

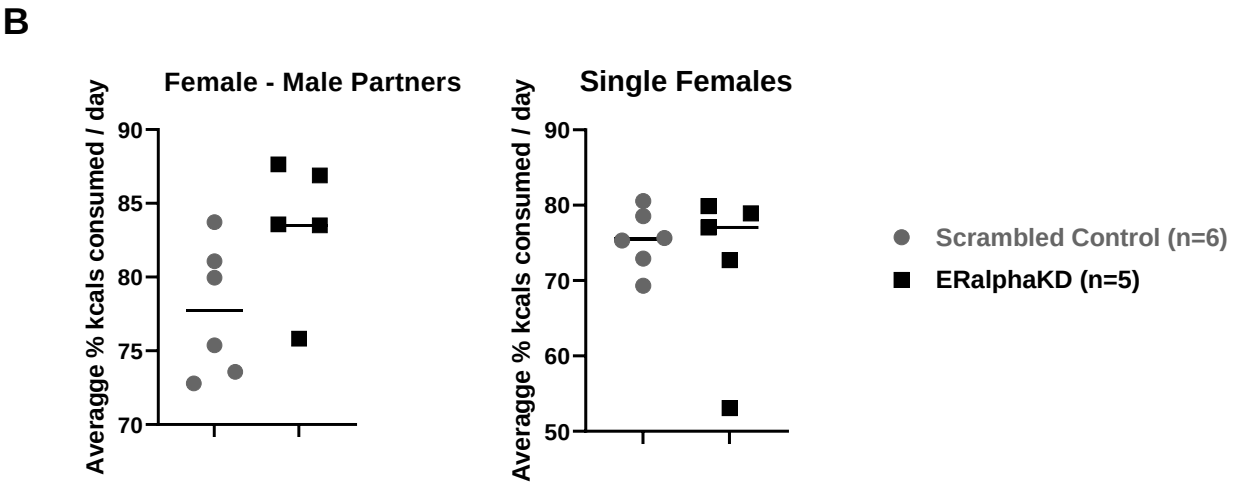

Figure 6. Average calories consumed while females singly housed (A) with corresponding AUC. Average percent of kcals consumed in female-male pairs and singly housed females (B). Plots expressed as mean ± SEM. Significance assessed via RM-ANOVA and student's t-test. P*<0.05.

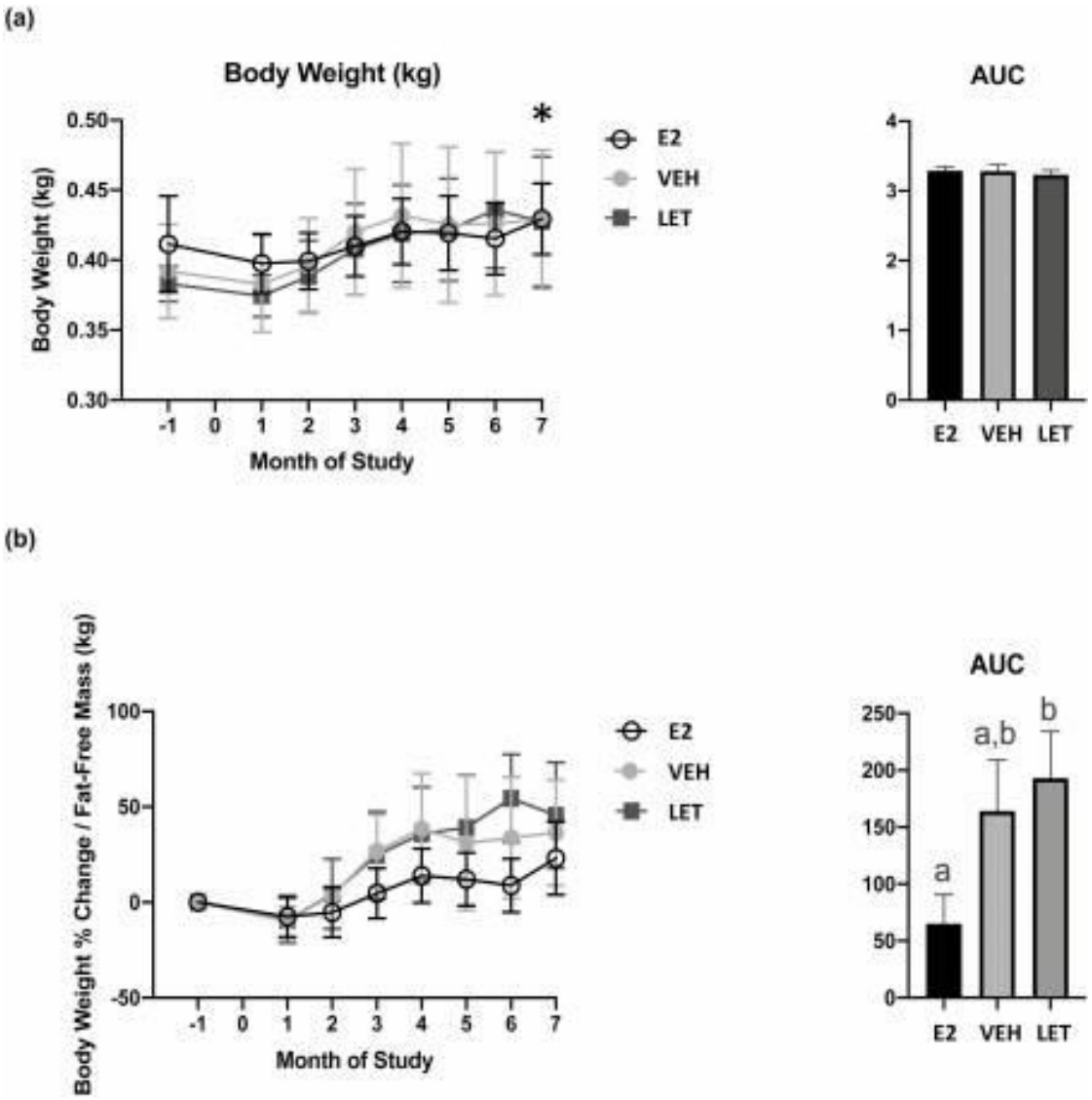

Figure 7. (A) Monthly body weights (mean ± SEM) of adult female marmoset monkeys from baseline until 7 months following ovariectomy, and (B) AUC body weights (mean ± SEM) incorporating all increments in body weight across the entire study, in E2 (open circles and black bars), VEH (light gray circles and bars), and LET (dark gray squares and bars) female groups.

Body region of interest	DXA parameter	Treatment group	Baseline	6 months	Change from baseline
Total body	Fat mass (g)	E2	121 ± 17	106 ± 19	-15 ± 18
		VEH	106 ± 22	156 ± 37	38 ± 33
		LET	113 ± 23	126 ± 35	5 ± 45
	Fat free mass (FFM)[a] (g)	E2	254 ± 15	270 ± 12	16 ± 7
		VEH	231 ± 11	251 ± 14	5 ± 11
		LET	234 ± 16	249 ± 7	22 ± 5
	Fat/FFM ratio	E2	0.5 ± 0.1	0.4 ± 0.1	-0.1 ± 0.1
		VEH	0.5 ± 0.1	0.6 ± 0.1	0.1 ± 0.1
		LET	0.5 ± 0.1	0.5 ± 0.1	-0.1 ± 0.1
	% fat	E2	31.6 ± 2.0	27.6 ± 3.8	-4.1 ± 3.2
		VEH	30.9 ± 4.2	36.6 ± 5.6	5.3 ± 6.3
		LET	32.3 ± 5.8	31.9 ± 6.3	-3.4 ± 7.1
	% FFM	E2	68.4 ± 2.0	72.4 ± 3.8	4.1 ± 3.2
		VEH	69.1 ± 4.2	63.4 ± 5.6	-5.3 ± 6.3
		LET	67.7 ± 5.8	68.1 ± 6.3	3.4 ± 7.1
Abdomen	Fat mass (g)	E2	27 ± 5	22 ± 6	-5 ± 7
		VEH	24 ± 8	43 ± 15	15 ± 14
		LET	23 ± 6	31 ± 13	19 ± 29
	FFM[b] (g)	E2	80 ± 9	85 ± 8	5 ± 3
		VEH	71 ± 8	92 ± 8	16 ± 3[c]
		LET	73 ± 5	81 ± 6	9 ± 5
	Fat/FFM ratio	E2	0.3 ± 0.1	0.3 ± 0.1	-0.1 ± 0.1
		VEH	0.3 ± 0.1	0.4 ± 0.2	0.1 ± 0.2
		LET	0.3 ± 0.1	0.4 ± 0.1	0.1 ± 0.2
	% Fat	E2	24 ± 2	20 ± 4	-5 ± 3
		VEH	24 ± 5	29 ± 7	4 ± 8
		LET	23 ± 5	24 ± 7	-3 ± 6
	% FFM	E2	76 ± 2	80 ± 4	5 ± 3
		VEH	76 ± 5	71 ± 7	-4 ± 1
		LET	77 ± 5	76 ± 7	2 ± 6
Chest	Fat (g)	E2	37 ± 9	34 ± 7	-4 ± 6
		VEH	32 ± 11	48 ± 14	12 ± 10
		LET	35 ± 10	42 ± 14	1 ± 12

Table 5A: Mean (+/- SEM) regional body composition parameters as determined by dual x-ray absorptiometry (DXA) in E2, VEH and LET female groups of marmosets at baseline and after six months of treatment (continued in Figure B).

Body region of interest	DXA parameter	Treatment group	Baseline	6 months	Change from baseline
Chest (contd.)	**FFM[c] (g)**	E2	57 ± 4	61 ± 4	4 ± 2
		VEH	50 ± 4	44 ± 5	-8 ± 4
		LET	52 ± 8	52 ± 8	5 ± 7
	Fat/FFM ratio	E2	0.7 ± 0.1	0.6 ± 0.1	-0.1 ± 0.1
		VEH	0.7 ± 0.3	1.2 ± 0.4	0.5 ± 0.4
		LET	0.8 ± 0.3	1.0 ± 0.4	0.1 ± 0.5
	% Fat	E2	38 ± 5	35 ± 6	-3 ± 4
		VEH	37 ± 10	48 ± 10	10 ± 7
		LET	40 ± 11	43 ± 12	-4 ± 9
	% FFM	E2	63 ± 5	65 ± 6	3 ± 4
		VEH	63 ± 10	52 ± 11	-10 ± 7
		LET	60 ± 11	57 ± 12	4 ± 9
Upper legs	Fat mass (g)	E2	14 ± 1	12 ± 2	-1 ± 2
		VEH	12 ± 1	16 ± 2	3 ± 3
		LET	13 ± 2	11 ± 3	-1 ± 6
	FFM[d] (g)	E2	48 ± 3	50 ± 2	2 ± 1
		VEH	42 ± 3	48 ± 3	2 ± 3
		LET	44 ± 3	45 ± 2	5 ± 4
	Fat/FFM ratio	E2	0.3 ± 0.1	0.2 ± 0.1	-0.1 ± 0.1
		VEH	0.3 ± 0.1	0.3 ± 0.1	0.1 ± 0.1
		LET	0.3 ± 0.1	0.2 ± 0.1	-0.1 ± 0.1
	% Fat	E2	22 ± 1	19 ± 3	-3 ± 3
		VEH	21 ± 2	24 ± 2	2 ± 5
		LET	23 ± 4	19 ± 3	-5 ± 7
	% FFM	E2	78 ± 1	81 ± 3	3 ± 3
		VEH	79 ± 2	76 ± 2	-2 ± 5
		LET	77 ± 4	81 ± 3	5 ± 7
Lower legs	Fat mass (g)	E2	13 ± 1	12 ± 2	-2 ± 1
		VEH	12 ± 1	14 ± 2	-1 ± 2
		LET	12 ± 1	11 ± 2	-1 ± 1
	FFM (g)	E2	20 ± 1	23 ± 2	3 ± 2
		VEH	21 ± 2	19 ± 1	-2 ± 2
		LET	18 ± 1	22 ± 1	4 ± 3
	Fat/FFM ratio	E2	0.7 ± 0.1	0.5 ± 0.1	-0.1 ± 0.1
		VEH	0.6 ± 0.1	0.7 ± 0.1	0.1 ± 0.2
		LET	0.7 ± 0.1	0.5 ± 0.1	-0.2 ± 0.1

Table 5B: Mean (+/- SEM) regional body composition parameters as determined by dual x-ray absorptiometry (DXA) in E2, VEH and LET female groups of marmosets at baseline and after six months of treatment (Continued in Figure 5C).

Body region of interest	DXA parameter	Treatment group	Baseline	6 months	Change from baseline
Lower legs	% Fat	E2	41 ± 2	34 ± 4	-6 ± 4
(contd.)		VEH	37 ± 1	41 ± 4	1 ± 4
		LET	40 ± 4	32 ± 3	-7 ± 1
	% FFM	E2	59 ± 2	66 ± 4	6 ± 4
		VEH	63 ± 1	59 ± 4	-1 ± 4
		LET	60 ± 4	68 ± 3	7 ± 1
Arms	Fat mass (g)	E2	14 ± 2	12 ± 1	-2 ± 1
		VEH	12 ± 1	14 ± 2	2 ± 3
		LET	13 ± 2	13 ± 2	0 ± 3
	FFM (g)	E2	27 ± 1	28 ± 1	1 ± 1
		VEH	26 ± 2	27 ± 2	0 ± 2
		LET	26 ± 2	26 ± 2	0 ± 2
	Fat/FFM ratio	E2	0.5 ± 0.1	0.4 ± 0.1	-0.1 ± 1
		VEH	0.5 ± 0.1	0.6 ± 0.1	0.1 ± 0.2
		LET	0.5 ± 0.1	0.5 ± 0.1	0 ± 0.2
	% Fat	E2	34 ± 2	30 ± 3	-2 ± 1
		VEH	31 ± 2	35 ± 4	2 ± 3
		LET	33 ± 5	33 ± 3	0 ± 3
	% FFM	E2	66 ± 2	70 ± 3	4 ± 3
		VEH	68 ± 2	65 ± 4	-4 ± 7
		LET	67 ± 5	67 ± 3	1 ± 6
Abdomen/Upper legs ratio	Fat	E2	1.9 ± 0.2	1.7 ± 0.1	-0.2 ± 0.2
		VEH	1.5 ± 0.3	2.2 ± 0.6	0.6 ± 0.5
		LET	2.2 ± 0.6	2.4 ± 0.5	0.1 ± 0.1

Table 5C: Mean (+/- SEM) regional body composition parameters as determined by dual x-ray absorptiometry (DXA) in E2, VEH and LET female groups of marmosets at baseline and after six months of treatment.

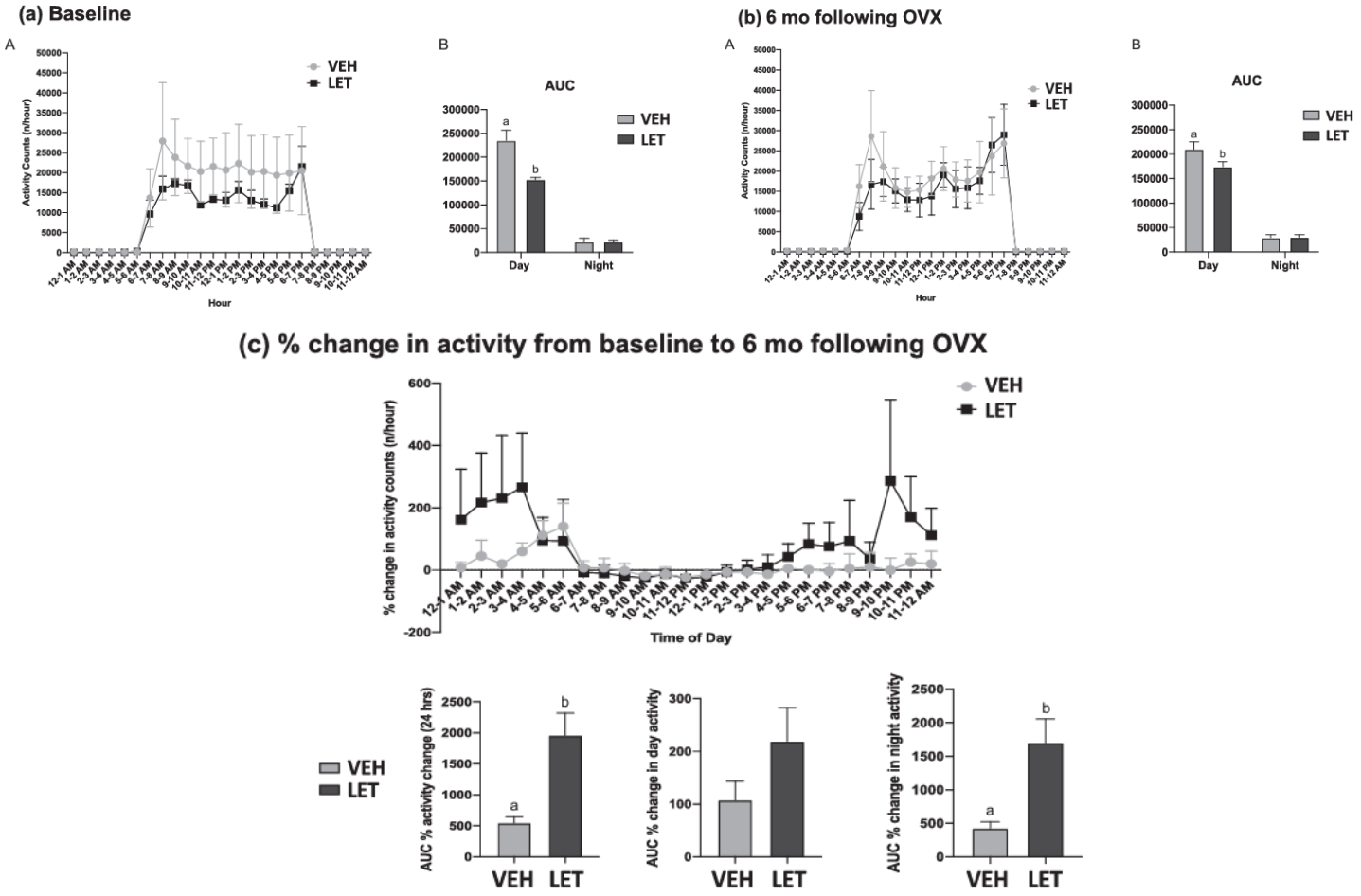

Figure 8. Actical collar determined body motion activity over 21 consecutive days (mean ± SEM) in adult female marmosets in VEH (light gray circles and bars) and LET (dark gray squares and bars) groups (a) at baseline illustrating (A) hourly activity during 12 hour daytime and 12 hour nighttime and (B) AUC activity for daytime and nighttime, a, b: P = 0.001, at (b) 6 months (months) following OVX illustrating (A) hourly activity during 12 hour daytime and 12 hour nighttime and (B) AUC activity for daytime and nighttime, a, b: P = 0.01, and (c) % change in activity from baseline to 6 months following OVX during 12 hour daytime and 12 hour nighttime and AUC % activity change for 24 hours/day, daytime only and nighttime only, a, b: P = 0.01.

Parameter	E2	VEH	LET	*P* value
Baseline				
Basal glucose (mg/dL)	114 ± 3	119 ± 3	111 ± 6	—
6 months after ovariectomy				
Basal glucose (mg/dL)[a]	120 ± 11	127 ± 9	137 ± 7	.149
AUC OGTT glucose (mg/dL*120 min)	21251 ± 2386	19380 ± 1548	20843 ± 4829	.555
2 hour OGTT glucose (mg/dL)	130 ± 16	128 ± 13	180 ± 48	.440

Table 6: Mean (±SEM) basal glucose at baseline and 6 months after ovariectomy, as well as oral glucose tolerance test (OGTT) derived glucose values at 6 months after ovariectomy in E2, VEH and LET females. Abbreviations: AUC, area under the curve; OGTT, oral glucose tolerance test. [a]P = .055, 6 mo > baseline, all female groups combined. SI unit conversion : glucose × 0.0551 mmol/L.

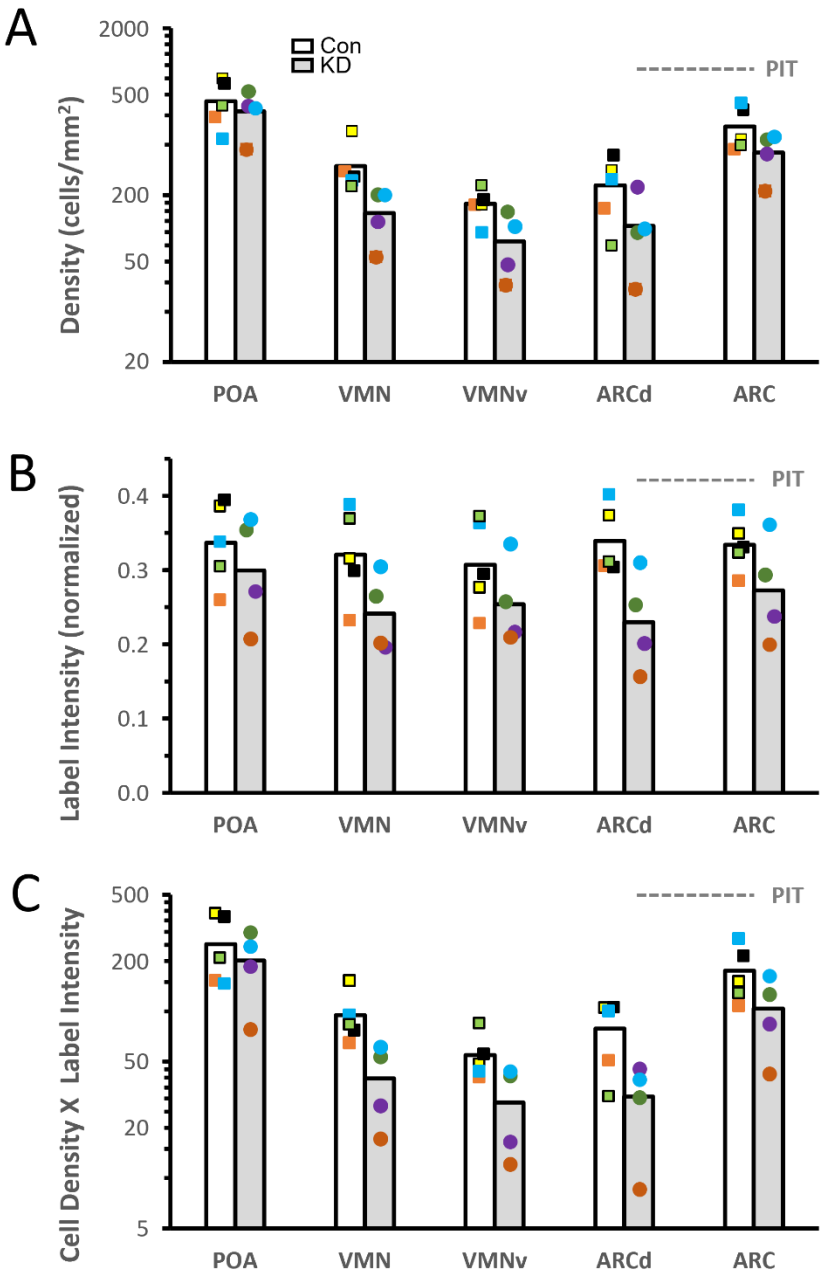

Figure 9: (A) The number of cells per unit area, or the ERα cell density is not statistically different between the groups in any of the hypothalamic nuclei analyzed. (B) ERα staining intensity in the VMN, but not the POA and ARC nuclei of the hypothalamus, is markedly less in the ERα gene silenced females (*p=0.04) compared with control females. (C) density * intensity in hypothalamic nuclei.

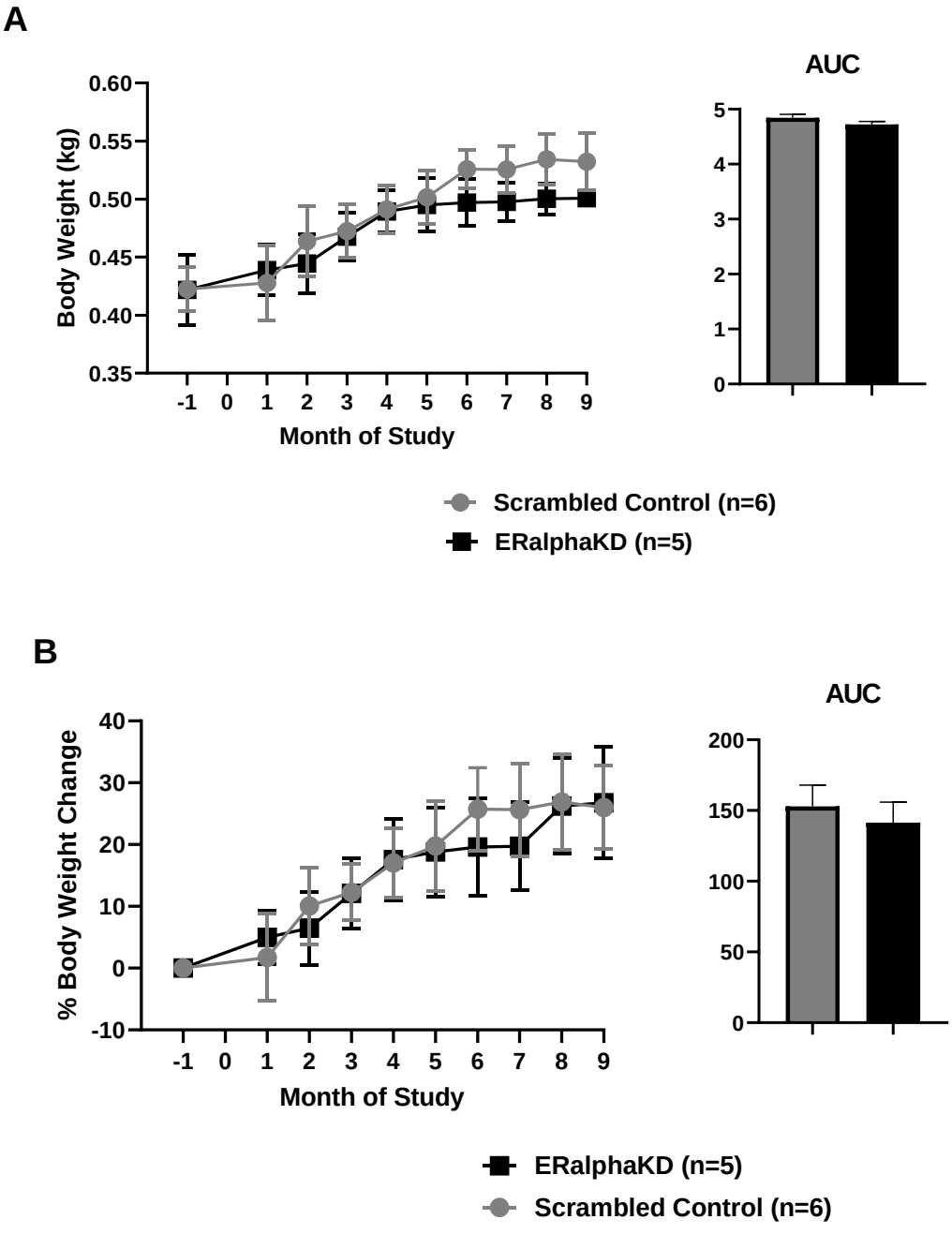

Figure 10: Body weight (kg) over duration of study with corresponding AUC bar graph (A) and body weight percent change from baseline weight over duration of study with corresponding AUC bar graph (B). Plots expressed as mean ± SEM. Significance assessed via RM-ANOVA and student's t-test.

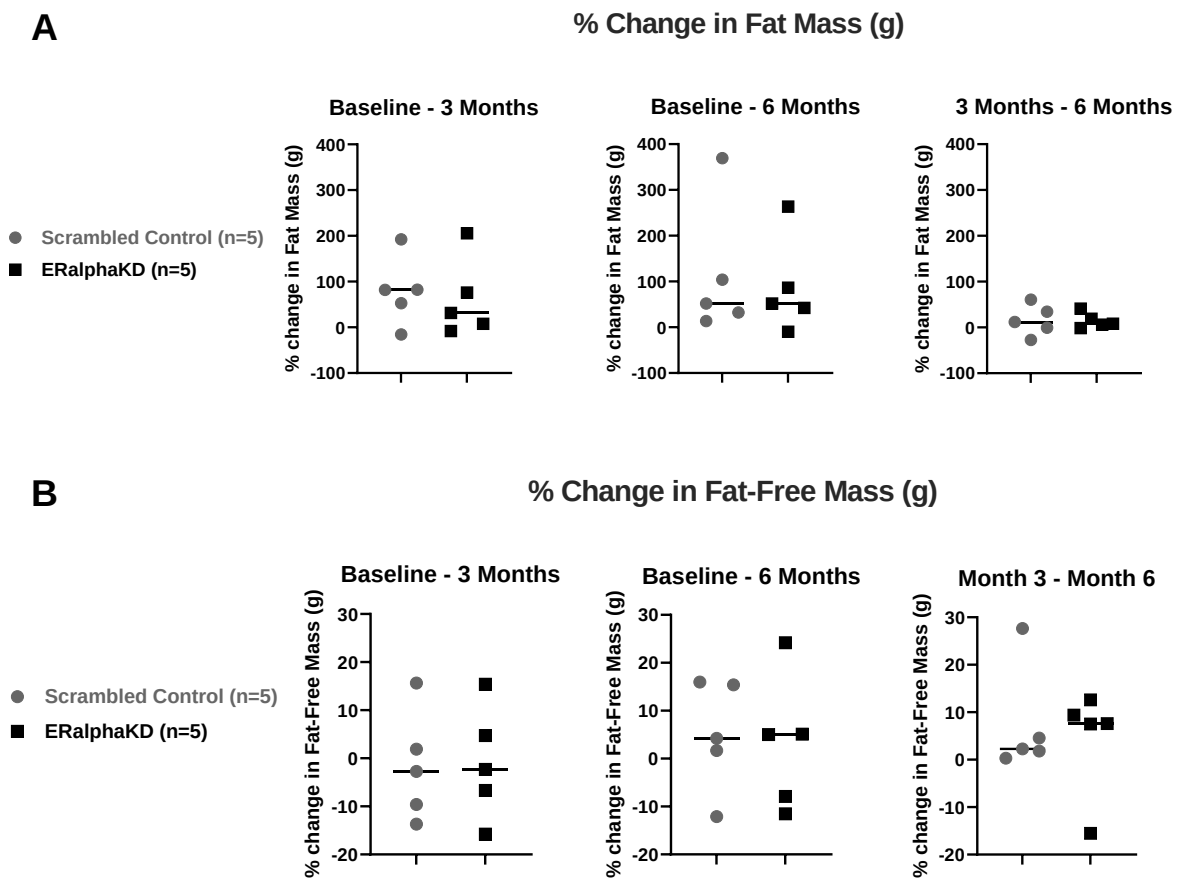

Figure 11: Percent change in fat mass (A) and fat-free mass (B) between DXA scans at baseline, 3-months, and 6-months post-treatment onset. Plots expressed as mean ± SEM. Significance assessed via student's t-test.

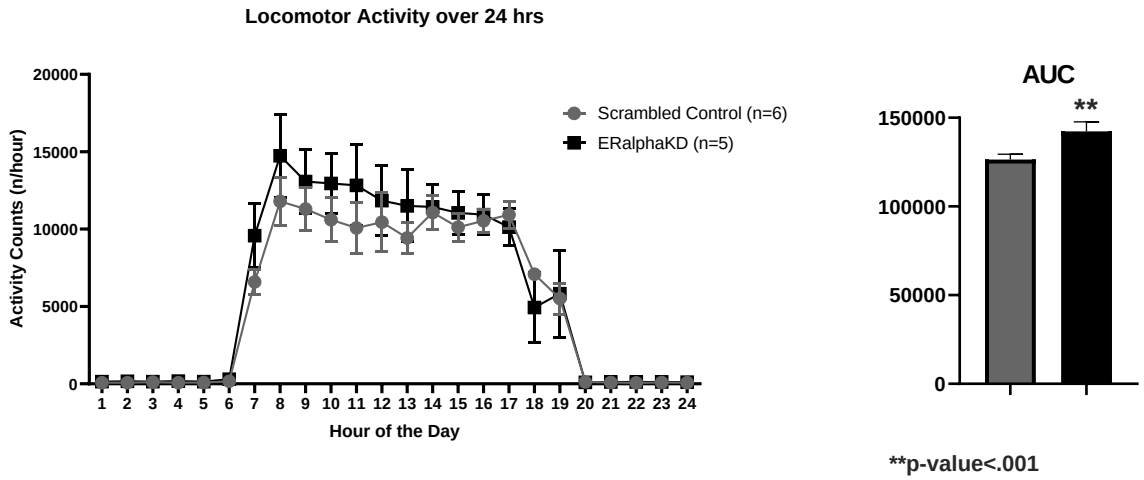

Figure 12: Locomotor activity over 24-hours averaged over the duration of the activity assessment with corresponding AUC histogram. Plots expressed as mean ± SEM. Significance assessed via RM-ANOVA and student's t-test. P**<0.001.

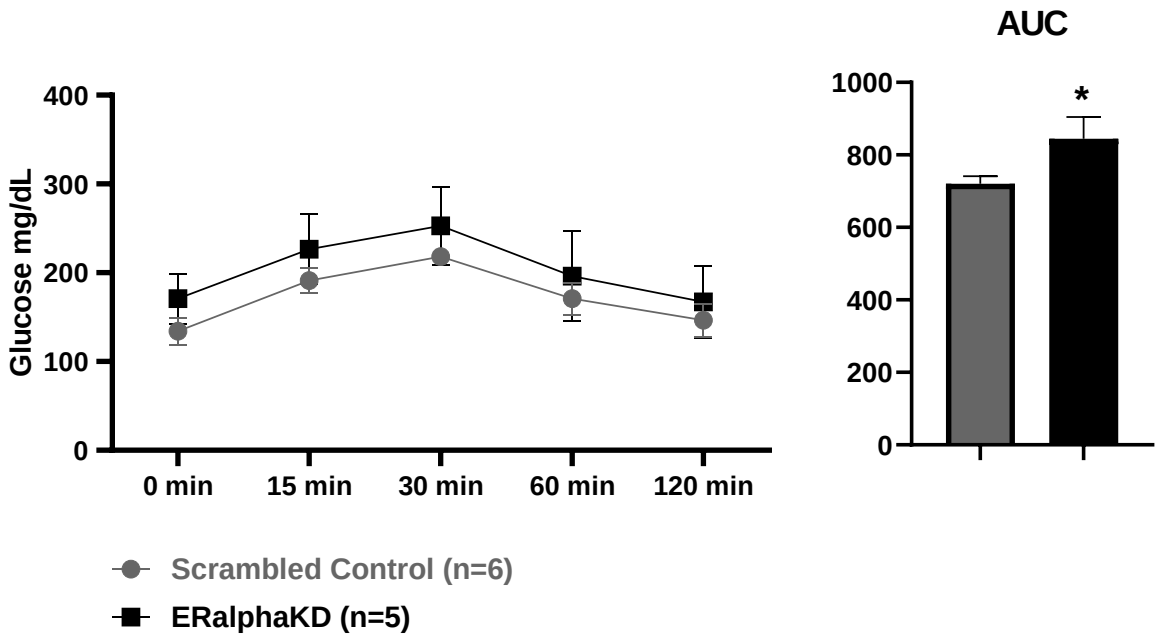

Figure 13: Glucose levels during oral glucose tolerance test at 6-months post-treatment onset. Plots expressed as mean ± SEM. Significance assessed via RM-ANOVA and student's t-test. P*<0.05.

2.7 References

1. Killinger DW, Perel E, Daniilescu D, Kharlip L, Blackstein ME. Aromatase activity in the breast and other peripheral tissues and its therapeutic regulation. *Steroids*. 1987 Oct-Dec;50(4-6):523-36. doi: 10.1016/0039-128x(87)90036-5. PMID: 3332939.
2. Kadioglu P, Oral G, Sayitoglu M, Erensoy N, Senel B, Gazioglu N, Sav A, Cetin G, Ozbek U. Aromatase cytochrome P450 enzyme expression in human pituitary. *Pituitary*. 2008;11(1):29-35. doi: 10.1007/s11102- 007-0065-3. PMID: 17703367
3. Weisz J. In vitro assays of aromatase and their role in studies of estrogen formation in target tissues. *Cancer Res.*1982;42(8Suppl):3295s-3298s
4. Amanatullah DF, Tamaresis JS, Chu P, et al.. Local estrogen axis in the human bone microenvironment regulates estrogen receptor-positive breast cancer cells. *Breast Cancer Res.* 2017;19(1):121.
5. Remage-Healey L, London SE, Schlinger BA. Birdsong and the neural production of steroids. *J Chem Neuroanat.* 2010;39(2):72-81.
6. Remage-Healey L, Saldanha CJ, Schlinger BA. Estradiol synthesis and action at the synapse: evidence for “synaptocrine” signaling. *Front Endocrinol (Lausanne).* 2011;2:28.
7. Liere P, Cornil CA, de Bournonville MP, et al.. Steroid profiles in quail brain and serum: sex and regional differences and effects of castration with steroid replacement. *J Neuroendocrinol.* 2019;31(2):e12681.
8. Baumgartner NE, Grissom EM, Pollard KJ, McQuillen SM, Daniel JM. Neuroestrogen-dependent transcriptional activity in the brains of ERE-luciferase reporter mice following short- and long-term ovariectomy. *eNeuro* 2019;6(5):ENEURO.0275ENE URO
9. Saito K, He Y, Yang Y, et al.. PI3K in the ventromedial hypothalamic nucleus mediates estrogenic actions on energy expenditure in female mice. *Sci Rep.* 2016;6:20166.
10. Amateau SK, Alt JJ, Stamps CL, McCarthy MM. Brain estradiol content in newborn rats: sex differences, regional heterogeneity, and possible de novo synthesis by the female telencephalon. *Endocrinology.* 2004;145(6):2906-17.
11. Konkle AT, McCarthy MM. Developmental time course of estradiol, testosterone, and dihydrotestosterone levels in discrete regions of male and female rat brain. *Endocrinology.* 2011;152(1):223-35.
12. Li J, Gibbs RB. Detection of estradiol in rat brain tissues: Contribution of local versus systemic production. *Psychoneuroendocrinology.* 2019;102:84-94.
13. Kenealy BP, Kapoor A, Guerriero KA, et al.. Neuroestradiol in the hypothalamus contributes to the regulation of gonadotropin releasing hormone release. *J Neurosci.* 2013;33(49):19051-9.
14. Kenealy BP, Keen KL, Kapoor A, Terasawa E. Neuroestradiol in the stalk median eminence of female rhesus macaques decreases in association with puberty onset. *Endocrinology.* 2016;157(1):70-6
15. Kenealy BP, Keen KL, Garcia JP, Kohlenberg LK, Terasawa E. Obligatory role of hypothalamic neuroestradiol during the estrogen-induced LH surge in female

ovariectomized rhesus monkeys. *Proc Natl Acad Sci USA.* 2017;114(52):13804-13809.
16. Gervais NJ, Remage-Healey L, Starrett JR, Pollak DJ, Mong JA, Lacreuse A. Adverse effects of aromatase inhibition on the brain and behavior in a nonhuman primate. *J Neurosci.* 2019;39(5):918-928.
17. Cornil CA. On the role of brain aromatase in females: why are estrogens produced locally when they are available systemically? *J Comp Physiol A Neuroethol Sens Neural Behav Physiol.* 2018;204(1):31-49.
18. Terasawa E, Kenealy BP. Neuroestrogen, rapid action of estradiol, and GnRH neurons. *Front Neuroendocrinol.* 2012;33(4):364-75.
19. Kraynak M, Flowers MT, Shapiro RA, Kapoor A, Levine JE, Abbott DH. Extraovarian gonadotropin negative feedback revealed by aromatase inhibition in female marmoset monkeys. *Am J Physiol Endocrinol Metab.* 2017;313(5):E507-E514.
20. Park CJ, Zhao Z, Glidewell-Kenney C, et al.. Genetic rescue of nonclassical ERα signaling normalizes energy balance in obese Erα-null mutant mice. *J Clin Invest.* 2011;121(2):604-12.
21. Xu Y, Nedungadi TP, Zhu L, et al.. Distinct hypothalamic neurons mediate estrogenic effects on energy homeostasis and reproduction. *Cell Metab.* 2011;14(4):453-65.
22. Zidon TM, Padilla J, Fritsche KL, et al.. Effects of ERβ and ERα on OVX-induced changes in adiposity and insulin resistance. *J Endocrinol.* 2020;245(1):165-178.
23. Heine PA, Taylor JA, Iwamoto GA, Lubahn DB, Cooke PS. Increased adipose tissue in male and female estrogen receptor-alpha knockout mice. *Proc Natl Acad Sci USA.* 2000;97(23):12729-12734.
24. Bryzgalova G, Gao H, Ahren B, et al.. Evidence that oestrogen receptor-alpha plays an important role in the regulation of glucose homeostasis in mice: insulin sensitivity in the liver. *Diabetologia.* 2006;49(3):588-97.
25. Ogawa S, Chan J, Gustafsson JA, Korach KS, Pfaff DW. Estrogen increases locomotor activity in mice through estrogen receptor alpha: specificity for the type of activity. *Endocrinology.* 2003;144(1):230-9.
26. Fester and Rune, 2021 Fester L, Rune GM. Sex neurosteroids: Hormones made by the brain for the brain. *Neurosci Lett*. 2021 May 14;753:135849. doi: 10.1016/j.neulet.2021.135849. Epub 2021 Mar 26. PMID: 33775739.
27. Stincic and Kelly, 2022 Stincic TL, Kelly MJ. Estrogenic regulation of reproduction and energy homeostasis by a triumvirate of hypothalamic arcuate neurons. *J Neuroendocrinol.* 2022 Jun;34(6):e13145. doi: 10.1111/jne.13145. Epub 2022 May 17. PMID: 35581942.
28. Wallen K, Winston LA, Gaventa S, Davis-DaSilva M, Collins DC. Periovulatory changes in female sexual behavior and patterns of ovarian steroid secretion in group-living rhesus monkeys. *Horm Behav.* 1984;18(4):431-50.
29. Van Wagenen G. Accelerated growth with sexual precocity in female monkeys receiving testosterone propionate. *Endocrinology.* 1949;45(5):544-546.
30. True CA, Takahashi DL, Burns SE, et al.. Chronic combined hyperandrogenemia and western-style diet in young female rhesus macaques causes greater

metabolic impairments compared to either treatment alone. *Hum Reprod.* 2017;32(9):1880-1891.
31. Aflatounian A, Edwards MC, Rodriguez Paris V, et al.. Androgen signaling pathways driving reproductive and metabolic phenotypes in a PCOS mouse model. *J Endocrinol.* 2020;245(3):381-395.
32. Binkley N, Kimmel D, Bruner J, et al.. Zoledronate prevents the development of absolute osteopenia following ovariectomy in adult rhesus monkeys. *J Bone Miner Res.* 1998;13(11):1775-1782.
33. Terasawa E. The mechanism underlying the pubertal increase in pulsatile GnRH release in primates. *J Neuroendocrinol*. 2022 May;34(5):e13119. doi: 10.1111/jne.13119. Epub 2022 May 1. PMID: 35491543; PMCID: PMC9232993.
34. Wade GN, Gray JM. Gonadal effects on food intake and adiposity: a metabolic hypothesis. *Physiol Behav.* 1979;22(3):583-93.
35. Barros RP, Gustafsson JA. Estrogen receptors and the metabolic network. *Cell Metab.* 2011;14(3):289-99.
36. Barros RP, Gabbi C, Morani A, Warner M, Gustafsson JA. Participation of ERalpha and ERbeta in glucose homeostasis in skeletal muscle and white adipose tissue. *Am J Physiol Endocrinol Metab.* 2009;297(1):E124-33.
37. Cignarella A, Bolego C, Pelosi V, et al.. Distinct roles of estrogen receptor-alpha and beta in the modulation of vascular inducible nitric-oxide synthase in diabetes. *J Pharmacol Exp Ther.* 2009;328(1):174-82.
38. Mauvais-Jarvis F. Estrogen and androgen receptors: regulators of fuel homeostasis and emerging targets for diabetes and obesity. *Trends Endocrinol Metab.* 2011;22(1):24-33.
39. Jones ME, Thorburn AW, Britt KL, et al.. Aromatase-deficient (ArKO) mice have a phenotype of increased adiposity. *Proc Natl Acad Sci USA.* 2000;97(23):12735-12740.
40. Riant E, Waget A, Cogo H, Arnal JF, Burcelin R, Gourdy P. Estrogens protect against high-fat diet-induced insulin resistance and glucose intolerance in mice. *Endocrinology.* 2009;150(5):2109-17.
41. Yonezawa R, Wada T, Matsumoto N, et al.. Central versus peripheral impact of estradiol on the impaired glucose metabolism in ovariectomized mice on a high-fat diet. *Am J Physiol Endocrinol Metab.* 2012;303(4):E445-56.
42. Hong J, Stubbins RE, Smith RR, Harvey AE, Núñez NP. Differential susceptibility to obesity between male, female and ovariectomized female mice. *Nutr J.* 2009;8:11.
43. Ludgero-Correia A Jr, Aguila MB, Mandarim-de-Lacerda CA, Faria TS. Effects of high-fat diet on plasma lipids, adiposity, and inflammatory markers in ovariectomized C57BL/6 mice. *Nutrition.* 2012;28(3):316-23.
44. Ziemian SN, Ayobami OO, Rooney AM, et al.. Low bone mass resulting from impaired estrogen signaling in bone increases severity of load-induced osteoarthritis in female mice. *Bone.* 2021;152:116071.
45. Gervais NJ, Mong JA, Lacreuse A. Ovarian hormones, sleep and cognition across the adult female lifespan: an integrated perspective. *Front Neuroendocrinol.* 2017;47:134-153

46. van der Kooi AL, van den Heuvel-Eibrink MM, van Noortwijk A, et al.. Longitudinal follow-up in female childhood cancer survivors: no signs of accelerated ovarian function loss. *Hum Reprod.* 2017;32(1):193-200.
47. van Dorp W, Mulder RL, Kremer LC, et al.. Recommendations for premature ovarian insufficiency surveillance for female survivors of childhood, adolescent, and young adult cancer: a report from the International Late Effects of Childhood Cancer Guideline Harmonization Group in collaboration with the PanCareSurFup Consortium. *J Clin Oncol.* 2016;34(28):3440-50
48. Deroo BJ, Korach KS. Estrogen receptors and human disease. *J Clin Invest.* 2006;116(3):561-70.
49. Zidon TM, Padilla J, Fritsche KL, et al.. Effects of ERβ and ERα on OVX-induced changes in adiposity and insulin resistance. *J Endocrinol.* 2020;245(1):165-178.
50. Nelson HD, Walker M, Zakher B, Mitchell J. Menopausal hormone therapy for the primary prevention of chronic conditions: a systematic review to update the U.S. Preventive Services Task Force recommendations. *Ann Intern Med.* 2012;157(2):104-13.
51. Sood R, Faubion SS, Kuhle CL, Thielen JM, Shuster LT. Prescribing menopausal hormone therapy: an evidence-based approach. *Int J Womens Health.* 2014;6:47-57.
52. Justenhoven C, Obazee O, Brauch H. The pharmacogenomics of sex hormone metabolism: breast cancer risk in menopausal hormone therapy. *Pharmacogenomics.* 2012;13(6):659-75.
53. Drew BG, Hamidi H, Zhou Z, et al.. Estrogen receptor (ER)α-regulated lipocalin 2 expression in adipose tissue links obesity with breast cancer progression. *J Biol Chem.* 2015;290(9):5566-81.
54. Hamilton, L.W. (1976). The Medial Forebrain Bundle and Related Hypothalamic Connections. In: Basic Limbic System Anatomy of the Rat. Springer, Boston, MA. https://doi.org/10.1007/978-1-4684-2247-4_8
55. Terasawa E, Noonan JJ, Nass TE, Loose MD. Posterior hypothalamic lesions advance the onset of puberty in the female rhesus monkey. Endocrinology. 1984 Dec;115(6):2241-50. doi: 10.1210/endo-115-6-2241. PMID: 6499768.
56. Musatov S, Chen W, Pfaff DW, Mobbs CV, Yang XJ, Clegg DJ, Kaplitt MG, Ogawa S. Silencing of estrogen receptor alpha in the ventromedial nucleus of hypothalamus leads to metabolic syndrome. *Proc Natl Acad Sci U S A.* 2007 Feb 13;104(7):2501-6. doi: 10.1073/pnas.0610787104. Epub 2007 Feb 6. PMID: 17284595; PMCID: PMC1892990.
57. Pfaff, D. W. et al. Autoradiographic localization of hormone-concentrating cells in the brain of the female rhesus monkey. *J Comp Neurol* 170, 279-293, doi:10.1002/cne.901700302 (1976)
58. Rissman, E. F., Wersinger, S. R., Taylor, J. A. & Lubahn, D. B. Estrogen receptor function as revealed by knockout studies: neuroendocrine and behavioral aspects. *Horm Behav* 31, 232-243, doi:10.1006/hbeh.1997.1390 (1997).
59. Montague, D. et al. Oestrogen receptor alpha localisation in the prefrontal cortex of three mammalian species. *J Neuroendocrinol* 20, 893-903, doi:10.1111/j.1365-2826.2008.01743.x (2008).

60. Fox J, Miller MA, Newman MK, Turner CH, Recker RR, Smith SY. Treatment of skeletally mature ovariectomized rhesus monkeys with PTH(1-84) for 16 months increases bone formation and density and improves trabecular architecture and biomechanical properties at the lumbar spine. *J Bone Miner Res.* 2007;22(2):260-273.
61. Lovejoy JC, Champagne CM, de Jonge L, Xie H, Smith SR. Increased visceral fat and decreased energy expenditure during the menopausal transition. *Int J Obes (Lond).* 2008;32(6):949-58.
62. Ley CJ, Lees B, Stevenson JC. Sex- and menopause-associated changes in body-fat distribution. *Am J Clin Nutr.* 1992;55(5):950-4.
63. Genazzani AR, Gambacciani M. Effect of climacteric transition and hormone replacement therapy on body weight and body fat distribution. *Gynecol Endocrinol.* 2006;22(3):145-50.
64. Sullivan EL, Daniels AJ, Koegler FH, Cameron JL. Evidence in female rhesus monkeys (*Macaca mulatta*) that nighttime caloric intake is not associated with weight gain. *Obes Res.* 2005;13(12):2072-80.
65. Sandoval-Guzmán T, Stalcup ST, Krajewski SJ, Voytko ML, Rance NE. Effects of ovariectomy on the neuroendocrine axes regulating reproduction and energy balance in young cynomolgus macaques. *J Neuroendocrinol.* 2004;16(2):146-53.
66. Wagner JD, Clarkson TB, St Clair RW, Schwenke DC, Shively CA, Adams MR. Estrogen and progesterone replacement therapy reduces low density lipoprotein accumulation in the coronary arteries of surgically postmenopausal cynomolgus monkeys. *J Clin Invest.* 1991;88(6):1995-2002.
67. Sullivan EL, Shearin J, Koegler FH, Cameron JL. Selective estrogen receptor modulator promotes weight loss in ovariectomized female rhesus monkeys (*Macaca mulatta*) by decreasing food intake and increasing activity. *Am J Physiol Endocrinol Metab.* 2012;302(7):E759-67.
68. Cefalu WT, Wagner JD, Bell-Farrow AD, et al.. The effects of hormonal replacement therapy on insulin sensitivity in surgically postmenopausal cynomolgus monkeys (Macaca fascicularis). *Am J Obstet Gynecol.* 1994;171(2):440-5.
69. Kittivanichkul D, Watanabe G, Nagaoka K, Malaivijitnond S. Changes in bone mass during the perimenopausal transition in naturally menopausal cynomolgus monkeys. *Menopause.* 2016;23(1):87-99.
70. Mann DR, Gould KG, Collins DC. A potential primate model for bone loss resulting from medical oophorectomy or menopause. *J Clin Endocrinol Metab.* 1990;71(1):105-10.
71. Lees CJ, Register TC, Turner CH, Wang T, Stancill M, Jerome CP. Effects of raloxifene on bone density, biomarkers, and histomorphometric and biomechanical measures in ovariectomized cynomolgus monkeys. *Menopause.* 2002;9(5):320-8.
72. Barnett DK, Bunnell TM, Millar RP, Abbott DH. Gonadotropin-releasing hormone II stimulates female sexual behavior in marmoset monkeys. *Endocrinology.* 2006;147(1):615-23.
73. Aubert Y, Allers KA, Sommer B, de Kloet ER, Abbott DH, Datson NA. Brain region-specific transcriptomic markers of serotonin-1A receptor agonist action

mediating sexual rejection and aggression in female marmoset monkeys. *J Sex Med.* 2013;10(6):1461-75.
74. Risal S, Pei Y, Lu H, et al.. Prenatal androgen exposure and transgenerational susceptibility to polycystic ovary syndrome. *Nat Med.* 2019;25(12):1894-1904.
75. Kraynak M, Colman RJ, Flowers MT, Abbott DH, Levine JE. Ovarian estradiol supports sexual behavior but not energy homeostasis in female marmoset monkeys. *Int J Obes (Lond).* 2019;43(5):1034-1045.
76. Gonçalves FB, Gonçalves BSB, Cavalcante JS, Azevedo CVM. Aging-related changes on social synchronization of circadian activity rhythm in a diurnal primate (*Callithrix jacchus*). *Chronobiol Int.* 2020;37(7):1-13.
77. Ziegler TE, Sosa ME, Peterson LJ, Colman RJ. Using snacks high in fat and protein to improve glucoregulatory function in adolescent male marmosets (Callithrix jacchus). *J Am Assoc Lab Anim Sci.* 2013;52(6):756-62.
78. Kraynak M, Willging MM, Kuehlmann AL, Kapoor AA, Flowers MT, Colman RJ, Levine JE, Abbott DH. Aromatase Inhibition Eliminates Sexual Receptivity Without Enhancing Weight Gain in Ovariectomized Marmoset Monkeys*. J Endocr Soc.* 2022 Apr 22;6(6):bvac063. doi: 10.1210/jendso/bvac063. PMID: 35592515; PMCID: PMC9113444.
79. Hardman CD, Ashwell KWS. Stereotaxic and Chemoarchitectural Atlas of the Brain of the Common Marmoset (Callithrix jacchus). *CRC Press,* Boca Raton, FL, USA. 2012.
80. Emborg ME, Joers V, Fisher R, Brunner K, Carter V, Ross C, Raghavan R, Brady M, Raschke J, Kubota K, Alexander A. Intraoperative intracerebral MRI-guided navigation for accurate targeting in nonhuman primates. *Cell Transplant.* 2010;19(12):1587-97. doi: 10.3727/096368910X514323. Epub 2010 Jun 29. PMID: 20587170; PMCID: PMC3278961.
81. McCarthy MM. The two faces of estradiol: effects on the developing brain. *Neuroscientist.* 2009 Dec;15(6):599-610. doi: 10.1177/1073858409340924. PMID: 19700741; PMCID: PMC2795061.
82. Remage-Healey, L., London, S. E. & Schlinger, B. A. Birdsong and the neural production of steroids. *J Chem Neuroanat* 39, 72-81, doi:10.1016/j.jchemneu.2009.06.009 (2010)
83. Masamizu, Y. et al. Local and retrograde gene transfer into primate neuronal pathways via adeno-associated virus serotype 8 and 9. *Neuroscience* 193, 249-258, doi:10.1016/j.neuroscience.2011.06.080 (2011).
84. Nadler RD, Collins DC, Miller LC, Graham CE. Menstrual cycle patterns of hormones and sexual behavior in gorillas. *Horm Behav.* 1983;17(1):1-17.
85. Emborg, M. E. et al. Induced pluripotent stem cell-derived neural cells survive and mature in the nonhuman primate brain. Cell Rep 3, 646-650, doi:10.1016/j.celrep.2013.02.016 (2013).
86. de Backer MW, Brans MA, Luijendijk MC, Garner KM, Adan RA. Optimization of adeno-associated viral vector-mediated gene delivery to the hypothalamus. Hum Gene Ther. 2010 Jun;21(6):673-82. doi: 10.1089/hum.2009.169. PMID: 20073991.

87. Li J, Gibbs RB. Detection of estradiol in rat brain tissues: Contribution of local versus systemic production. *Psychoneuroendocrinology*. 2019 Apr;102:84-94. doi: 10.1016/j.psyneuen.2018.11.037. Epub 2018 Dec 1. PMID: 30529907.
88. Rossetti MF, Cambiasso MJ, Holschbach MA, Cabrera R. Oestrogens and progestagens: synthesis and action in the brain. *J Neuroendocrinol.* 2016;28(7).
89. Muhammad A, Ibrahim MA, Erukainure OL, Malami I, Sani H, Mohammed HA. Metabolism and toxicological implications of commonly used chemopreventive drugs against breast cancer/carcinogenesis. *Curr Drug Metab*. Accessed Nov 16, 2016. Epub ahead of print.
90. Ghizzani A, Bruni S, Luisi S. The sex life of women surviving breast cancer. *Gynecol Endocrinol.* 2018;34(10):821-825.
91. Lizcano F, Guzmán G. Estrogen deficiency and the origin of obesity during menopause. *Biomed Res Int.* 2014;2014:757461.
92. Kohn GE, Rodriguez KM, Hotaling J, Pastuszak AW. The history of estrogen therapy. *Sex Med Rev.* 2019;7(3):416-421.
93. Assogba ELF, Kamga AM, Costaz H, et al.. What are young women living conditions after breast cancer? Health-related quality of life, sexual and fertility issues, professional reinsertion. *Cancers (Basel)6* 2020;12(6):1564.
94. Gibb FW, Dixon JM, Clarke C, et al.. Higher insulin resistance and adiposity in postmenopausal women with breast cancer treated with aromatase inhibitors. *J Clin Endocrinol Metab.* 2019;104(9):3670-3678.
95. Gennari L, Merlotti D, Nuti R. Aromatase activity and bone loss. *Adv Clin Chem.* 2011;54:129-164.
96. Sriprasert I, Hodis HN, Bernick B, Mirkin S, Mack WJ. Effects of estradiol dose and serum estradiol levels on metabolic measures in early and late postmenopausal women in the REPLENISH Trial. *J Womens Health (Larchmt).* 2020;29(8):1052-1058.
97. Naftolin F, Friedenthal J, Nachtigall R, Nachtigall L. Cardiovascular health and the menopausal woman: the role of estrogen and when to begin and end hormone treatment. *F1000Res.* 2019;8:F1000 Faculty Rev-F1000 Faculty1576.
98. Ellis AJ, Hendrick VM, Williams R, Komm BS. Selective estrogen receptor modulators in clinical practice: a safety overview. *Expert Opin Drug Saf.* 2015;14(6):921-934.
99. Merchenthaler I, Lane M, Sabnis G, et al.. Treatment with an orally bioavailable prodrug of 17β-estradiol alleviates hot flushes without hormonal effects in the periphery. *Sci Rep.* 2016;6:30721.
100. Clegg DJ, et al.. Sex Hormones and Cardiometabolic Health: Role of Estrogen and Estrogen Receptors. *Endocrinology* 2017;158(6):1095-1105.
101. Al-Safi ZA, Polotsky AJ. Obesity and menopause. *Best Pract Res Clin Obstet Gynaecol.* 2015;29(4):548-553.
102. Davis SR, Castelo-Branco C, Chedraui P, et al.; Writing Group of the International Menopause Society for World Menopause Day 2012. Understanding weight gain at menopause. *Climacteric.* 2012;15(5):419-429.

103. Bracht JR, Vieira-Potter VJ, De Souza Santos R, Öz OK, Palmer BF, Clegg DJ. The role of estrogens in the adipose tissue milieu. *Ann N Y Acad Sci.* 2020;1461(1):127-143.
104. Ryan AS, Nicklas BJ, Berman DM. Hormone replacement therapy, insulin sensitivity, and abdominal obesity in postmenopausal women. *Diabetes Care.* 2002;25(1):127-133.
105. Moreno M, Ordoñez P, Alonso A, Díaz F, Tolivia J, González C. Chronic 17beta-estradiol treatment improves skeletal muscle insulin signaling pathway components in insulin resistance associated with aging. *Age (Dordr).* 2010;32(1):1-13.
106. Wegorzewska IN, Walters K, Weiser MJ, et al.. Postovariectomy weight gain in female rats is reversed by estrogen receptor alpha agonist, propylpyrazoletriol. *Am J Obstet Gynecol.* 2008;199(1):67.e1-67.e5.
107. de Souza Santos R, Feijó da Silva Santos A, Clegg DJ, Iannetta O, Marchini JS, Marques Miguel Suen V. Overweight postmenopausal women with different plasma estradiol concentrations present with a similar pattern of energy expenditure and substrate oxidation rate before and after a fatty meal challenge. *Clin Nutr ESPEN.* 2016;15:21-27.
108. Shea KL, Gavin KM, Melanson EL, et al.. Body composition and bone mineral density after ovarian hormone suppression with or without estradiol treatment [published correction appears in *Menopause*. 2018;25(3):359]. *Menopause* 2015;22(10):1045-1052
109. Gambacciani M, Ciaponi M, Cappagli B, Genazzani AR. Effects of low-dose continuous combined conjugated estrogens and medroxyprogesterone acetate on menopausal symptoms, body weight, bone density, and metabolism in postmenopausal women. *Am J Obstet Gynecol.* 2001;185(5):1180-1185.
110. Lahmann PH, Lissner L, Gullberg B, Berglund G. Sociodemographic factors associated with long-term weight gain, current body fatness and central adiposity in Swedish women. *Int j Obes Relat Metab Disord.* 2000;24(6):685-694.
111. Salpeter SR, Walsh JM, Ormiston TM, Greyber E, Buckley NS, Salpeter EE. Meta-analysis: effect of hormone-replacement therapy on components of the metabolic syndrome in postmenopausal women. *Diabetes Obes Metab.* 2006;8(5):538-554.
112. Chmouliovsky L, Habicht F, James RW, Lehmann T, Campana A, Golay A. Beneficial effect of hormone replacement therapy on weight loss in obese menopausal women. *Maturitas.* 1999;32(3):147-153.
113. dos Reis CM, de Melo NR, Meirelles ES, Vezozzo DP, Halpern A. Body composition, visceral fat distribution and fat oxidation in postmenopausal women using oral or transdermal oestrogen. *Maturitas.* 2003;46(1):59-68.
114. O'Sullivan AJ, Hoffman DM, Ho KK. Estrogen, lipid oxidation, and body fat. *N Engl J Med.* 1995;333(10):669-670.
115. Duncan AC, Lyall H, Roberts RN, et al.. The effect of estradiol and a combined estradiol/progestagen preparation on insulin sensitivity in healthy postmenopausal women. *J Clin Endocrinol Metab.* 1999;84(7):2402-2407.
116. Mattiasson I, Rendell M, Törnquist C, Jeppsson S, Hulthén UL. Effects of estrogen replacement therapy on abdominal fat compartments as related to

glucose and lipid metabolism in early postmenopausal women. *Horm Metab Res.* 2002;34(10):583-588.
117. Sites CK, L'Hommedieu GD, Toth MJ, Brochu M, Cooper BC, Fairhurst PA. The effect of hormone replacement therapy on body composition, body fat distribution, and insulin sensitivity in menopausal women: a randomized, double-blind, placebo-controlled trial. *J Clin Endocrinol Metab.* 2005;90(5):2701-2707.
118. Saltzman W, Abbott DH, Binkley N, Colman RJ. Maintenance of bone mass despite estrogen depletion in female common marmoset monkeys (Callithrix jacchus). *Am J Primatol.* 2019;81(2):e2905.
119. Power ML, Adams J, Solonika K, Colman RJ, Ross C, Tardif SD. Diet, digestion, and energy intake in captive common marmosets (Callithrix jacchus): research and management implications. *Sci Rep.* 2019;9(1):12134.
120. Riesche L, Tardif SD, Ross CN, deMartelly VA, Ziegler T, Rutherford JN. The common marmoset monkey: avenues for exploring the prenatal, placental, and postnatal mechanisms in developmental programming of pediatric obesity. *Am J Physiol Regul Integr Comp Physiol.* 2018;314(5):R684-R692.
121. Yang JA, Yasrebi A, Snyder M, Roepke TA. The interaction of fasting, caloric restriction, and diet-induced obesity with 17β-estradiol on the expression of KNDy neuropeptides and their receptors in the female mouse. *Mol Cell Endocrinol.* 2016;437:35-50.
122. Kemnitz JW, Sladky KK, Flitsch TJ, Pomerantz SM, Goy RW. Androgenic influences on body size and composition of adult rhesus monkeys. *Am J Physiol.* 1988;255(6 Pt 1):E857-E864.
123. Elbers JM, Asscheman H, Seidell JC, Gooren LJ. Effects of sex steroid hormones on regional fat depots as assessed by magnetic resonance imaging in transsexuals. *Am J Physiol.* 1999;276(2):E317-E325.
124. Obici S, Rossetti L. Minireview: nutrient sensing and the regulation of insulin action and energy balance. *Endocrinology.* 2003;144(12):5172-5178.
125. Obici S, Zhang BB, Karkanias G, Rossetti L. Hypothalamic insulin signaling is required for inhibition of glucose production. *Nat Med.* 2002;8(12):1376-1382.
126. Pocai A, Lam TK, Gutierrez-Juarez R, et al.. Hypothalamic K(ATP) channels control hepatic glucose production. *Nature.* 2005;434(7036):1026-1031.
127. Wachtman LM, Kramer JA, Miller AD, Hachey AM, Curran EH, Mansfield KG. Differential contribution of dietary fat and monosaccharide to metabolic syndrome in the common marmoset (Callithrix jacchus). *Obesity (Silver Spring).* 2011;19(6):1145-1156.
128. Kaspareit J, Friderichs-Gromoll S, Buse E, Habermann G. Background pathology of the common marmoset (Callithrix jacchus) in toxicological studies. *Exp Toxicol Pathol.* 2006;57(5-6):405-410.
129. Sherigar JM, Castro J, Yin YM, Guss D, Mohanty SR. Glycogenic hepatopathy: A narrative review. *World j Hepatol.* 2018;10(2):172-185.
130. Pattison JC, Abbott DH, Saltzman W, Conley AJ, Bird IM. Plasticity of the zona reticularis in the adult marmoset adrenal cortex: voyages of discovery in the New World. *J Endocrinol.* 2009;203(3):313-326.

131. Mannerås L, Cajander S, Holmäng A, et al.. A new rat model exhibiting both ovarian and metabolic characteristics of polycystic ovary syndrome. *Endocrinology.* 2007;148(8):3781-3791.
132. Kemnitz JW, Sladky KK, Flitsch TJ, Pomerantz SM, Goy RW. Androgenic influences on body size and composition of adult rhesus monkeys. *Am J Physiol.* 1988;255(6 Pt 1):E857-E864.
133. Fox J, Miller MA, Newman MK, Turner CH, Recker RR, Smith SY. Treatment of skeletally mature ovariectomized rhesus monkeys with PTH(1-84) for 16 months increases bone formation and density and improves trabecular architecture and biomechanical properties at the lumbar spine. *J Bone Miner Res.* 2007;22(2):260-273.
134. Colman RJ, Kemnitz JW, Lane MA, Abbott DH, Binkley N. Skeletal effects of aging and menopausal status in female rhesus macaques. *J Clin Endocrinol Metab.* 1999;84(11):4144-4148.
135. Florio M, Gunasekaran K, Stolina M, et al.. A bispecific antibody targeting sclerostin and DKK-1 promotes bone mass accrual and fracture repair. *Nat Commun.* 2016;7:11505.
136. Havill LM, Levine SM, Newman DE, Mahaney MC. Osteopenia and osteoporosis in adult baboons (Papio hamadryas). *J Med Primatol.* 2008;37(3):146-153.
137. Seidlová-Wuttke D, Schlumbohm C, Jarry H, Dullin C, Wuttke W. Orchidectomized (orx) marmoset (Callithrix jacchus) as a model to study the development of osteopenia/osteoporosis. *Am J Primatol.* 2008;70(3):294-300.
138. Chalmers DT, Murgatroyd LB, Wadsworth PF. A survey of the pathology of marmosets (Callithrix jacchus) derived from a marmoset breeding unit. *Lab Anim.* 1983;17(4):270-279.
139. Baxter VK, Shaw GC, Sotuyo NP, et al.. Serum albumin and body weight as biomarkers for the antemortem identification of bone and gastrointestinal disease in the common marmoset. *PLoS One.* 2013;8(12):e82747.
140. Abbott DH. Reproduction in nonhuman primates. In: Skinner MK, ed. *Encyclopedia of Reproduction,* Vol. 6. Elsevier; 2018: 672–677.
141. Abbott DH, Barnett DK, Colman RJ, Yamamoto ME, Schultz-Darken NJ. Aspects of common marmoset basic biology and life history important for biomedical research. *Comp Med.* 2003;53(4):339-350.

3. CHAPTER THREE: Hypothalamic *ESR1* Knockdown Induces Weight Gain and Reduces Morning Activity in Adult Female Rhesus Macaques

Willging MM, Greinwald EP, Jacobs AM, Byington NC, Woida AM, Uhlrich DJ, Flowers MT, Kapoor AA, Williams SM, Marrah R, Abbott DH, and Levine JE.

[Manuscript is being prepared for submission to Journal of the Endocrine Society. Contribution to this manuscript: Designed/carried out experiments, analyzed data, and prepared the manuscript for this thesis and subsequent publication]

3.1 Abstract

Estradiol (E_2), the major bioactive estrogen, has been well documented as a major regulator of female metabolism in rodents. Estrogen receptor alpha (ERα) in the ventromedial nucleus (VMN) and arcuate nucleus (ARC) of the mediobasal hypothalamus (MBH) is the predominate estrogen receptor mediating female rodent metabolic homeostasis. In primates, however, it remains unknown if hypothalamic ERα similarly mediates E_2 metabolic actions. We hypothesized that reducing expression of ERα in the VMN and ARC of female rhesus macaques would induce metabolic dysfunction by way of increased body weight, hyperphagia, decreased energy expenditure and insulin insensitivity. Adult female rhesus macaques were randomly assigned to one of two conditions: (1) control, scrambled shRNA (control, n=5) and (2) selective ERα protein knockdown with *ESR1* gene silencing shRNA (ERαKD, n=6). MRI-guided neural viral vector infusion surgery enabled delivery of scrambled or gene silencing shRNA into our target regions, VMN and ARC. Neurohistochemical visualization of green fluorescent protein (GFP) infected neurons confirmed accuracy of targeting as well as quantification of hypothalamic density and intensity of ERα protein expression at study completion. ERα expression was successfully diminished in our target regions of interest (ROIs); VMN ROIs of VMNv ($p=0.03$) and VMNd1 ($p=0.05$) and in ARC ROIs of ARC ($p=0.02$) and ARCd ($p=0.02$). The ERαKD group presented with increased cumulative body weight % change (AUC, $p=0.02$) and decreased morning locomotion between 0600h-0900h ($p<0.01$). In both control and ERαKD female groups, ERα density in the ARC trended to be negatively correlated with body weight % change AUC ($p=0.08$). Together, our findings highlight

ERα activation within hypothalamic nuclei as crucial for regulating metabolic homeostasis in female NHPs, and likely, women.

3.2 Introduction

The major bioactive estrogen, E_2, is synthesized throughout the body by aromatase, a cytochrome P450 enzyme, encoded by the CYP19A1 gene[1-4]. While the main source of E_2 is synthesized in the ovaries, E_2 is also produced in extra-ovarian sites including adipose tissue, adrenal glands, skin, bone, pituitary gland, and multiple brain areas[1-4]. Rodent research has shown estrogen receptor alpha (ERα), encoded by the gene, *ESR1*, to be the predominant estrogen receptor involved in female energy balance[5-8], yet this has not yet been determined in nonhuman primates (NHPs). In female rodents, E_2 activates ERα in both the ventromedial nucleus (VMN) and arcuate nucleus (ARC) of the hypothalamus to initiate downstream neuroendocrine metabolic effects. In many experimental animal models, ovarian E_2 regulates body weight and composition, energy balance, and glucoregulation[9]. In rodent models, ovarian E_2-regulated control mechanisms are well established since OVX mediated E_2 depletion reliably disrupts energy balance, including, increased body weight and visceral adiposity, reduced physical activity and energy expenditure[10,11], and diminished insulin sensitivity[10]. All of these effects on metabolic function can be diminished or reversed by E_2 replacement[12,13]. Further, these E_2 actions are mediated by ERα, as complete knockout of *ESR1* in female mice (ESR1KO) increases body weight, adiposity and diminishes energy metabolism producing a phenotype that largely mimics that observed in long-term OVX mice[14]. Resulting from the vast research on the metabolic impact of ovarian E_2 via ERα in rodents, multiple mechanisms have been identified by which E_2 regulates of female energy balance. These include direct actions of E_2 on metabolically active tissues such as adipose tissue, liver, muscle, and pancreas[15], E_2 activation of brown fat (BAT) via the

sympathetic nervous system (SNS)[16] and E_2-induced alterations in neural and peripheral control of food intake and energy expenditure. Rodent models of ovarian E_2 regulation have also highlighted the critical role of neural ERα signaling in hypothalamic nuclei, VMN and ARC, to maintain energy homeostasis[8,17]. Importantly, one study demonstrated that viral vector mediated *ESR1* gene silencing in the VMN of both female mice and rats largely recapitulates a metabolic phenotype observed in complete ERα knockout mice, including obesity, hyperphagia, impaired glucose tolerance and reduced energy expenditure[8]. It remains unknown whether the same mechanisms of E_2 signaling, and metabolic regulation apply to female NHPs and women. Human studies suggest declining serum E_2 levels during the menopausal transition are associated with reduced energy expenditure and activity, increased central adiposity and insulin resistance[12,13,18-20], but not all studies are consistent in these regards. In additional recently completed studies, we examined the role of ERα in the regulation of metabolic function in a female new-world, NHP, the common marmoset monkey (Chapter 2). Using a viral vector containing either a scrambled shRNA without known gene targets (control treatment) or gene silencing shRNA targeting *ESR1*, we assessed the metabolic effects of diminishing ERα protein expression in the mediobasal hypothalamus (MBH) of adult female marmoset monkeys. Our results suggested hyperglycemia and a reduction in daily caloric intake, despite increased body weight, induced by reduced ERα expression in VMN and ARC neurons in the MBH (Chapter 2), as found in female mice[8]. Taken together, our controlled NHP studies provide the first evidence that hypothalamic ERα signaling, in a diet-induced obesity (DIO) environment, is critically important in regulating energy balance in female NHPs. Moreover, recent research from our laboratory has shown that in female marmoset

monkeys, depletion of ovarian or both ovarian and extra-ovarian E_2 production removes protection from diet-induced obesity (DIO) and increased daily calorie consumption, suggesting that E_2 plays an important role in metabolic regulation in female NHPs (Chaper 2), and thus, possibly likely women[21].

These findings reveal the importance of E_2 produced by the ovary, alone, as the primary organ source for E_2 activating hypothalamic ERα in at least one female primate NHP. Being able to replicate these findings that E2 signaling hypothalamic ERα mediates similar regulation of metabolic homeostasis in a female NHP model with greater genetic, developmental, and physiological similarities to humans, such as rhesus macaques, will therefore be crucial to understanding how E_2 regulates female energy homeostasis and neuroendocrine-related functions in humans.

3.3 Methods

Animals

Eleven adult female rhesus macaques (6-11 years of age) from the Wisconsin National Primate Research Center colony were randomized based on age, body weight and body mass index (BMI) into two groups: 1) estrogen receptor knockdown (ERaKD; n=6) in which monkeys received a viral vector infusion of a gene silencing shRNA targeting *ESR1* in the VMN and ARC of the hypothalamus and 2) scrambled control (scrambled control, SC; n=5) in which monkeys received a scrambled shRNA instead (Table 1). Monkeys were maintained in these two groups for ~34 months, pair-housed, in enclosures under 12-h lighting, ambient temperature of ~27°C and humidity of ~50%. (Figure 1). The protocol for this study was approved by the Animal Care and Use Committee of the Office of the Vice Chancellor for Graduate Research and Education of

the University of Wisconsin–Madison, an AAALAC-accredited program. Animals were fed chow twice a day, between 0700h-0900h and 1200h-1400h (Teklad Global 20% Protein Primate Diet, ENVIGO, Madison, WI). The calorie distribution of the biscuits was 29% protein, 14% fat and 57% carbohydrates with an energy density of 2.8 kcal/g. Animals were supplemented with daily fruit enrichment (<100 kcals), weekly tactile enrichments (<100 kcals), and weekly destructible enrichments (<100 kcals).

Neural Infusion Surgery and Knockdown of ERα

OVX adult female rhesus monkeys received bilateral stereotaxic injections into the hypothalamic VMN and ARC of adeno-associated virus 8 (AAV8) expressing shRNA targeting *ESR1* for *in vivo* RNAi, and thus diminishing *ESR1* translation into ERα (ERαKD, n=6), or a control scrambled shRNA (Control, n=5). Treatment onset (0 months) was the day of neural infusion surgery.

Since accurate, within-brain placement of viral vector was essential for gene silencing efficacy and specificity, we used a single, presurgical, neuro-anatomical MRI scan to refine the unique locations of each VMN and ARC within each rhesus macaque, refined and adapted from[22]. To accomplish this, each female rhesus macaque was food deprived overnight, sedated with an intramuscular (IM) injection of ketamine (10 mg), anesthesia was continued with an IM injection of meloxicam (2 mg), 10 ml isotonic saline was injected subcutaneously (SC) to provide fluid administration and atropine (0.218 mg) was administered IM, followed by placement of the rhesus macaque into an MRI-compatible stereotaxic frame. Lateral placements of both left and right earbars, as well as vertical placements of palate and left and right eye bars, were all noted. Three-dimensional coordinate locations of both left and right VMN and ARC were subsequently

obtained from an ~23 min, T1 MRI anatomical scan adapted for rhesus monkeys[23] in a next-generation 3T MRI system MR750 (GE Healthcare, Waukesha, WI) and performed at least 3 days prior to viral vector infusion (Figure 2).

Each presurgical scan employed a 3-inch surface coil and comprised 3D T1-weighted (T1W) images with an inversion-recovery (IR) prepped, fast gradient-echo (IR-fGRE) sequence adapted for rhesus monkeys[23]. Scanning parameters included an inversion time (TI) of 450 ms, repetition time (TR) of 6.8 ms, echo time (TE) of 2.9 ms, and receiver bandwidth of 62.5 kHz. The matrix size was 256 × 256 × 128 (X × Y × Z). The 3D T1W scans produced 248 coronal 0.3-mm-thick contiguous slices. Using coronal slices incorporating the hypothalamus from each monkey's presurgical scan, we utilized contrast-agent filled earbars in the stereotaxic frame to provide a rostral-caudal (RC) zero plane (Z coordinates), the middle of the 3rd ventricle at the level of the mediobasal hypothalamus to generate a medial zero plane (X coordinates), and the farthest lateral point of each earbar to provide a dorso-ventral zero plane for right and left sides separately (X coordinates). Based on these 3D parameter sets, target coordinates for entry into the skull, as well as for rostral, medial-rostral, medial-caudal and caudal left and right VMN, and analogous locations for both left and right ARC, were estimated based on marmoset neuroanatomy atlas coordinates[23].

For viral vector infusion surgery, each rhesus macaque was sedated and prepped as described for their presurgical MRI scan. In addition, each monkey received buprenorphine (0.072 mg) and cefazolin (174.9 mg) and was intubated with anesthesia continuing under isoflurane (1-2%). Each rhesus macaque was re-positioned into similar stereotaxic frame parameters as noted during for their presurgical MRI scan. Vital signs

(heart rate, blood oxygen, respiration, and temperature) were regularly monitored during the procedure and the animals were wrapped for warmth. A series of small-volume, subcutaneous (SC) injections of lidocaine (6 mg, total) were given along the anticipated incision site to provide local anesthesia. A ~60mm incision was made on the top of the animal's head. Stereotaxic coordinates, estimated from our pre-surgery anatomical MRI scan, allowed calculation for the insertion sites of a 22-gauge guide cannula housing a 28-gauge stylet to target the VMN and ARC in the hypothalamus. The estimated midline location between the medial sites for both VMN and ARC was marked on the skull to enable excision of a ~15 mm diameter portion of skull using a surgical bone drill. A micromanipulator, with cannula holder and guide cannula with screw-in solid stylet, were placed on the stereotaxic frame to confirm midline of the brain from the medial location of the superior sagittal sinus, and presurgical scan estimated target coordinates for left VMN and ARC sites were revised accordingly. A 27g needle, customized into a miniature scalpel blade, was used to open a ~10mm incision in the dura mater about 5-7mm to the right of the mid-sagittal sinus, lateral to potential hypothalamic locations on the right side of the rhesus monkey brain, to permit a 4-degree-to-the-vertical angled approach.

At a trajectory angle of 4° (offset from vertical, 0°), with the flaps of the dura held apart, a 22-gauge guide cannula housing a sterile 28-gauge stylet was lowered into the medial-rostral estimated extent of the right ARC[24,25]. The stylet was then replaced by a 28-gauge infusion cannula attached to a Hamilton syringe controlled by a programmable infusion pump, A solution of viral vector (~3.06 x 10^{10} packaged genomic particles of AAV8 in 12.0 µL of sterile saline) mixed with gadolinium-containing Multihance MRI

contrast agent (2 mM gadobenate dimeglumine, Bracco Diagnostics Inc.), was infused at 2 µL per minute for a total of six minutes. The AAV8 virus utilized in this study was shown to readily infect neurons[26] and was without notable inflammation in NHP brain[24]. To minimize dorsal tracking of viral particles and contrast agent when the guide and infusion cannulae were raised, there was a 5-min delay following cessation of infusion before the cannulae were raised approximately 1 mm to the VMN infusion site, all at a 4 degree-angle-to-the vertical. Viral vector infusion and delayed raising of the cannula were then performed at the VMN, as undertaken at the ARC. The infusion cannula alone was raised and removed from the guide cannula to permit its flushing of sufficient fluid while outside the brain to confirm infusion integrity of the system. The stylet was re-positioned inside the guide cannula. Both guide cannula and stylet were initially raised 0.5 mm, pausing for 30 sec to minimize dorsal tracking of viral particles and contrast agent, and then both were gradually removed from the brain. Superficial skin sutures were placed using 4/0 vicryl suture to temporarily close the incision site during transfer to the MRI scanning room while the rhesus macaque remained in the stereotaxic frame.

The contrast agent remaining at the right medial ARC and VMN infusion sites was used to confirm accuracy of the infusion site location from a mid-surgery, ~23-min MRI T1 scan obtained approximately 20 min following the first infusion on the right side. When necessary, presurgical scan estimated target coordinates for right VMN and ARC sites were revised. Guide cannula, stylet and infusion cannula insertion, infusion and removal procedures were then repeatedly performed to enable AAV8 infusion into rostral, medial-rostral, medial-caudal and caudal VMN and ARC target sites on the right side of the brain.

Following all right side infusions, a 27g needle customized into a miniature scalpel blade, was used to open a ~10mm incision in the dura mater about 5-7mm to the left of the mid-sagittal sinus, lateral to potential hypothalamic locations on the left side of the rhesus monkey brain, to permit a 4-degree-to-the-vertical angled approach. A similar series of procedures, infusions, and MRI scan were performed on the left side of the brain analogous to those performed on the right. When necessary, adjustments to presurgical estimates for rostral, medial-rostral, medial-caudal and caudal left VMN and ARC target sites were made following the 2nd within-surgery MRI scan.

Efficacy of RNAi activity for shRNA specific to ESR1 and absence of RNAi in control scramble sequence shRNA

Two viruses were designed for this experiment, 1) ERα34 shRNA driven by the H1 promoter and 2) ERα78 shRNA driven by the U6 promoter. Vector Biolabs performed all recombinant AAV8 production, and the Dharmacon shRNA design center online was employed to design the shRNAs. Candidate shRNAs were only advanced to the next round if the chosen sequence was identical in marmoset and rhesus monkeys, human and mouse. Furthermore, candidate shRNAs were required to target a region of ERα that was common to all isoforms. Candidates were further scrutinized by examining potential off-target effects using BLAST analysis against the database for rhesus monkeys.

We obtained the AAV-H1-EGFP (green fluorescent reporter gene) or AAV-U6-RFP (red fluorescent reporter gene) plasmids from Vector Biolabs that were pre-designed, and then cloned in the shRNA sequence that we designed. Once the shRNA was chosen, and cloning completed, we transfected the shRNA expressing plasmids into MCF7 cells (a human breast cancer cell line with estrogen, progesterone, and glucocorticoid reporters[27]

at two different doses compared to mock transfected cells and ERα protein expression assessed by western blot quantified the ability of each shRNA to knockdown ERα. The pAAV-H1-ERa34-EGFP plasmid was used to transfect MCF7 cells to validate the knockdown. Three candidate shRNA were screened: ERα12, ERα34, ERα56. After initial screening all three shRNAs, ERα34 and ERα56 were more successful than ERα12 (validation blots, Figure 3) so ERα34 and ERα56 were compared in the follow up experiment.

The ERα78 shRNA sequence mimicked that of the ERα34 shRNA, except the leading nucleotide was changed from "A" to "G" to make it more compatible and efficient when employing the U6 promoter. Additionally, the pAAV-H1-ERα34-EGFPengaged the GFP reporter for identifying hypothalamic areas infected during subsequent neuroimmunohistochemical morphological analyses, and the pAAV-U6-ERα78-RFP engaged the RFP reporter for subsequent identification of infected hypothalamic areas. The oligos used for subcloning the shRNAs into the pAAV-H1-GFP and pAAV-U6-RFP plasmids are illustrated in Figure 4.

Immunohistochemical processing of rhesus monkey brain for visualizing and quantifying green or red fluorescent protein (GFP or RFP) and ERα protein expression

Following upper body perfusion with 4% paraformaldehyde (PFA) (pH 7.6) at necropsy, each female rhesus macaque brain was removed, post-fixed at 4C for an additional 12-16h and cryoprotected in graded (10-30%) sucrose/PBS (pH 7.2) solutions. Each post-fixed, dehydrated brain was placed in a customized plastic mold designed to accommodate the dorsal surface of an adult rhesus brain and expose the ventral surfaces landmarks, enabling placement of mold-guided, microtome blades cutting the brain into

coronal plane portions. The medial rostral-caudal portion (~8-10 mm), including the hypothalamus, was separated, comprising immediately rostral to the optic chiasm to immediately caudal to the mammillary bodies. This medial rostral-caudal portion of whole-brain was cryosectioned into consecutive 40µm frozen sections in the coronal plane to include the rostral-caudal extent of the hypothalamus from the rostral extent of the mPOA to the caudal extent of the ARC.

Immunohistochemistry (IHC) procedures for ERα, GFP (control monkeys) and RFP (ERαKD monkeys). Cryo-sections of 40 µm, at regular intervals, were immunostained for ERα using the mouse monoclonal antibody, 6F11 (Thermo Fisher Scientific, Hampton, NH)[29]. DAB-staining was subsequently used to detect specific primary antibody binding. Sections adjacent to those selected for ERα immunostaining were stained for GFP using the rabbit polyclonal antibody, AB3080 (MilliporeSigma, Burlington, NH)[30] (control monkeys) or for RFP using the polyclonal antibody, R10367 (Invitrogen, Waltham, MA) (ERαKD monkeys).

Confirmation of neural targeting accuracy from immunohistochemical analyses of GFP or RFP expression in the mediobasal hypothalamus

Digital images from coronal brain sections immunostained for GFP and RFP were obtained with a Nikon Eclipse Ti microscope and Nikon NIS Elements software. Images were acquired of the hypothalamus and peri-hypothalamic areas from the rostral preoptic area to the caudal arcuate nucleus and mammillary bodies at 4x objective. Each hypothalamic section image was the composite of several images stitched together by the Nikon system during the photo acquisition process. As illustrated by a coronal section from approximately the mid-rostral-caudal extents of VMN and ARC within the

hypothalamus (Figure 5), abundant GFP-immunoreactive (ir) labeling was demonstrated in VMN (Figure 5B) and ARC (Figure 5B) from a control monkey, and in VMN and ARC (Figure 5C) from an ERαKD monkey. Selected images from each rostral-caudal series of coronal sections of GFP-ir labeling, including the POA, VMN and ARC, for each rhesus macaque were positioned at appropriate rostral-caudal locations associated with quantification of ERα immunostaining, as illustrated in Figure 5 for a representative control (Figure 5A) and ERαKD female rhesus monkeys (Figure 5C) to confirm AAV8 infection in both VMN and ARC.

Analysis of Neural Targeting of ERα Gene Silencing

Digital images from sections immunostained for ERα were obtained as described above for GFP and RFP imaging and analyzed with NIS Elements Advanced Research (AR) image analysis software (ver. 5.02) was then used to quantify the amount of ERα-immunoreactive (ir) labeling in the POA, VMN and ARC, employing measures of cell counts, cell density per unit area (number of cells/mm^2), and labeling intensity (pixel intensity) of individual cells. Labeled cells were detected using the NIS Elements AR Dark Spot Detection feature. The contrast threshold in the detection algorithm was determined for each monkey by adjusting contrast settings in the spot detection algorithm to match cell counts made by three observers on a series of six cropped images of the hypothalamic section to be analyzed. Observer counts differed by less than 15 %, and NIS threshold values were adjusted so NIS-derived cell counts fell within 5% of the average counts of all observers. The NIS threshold value for labeled cells was then applied across all hypothalamic sections to derive cell counts for that monkey.

The NIS Elements AR software calculated the mean pixel intensity of each identified cell, and we used this to estimate the intensity of ERα staining. Threshold staining intensity was determined by the threshold process described above, and the threshold value was quantified as lowest 1% intensity of all stained cells. The darkest staining label was defined as the pixel intensity of the darkest 2% of ERα expressing cells; these were typically a subset of cells in the POA and anterior pituitary, which were distant from the infusion and served as a positive control within each monkey. This established a range from threshold to dark for each monkey. Staining of each labeled cell was normalized within this range, and staining intensity measures were calculated from the normalized intensity values.

Density of individual neuronal nuclear immunostaining for ERα in each of the hypothalamic areas was determined by counting the number of immunostained neurons within regions of interest (ROIs) of 1000μm X 500μm ellipses (areas of 0.395 mm^2) positioned within POA, VMN and ARC. Multiple ROIs were used in the VMN (VMNv, VMN, VMNd1, VMNd2, ventral to dorsal) and ARC (ARC and ARCd) because of the broad extent of the ERα cells they contained (Figure 6). For each hypothalamic ROI within each female, we used the average of the three most densely-staining sections as an overall density measure for that ROI.

Quantitative analyses were performed on digital images obtained while the microscope lens was focused on the middle depth of each hypothalamic section. At that focal point, the depth of field with a 4X objective allowed visualization of labeled cells throughout the entire depth of the hypothalamic section (Chapter 2). To confirm validity of this strategy, we compared cell counts from images acquired when focus was on the

surface of the hypothalamic section, middle of the hypothalamic section and bottom of the hypothalamic section. Cell counts obtained from center-focused images varied less than 5% from those obtained from top-of-section or bottom-of-section focused images.

Hormone and Metabolic Analyte Determinations

Steroid hormone analysis was adapted from methods previously described[31,32]. Briefly, internal standard was added to rhesus serum samples (1mL) and then they were extracted twice using methyl tert butyl ether followed by dichloromethane. Samples were derivatized using dansyl chloride and then analyzed by LC-MS/MS (Sciex QTRAP 5500). Individual calibration curves were constructed for each analyte with at least 8 points. The linearity was $r > 0.9990$ and the curve fit was linear with $1/x$ weighting. None of the compounds of interest were detected in blank or double blank samples. Inter-assay coefficient of variation was determined by 3 levels of human serum and ranged from 5.6-9.7%.

Body Weight, Body Composition & Bone Mass

Animals were weighed weekly. Incremental area under the curve (AUC) assessment of weight parameters over time, calculated by the trapezoid rule, was used to better detect recurring differences in weight gain. At ~18 months post-neurosurgery and ~28 months post- neurosurgery, total body composition was assessed by dual-energy X-ray absorptiometry (DXA, iDXA, GE/Lunar Corp., Madison, WI) on sedated animals. Monkeys received up to 7 mg/kg ketamine IM and up to 0.03 mg/kg dexmedetomidine IM, to be reversed on conclusion of the procedure by up to 0.3 mg/kg atipamezole IM. After placing the anesthetized monkey onto the scanner bed, DXA-compliant cushioning was used to position the monkey with arms and tail flat on the

scanner bed, clearly distinct from it's trunk and other extremities. A DXA scan was then performed for approximately 30 minutes. The scanner room was maintained at 27-28°C during the performance of all scans to minimize the risk of hypothermia. Monitoring of anesthesia recovery was documented every 15 min until the monkey was sitting upright, then every 30 minutes until the animal was fully recovered from the anesthesia. Fat mass, fat-free mass, bone mineral content (BMC) and bone mineral density (BMD) were determined for total body as well as regions of interest, including abdomen, chest, thighs and extremities[33]. Body mass index was calculated using $\frac{Body\ Weight\ (kg)}{Crown\ Rump\ Length\ (m^2)}$ [34].

Somatometric Measurements

Somatometric parameters were measured using tape measure or calipers while monkeys were anesthetized for DXA imaging. Measurements included femur length; abdomen, chest, pelvis, arm, leg, and head circumferences; head diameter; and chest and abdomen skinfolds. Additionally, monkeys were placed on an osteometric board for measurement of crown rump and crown-heel lengths.

Indirect calorimetry

At ~28-months post treatment onset, monkeys were singly housed in a transparent metabolic chamber (75 cm x 75 cm x 80 cm (0.45 m^3) with respiratory system (Sable Systems, North Las Vegas, NV) for 48 hours. While occupying the chamber, each monkey was able to see and hear its cagemate or another monkey residing in a standard cage or another metabolic chamber within the same room; no other monkeys resided in the room. Monkeys were fed chow, fruit enrichment (~1,000 total kcal a day) split between two feeding periods, 0700h-1000h and 1200h-1400h while in the chamber. Oxygen (O_2) consumption and carbon dioxide (CO_2) productions

were measured. As determined by behavioral observations in an acclimation period of 24 hours, such circumstances were not stressful for these monkeys. Room air was drawn through the chamber and flow rate was continuously monitored. Exhaust air was sampled for analysis of O_2, and CO_2 content. Energy expenditure, respiratory quotient, daily, daytime and nighttime metabolic rate, and meal-induced thermogenesis, noted as the energy expenditure in the five hours post meal consumption, was determined from these data.

Locomotor Activity Assessment

At ~18 months and ~28 months post-treatment onset Actical accelerometers (Respironics, Murrysville, PA) were attached to a fabric collar and placed around each monkey's neck. Activity and intensity of movement were recorded over a ~4-week period after which the accelerometers were removed. Activity was recorded in counts (n), where one count represented body movements on an x, y, or z axis. The accelerometer sampled such activity counts every minute and these data were averaged for every hour (h), day (during lights on, 0600-1800 h), night (during lights off, 1800-0600 h), morning (0600–1200 h), afternoon (1200–1800 h), and over 24 hours. Incremental area under the curve activity values were also assessed to detect cumulative differences over the course of the study.

Caloric Intake Assessment

At ~28 months post-treatment onset, monkeys were singly housed 0700-1800 for 7-21 days. Monkeys were fed 9 biscuits of standard chow twice a day at 0700-0900 and 1200-1400. At each feeding, monkeys received on average ~423 kilocalories from chow. In addition, monkeys received daily fruit enrichment (i.e., pear, banana, green

pepper, kiwi and apple) totaling on average ~100 kilocalories per enrichment occurrence. Daily chow and enrichment were weighed prior to be given each day (Calories Offered). At 1800h, any chow or enrichment not consumed from the day was weighed (Calories Left) and returned to each monkey for the overnight period (1800h-0700h). Average calories (kcals) consumed was calculated by multiplying the weight (g) of chow consumed each day by the chow's energy density of 2.8 kcal/g and averaged over the 20-day food assessment period. Monkeys were repaired with their partner for the overnight period (1800h-0700h).

Intravenous Glucose Tolerance Test (ivGTT)

The ivGTT was conducted according to the Modified Minimal Model (MMM) protocol as adapted for rhesus monkeys[35]. A catheter was inserted through the saphenous or femoral vein and the tip positioned in the inferior vena cava. Four pretreatments ~1.5 ml blood samples were taken at approximately -15, -10, -5, and -1 minutes to establish fasted baseline values of insulin and glucose. A ~300 mg/kg glucose bolus was administered over about one minute starting at ~ 0 min, and ~1.5 ml blood samples were drawn at 2, 3, 4, 5, 6, 8, 10, 12, 14, 16, 19, 22, 23, 24, 25, 27, 30, 40, 50, 60, 70, 80, 90, 100, 120, 140, 160, and 180 minutes after glucose administration. Blood volume availability for individual animals was calculated by body weight (animal's body weight (kg) x 60 = estimated total volume of blood). If a monkey's blood volume availability did not meet the required volume for the full ivGTT (48 ml), samples at timepoints of 100, 120, 140 and/or 160 were omitted. Twenty minutes after glucose bolus administration, tolbutamide (~25mg/ml up to a maximum volume of ~5ml 1N sodium hydroxide, 0.1N hydrochloric acid in sterile saline solution) was administered

via the catheter to induce an additional increment in insulin secretion to enhance MMM calculations. Maintenance of catheter patency and fluid volume was accomplished with intravenous Plasma-Lyte A provided by an infusion pump hooked up to the indwelling catheter. Additional fluid replacement was provided by 1-2ml cannula line flushes following each blood sample withdrawal. The duration of anesthesia was approximately 240 minutes. Monkeys were maintained under warm heat lamps (with a 24-inch minimum space between the monkey and the heating lamp), a heated air warming unit and/or a water-circulating heating pad. During the procedure, each monkey's blood oxygen, heart rate and rectal temperature were continuously monitored and recorded every 15 minutes. After completion of the procedure, progress of anesthesia recovery was documented every 15 min until the monkey was sitting upright, then every 30 min until the monkey was fully recovered from the anesthesia.

Statistical Analysis

Data collected was analyzed utilizing GraphPad PRISM and SPSS software. Metabolic parameters collected at both time points (~18 mo and ~28 mo) were compared by ANOVA with repeated measures (RM-ANOVA). Neuronal nuclear ERα immunostaining intensity, immunostained cell density within neurons, as well as metabolic, endocrine and somatometric parameters were analyzed using independent t-tests to compare means. Plots are expressed as means+/-SEM. Relationships between hormones, metabolic parameters, and ERα immunostaining intensity and density were assessed via nonparametric Spearman's correlation tests. Statistical significance was determined as $p<=0.05$ and trending towards significance was determined as $0.05<p<0.1$.

3.4 Results

Targeted knockdown of ERα within VMN and ARC

ERαKD monkeys typically demonstrated less ERα protein density and ERα density*intensity in multiple VMN and ARC ROIs as determined by immunohistochemical analysis when compared to controls (Figure 7). In addition, ERα density was less in the VMN ROIs of VMNv (p=0.03) and VMNd1 (p=0.05) and ERα density*intensity was less in the VMNv (p=0.05) and tended to be less in the VMNd1 (p=0.06) in ERαKD monkeys compared to controls. Additionally, there was reduced ERα density in the ARC (p=0.02) and ARCd (p=0.02) and reduced ERα density*intensity in the ARC (p=0.02) and ARCd (p=0.03) in ERαKD compared to control monkeys.

Certain metabolic and hormone parameters involving all females combined across both groups correlated with degree of ERα knockdown in specific brain regions. In the ARC, there was a trend towards a negative correlation between body weight percent change AUC with ERα expression density (Figure 8A; R^2=0.33, p=0.08). In each of the VMNv, VMNd1, ARC, and ARCd, luteinizing hormone (LH) AUC between 18-30 months negatively correlated with ERα expression density (VMNv, R^2=0.58, p=0.02 (Figure 8B), VMNd1, R^2=0.42, p=0.057 (trend), ARC, R^2=0.75, p=0.001, ARCd, R^2=0.52, p=0.02) and ERalpha expression density x intensity (VMNd1, R^2=0.37, p=0.08 (trend), ARC, R^2=0.63, p=0.006, ARCd, R^2=0.48, p=0.03).

Steroid Hormones

There were no treatment differences observed in steroid hormone measurements of E_2, estrone (E_1), testosterone (T), androstenedione (A_4), DHEA, progesterone (P_4), 17-OHP, LH and FSH at baseline, 18-months, and 30-months post-treatment onset (Table

2). Area under the curve analyses of hormones revealed increased LH ($p<0.001$) and A_4 ($p=0.03$) between 18-months and 30-months of the study.

Body Composition

Weekly weight measurements were averaged for each month of the study. Body weight via AUC over the duration of the study was increased in ERαKD compared to control females ($p=0.01$, Figure 9A). Body weight percent change AUC was also increased in the ERαKD compared to the control females ($p=0.02$, Figure 9B). Although there was a cumulative increase in body weight % change over the course of the 34-month study in the ERαKD monkeys, DXA scans at 18-months and 28-months of the study indicated no differences between ERαKD and control females with regard to total fat mass (1st DXA, $p=0.39$; 2nd DXA, $p=0.38$) and total fat-free mass (1st DXA, $p=.18$; 2nd DXA, $p=0.33$) (Figure 10). Additionally, percent change of fat mass ($p=0.45$) and fat-free mass ($p=0.85$) between the 18-month and 28-month DXA scans did not differ between female groups (Figure 9). There were also no differences in fat mass or fat-free mass in any defined region of interest (abdomen, extremities, thigh, or head) between female groups (Table 3).

Caloric Intake

There were no differences between female groups in average kcals consumed ($p=0.29$, Figure 11) or average kcals assumed when adjusted for kilogram of body weight ($p=0.12$, Figure 11). There was a trend, however, towards reduced kcal consumed when adjusted for kilogram of FFM in the ERαKD compared to control females ($p=.085$, Figure 11).

Indirect Calorimetry

The metabolic chamber analysis enabled investigation into energy expenditure (EE) per minute (EE/min) with EE values adjusted for kilogram of fat-free mass. Cumulative EE assessed via AUC analysis indicated there were no female group differences in EE over the course of the 48-hour period the monkeys occupied the metabolic chambers (Figure 12). More specifically, there was also no difference in averaged EE with or without being adjusted for fat-free mass for 24-hours ($p=0.80$, w/FFM adjustment, $p=0.35$, Figure 13) daytime EE, defined as 0600-1800 ($p=0.53$, w/FFM adjustment, $p=0.31$, Figure 13) and nighttime EE, defined as 1800-0600 ($p=0.65$, w/FFM adjustment, $p=0.59$, Figure 13) between female groups. Energy expended was calculated from the difference of averaged nighttime EE from daytime EE. Energy expended with ($p=0.32$, Figure 14) and without FFM ($p=0.40$, Figure 14) adjustment showed no between female group difference. Sleeping EE, defined as the lowest continuous 3-hour EE period during the night also showed no between female group difference ($p=0.46$, w/FFM adjustment, $p=0.54$, Figure 15).

Locomotor Activity

Activity counts were averaged over 24-hrs, daytime (0600-1800), nighttime (1800-0600), morning (0600-1200) and afternoon (1200-1800) for the duration of the activity assessment at ~28-months post-treatment onset. There were no between group differences in 24-hr, day, night, morning, or afternoon periods (Figure 16). Although there was not a between group difference in the morning period (0600h-1200h), during the hours of 0600h-0900h, the ERαKD females exhibited reduced morning activity compared to the controls (0600h-0700h, $p<0.001$; 0700h-0800h, $p<0.001$, 0800h-0900h, $p<0.05$; Figure 17).

Glucoregulation via ivGTT

Glucoregulatory values were calculated via the Bergman-Cobelli Minimal Model software. There were no treatment differences in insulin sensitivity (S_I, p=0.45), disposition index (DI, p=0.95), acute insulin response (AIRg, p=0.27), glucose effectiveness (S_G, p=0.58), and basal insulin (I_b, p=0.68). There was a trend towards reduced basal glucose (G_b) in the ERαKD compared to control females (p=0.06, Figure 18).

3.5 Discussion

Hypothalamic ERα has been well documented as the main estrogen receptor governing E_2-dependent energy homeostatic mechanisms in female adult rodents, yet, prior to this study the role of ERα in a female adult NHP model with close physiological, reproductive, and genetic similarities to humans was unknown. Our results suggest that NHP hypothalamic ERα is an important neural target for E_2 to maintain energy balance in adult female rhesus macaques and likely, women.

In the present study, we demonstrated that mediobasal hypothalamic ERα mediates energy balance in terms of body weight regulation as well as locomotion activity in adult female rhesus macaques. The hypothalamic nuclei regions, VMN and ARC, targeted for MRI-guided viral vector infusion diminishing ERα protein expression were divided into multiple regions of interests (ROIs) for immunohistochemical (IHC) analysis. The ROIs VMNv, VMNd1, ARC and ARCd demonstrated significantly less ERα expression density and ERα density x intensity in ERαKD compared to control monkeys. Twelve months after neural ERα knockdown surgery, visually, ERαKD females began diverging in body weight percent increase compared to the controls.

Incremental AUC analyses were used to highlight the subtle cumulative weight gain induced by reduced hypothalamic ERα expression. We also demonstrated reduced ERα expression contributing to reduced locomotion in specific morning hours compared to control monkey activity. The positive energy balance of body weight gain and reduced morning locomotion resembles previous studies in rodents[10,14] and humans[18] that demonstrated menopause-associated body weight gain and reduced spontaneous activity. Similarly, to previous human studies[18], we found no caloric intake differences in menopausal compared with premenopausal women despite weight gain and reduced spontaneous activity.

In contrast to our findings of body weight percent increase and reduced locomotor activity in specific morning hours, mice subjected to ERα knockdown in the VMN exhibit a more robust metabolic phenotype. ERαKD mice demonstrate increased body weight, reduced energy expenditure, hyperphagia and impaired glucose tolerance within 10 weeks compared to control mice[8]. The difference in severity of metabolic phenotype after ERα knockdown could be due to a more complete knockdown of ERα protein expression in the mice compared to the rhesus monkeys in our study[8]. Additionally, we saw similar contrasts in our recently completed adult female marmoset monkey ERα knockdown study. In ERαKD female marmosets, we observed reduced 24-hour locomotor activity and a trend towards impaired glucose tolerance. Due to the less robust metabolic phenotypes observed in our ERαKD female marmoset and rhesus monkey studies, we speculate that fewer metabolic processes are mediated by hypothalamic ERα within the VMN and ARC in adult female rhesus monkeys compared

to adult female mice. Perhaps, one metabolic process mediated by ERα and conserved across species is the regulation of locomotion.

Previously, our group investigated the metabolic consequence of silencing hypothalamic ERα expression in a marmoset monkey model and provided similar evidence that mediobasal hypothalamic ERα expression is crucial for maintenance of female energy homeostasis in female NHPs (Chapter 2). The female marmoset study, in contrast to the present study employing female rhesus macaques, diet-induced obesity (DIO). Estradiol and functional ERα have been shown in rodent models to have a protective effect against DIO attributed weight gain. We speculate that adoption of a DIO methodology in this rhesus monkey study, may have exaggerated the weight gains and reductions in morning activities in ERαKD compared to control females that we observed in the present study. Although the present rhesus monkey study approximated 3 years in duration, the menopausal transition in humans averages 3-4 years and can proceed over a decade[36]. It is plausible that the specific metabolic differences detected are only the first indications of metabolic dysfunction due to reduced ERα expression and disruption of E_2 mediated energy homeostatic mechanisms. Moreover, it is possible that ERα and E_2 independent mechanisms of energy balance can compensate in the absence of hypothalamic ERα action, such as increased signaling through leptin-mediated melanocortin pathways that are not all regulated by ERα. It had been assumed that E_2's effect on energy balance acts in tandem with leptin's role via co-expression of leptin receptor (LepRb) and ERα in the mediobasal hypothalamus, but recent research in rodents has shown co-expression is more pronounced in the preoptic area (POA) and is limited in the mediobasal

hypothalamus. Quantification of LepRb and ERα colocalization throughout the murine hypothalamus has revealed that robust colocalization does not occur in all areas aside from the POA and one month after OVX, co-expression tended to decline[37]. Further, STAT3 or ERα deletion from LepRb cells does not inhibit E_2's ability to regulate body weight[38]. It has been shown that circulating levels of E_2 may enhance the anti-obesity effects of leptin and specifically modulate leptin sensitivity in certain metabolic tissues like adipose and skeletal muscle[39]. Taken together, E_2 mediation of energy homeostasis via ERα is not dependent on activation of LepRb on co-expressing cells and circulating levels of E_2 may act indirectly on the leptin-melanocortin pathway and it can be posited that in the absence of ERα expression, leptin control of energy balance may partially compensate, enough, if not further stressed by DIO or a sedentary lifestyle.

In summary, partial silencing of ERα in the VMN and ARC of rhesus macaques results in significant body weight gain and a significant reduction in locomotion during the peak hours of physical activity. These findings replicate only some of much more extensive effects of similar treatments in rodents, a difference that may be attributable to technical limitations in deploying RNAi strategies in NHPs vs. rodents, or incompletely overlapping metabolic roles of ERα in these differing experimental models. Nevertheless, our findings confirm ERα as a crucial neural receptor of E_2 action in female NHPs and reveal the potential for therapies to engage this specific neural target as a way to combat obesity and E_2-associated metabolic disorders.

3.6 Tables & Figures

	Age (years)	Body Weight (kg)
Scrambled Controls (n=6)	10.75±1.16	7.71±1.05
ERα Knockdown (n=6)	11.26±0.77	8.35±0.51
p-value	0.71	0.56

Table 1: Comparable ages and body weights between both female rhesus treatment groups. Scrambled control (n=6) and ERalpha knockdown (n=6) at the start of the study. P-values calculated via student's t-test.

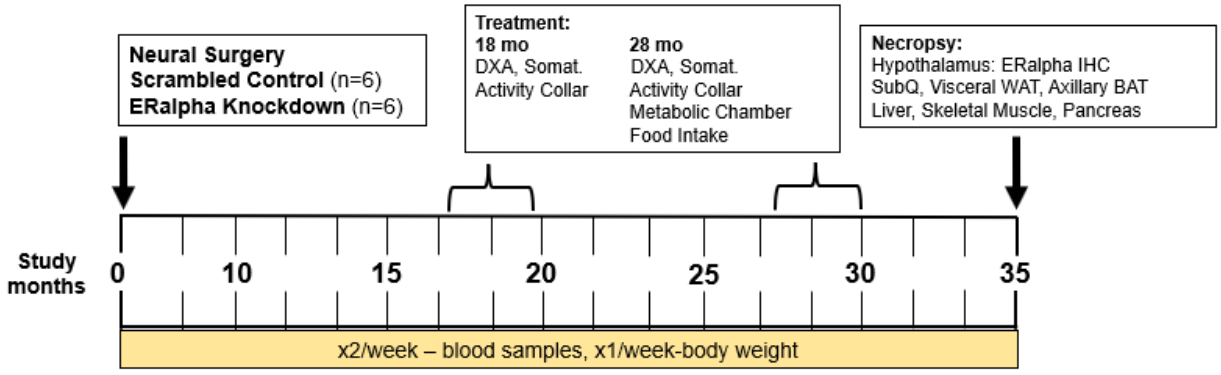

Figure 1: Timeline of treatment onset, metabolic procedures, and end of study**.**

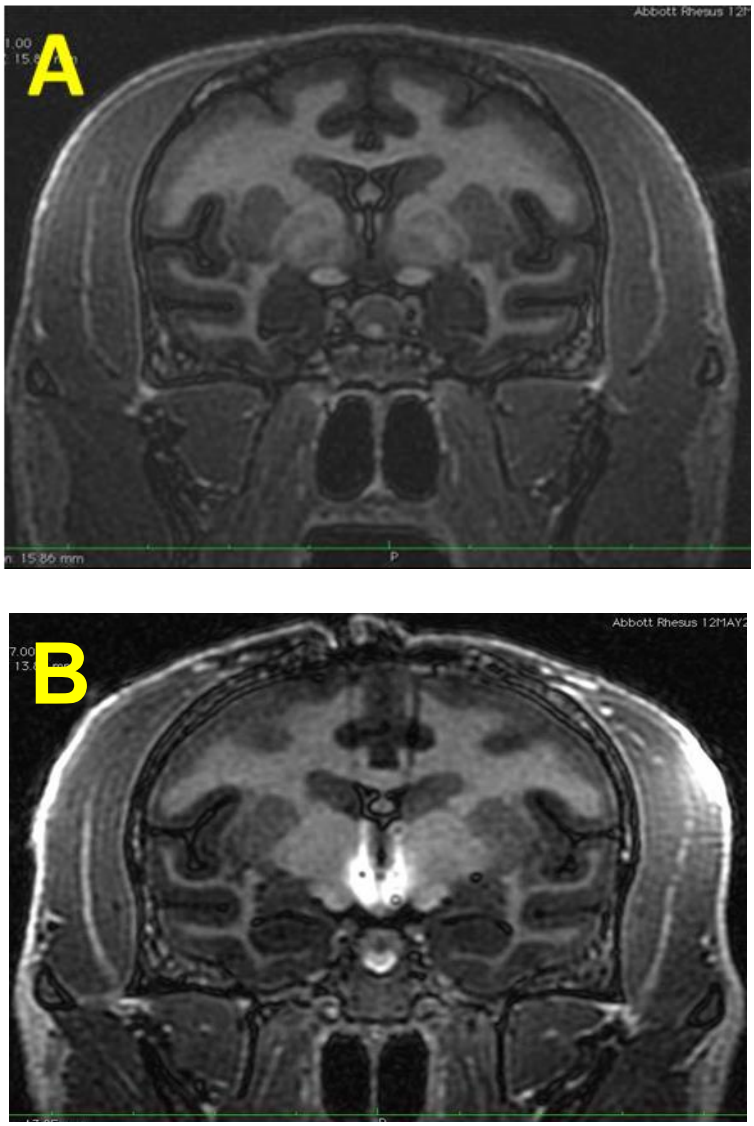

Figure 2: (**A**) Coronal anatomical MRI images used to determine targeting of the MBH prior to neural surgery. (**B**) During surgery, infusions contained a contrast agent (white) to enable MRI imaging of infusion placement.

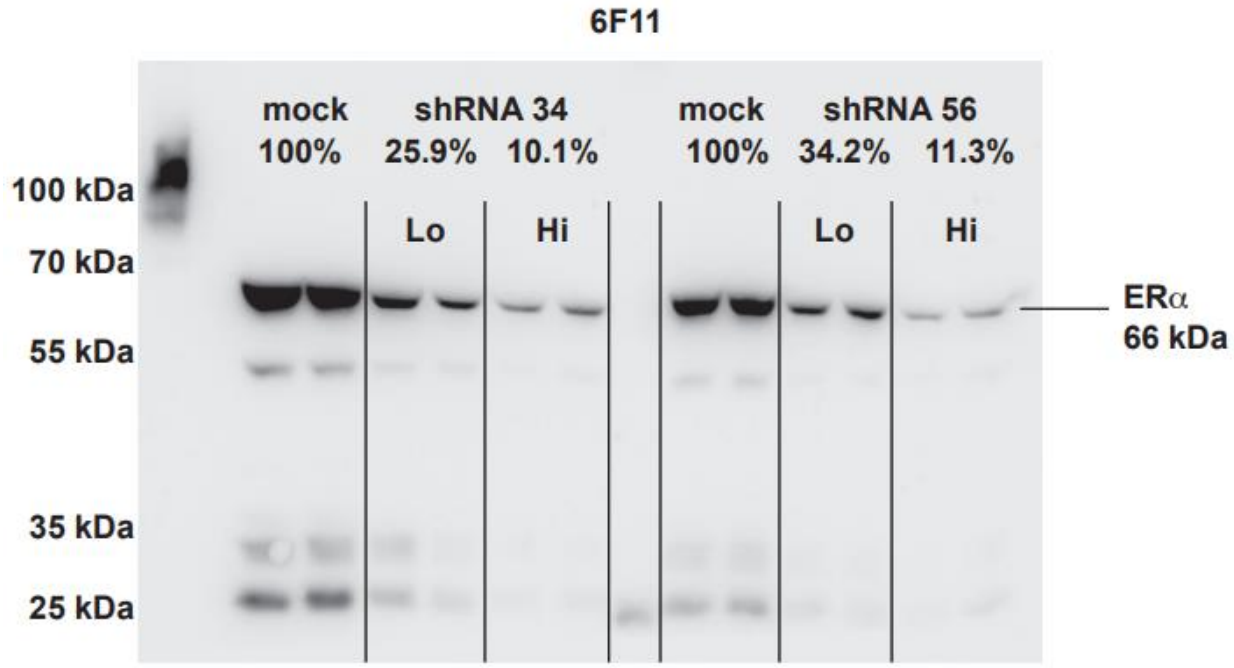

Figure 3: Western blots validated the knockdown of ERα protein expression for shRNA 34 and shRNA 56 employing antibody 6F11.

A

ERa34 oligo 1
5'-GATCCACCTACTACCTGGAGAACGACTTCCTGTCATCGTTCTCCAGGTAGTAGGTTTTTTGGAAA-3'

ERa34 oligo 2
5'-AGCTTTTCCAAAAAACCTACTACCTGGAGAACGATGACAGGAAGTCGTTCTCCAGGTAGTAGGTG-3'

Oligos 1 and 2 annealed:

5'-GATCCACCTACTACCTGGAGAACGACTTCCTGTCATCGTTCTCCAGGTAGTAGGTTTTTTGGAAA-3'
3'-GTGGATGATGGACCTCTTGCTGAAGGACAGTAGCAAGAGGTCCATCATCCAAAAAACCTTTTCGA-5'

pAAV-H1-EGFP from VB: clone into 5' BamHI (GGATCC) and 3' HindIII (AAGCTT)
BamH1: GGATCC HindIII: AAGCTT
CCTAGG TTCGAA

B

ERa78 oligo 1
5'-GATCCGCCTACTACCTGGAGAACGACTTCCTGTCATCGTTCTCCAGGTAGTAGGTTTTTTGGAAA-3'

ERa78 oligo 2
5'-AGCTTTTCCAAAAAACCTACTACCTGGAGAACGATGACAGGAAGTCGTTCTCCAGGTAGTAGGCG-3'

Oligos 1 and 2 annealed:

5'-GATCCGCCTACTACCTGGAGAACGACTTCCTGTCATCGTTCTCCAGGTAGTAGGTTTTTTGGAAA-3'
3'-GCGGATGATGGACCTCTTGCTGAAGGACAGTAGCAAGAGGTCCATCATCCAAAAAACCTTTTCGA-5'

pAAV-H1-EGFP from VB: clone into 5' BamHI (GGATCC) and 3' HindIII (AAGCTT)
BamH1: GGATCC HindIII: AAGCTT
CCTAGG TTCGAA

Figure 4: Oligo sequences for ERα34 (A) and ERα78 (B) shRNA candidates for virus production. Green highlighted is the shRNA portion. Bold in between highlighted regions are the loop.

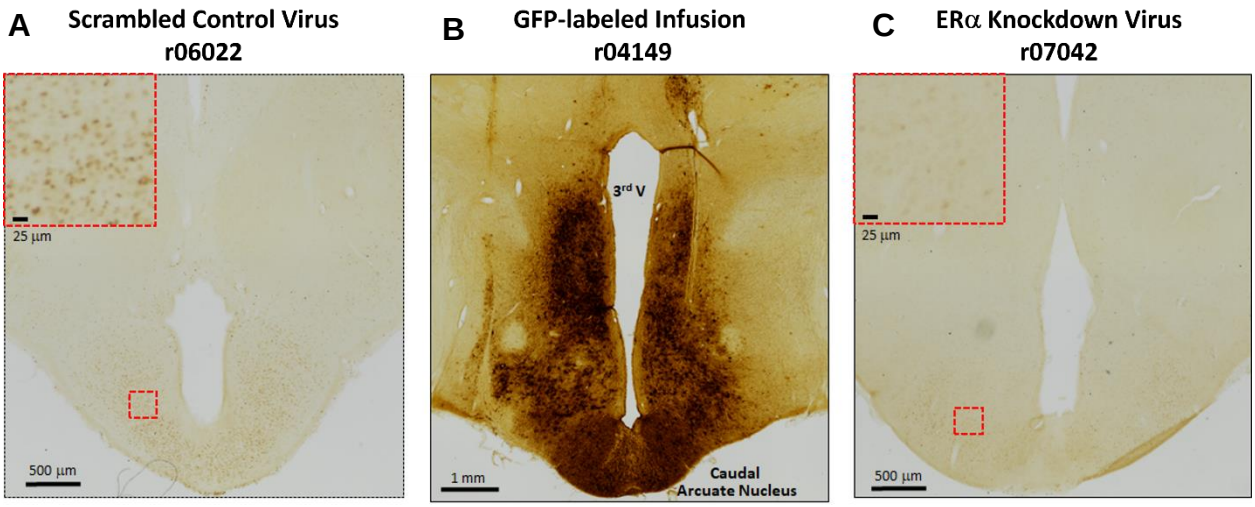

Figure 5: Adult rhesus macaque coronal sections from approximately the caudal extents of the ARC within the hypothalamus. Abundant GFP-immunoreactive (ir) labeling was demonstrated in ARC (B). ERα protein expression was abundant in scrambled control (A) and was less obvious in ERαKD females (C).

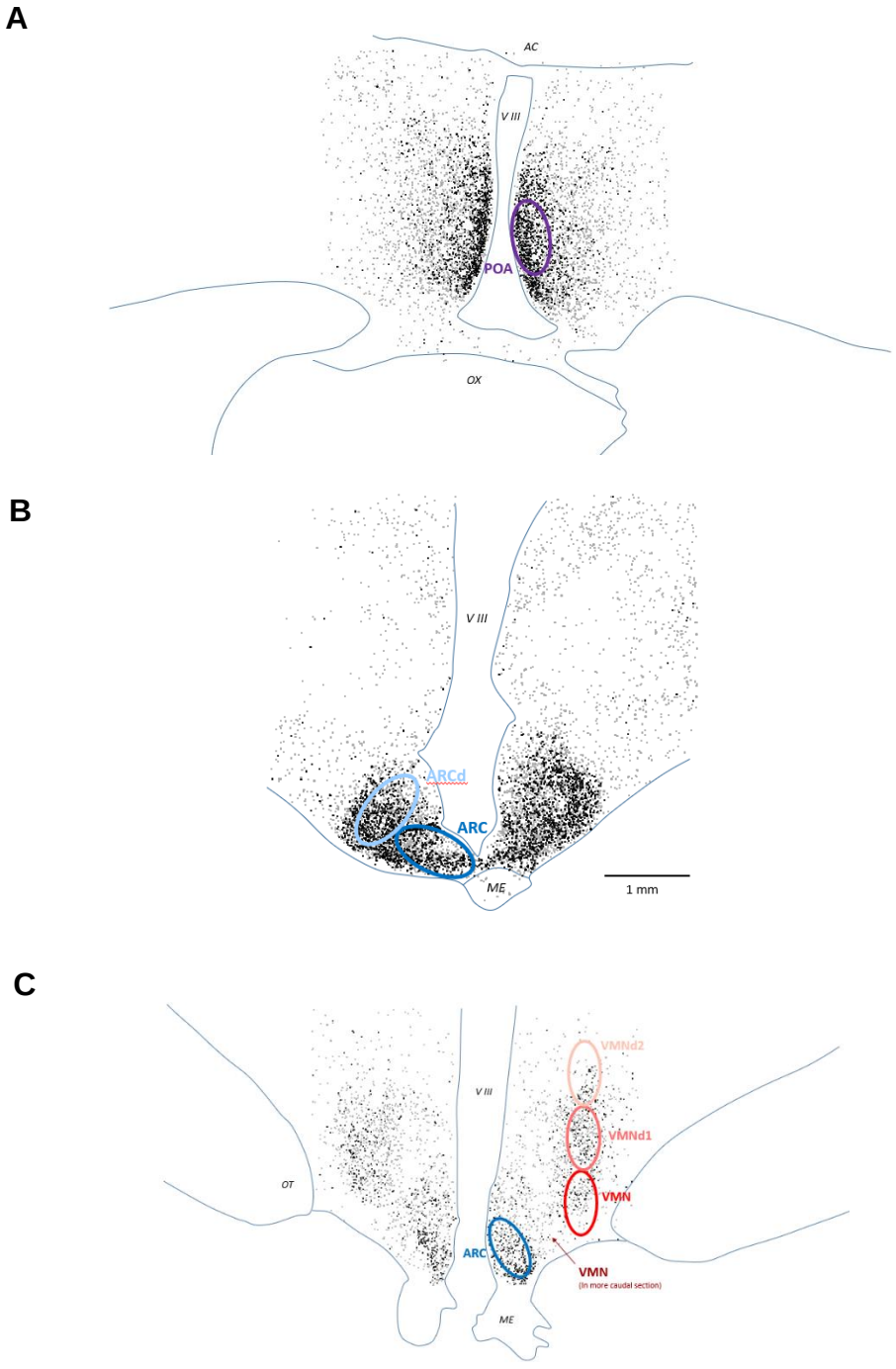

Figure 6: Regions of interest (ROIs) drawn for the POA (A, purple), ARC (B, blue) and VMN (C, red) ERα density and intensity analyses from a control monkey.

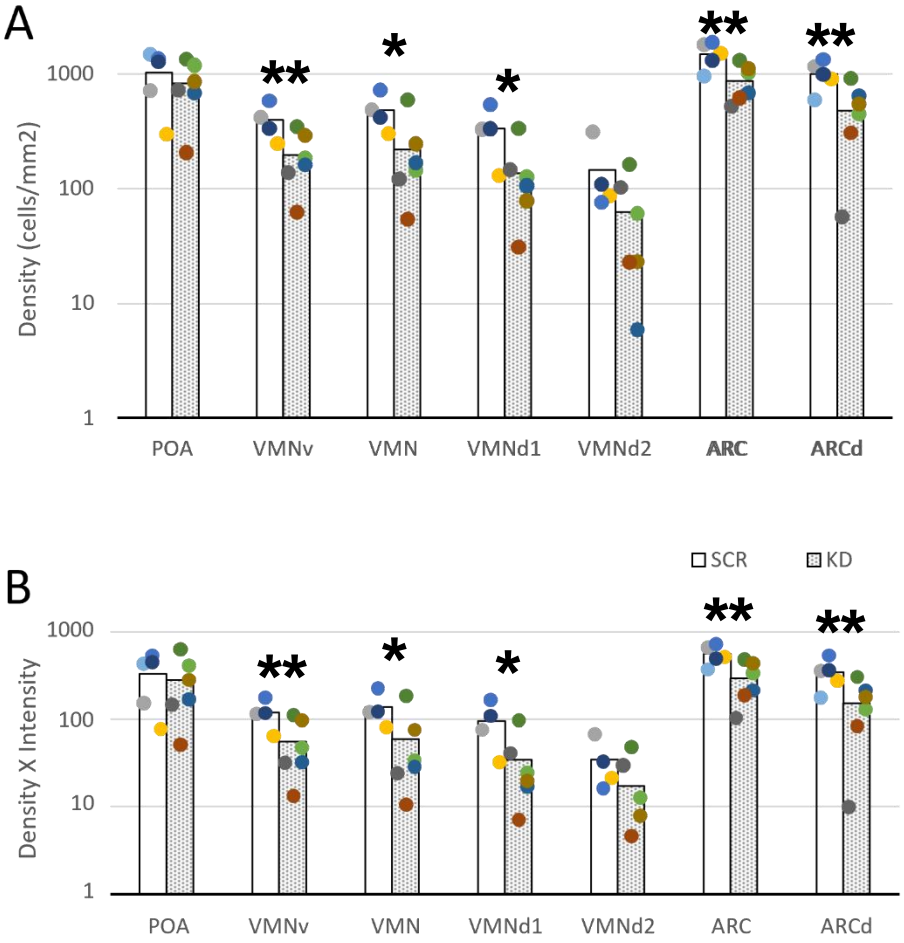

Figure 7: ERα density (A) and density*intensity (B) for control (SCR, white bars) and ERαKD females (KD, shaded bars). Dots represent individual values for each monkey. Bars represent mean of each female group. p*<0.1, p**<0.05.

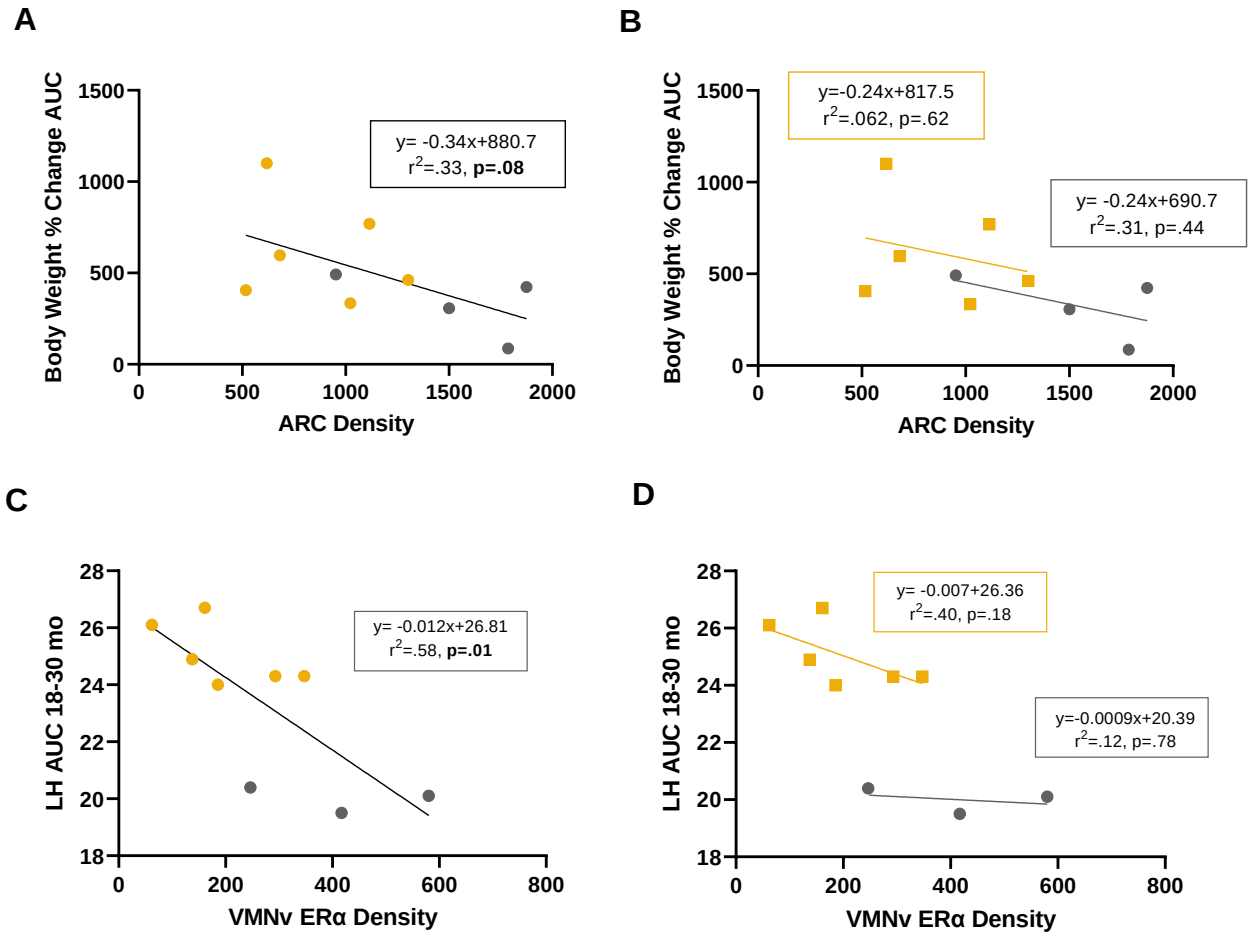

Figure 8. Associations between ARC ERα expression density and body weight percent change AUC for all females combined (A) and by female group (B). Relationships of VMNv ERα density and LH AUC 18-30 months for all females combined (C) and by female group (D). There was a trend (p=0.08) towards a negative correlation between ARC ERα expression and body weight percent change AUC, all females combined (A) and a negative correlation (p=0.01) between ARC ERα expression and LH AUC 18-30 months, all females combined (C). Scrambled control (grey) and ERαKD (yellow) females.

		Female Group		
		Scrambled Control (n=4)	**ERα Knockdown (n=6)**	**p-value**
Estradiol (pg/mL)	Baseline	64.85±17.45	60.02±2.91	0.80
	18-months	63.80±16.97	59.50±12.40	0.84
	30-months	77.70±14.13	54.37±5.25	0.20
Estrone (pg/mL)	Baseline	37.85±12.10	23.80±3.25	0.33
	18-months	12.48±3.57	8.87±1.75	0.41
	30-months	13.93±6.10	13.05±4.19	0.91
Testosterone (ng/mL)	Baseline	0.24±0.03	0.20±0.03	0.32
	18-months	0.16±0.01	0.17±0.02	0.64
	30-months	0.17±0.01	0.18±0.12	0.87
Androstenedione (ng/mL)	Baseline	0.44±0.03	0.42±0.05	0.80
	18-months	0.25±0.03	0.31±0.03	0.20
	30-months	0.33±0.05	0.37±0.04	0.50
DHEA (ng/mL)	Baseline	20.79±2.85	14.84±1.15	0.13
	18-months	12.60±3.00	14.87±2.89	0.60
	30-months	21.04±4.13	20.70±2.98	0.95
LH (ng/mL)	Baseline	1.63±0.29	1.38±0.07	0.48
	18-months	1.75±0.29	1.82±0.16	0.85
	30-months	1.60±0.20	2.17±0.26	0.12
Progesterone (ng/mL)	Baseline	0.24±0.03	0.20±0.03	0.32
	18-months	0.15±0.03	0.15±0.03	0.93
	30-months	0.17±0.01	0.18±0.01	0.87

Table 2: Circulating steroid hormones during the follicular phase at baseline, 18-months, and 30-months post-treatment onset. Significance assessed via student's t-test. Values represented as mean ± SEM.

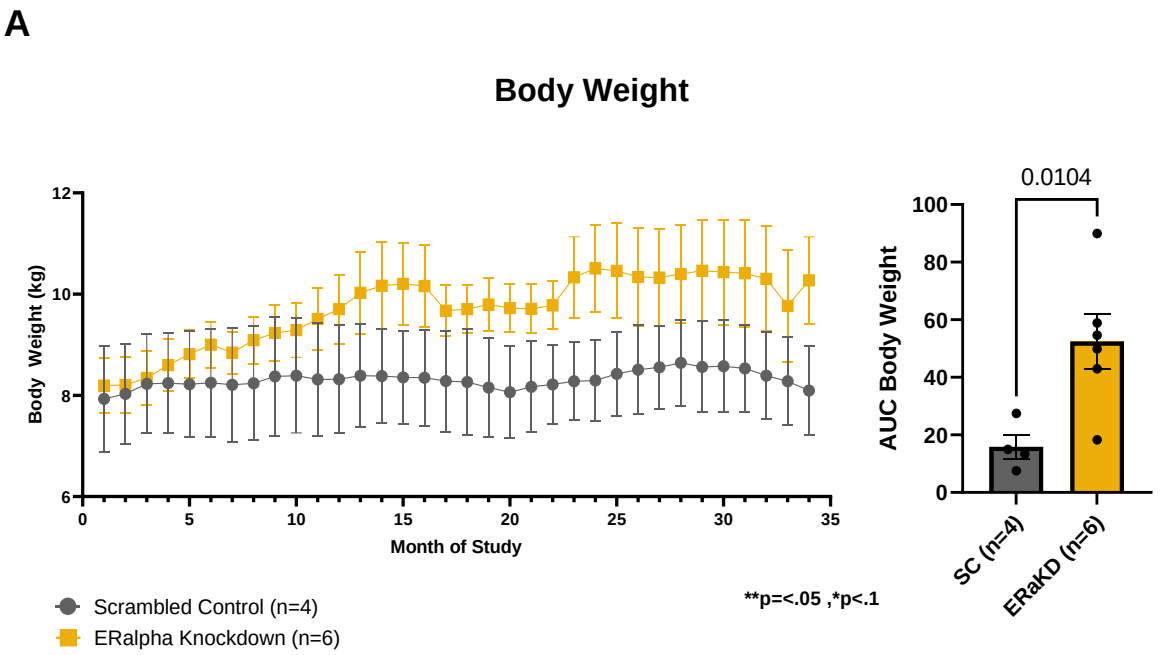

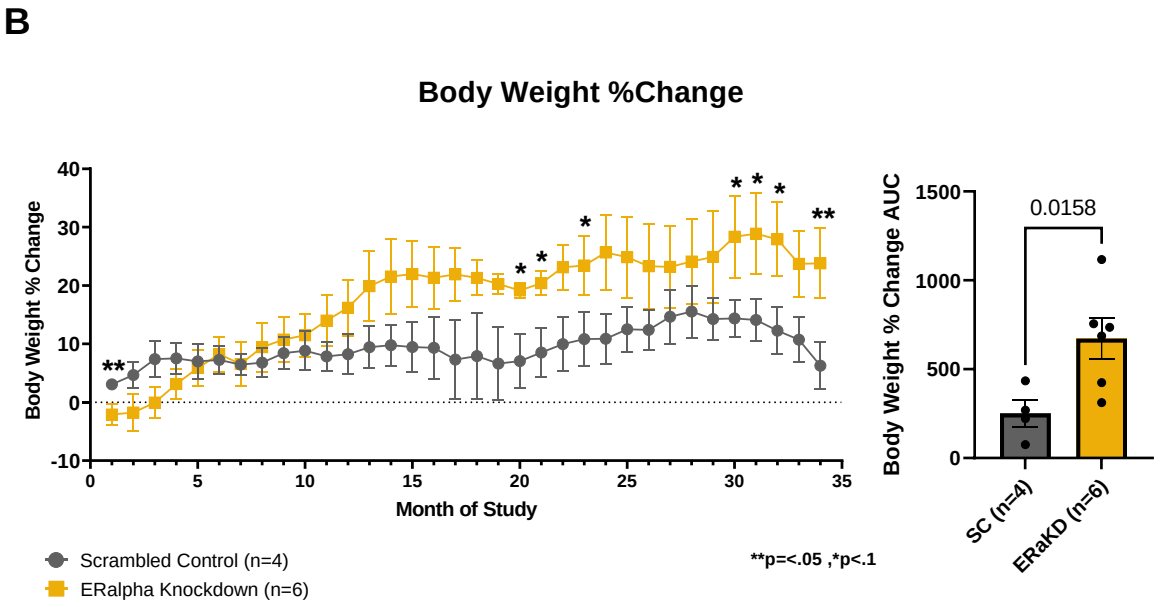

Figure 9. Body weight (A) and body weight percent change (B) over 34-months of the study with corresponding area under the curve (AUC) measurements. Asterisks represent months significant, ERαKD compared to control females from repeated-measures ANOVA time effect (*p<0.1, **p<0.05). Plots are expressed as means+/-SEM.

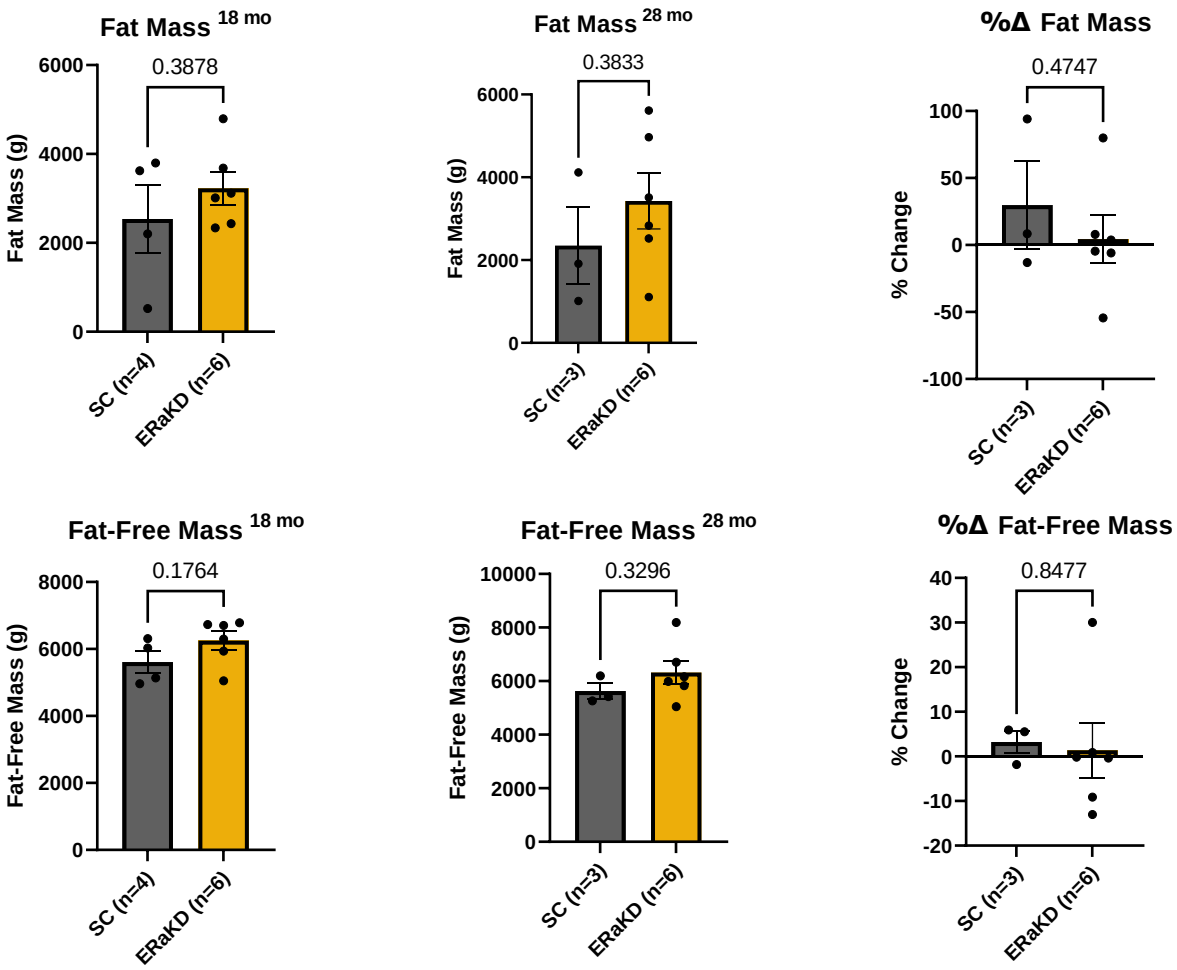

Figure 10: Total fat mass and fat-free mass from DXA scan at 18-months and 28-months of the study with corresponding percent change between the two scans. There were no significant differences between the female groups. Significance assessed via student's t-test. Plots are expressed as means+/-SEM.

		Treatment Group					
		Scrambled Control (n=4)		**ERα Knockdown (n=6)**		**p-value**	**p-value**
		Fat Mass (kg)	Fat-Free Mass (kg)	Fat Mass (kg)	Fat-Free Mass (kg)	Fat-Mass	Fat-Free Mass
Abdomen	18-mo 28-mo	1.07±0.38 0.87±0.40	**1.67±0.07** 1.68±0.07	1.33±0.21 1.32±0.30	**2.04±0.11** 2.05±0.23	0.58 0.41	**0.02*** 0.17
Upper Legs	18-mo 28-mo	0.30±0.09 0.29±0.10	1.13±0.17 1.08±0.21	0.40±0.06 0.38±0.09	1.22±0.07 1.26±0.11	0.38 0.54	0.63 0.50
Chest	18-mo 28-mo	0.56±0.18 0.60±0.27	1.12±0.13 1.09±0.03	0.80±0.09 0.97±0.18	1.21±0.08 1.23±0.07	0.29 0.33	0.70 0.13
Lower Legs	18-mo 28-mo	0.19±0.04 0.19±0.03	0.53±0.04 0.58±0.04	0.21±0.02 0.21±0.03	0.52±0.04 0.55±0.04	0.61 0.70	0.92 0.61
Arms	18-mo 28-mo	0.29±0.03 0.25±0.09	0.71±0.01 0.72±0.02	0.33±0.03 0.37±0.09	0.75±0.04 0.71±0.04	0.63 0.42	0.39 0.80

Table 3: Regions of interest analyzed at ~18-months and ~28-months post-treatment onset via DXA scan. Significance assessed via student's t-test ($p^*<0.05$) between ERαKD and control females. Values represented as mean ± SEM.

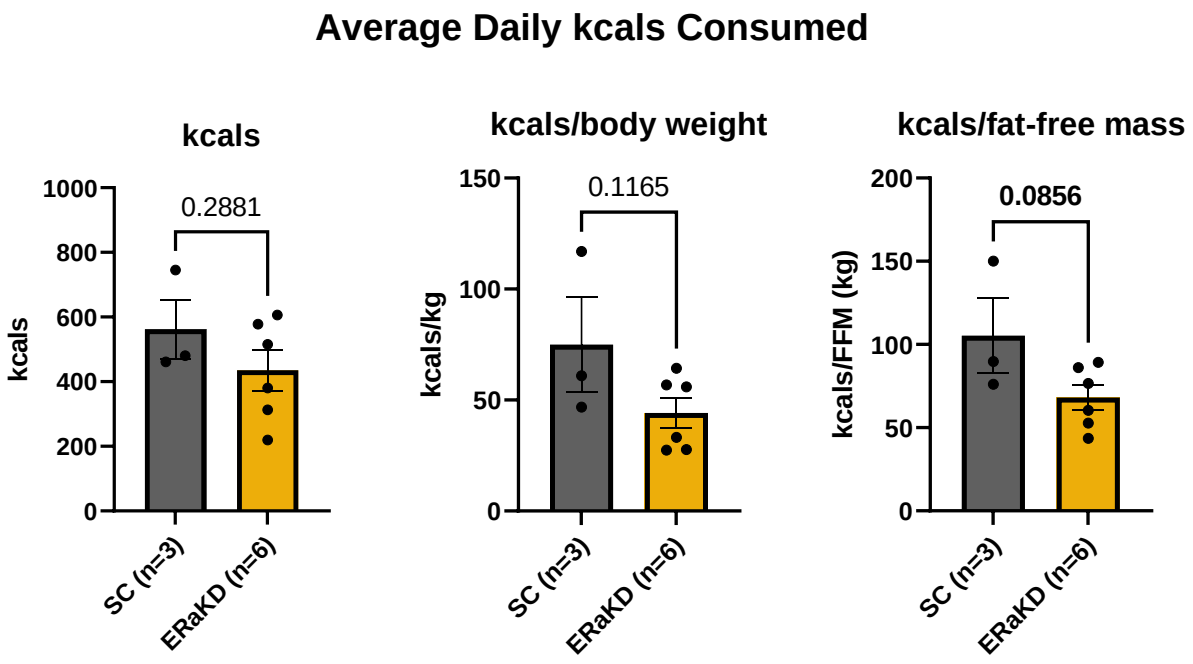

Figure 11: Average kcals consumed throughout the food assessment without adjustment and with body weight (kg) and fat-free mass (kg) adjustments. Trend (p=.08) towards reduced kcals consumed when adjusted for kilogram of fat-free mass in ERαKD compared to control females. Significance assessed via student's t-test. Plots are expressed as means+/-SEM.

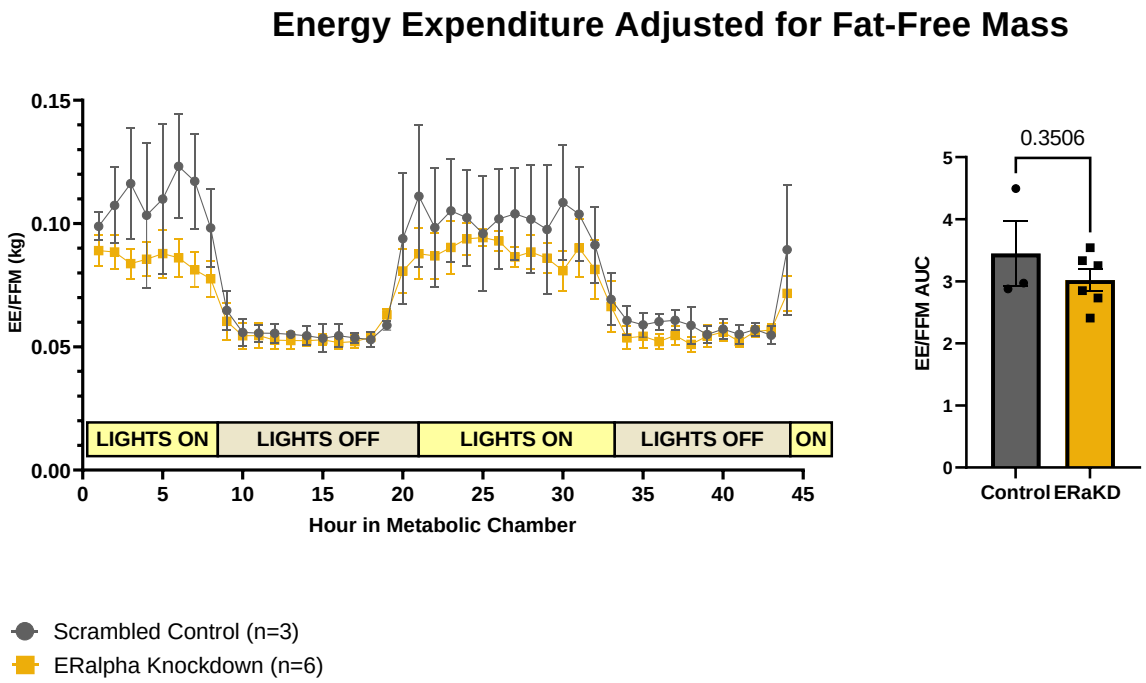

Figure 12. Averaged hourly energy expenditure (EE) adjusted for kilogram of fat-free mass (FFM) with corresponding area under the curve (AUC) measurement. There were no between female group differences. Significance assessed via student's t-test and RM-ANOVA. Plots are expressed as means+/-SEM.

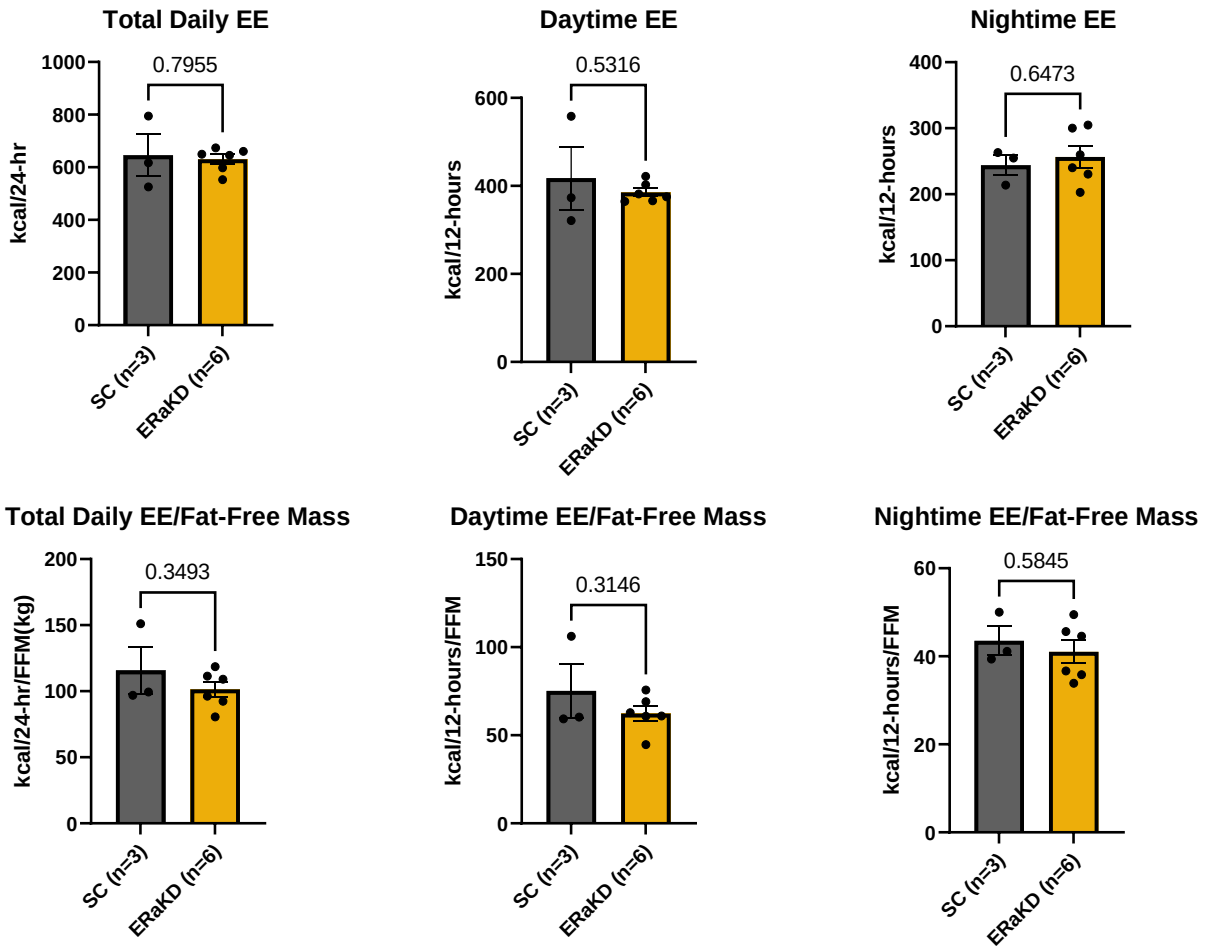

Figure 13. Summaries of energy expenditure over 24-hr, daytime (0600-1800) and nighttime (1800-0600) periods within the metabolic chamber with and without adjustments for fat-free mass (kg). There were no observed differences between female groups. Significance assessed via student's t-test. Plots are expressed as means+/-SEM.

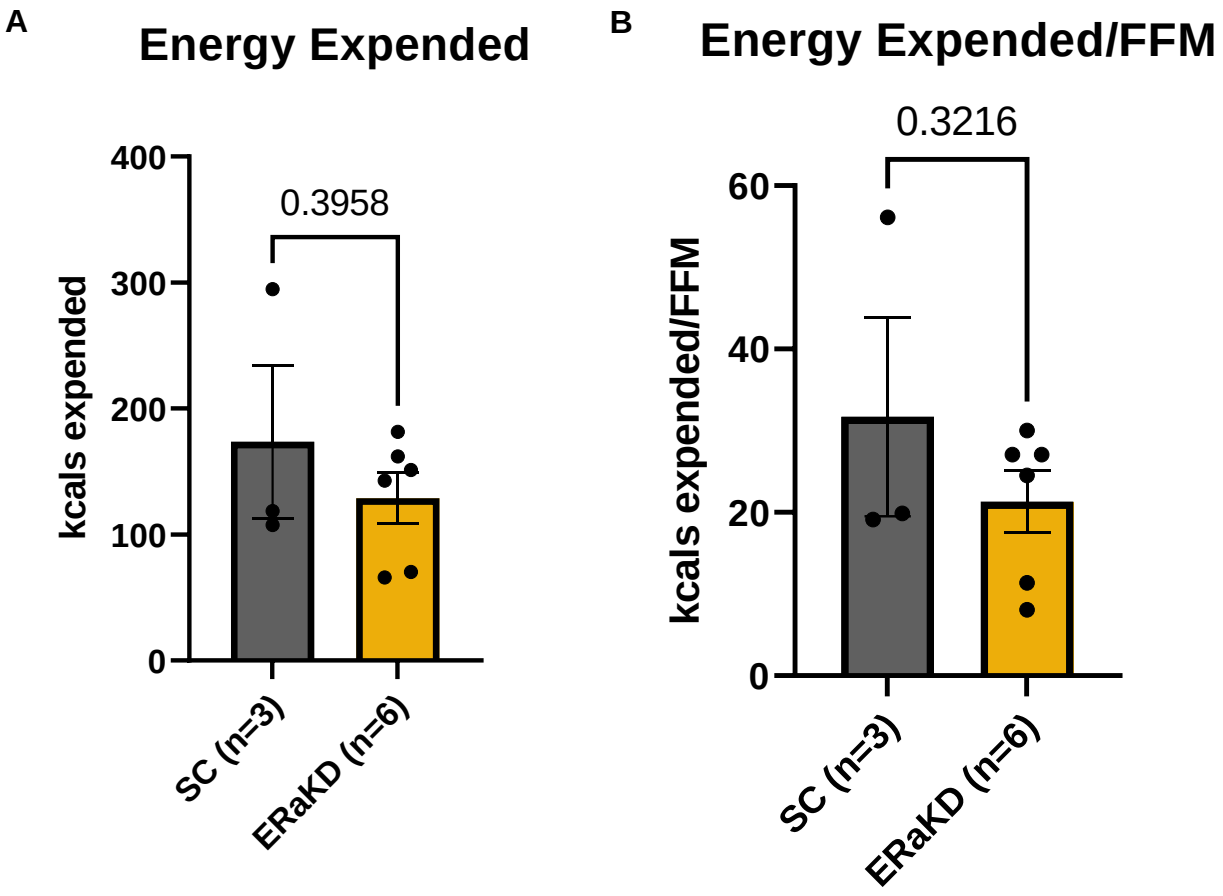

Figure 14. Average energy expenditure over duration in metabolic chamber with and without correction for fat-free mass (kg). No observed differences between female groups. Significance assessed via student's t-test. Plots are expressed as means+/- SEM.

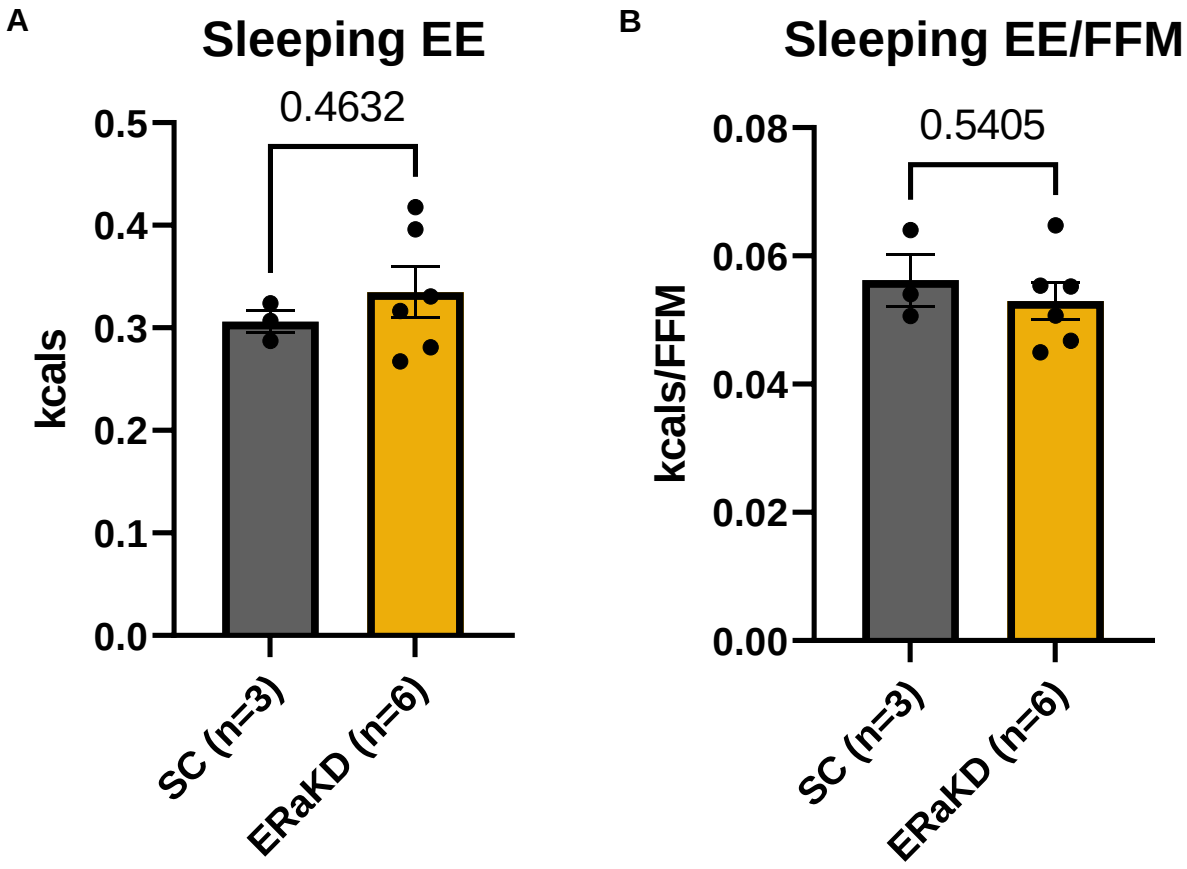

Figure 15. Average sleeping energy expenditure averaged over both nights in the metabolic chamber with and without adjustment for fat-free mass (kg). No observed differences between female groups. Significance assessed via student's t-test. Plots are expressed as means+/-SEM.

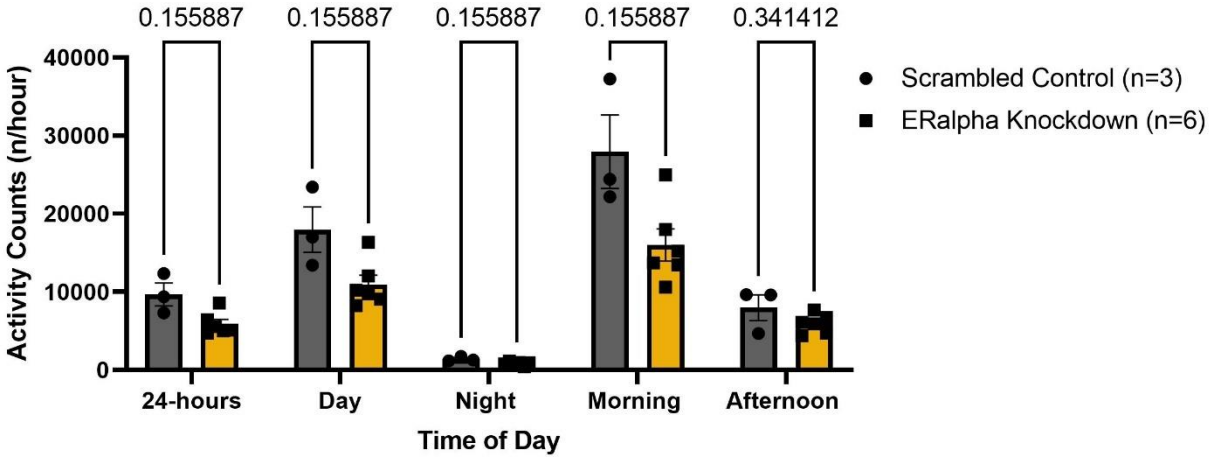

Figure 16: Activity counts averaged over 24-hours, Day (0600-1800), Night (1800-0600), Morning (0600-1200) and Afternoon (1200-1800). There were no observed differences between female groups. Significance assessed via student's t-test. Plots are expressed as means+/-SEM.

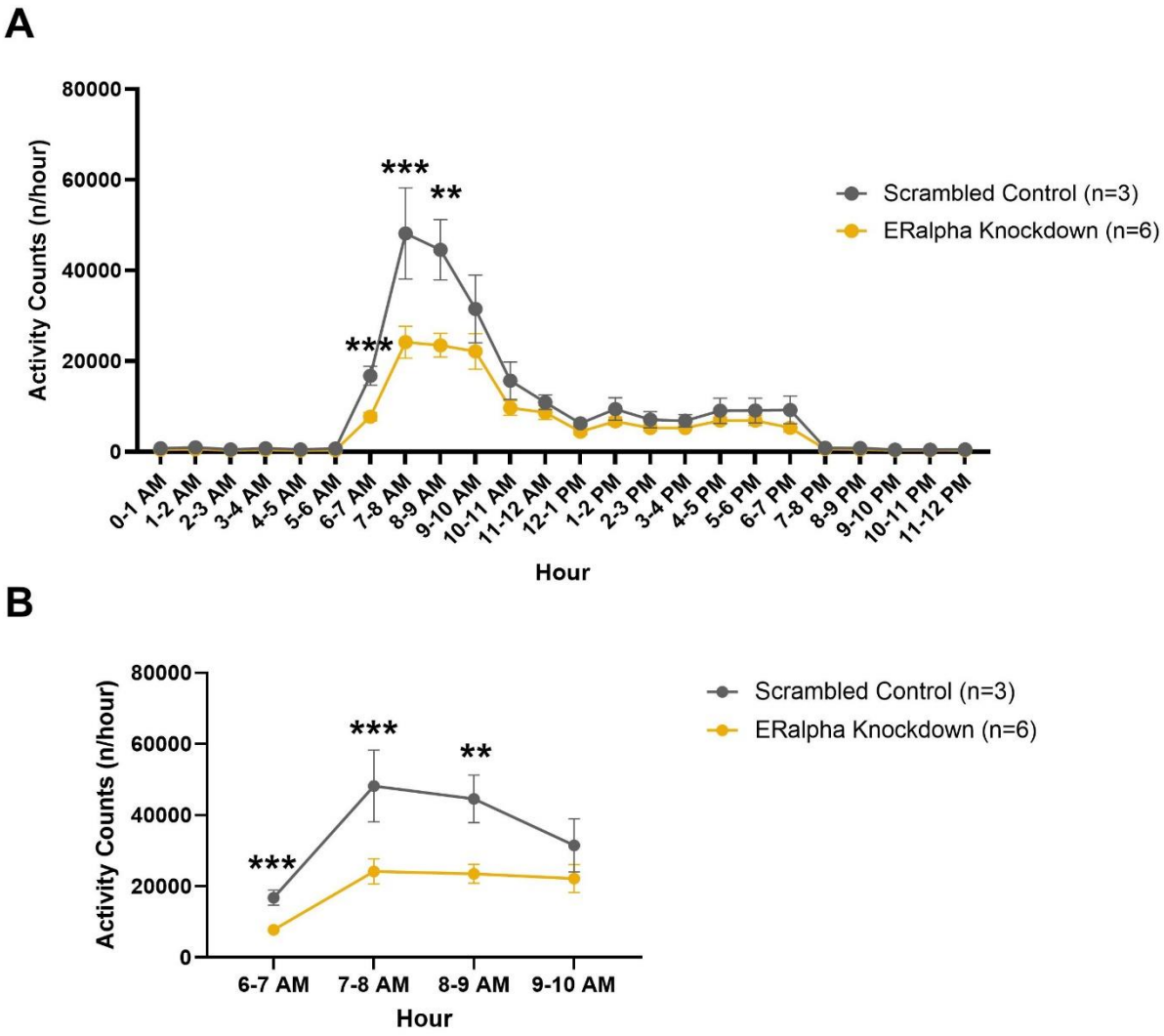

Figure 17: Activity counts (n) averaged per hour over the duration of the locomotor assessment (A) and activity counts over the morning period, 6 AM – 10 AM (B). Significance assessed via RM-ANOVA (p*<0.05, p**<0.001, p****<0.0001) ERαKD compared to control females. Plots are expressed as means+/-SEM.

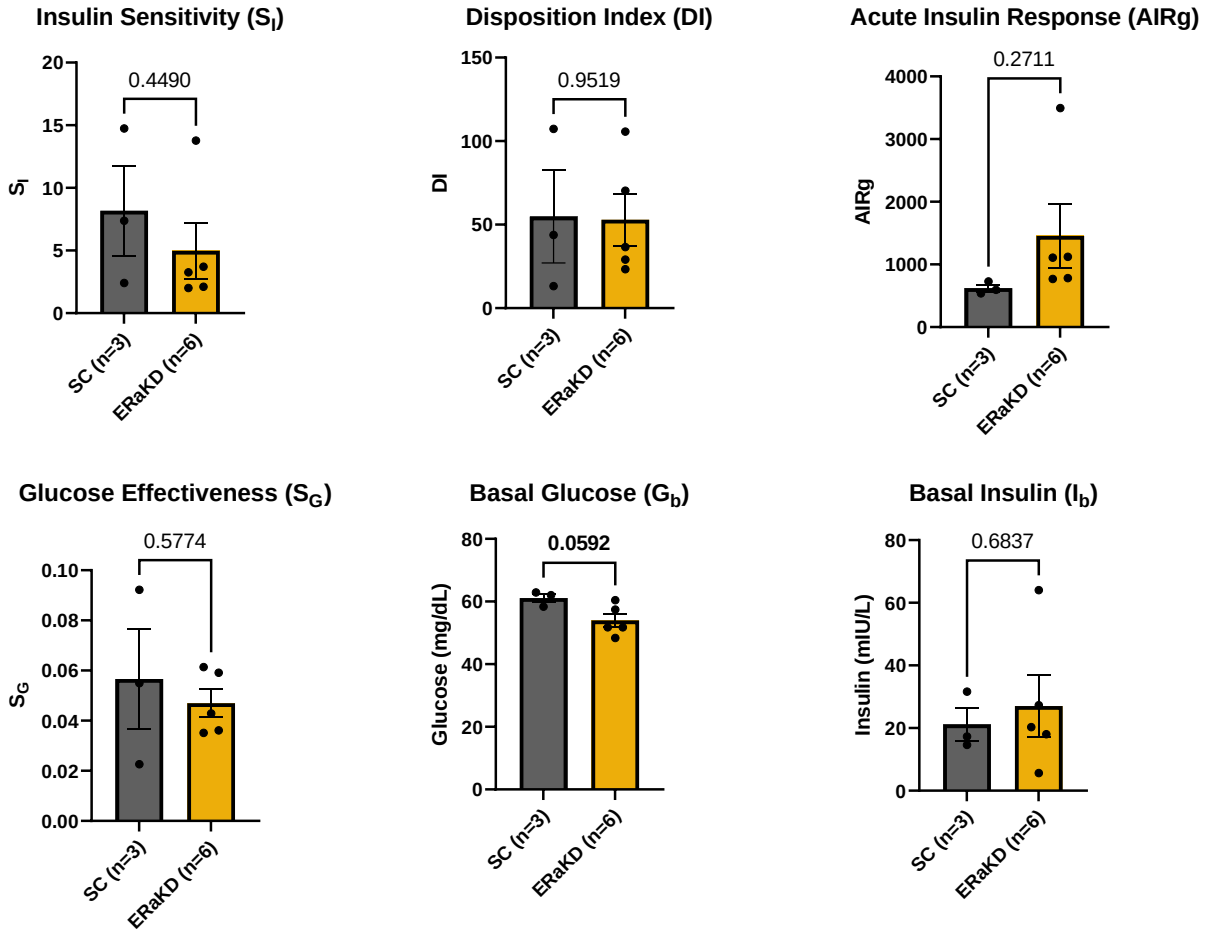

Figure 18. Summary of values computed from the Bergman Modified Minimal Model (MMM) for glucoregulation. No observed differences between female groups aside from a trend towards reduced basal glucose in ERαKD compared to control females (p=.0592). Significance assessed via student's t-test. Plots are expressed as means+/-SEM.

3.7 References

1. Killinger DW, Perel E, Daniilescu D, Kharlip L, Blackstein ME. Aromatase activity in the breast and other peripheral tissues and its therapeutic regulation. *Steroids.* 1987 Oct-Dec;50(4-6):523-36. doi: 10.1016/0039-128x(87)90036-5. PMID: 3332939.
2. Kadioglu P, Oral G, Sayitoglu M, Erensoy N, Senel B, Gazioglu N, Sav A, Cetin G, Ozbek U. Aromatase cytochrome P450 enzyme expression in human pituitary. *Pituitary.* 2008;11(1):29-35. doi: 10.1007/s11102- 007-0065-3. PMID: 17703367
3. Weisz J. In vitro assays of aromatase and their role in studies of estrogen formation in target tissues. *Cancer Res*.1982;42(8Suppl):3295s-3298s
4. Amanatullah DF, Tamaresis JS, Chu P, Bachmann MH, Hoang NM, Collyar D, Mayer AT, West RB, Maloney WJ, Contag CH, King BL. Local estrogen axis in the human bone microenvironment regulates estrogen receptor-positive breast cancer cells. *Breast Cancer Res.* 2017 Nov 15;19(1):121. doi: 10.1186/s13058-017-0910-x. PMID: 29141657; PMCID: PMC5688761.5
5. Xu P, Cao X, He Y, Zhu L, Yang Y, Saito K, Wang C, Yan X, Hinton AO Jr, Zou F, Ding H, Xia Y, Yan C, Shu G, Wu SP, Yang B, Feng Y, Clegg DJ, DeMarchi R, Khan SA, Tsai SY, DeMayo FJ, Wu Q, Tong Q, Xu Y. Estrogen receptor-α in medial amygdala neurons regulates body weight. *J Clin Invest*. 2015 Jul 1;125(7):2861-76. doi: 10.1172/JCI80941. Epub 2015 Jun 22. PMID: 26098212; PMCID: PMC4563687.
6. Bryzgalova, G. et al. Evidence that oestrogen receptor-alpha plays an important role in the regulation of glucose homeostasis in mice: insulin sensitivity in the liver. *Diabetologia* 49, 588-597, doi:10.1007/s00125- 005-0105-3 (2006).
7. Park CJ, Zhao Z, Glidewell-Kenney C, Lazic M, Chambon P, Krust A, Weiss J, Clegg DJ, Dunaif A, Jameson JL, Levine JE. Genetic rescue of nonclassical ERα signaling normalizes energy balance in obese Erα-null mutant mice. *J Clin Invest.* 2011 Feb;121(2):604-12. doi: 10.1172/JCI41702. Epub 2011 Jan 18. PMID: 21245576; PMCID: PMC3026715.
8. Musatov S, Chen W, Pfaff DW, Mobbs CV, Yang XJ, Clegg DJ, Kaplitt MG, Ogawa S. Silencing of estrogen receptor alpha in the ventromedial nucleus of hypothalamus leads to metabolic syndrome. *Proc Natl Acad Sci U S A.* 2007 Feb 13;104(7):2501-6. doi: 10.1073/pnas.0610787104. Epub 2007 Feb 6. PMID: 17284595; PMCID: PMC1892990.
9. Roberta Diaz Brinton, Minireview: Translational Animal Models of Human Menopause: Challenges and Emerging Opportunities, *Endocrinology,* Volume 153, Issue 8, 1 August 2012, Pages 3571– 3578, https://doi.org/10.1210/en.2012-1340
10. Yonezawa R, Wada T, Matsumoto N, Morita M, Sawakawa K, Ishii Y, Sasahara M, Tsuneki H, Saito S, Sasaoka T. Central versus peripheral impact of estradiol on the impaired glucose metabolism in ovariectomized mice on a high-fat diet. *Am J Physiol Endocrinol Metab*. 2012 Aug 15;303(4):E445-56. doi: 10.1152/ajpendo.00638.2011. Epub 2012 May 1. PMID: 22550066.

11. Hong, J., Stubbins, R. E., Smith, R. R., Harvey, A. E. & Nunez, N. P. Differential susceptibility to obesity between male, female and ovariectomized female mice. *Nutr J* 8, 11, doi:10.1186/1475-2891-8-11 (2009)
12. Gambacciani, M., Ciaponi, M., Cappagli, B. & Genazzani, A. R. Effects of low-dose continuous combined conjugated estrogens and medroxyprogesterone acetate on menopausal symptoms, body weight, bone density, and metabolism in postmenopausal women. *Am J Obstet Gynecol* 185, 1180-1185, doi:10.1067/mob.2001.117669 (2001).
13. Mattiasson, I., Rendell, M., Tornquist, C., Jeppsson, S. & Hulthen, U. L. Effects of estrogen replacement therapy on abdominal fat compartments as related to glucose and lipid metabolism in early postmenopausal women. *Horm Metab Res* 34, 583-588, doi:10.1055/s-2002-35420 (2002)
14. Park CJ, Zhao Z, Glidewell-Kenney C, Lazic M, Chambon P, Krust A, Weiss J, Clegg DJ, Dunaif A, Jameson JL, Levine JE. Genetic rescue of nonclassical ERα signaling normalizes energy balance in obese Erα-null mutant mice. *J Clin Invest.* 2011 Feb;121(2):604-12. doi: 10.1172/JCI41702. Epub 2011 Jan 18. PMID: 21245576; PMCID: PMC3026715.
15. Mauvais-Jarvis F, Clegg DJ, Hevener AL. The role of estrogens in control of energy balance and glucose homeostasis. *Endocr Rev.* 2013 Jun;34(3):309-38. doi: 10.1210/er.2012-1055. Epub 2013 Mar 4. PMID: 23460719; PMCID: PMC3660717.
16. Martínez de Morentin PB, González-García I, Martins L, Lage R, Fernández-Mallo D, Martínez-Sánchez N, Ruíz-Pino F, Liu J, Morgan DA, Pinilla L, Gallego R, Saha AK, Kalsbeek A, Fliers E, Bisschop PH, Diéguez C, Nogueiras R, Rahmouni K, Tena-Sempere M, López M. Estradiol regulates brown adipose tissue thermogenesis via hypothalamic AMPK. *Cell Metab.* 2014 Jul 1;20(1):41-53. doi: 10.1016/j.cmet.2014.03.031. Epub 2014 May 22. PMID: 24856932; PMCID: PMC4082097.
17. van Veen JE, Kammel LG, Bunda PC, Shum M, Reid MS, Massa MG, Arneson D, Park JW, Zhang Z, Joseph AM, Hrncir H, Liesa M, Arnold AP, Yang X, Correa SM. Hypothalamic estrogen receptor alpha establishes a sexually dimorphic regulatory node of energy expenditure. *Nat Metab.* 2020 Apr;2(4):351- 363. doi: 10.1038/s42255-020-0189-6. Epub 2020 Apr 13. PMID: 32377634; PMCID: PMC7202561.
18. Lovejoy, J. C., Champagne, C. M., de Jonge, L., Xie, H. & Smith, S. R. Increased visceral fat and decreased energy expenditure during the menopausal transition. *Int J Obes (Lond*) 32, 949-958, doi:10.1038/ijo.2008.25 (2008).
19. de Souza Santos R, Feijó da Silva Santos A, Clegg DJ, Iannetta O, Marchini JS, Marques Miguel Suen V. Overweight postmenopausal women with different plasma estradiol concentrations present with a similar pattern of energy expenditure and substrate oxidation rate before and after a fatty meal challenge. *Clin Nutr* ESPEN. 2016 Oct;15:21-27. doi: 10.1016/j.clnesp.2016.05.003. Epub 2016 Jun 2. PMID: 28531779.

20. Lahmann, P. H., Lissner, L., Gullberg, B. & Berglund, G. Sociodemographic factors associated with longterm weight gain, current body fatness and central adiposity in Swedish women. *Int J Obes Relat Metab Disord* 24, 685-694 (2000).
21. Kraynak M, Willging MM, Kuehlmann AL, Kapoor AA, Flowers MT, Colman RJ, Levine JE, Abbott DH. Aromatase Inhibition Eliminates Sexual Receptivity Without Enhancing Weight Gain in Ovariectomized Marmoset Monkeys. *J Endocr Soc.* 2022 Apr 22;6(6):bvac063. doi: 10.1210/jendso/bvac063. PMID: 35592515; PMCID: PMC9113444.
22. Park YW, Zhu S, Palaniappan L, Heshka S, Carnethon MR, Heymsfield SB. The metabolic syndrome: prevalence and associated risk factor findings in the US population from the Third National Health and Nutrition Examination Survey, 1988-1994. *Arch Intern Med*. 2003 Feb 24;163(4):427-36. doi: 10.1001/archinte.163.4.427. PMID: 12588201; PMCID: PMC3146257.
23. Emborg ME, Joers V, Fisher R, Brunner K, Carter V, Ross C, Raghavan R, Brady M, Raschke J, Kubota K, Alexander A. Intraoperative intracerebral MRI-guided navigation for accurate targeting in nonhuman primates. Cell Transplant. 2010;19(12):1587-97. doi: 10.3727/096368910X514323. Epub 2010 Jun 29. PMID: 20587170; PMCID: PMC3278961.
24. Kenealy BP, Keen KL, Kapoor A, Terasawa E. Neuroestradiol in the stalk median eminence of female rhesus macaques decreases in association with puberty onset. *Endocrinology.* 2016;157(1):70-6. 15.
25. Kenealy BP, Keen KL, Garcia JP, Kohlenberg LK, Terasawa E. Obligatory role of hypothalamic neuroestradiol during the estrogen-induced LH surge in female ovariectomized rhesus monkeys. *Proc Natl Acad Sci USA.* 2017;114(52):13804-13809.
26. Molly C. Carr, The Emergence of the Metabolic Syndrome with Menopause, *The Journal of Clinical Endocrinology & Metabolism,* Volume 88, Issue 6, 1 June 2003, Pages 2404– 2411, https://doi.org/10.1210/jc.2003-030242
27. Kravitz HM, Kazlauskaite R, Joffe H. Sleep, Health, and Metabolism in Midlife Women and Menopause: Food for Thought. *Obstet Gynecol Clin North Am.* 2018 Dec;45(4):679-694. doi: 10.1016/j.ogc.2018.07.008. Epub 2018 Oct 25. PMID: 30401550; PMCID: PMC6338227.
28. Davis SR, Castelo-Branco C, Chedraui P, Lumsden MA, Nappi RE, Shah D, et al. Understanding weight gain at menopause. *Climacteric.* 2012;15(5):419–29.
29. Hassanzadeh Makoui M, Mobini M, Khoshnoodi J, Judaki MA, Bahadori T, Ahmadi Zare H, Golsaz-Shirazi F, Moradi Tabriz H, Madjd Z, Jeddi-Tehrani M, Zarnani AH, Amiri MM, Shokri F. Generation and Characterization of Novel Diagnostic Mouse Monoclonal Antibodies Against Human Estrogen Receptor Alpha and Progesterone Receptor. *Asian Pac J Cancer Prev*. 2022 Sep 1;23(9):2999-3007. doi: 10.31557/APJCP.2022.23.9.2999. PMID: 36172662; PMCID: PMC9810286.
30. de Backer MW, Brans MA, Luijendijk MC, Garner KM, Adan RA. Optimization of adeno-associated viral vector-mediated gene delivery to the hypothalamus. Hum Gene Ther. 2010 Jun;21(6):673-82. doi: 10.1089/hum.2009.169. PMID: 20073991.

31. Kenealy, B.P., Kapoor, A., Guerriero, K.A., Keen, K.L., Garcia, J.P., Kurian, J.R., Ziegler, T.E., and Terasawa, E. (2013). Neuroestradiol in the Hypothalamus Contributes to the Regulation of Gonadotropin Releasing Hormone Release. *Journal of Neuroscience* 33, 19051–19059.
32. Kenealy, B.P., Keen, K.L., Garcia, J.P., Kohlenberg, L.K., and Terasawa, E. (2017). Obligatory role of hypothalamic neuroestradiol during the estrogen-induced LH surge in female ovariectomized rhesus monkeys. *Proc. Natl. Acad. Sci. U.S.A.* 114, 13804–13809.
33. Clément K, Vaisse C, Lahlou N, Cabrol S, Pelloux V, Cassuto D, Gourmelen M, Dina C, Chambaz J, Lacorte JM, Basdevant A, Bougnères P, Lebouc Y, Froguel P, Guy-Grand B. A mutation in the human leptin receptor gene causes obesity and pituitary dysfunction. *Nature.* 1998 Mar 26;392(6674):398-401. doi: 10.1038/32911. PMID: 9537324.
34. Aarthi Raman, Ricki J. Colman, Yu Cheng, Joseph W. Kemnitz, Scott T. Baum, Richard Weindruch, Dale A. Schoeller, Reference Body Composition in Adult Rhesus Monkeys: Glucoregulatory and Anthropometric Indices, *The Journals of Gerontology*: Series A, Volume 60, Issue 12, December 2005, Pages 1518–1524, https://doi.org/10.1093/gerona/60.12.1518
35. Zhou R, Bruns CM, Bird IM, Kemnitz JW, Goodfriend TL, Dumesic DA, Abbott DH. Pioglitazone improves insulin action and normalizes menstrual cycles in a majority of prenatally androgenized female rhesus monkeys. *Reprod Toxicol.* 2007 Apr-May;23(3):438-48. doi: 10.1016/j.reprotox.2006.12.009. Epub 2007 Jan 14. PMID: 17306503; PMCID: PMC2705750.
36. Avis NE, Crawford SL, Greendale G, Bromberger JT, Everson-Rose SA, Gold EB, Hess R, Joffe H, Kravitz HM, Tepper PG, Thurston RC; Study of Women's Health Across the Nation. Duration of menopausal vasomotor symptoms over the menopause transition. *JAMA Intern Med.* 2015 Apr;175(4):531-9. doi: 10.1001/jamainternmed.2014.8063. PMID: 25686030; PMCID: PMC4433164.
37. Laque A, Zhang Y, Gettys S, Nguyen TA, Bui K, Morrison CD, Münzberg H. Leptin receptor neurons in the mouse hypothalamus are colocalized with the neuropeptide galanin and mediate anorexigenic leptin action. *Am J Physiol Endocrinol Metab.* 2013 May 1;304(9):E999-1011. doi: 10.1152/ajpendo.00643.2012. Epub 2013 Mar 12. PMID: 23482448; PMCID: PMC3651648.
38. Joon S. Kim, Mohammed Z. Rizwan, Deborah J. Clegg, Greg M. Anderson, Leptin Signaling Is Not Required for Anorexigenic Estradiol Effects in Female Mice, *Endocrinology*, Volume 157, Issue 5, 1 May 2016, Pages 1991–2001, https://doi.org/10.1210/en.2015-1594
39. Pereira S, Cline DL, Glavas MM, Covey SD, Kieffer TJ. Tissue-Specific Effects of Leptin on Glucose and Lipid Metabolism. *Endocr Rev.* 2021 Jan 28;42(1):1-28. doi: 10.1210/endrev/bnaa027. PMID: 33150398; PMCID: PMC7846142.

4. CHAPTER FOUR: Ovarian and Extra-Ovarian Estradiol Depletion Both Contribute to Bone Loss but not to Body Weight Gain or Diminished Energy Expenditure in Adult Female Rhesus Monkeys

Willging MM, Greinwald EP, Jacobs AM, Peterson SM, Byington NC, Williams SJ, Woida AM, Shankar S, Kapoor AA, Ravelli MN, Shriver T, Gutkes JR, Beck RT, Abbott DH, and Levine JE.

[Manuscript is being prepared for submission to the Journal of the Endocrine Society. Contribution to this manuscript: Designed/carried out experiments, analyzed data, and prepared the manuscript for this thesis and subsequent publication]

4.1 Abstract

Declining serum estradiol (E_2) levels during the menopausal transition are associated with increased central adiposity and heightened risk for metabolic disease. Ovarian estradiol, E_2, supports female metabolic function in rodents. While ovariectomy (OVX) in rodents enables obesity, OVX in nonhuman primates (NHPs) inconsistently alters weight gain. We therefore hypothesized that in female NHPs, extra-ovarian E_2 provides key support for metabolic homeostasis. To test this, we employed aromatase inhibition, via letrozole, to eliminate extra-ovarian E_2 biosynthesis. Nineteen adult female rhesus monkeys were OVX and received: (1) E_2-containing capsules and daily oral treatments of letrozole (E2; n=5); empty capsules and daily oral treatments of either vehicle (VEH, 1ml vehicle/kg, n=7), or (3) letrozole (LET, 1 mg/kg in 1ml vehicle/kg, n=7). After 12 months, we demonstrated reduced percent change of bone mineral density in LET (p=0.005) and VEH (0.06, trend) females compared to E2 females. We also demonstrated a trend (p=0.08) in reduced glucose effectiveness for VEH and LET compared to E2 females at 12-months, despite no other differences in metabolic components such as body weight, body composition and locomotor activity. Our findings demonstrate that ovarian and ovarian + extra-ovarian E_2 depletion results in decreased bone mineral content and bone mineral density and contributes to reduced ability for glucose uptake independent of insulin action in adult female rhesus macaques.

4.2 Introduction

Women largely spend the last third of their lives in a post-menopausal state. Menopause is characterized as the cessation of menstrual cyclicity and ovarian estrogen production. The depletion of the ovarian follicular pool and consequent reduction of circulating estradiol (E_2) during menopause has been suggested by some investigators to contribute to post-menopausal weight gain, reduced energy expenditure, osteoporosis, hot flashes, cardiovascular disease, and cognitive decline[1-6]. There is greater consensus supporting the idea that menopause is associated with an increase in visceral relative to subcutaneous adiposity, with or without an increase in overall body weight[7]. Women experiencing personally distressing symptoms of menopause are prescribed hormonal replacement therapy (HRT), comprising of estrogen only therapies and combinations of estrogens and progestins, including synthetic forms of progesterone, to alleviate symptoms and help reduce osteoporosis induced by declining circulating E_2 levels. While HRT has been shown in some studies[8-9], but not others[10-12], to reduce weight gain and slow skeletal bone loss, HRT use has been greatly reduced since the WHO-sponsored studies originally reported small but significant increases in the risks of blood clots, dementia, and breast cancer[13-14].

E_2 supports optimal female metabolic function in multiple female laboratory animals, including, mice, rats, and sheep[15-17]. E_2 action is mediated through estrogen receptors, predominately, estrogen receptor alpha (ERα) and estrogen receptor beta (ERβ). ERα has been shown extensively to be the predominant estrogen receptor regulating E_2 action in rodents[18] and as we have recently shown, ERα, is an important hypothalamic regulator of metabolic homeostasis in adult female rhesus macaques

(Chapter 3). Thus, while ovarian E_2 has been established as a major contributor to female metabolism in female rodents and sheep, its role in female NHPs is less well understood. While ovariectomy (OVX) in female rodents enables obesity, OVX in female NHPs inconsistently alters weight gain[18-20], highlighting the possibility of E_2 produced outside the ovaries as an important site of E_2 synthesis signaling through ERα in female NHPs.

Aromatase, a cytochrome P450 enzyme, encoded by the CYP19A1 gene, converts testosterone (T) to E_2, as well as androstenedione (A_4) to estrone (E_1). The ovaries serve as the major site of E_2 synthesis in female non-primates, NHPs and humans. E_2, however, is also produced in various other tissues in which aromatase is expressed, such as adipose depots, adrenal glands, liver, skin, and in various brain regions. In particular, neural production of E_2 (neuro-E_2) has been characterized in birds, rats, and in NHPs. Brain aromatase is expressed at its highest levels in the medial basal hypothalamus (MBH), preoptic area (POA) and amygdala in rodents, monkeys, and humans.

We hypothesize that the failure for OVX to increase female NHP body weight is due to the residual actions of neuro-E_2 orchestrating energy balance in the hypothalamus of OVX female NHPs. Rodent research models have provided comprehensive evidence supporting roles played by ovarian E_2 in female energy balance and body composition, yet there are few studies in female NHPs assessing ovarian and extra-ovarian E2, possibly neuro-E2, in regulating aspects of energy balance. To test this hypothesis, we employed the aromatase inhibitor, letrozole, to diminish systemic and central E_2 production in OVX adult female rhesus macaques to

enable investigation into extraovarian E_2 source(s) regulating of female metabolism in a NHP. We propose that an extra-ovarian source of E_2, likely from the brain, will be greatly diminished or extinguished by body-wide aromatase inhibition and resulting in metabolic dysfunction via increased body weight, increased adiposity and reduced energy expenditure in female rhesus macaques compared with both E_2 replaced females and those experiencing depleted ovarian E_2, alone.

4.3 Methods

Animals

Nineteen adult female rhesus macaques (5-11 years of age) from the Wisconsin National Primate Research Center colony were all OVX assigned to one of three female groups so that age, body weight and body mass index (BMI) were comparable (Table 1): 1) OVX + letrozole + E_2 replacement via subcutaneous capsules (E2, n=5), 2) OVX + vehicle subcutaneous capsules (VEH, n=7) and 3) OVX + letrozole + vehicle capsules (LET, n=7) (Table 1). E_2 replacement was achieved through subcutaneous E_2-filled capsules that maintained a sufficient systemic level of E_2 (40-100 pg/mL) to suppress gonadotropin secretion and resembled E_2 values observed during the early-to-late follicular of the menstrual cycle[21]. To maintain constant E_2 levels, capsules were replaced every 3 months throughout the study. OVX females received a daily oral dose of 1ml/kg low calorie pudding as a vehicle control. LET and E2 females were given a daily oral dose of 1 mg/kg of letrozole dissolved in 1ml/kg low calorie pudding. Monkeys were maintained in these three groups for ~17 months, pair-housed, in enclosures under 12-h lighting, ambient temperature of ambient temperature of ~27°C and humidity of ~50%. (Figure 1). The protocol for this study was approved by the Animal Care and Use Committee of the

Office of the Vice Chancellor for Graduate Research and Education of the University of Wisconsin–Madison, an AAALAC-accredited program.

Diet

Monkeys were fed chow twice a day, between 0700h-0900h and 1200h-1400h (Teklad Global 20% Protein Primate Diet, ENVIGO, Madison, WI). The calorie distribution of the biscuits was 29% protein, 14% fat and 57% carbohydrates with an energy density of 2.8 kcal/g. Monkeys were supplemented with daily fruit enrichment (<100 kcals), weekly tactile enrichments (<100 kcals), and weekly destructible enrichments (<100 kcals).

Hormone and Metabolic Analyte Determinations

Steroid hormone analysis was adapted from methods previously described[22,23]. Briefly, internal standard was added to rhesus serum samples (1mL) and then they were extracted twice using methyl tert butyl ether followed by dichloromethane. Samples were derivatized using dansyl chloride and then analyzed by LC-MS/MS (Sciex QTRAP 5500). Individual calibration curves were constructed for each analyte with at least 8 points. The linearity was $r > 0.9990$ and the curve fit was linear with $1/x$ weighting. None of the compounds of interest were detected in blank or double blank samples. Inter-assay coefficient of variation was determined by 3 levels of human serum and ranged from 5.6-9.7%.

Serum samples were analyzed for estradiol (25uL) and progesterone (20uL) using a cobas e411 analyzer equipped with ElectroChemiLuminescence technology (Roche, Basal, Switzerland) according to manufacturer instructions. Results were determined via a calibration curve which was instrument generated by 2-point calibration using traceable

standards and a master curve provided via the reagent barcode. Inter-assay coefficient of variation (CV) was determined by a pool of rhesus plasma. For estradiol, the limit of quantitation (LOQ) was 25 pg/mL, the intra-assay CV was 2.02%, and the inter-assay CV was 5.05%. For progesterone, the LOQ was 0.2 ng/mL, the intra-assay CV was 1.37%, and the inter-assay CV was 4.63%.

Metabolic peptides were measured with a Milliplex Non-Human Primate Metabolic Magnetic Bead Panel (NHPMHMAG-45K; EMD Millipore). The assay was run according to the kit insert using a BioPlex 200 (BioRad). The intra-assay CV was determined by two pools of rhesus serum and ranged from 2.2-9.3%.

Hypothalamic Hormone Determinations

The method for measurement of steroid hormone measurement in the hypothalamus was adapted from Bertin et al., 2015[24]. Briefly, up to 100 mg of brain tissue was homogenized in methanol. Internal standard was added, and the methanol was run through solid phase extraction using Oasis HLB cartridges (Waters Corporation). The eluate was derivatized and analyzed by LC-MS/MS (Sciex 6500+). Individual calibration curves were constructed for each analyte with at least 8 points. The linearity was $r > 0.9990$ and the curve fit was linear with $1/x$ weighting. Inter-assay coefficient of variation was determined by two pools of spiked macaque cerebellum and ranged from 8.9-17.2%.

Body Weight, Body Composition & Bone Mass

All monkeys were weighed weekly. Incremental area under the curve (AUC) assessment of weight parameters over time, calculated by the trapezoid rule, was used to better detect recurring differences in weight gain, as previously employed by Risal

and colleagues (2019). At baseline, 6-months, and 12-months post-OVX, total body composition was assessed by dual-energy X-ray absorptiometry (DXA, iDXA, GE/Lunar Corp., Madison, WI) on sedated animals. Monkeys received up to 7 mg/kg ketamine IM and up to 0.03 mg/kg dexmedetomidine IM, and the latter was reversed on conclusion of the procedure by up to 0.3 mg/kg atipamezole IM. After placing the anesthetized animal onto the scanner bed, DXA-compliant cushioning was used to position the animal with arms and tail flat on the scanner bed, clearly distinct from the monkey's trunk and other extremities. A DXA scan was then performed for approximately 30 minutes. The scanner room was maintained at 27-28°C during the performance of all scans to minimize the risk of hypothermia. Monitoring of anesthesia recovery was documented every 15 min until the monkey was sitting upright, then every 30 minutes until it was fully recovered from the anesthesia. Fat mass, fat-free mass, bone mineral content (BMC) and bone mineral density (BMD) were determined for total body as well as regions of interest, including abdomen, chest, thighs and extremities. Body mass index was calculated using $\frac{Body\ Weight\ (kg)}{Crown\ Rump\ Length\ (m^2)}$ [25].

Somatometric Measurements

Somatometric parameters were measured using tape measure or calipers while monkeys were anesthetized for DXA imaging. Measurements included femur length; abdomen, chest, pelvis, arm, leg, and head circumferences; head diameter; and chest and abdomen skinfolds. Additionally, monkeys were placed on an osteometric board for measurement of crown rump and crown-heel lengths.

Caloric Intake Assessment

At baseline, 6-months post-OVX and 12-months post-OVX, monkeys were singly housed 0700h-1800h for 7-21 days. Animals were fed 9 biscuits of standard chow twice a day at 0700h-0900h and 1200h-1400h. At each feeding, monkeys received on average ~423 kilocalories from chow. In addition, animals received daily fruit enrichment (i.e., pear, banana, green pepper, kiwi and apple) totaling on average ~100 kilocalories per enrichment occurrence. Daily chow and enrichment were weighed prior to being given each day (Calories Offered). At 1800h, any chow or enrichment not consumed from the day was weighed (Calories Left) and returned to each monkey for the overnight period (1800h-0700h). Calories Consumed was calculated by subtracting Calories Left from Calories Offered. The weight of chow of Calories Consumed was multiplied by the chow's energy density of 2.8 kcal/g to convert to calories. Monkeys were repaired with their partner for the overnight period (1800h-0700h).

Locomotor Activity Assessment

At baseline, as well as at 6-months and 12-months post-OVX accelerometers were attached to a fabric collar and placed around each monkey's neck. Activity and intensity of movement were recorded over a ~4-week period after which the accelerometers were removed. Activity was recorded in counts (n), where one count represented body movements on an x, y, or z axis. The accelerometer sampled such activity counts every minute and these data were averaged for every hour (h), day (during lights on, 0600h-1800h), night (during lights off, 1800h-0600h), morning (0600h–1200h), afternoon (1200h–1800h), and over 24 hours. Incremental areas under the

curve activity values were also assessed to detect cumulative differences over the course of the study.

Doubly Labeled Water (DLW) Procedures

Total energy expenditure was measured during a 4-day period by the two-point doubly-labeled water (DLW) methodology[26]. Monkeys were injected IV with 1.0 g/kg of body weight of a premixed cocktail. The mixture comprised 0.147 g of 98 APE 18O water (Medical Isotopes, Inc., Pelham, NH), 0.083 g of at 99.9 APE deuterium oxide (2H2O, Cambridge Isotope Laboratories, Andover, MA), 0.650g of sterile water, and 0.125 g of 7.2% hypertonic NaCl to achieve physiological osmolarity. Blood samples were collected from non-anesthetized monkeys prior to (baseline), two hours, and four days after DLW injection. Immediately after blood collection, the samples were centrifuged for 10 min for serum separation. Serum was stored at −20°C in cryogenically stable tubes until analysis by isotope ratio mass spectrometry.

Water from serum samples was extracted by centrifugation (4°C, 30 minutes at 4,500 rpm, RCF 3,100 ×g, Centrifuge Marathon 21k/BR, Thermo Fisher Ltd) on regenerated cellulose filters (Amicron Ultra-4, Ultracel-30K, Merk Millipore Ltd). Isotope enrichments were determined as previously described (Blanc et al., 2003). Carbon dioxide production was calculated according to the equation proposed by Speakman et al. (2021): rCO2 = 0.4554 * N * [(1.007 * ko) – (1.043 * kd)] * 22.26, in which total body water (N) was calculated by the average of dilution spaces of stable isotopes (2H218O) obtained by the plateau method (Coward et al., 1990) using the 2-h post-dose sample and corrected for isotope exchange by the factors 1.043 and 1.007, respectively (Speakman, et al 2021). The observed isotope dilution space ratio was 1.037 ± 0.019

(mean ± SD). The isotope constant elimination rates (ko and kd) were calculated by linear regression of the natural logarithm of isotope enrichment as a function of elapsed time from 2h samples. TEE was calculated by Wier's equation (1949) using a food quotient of 0.93 estimated from the animal's diet.

Intravenous Glucose Tolerance Test (ivGTT)

At baseline, 6-months post-OVX and 12-months post-OVX, an ivGTT was conducted according to the Modified Minimal Model (MMM) protocol as adapted for rhesus monkeys[27]. A catheter was inserted through the saphenous or femoral vein and the tip positioned in the inferior vena cava. Four pretreatments ~1.5 ml blood samples were taken at approximately -15, -10, -5, and -1 minutes to establish fasted baseline values of insulin and glucose. A ~300 mg/kg glucose bolus was administered over about one minute starting at ~ 0 min, and ~1.5 ml blood samples were drawn at 2, 3, 4, 5, 6, 8, 10, 12, 14, 16, 19, 22, 23, 24, 25, 27, 30, 40, 50, 60, 70, 80, 90, 100, 120, 140, 160, and 180 minutes after glucose administration. Blood volume availability for individual animals was calculated by body weight (animal's body weight (kg) x 60 = estimated total volume of blood). If a monkey's blood volume availability did not meet the required volume for the full ivGTT (48 ml), samples at timepoints of 100, 120, 140 and/or 160 were omitted. Twenty minutes after glucose bolus administration, tolbutamide (~25mg/ml up to a maximum volume of ~5ml 1N sodium hydroxide, 0.1N hydrochloric acid in sterile saline solution) was administered via the catheter to induce an additional increment in insulin secretion to enhance MMM calculations. Maintenance of catheter patency and fluid volume was accomplished with intravenous Plasma-Lyte A provided by an infusion pump hooked up to the indwelling catheter. Additional fluid replacement

was provided by 1-2ml cannula line flushes following each blood sample withdrawal. The duration of anesthesia was approximately 240 minutes. Monkeys were maintained under warm heat lamps (with a 24-inch minimum space between the animal and the heating lamp), a heated air warming unit and/or a water-circulating heating pad. During the procedure, the monkey's blood oxygen, heart rate and rectal temperature were continuously monitored and recorded every 15 minutes. After completion of the procedure, progress of anesthesia recovery was documented every 15 min until the monkey was sitting upright, then every 30 min until it was fully recovered from the anesthesia.

Statistical Analysis

Data collected was analyzed utilizing GraphPad PRISM and SPSS software. Metabolic parameters collected at multiple timepoints were compared by ANOVA with repeated measures (RM-ANOVA). Metabolic parameters at individual timepoints between three treatment groups were assessed via one-way ANOVA. Plots are expressed as means+/-SEM. Relationships between hormones, metabolic parameters and hypothalamic hormones were assessed via nonparametric Spearman's correlation tests. To determine cumulative differences over time, incremental area under the curve (AUC) was calculated via the trapezoid rule using GraphPad Prism software. Outliers were determined via Grubbs test at alpha=0.05 level. If outliers were determined, appropriate statistical tests were completed after removal of outlier(s). Data presented includes all monkey values, nevertheless. Normality was assessed via GraphPad software. If normality was not met, $\log_{10}$ transformations were performed prior to statistical

analysis. Untransformed data, however, are reported. Statistical significance was determined as $p<0.05$ and trending towards significance was determined as$0.05< p<0.1$.

4.4 Results

Hypothalamic and Circulating Hormone Levels

Circulating hormones values averaged over the duration of the study and compared between groups, revealed reductions in estrogens but increases in androgens in both the VEH and LET E_2-depleted groups compared to the E2 group (Figure 2). In VEH and LET females, levels of both circulating estradiol (VEH, $p<0.0001$; LET, $p<0.0001$) and estrone (VEH, $p=0.02$; LET, $p=0.005$) were diminished in both E_2-depleted groups compared to the E2 group. In contrast, VEH and LET females exhibited hyperandrogenism compared to E2 by way of increased circulating T (VEH, $p=0.002$; LET, $p<0.0001$) and DHEA (VEH, $p=0.008$; LET, $p=0.003$) compared to the E2 females. LET females also developed elevated androstenedione levels compared to both VEH ($p=0.09$, trend) and E2 ($p=0.008$) females. There were no observed between female group differences in circulating progesterone levels (Figure 2). With regard to ratios between circulating steroid hormones, the T: E_2 ratio favored testosterone in LET ($p=0.0003$) and VEH (0.07) females compared to the E2 group. Additionally, the T: A_4 ratio trended to favor to testosterone in VEH ($p=0.08$) compared to E2 females (Figure 2).

Hypothalamic hormone content measured by LC-MS/MS from the right hemi-hypothalamus at 17-months from study onset revealed largely undetectable hypothalamic E_2 in both the VEH and LET groups, significantly reduced compared to E2 females (VEH, $p=<0.0001$; LET, $p=0.0001$, Figure 3A). E_1 was significantly reduced in

LET compared to E2 females (p=0.00.02, Figure 3B). Hypothalamic content of T, DHEA, A_4, progesterone, 17-OHP, and cortisol all showed no between female group differences (Figure 3C-H). Hypothalamic hormone ratios between T and E_2 and T and A_4 showed no between female group differences (Figure 4A-B). The hypothalamic ratio of E_1 to E_2, however, was reduced in E2 compared to VEH females (p=0.04, Figure 4C).

Circulating Metabolic Analytes

At baseline pre-OVX, there were no between female group differences in circulating levels of leptin, glucagon, GIP, c-peptide, and amylin (Table 2). There was a trend towards increased GLP-1 in LET compared to E2 females (p=0.07), but this trend disappeared at 6-months and 12-months post-OVX. At 6-months post-OVX, there was a trend towards reduced c-peptide in LET compared to E2 females (p=0.07) and increased leptin in VEH compared to E2 females (p=0.08), while there was no observed between group differences in any of the other metabolic analytes between female groups (Table 2). At 12-months post-OVX, no observed trends or differences between female groups remained for any metabolic analyte (Table 2).

Body Weight, Body Composition and Bone Analysis

Monthly body weights were calculated by averaging the weekly body weights for all animals in each treatment group. There were no differences in body weight or body weight percent change between the three female groups (Figure 5A, 5C). Additionally, there were no differences in AUC analyses performed on body weight and body weight percent change through 17 months of the study (Figure 5B,5D). Body mass index (BMI) calculated at baseline, 6-months post-OVX and 12-months post-OVX (Figure 6A) and percent change from baseline to 12-months post-OVX (Figure 6B) showed no

difference between female groups. Body composition via DXA scans at baseline, 6-months post-OVX and 12-months post-OVX showed no between female group difference in total body fat mass or total body fat-free mass. Additionally, there were no between female group differences in calculated percent change of fat mass and fat-free mass between baseline and 12-months post-OVX (Figure 7). In all validated regions of interest (abdomen, thighs, extremities) there were no between female group differences in fat mass or fat-free mass (Table 3).

Bone mineral content (BMC) was reduced at 6-months and 12-months post-OVX in the LET females compared to their baseline values ($p=<0.0001$; $p=0.0011$, Figure 8A). In contrast, E2 females presented with increased BMC at 12-months post-OVX compared to their baseline values ($p=0.045$, Figure 8A). Both VEH and LET females presented with negative percent change of BMC from baseline to 12-months post-OVX compared to E2 females (VEH vs E2, $p=0.007$; LET vs E2, $p=0.0002$; Figure 8B). Similarly with bone mineral density (BMD), LET females presented with reduced, while VEH females presented with a trend towards reduced percent change from baseline to 12-months post-OVX compared to E2 females (VEH vs E2, $p=0.06$; LET vs E2, $p=0.005$; Figure 8D). Only VEH females demonstrated a time effect of reduced BMD between 6-months and 12-months post-OVX ($p=0.03$; Figure 8B), in contrast to E2 and LET females.

Caloric Intake

Total daily calories (kcals) consumed were averaged between all the days of the caloric intake assessment at each timepoint. There were no differences in average calories consumed at baseline, 6-months post-OVX or 12-months post-OVX between

the three female groups (Figure 9A). Additionally, when daily average calories consumed were adjusted for body weight (kg) and fat-free mass (kg) for each animal at each timepoint, there were no observed between female group differences (Figure 9B).

Locomotor Activity

Locomotor activity data was calculated for a total of 24-hours and specific periods of the day. Total 24-hrs was an average of all the activity counts over 24-hrs averaged over the number of days the collar was worn. Daytime activity was the average of activity counts between 0600h-1800h, nighttime was 1800h-0600h, morning was 0600h-1200h and afternoon was 1200h-1800h. There were no observed between female group differences in total locomotor activity counts at baseline, pre-OVX and 12-months post-OVX (Figure 10, Figure 11). Additionally, there was no between female group differences in percent change of activity counts from baseline to 12-months post-OVX (Figure 12).

Doubly labeled water (DLW) Energy Expenditure

Total energy expenditure (TEE, kcal/d) was adjusted for fat-free mass (FFM, kg) at baseline, 6-months, and 12-months. There were no observed between female group differences in TEE adjusted for FFM at baseline, 6-months, or 12-months post-OVX (Figure 13A-C). Additionally, there was no observed between female group differences in percent change between baseline and 12 months in TEE adjusted for FFM (Figure 13D).

Glucoregulation via ivGTT

Glucoregulatory values were calculated via the Bergman-Cobelli Modified Minimal Model for rhesus macaques (Table 4). There were no between female group differences at baseline (B) and 12-months post-OVX for insulin sensitivity (SI, baseline, p=0.38; 12-mo, p=0.46), disposition index (DI, baseline, p=0.86; 12-mo, p=0.34), acute insulin response (AIRg, baseline, p=0.88; 12-mo, p=0.67), basal glucose (Gb, baseline, p=0.62; 12-mo, p=0.79) and basal insulin (Ib, baseline, p=0.54; 12-mo, p=0.30). At 12-months post-OVX, there was a trend towards reduced glucose effectiveness (Sg) in LET females (p=0.07) compared to E2 and VEH female groups, suggesting reduced ability for insulin-independent glucose uptake in LET females. Percent change between baseline and 12-months post-OVX revealed no between female group differences in any glucoregulatory measure (SI, p=0.11, AIRg, p=0.34, DI, p=0.59, Sg, p=0.37, Ib, p=0.42 and Gb, p=0.39).

4.5 Discussion

In the present study, we comprehensively demonstrate that neither ovarian E_2 depletion nor ovarian + extra-ovarian E_2 depletion for 17-months elicits a disruption in energy balance in adult female rhesus macaques. We hypothesized that extra-ovarian E_2, specifically neuro-E_2, would be the source of E_2 signaling through hypothalamic ERα to maintain female metabolic homeostasis, but our findings reveal that neither long-term ovariectomy alone, nor ovariectomy and complete estrogen synthesis inhibition, produced any major alterations in body weight, body composition, adiposity, energy expenditure, food intake, or glucose homeostasis. Our observations suggest that

neither ovarian nor extra-ovarian estrogens are required to maintain metabolic homeostasis in a non-human primate under normal dietary conditions.

Our results surprisingly revealed that the hypothalamic from ovariectomized animals treated with either vehicle or letrozole contained largely both the VEH and LET females exhibited undetectable levels of circulating and hypothalamic E_2 content. E2 females nevertheless demonstrated early to late follicular phase levels of circulating E_2 due to E_2 replacement and averaged 0.89 pg of E_2 in the right hemi-hypothalamus. It is interesting that both VEH and LET females exhibited comparable undetectable hypothalamic content of E_2 despite administration of high doses (1 mg/kg/day) of the aromatase inhibitor, letrozole, to LET females. Despite a highly sensitive limit of assay quantification for E_2 of 250 fg, it is possible that we were not able to identify aromatase inhibition driven differences as both systemic E_2 levels and hypothalamic E_2 content were below this limit. In addition, hypothalamic E_2 content in E2 females could be derived from circulating E_2 crossing the blood brain barrier, highlighting the possibility that hypothalamic E_2 in adult female rhesus macaques may not be synthesized in the hypothalamus or is only synthesized for brief periods following acute elevations in systemic E_2 levels[28].

In contrast to hypothalamic E_2 content, hypothalamic content of E_1 was reduced in LET, but not VEH female groups compared to the E2 group. This latter finding clearly demonstrates that the adult female rhesus monkey hypothalamus does express aromatase since aromatase inhibition and OVX diminished hypothalamic E_1 content more than OVX alone. Since this effect of aromatase inhibition was only observed for the hypothalamic E_1 and not hypothalamic E_2, content it is possible that hypothalamic

conversion of A_4 to E_1 was favored over hypothalamic conversion of A_4 to T. This motion of neuro-steroidogenic pathways having a bias towards A_4 and E_1 production relative to T and E_2 would be consistent with studies of bird brain neurosteroidogensis[29]. Interestingly, hypothalamic A_4 content was nearly undetectable in all female groups and there were no between female group differences of hypothalamic A_4 and T. The greater hypothalamic content of E_1 over E_2 is also consistent with research identifying E_1 as the predominate active estrogen in post-menopausal women.

In the systemic circulation of adult female rhesus monkeys in this study, E_1, like E_2, was below the limit of quantitation for most VEH and LET females. T and A_4 were nevertheless both increased to a greater extent in LET females, compared to VEH and E2 females, strongly implicating aromatase inhibition induced hyperandrogenism. The contrast between systemic circulation hormone levels and hypothalamic hormone content could be due to tissue specific regulation of estrogens as circulating levels of E_2 decline experimentally or naturally, with menopause. Investigation into the hormonal and genetic profiles of metabolically relevant tissues such as adipose and liver could reveal specific changes within a tissue.

With regard to E_2 depletion association with impaired female metabolic function, we found a subtle trend in reduced glucose effectiveness in the VEH and LET group compared to the E2 group. This suggests that reduced ovarian as well as reduced ovarian + extra-ovarian E_2 contributes to reduced ability for glucose uptake independent of insulin action. The menopausal transition in women lasts on average 4 years but can last up to a decade. During this period of vast hormonal and metabolic changes, E_2 levels decline. Our study duration was only 17 months so while it exceeded a year, the

representative time compared to humans experiencing reduced E_2 is short. In the absence of body weight gain and lipid accumulation, it is possible we are highlighting only early onset disruptions of energy balance due to reduced estrogens. The reduced ability of glucose effectiveness could elicit pancreatic islets to compensate and if stressed by a Western style diet or sedentary lifestyle, could evolve into insulin intensity and subsequently, diabetes.

With regard to E_2 depletion and the development of osteoporosis, we provided evidence that ovarian and ovarian + extra-ovarian E2 depletion results in decreased bone mineral content and bone mineral density. Percent change of bone mineral density from baseline to 12-months post-OVX trended towards greatest bone loss in LET females. Understanding the effects of aromatase inhibitor use and bone loss is incredibly important as aromatase inhibition is used as a frontline treatment for breast cancer patients[30]. Bone loss has been shown to occur rapidly in post-menopausal women with an estimated 10-20% of bone loss around the first 5 years[31] and occurs more severely in post-menopausal breast cancer patients receiving aromatase inhibition therapy[32]. In the present female monkey study, reductions in bone mineral content started to appear six-months post-treatment onset in LET females, confirming past literature of rapid deterioration of bone[33]. In contrast to other components of energy balance such as body weight and energy expenditure, our study confirms that bone metabolism appears sensitive to changes in circulating estrogens and is exaggerated by aromatase inhibition.

In summary, we demonstrated that OVX + aromatase inhibition exaggerates circulating hyperandrogenism and induces hypothalamic E_1:E_2 ratios favorable to E_1.

While all but one of these endocrine differences failed to diverge from just OVX alone, except for E_1, only bone loss differed in phenotypic outcomes between female groups. Potentially, the subtle difference in reduced glucose effectiveness in the E_2 depleted groups is highlighting the first disruption to energy balance and unless compensated for effectively, and even without achieving a positive energy balance, could lead to diabetes.

4.6 Tables/Figures

	Age (years)	Body Weight (kg)
E2 (n=7)	7.40 ± 3.31	6.59 ± 1.10
VEH (n=7)	7.50 ± 2.10	7.00 ± 1.16
LET (n=7)	9.94 ± 1.79	7.06 ± 1.03
p-value	0.13	0.75

Table 1: Comparable ages and body weights between all three female rhesus treatment groups. OVX+LET+E2 (n=7), OVX+VEH (n=7) and OVX+LET (n=7) at the start of the study. Values expressed as mean ± SEM. P-values calculated via ordinary one-way ANOVA.

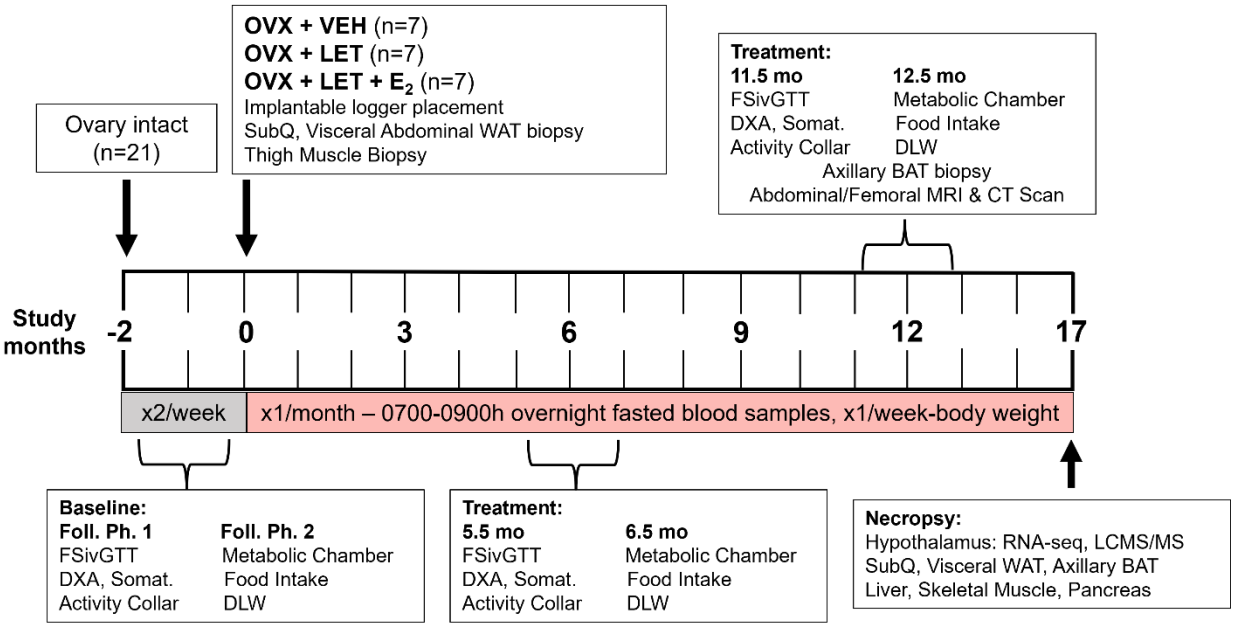

Figure 1: Timeline of treatment onset, metabolic procedures, and end of study**.**

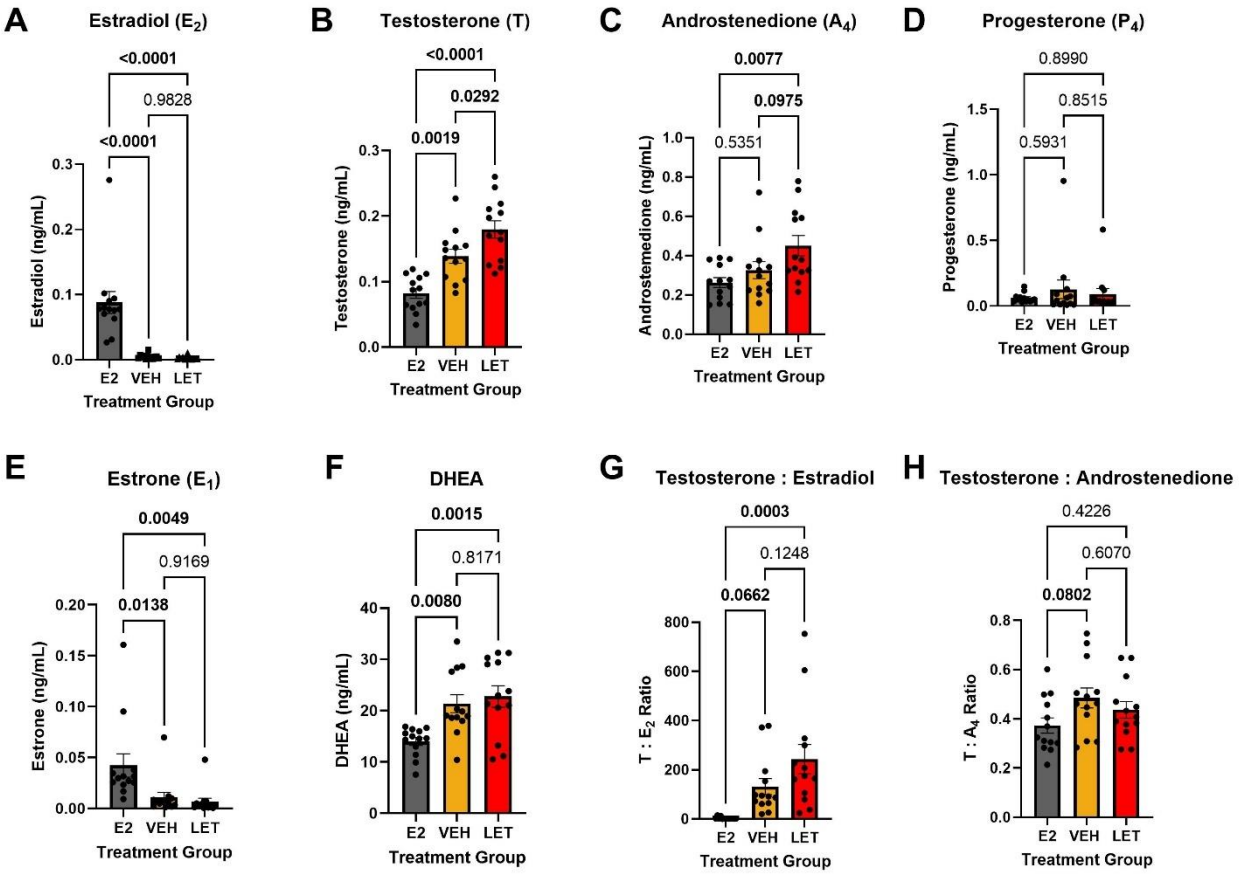

Figure 2: Circulating hormones averaged over 17 months of the study. Plots expressed as mean ± SEM. Significance assessed via ordinary one-way ANOVA. VEH and LET group presented with reduced E_1 and E_2 and increased T, A_4 and DHEA compared to the E2 group. T: E_2 ratio was favored to T in VEH and LET group and T: A_4 ratio favored to T in VEH group. E2 (grey, n=5), VEH (yellow, n=7) and LET (red, n=7).

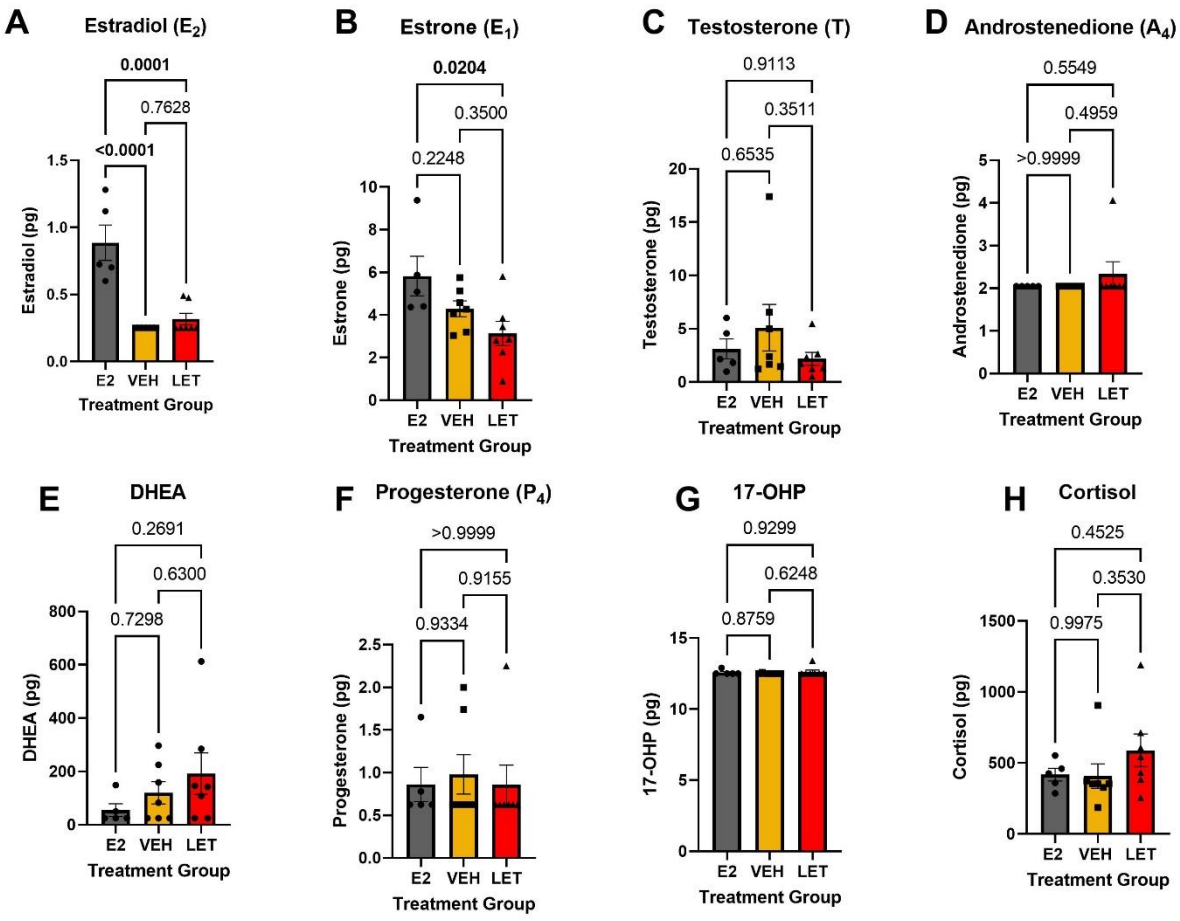

Figure 3. Hypothalamic steroid hormone content from the right hemi-hypothalamus 17-months following study onset. Individual values and mean ± SEM values are illustrated. E2 (grey, n=5), VEH (yellow, n=7) and LET (red, n=7).

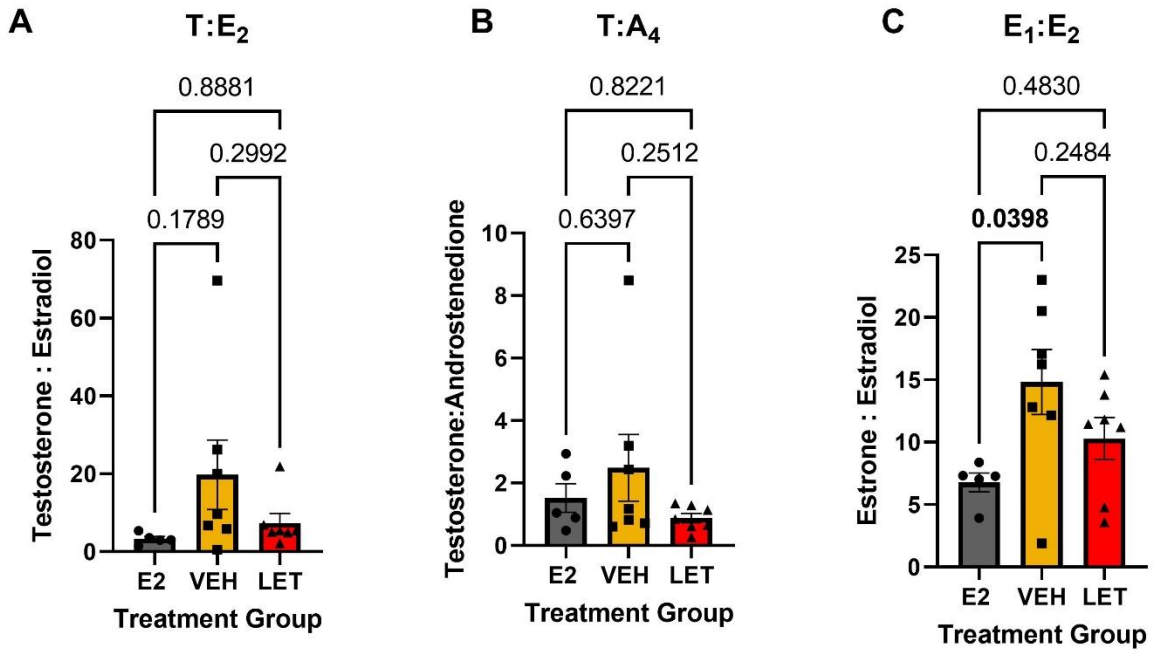

Figure 4: Ratio of hypothalamic hormones (T= testosterone, A_4=androstenedione, E2= estradiol and E1= estrone). Plots expressed as mean ± SEM. Significance assessed via ordinary one-way ANOVA. E2 (grey, n=5), VEH (yellow, n=7) and LET (red, n=7).

		Treatment Group			
		E2	**VEH**	**LET**	**p-value**
Leptin	Baseline	168.9±68.4	372.7±164.8	375.5±95.04	0.49
	6-months	**253.7±108.3**	**949.4±337.7**	**314.9±85.8**	**0.08**
	12-months	231.3±92.6	519.5±155.7	479.8±115.2	0.32
Ghrelin	Baseline	NA	NA	NA	NA
	6-months	20.15±6.43	13.93±0.21	18.27±2.15	0.40
	12-months	55.41±23.18	27.72±11.78	39.61±14.50	0.56
GLP-1	Baseline	**30.83±14.46**	**27.86±6.27**	**59.58±9.80**	**0.07**
	6-months	209.8±102.4	233.4±93.8	146.7±71.6	0.76
	12-months	30.37±3.58	44.14±7.12	47.73±14.50	0.53
Glucagon	Baseline	127.3±40.85	117.5±39.27	33.58±12.56	0.14
	6-months	36.60±8.95	37.48±7.00	44.63±18.59	0.11
	12-months	50.58±6.43	31.68±3.99	34.00±12.58	0.34
GIP	Baseline	49.00±10.8	32.04±5.3	41.25±7.4	0.32
	6-months	38.43±11.2	34.82±5.5	32.75±6.6	0.87
	12-months	52.50±12.0	59.00±5.6	70.69±13.9	0.52
C-peptide	Baseline	2002±637	1927±491	1655±183	0.86
	6-months	**963.8±218**	**1577±411**	**594.5±127**	**0.07**
	12-months	2091±315	2948±891	1754±161	0.34
Amylin	Baseline	3061±10.9	25.18±10.6	51.19±18.4	0.68
	6-months	13.72±0.00	19.26±5.54	54.22±40.50	0.71
	12-months	13.72±0.00	16.63±2.91	20.49±6.77	0.49

Table 2: Metabolic analytes measured at baseline pre-OVX, 6-months and 12-months post-OVX. Percent (%) change is the percentage change between baseline pre-OVX and 12-months post-OVX. Values expressed as mean ± SEM. Trending significance is represented by p-value <0.1.

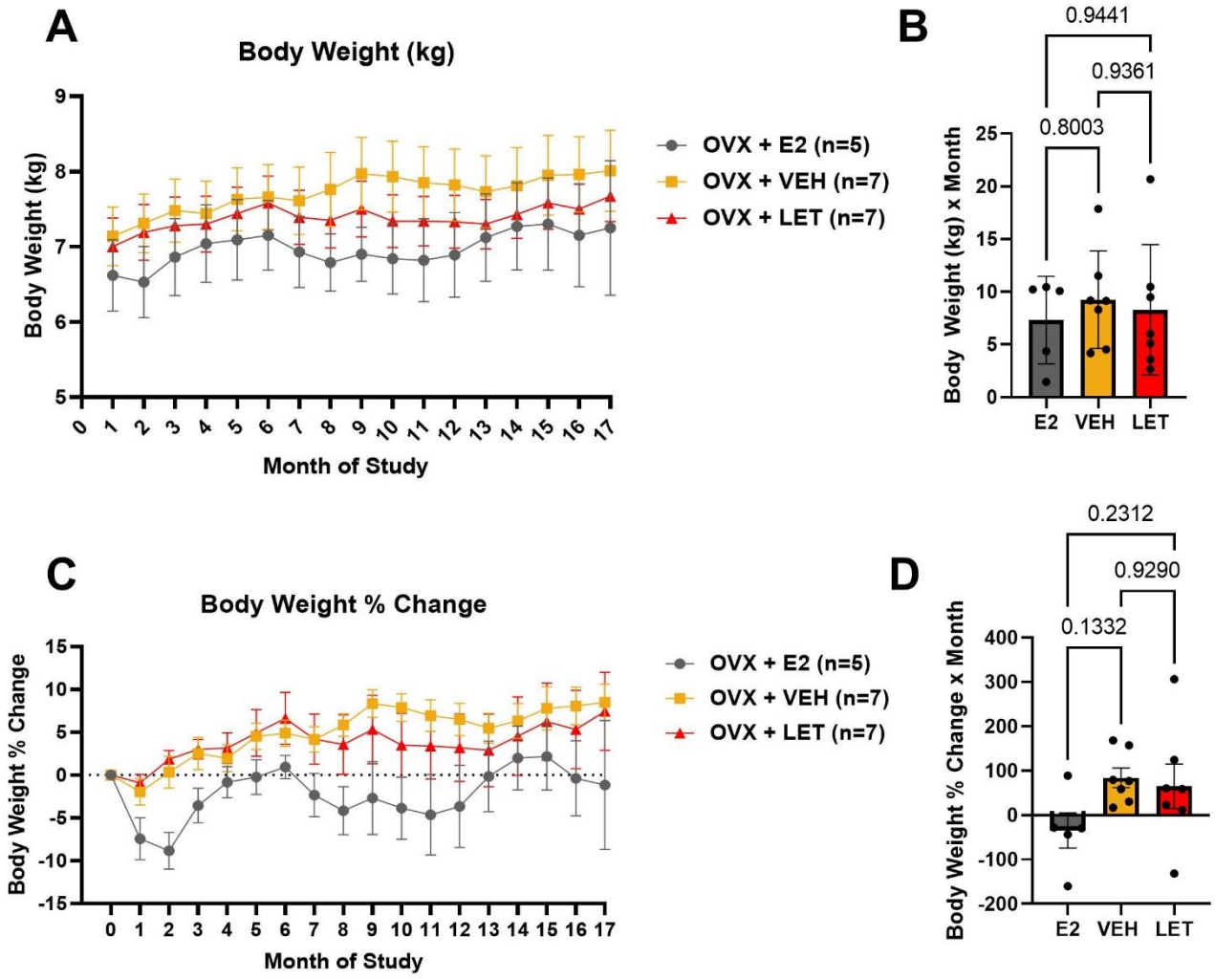

Figure 5: Body weight (A) over 17 months of the study with corresponding AUC bar graph (B) and body weight percent change from month 0 (C) over 17 months with corresponding AUC bar graph (D). Plots are expressed as mean ± SEM. Significance assessed via RM-ANOVA (A, C) and ordinary one-way ANOVA (B,D). E2 (grey, n=5), VEH (yellow, n=7) and LET (red, n=7).

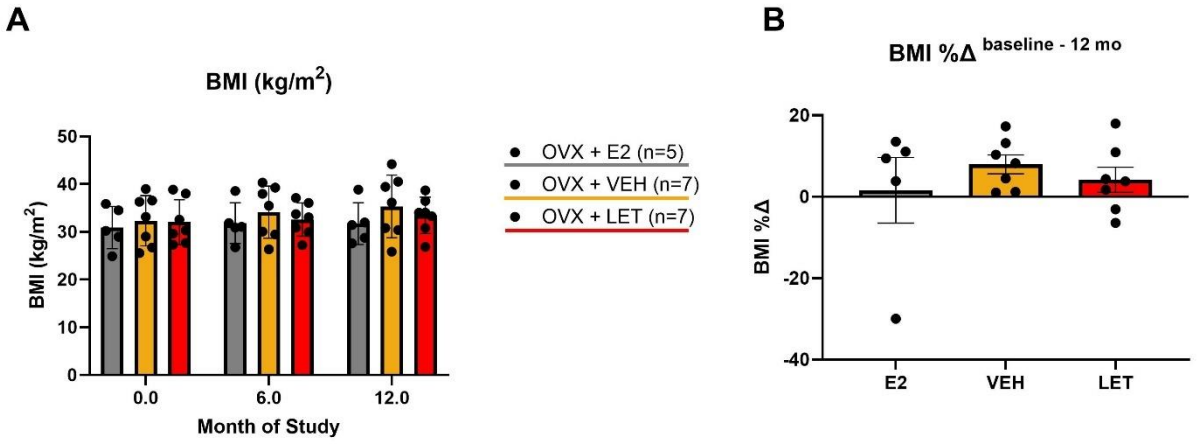

Figure 6. Body mass index (BMI) at baseline, 6-months and 12-months post-OVX (A) and BMI percent change between baseline and 12-months post-OVX (B). Plots are expressed as mean ± SEM. Signficance was assed via RM-ANOVA (A) and ordinary one-way ANOVA (B). E2 (grey, n=5), VEH (yellow, n=7) and LET (red, n=7).

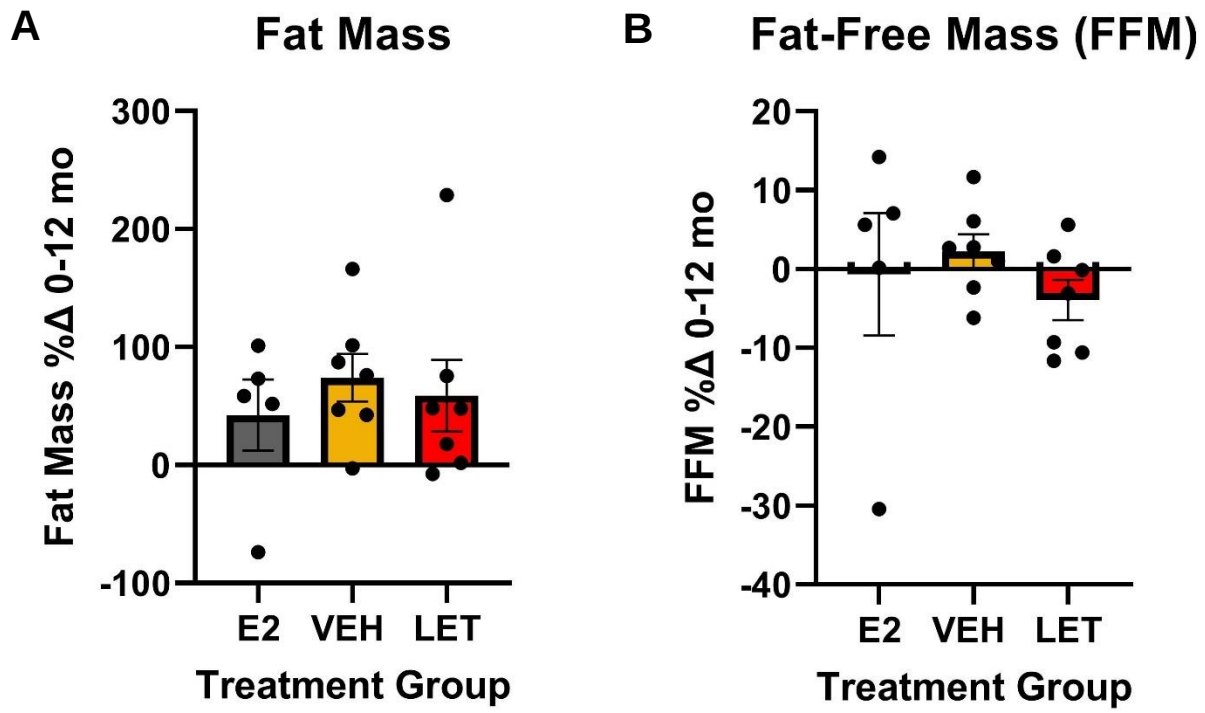

Figure 7. Fat mass and fat-free mass percent change from baseline to 12-months post-OVX. Plots are expressed as mean ± SEM. Significance was assessed via ordinary one-way ANOVA. E2 (grey, n=5), VEH (yellow, n=7) and LET (red, n=7).

		Treatment Group			
Fat-Mass (kg)		E2	VEH	LET	p-value
Abdomen	Baseline 6-months 12-months	0.29±0.11 0.34±0.11 0.38±0.16	0.56±0.17 0.86±0.19 0.98±0.20	0.48±0.13 0.78±0.14 0.82±0.14	0.13
Upper Legs	Baseline 6-months 12-months	0.18±0.06 0.21±0.04 0.02±0.03	0.22±0.06 0.28±0.04 0.29±0.05	0.22±0.04 0.29±0.04 0.27±0.04	0.39
Chest	Baseline 6-months 12-months	0.23±0.08 0.29±0.08 0.24±0.01	0.33±0.09 0.54±0.09 0.44±0.11	0.29±0.08 0.44±0.11 0.38±0.08	0.27
Lower Legs	Baseline 6-months 12-months	0.12±0.02 0.14±0.02 0.15±0.03	0.13±0.02 0.16±0.01 0.15±0.02	0.13±0.02 0.14±0.01 0.15±0.02	0.91
Arms	Baseline 6-months 12-months	0.14±0.02 0.16±0.02 0.16±0.02	0.17±0.04 0.22±0.04 0.20±0.03	0.17±0.03 0.23±0.04 0.21±0.03	0.53
Fat-Free Mass (kg)					
Abdomen	Baseline 6-months 12-months	1.60±0.09 1.51±0.09 1.76±1.24	1.57±0.07 1.54±0.09 1.68±0.07	1.69±0.08 1.54±0.07 1.68±0.07	0.89
Upper Legs	Baseline 6-months 12-months	1.02±0.99 1.00±0.86 0.80±0.21	1.07±0.08 1.09±0.07 1.01±0.03	0.96±0.09 0.99±0.09 0.92±0.07	0.48
Chest	Baseline 6-months 12-months	1.06±0.07 1.11±0.06 1.06±0.06	1.02±0.06 0.99±0.06 1.00±0.10	1.15±0.05 1.07±0.05 1.03±0.06	0.49
Lower Legs	Baseline 6-months 12-months	0.55±0.05 0.48±0.02 0.51±0.05	0.48±0.03 0.48±0.02 0.53±0.02	0.47±0.02 0.47±0.02 0.47±0.02	0.51
Arms	Baseline 6-months 12-months	0.73±0.05 0.73±0.03 0.71±0.04	0.67±0.04 0.62±0.04 0.66±0.02	0.71±0.02 0.62±0.03 0.64±0.02	0.21

Table 3. Fat-mass (kg) and fat-free mass (kg) values from DXA scan ROIs (abdomen, upper legs, chest, lower legs, and arms). P-values represent treatment factor from RM-ANOVA over baseline, 6-months, and 12-months.

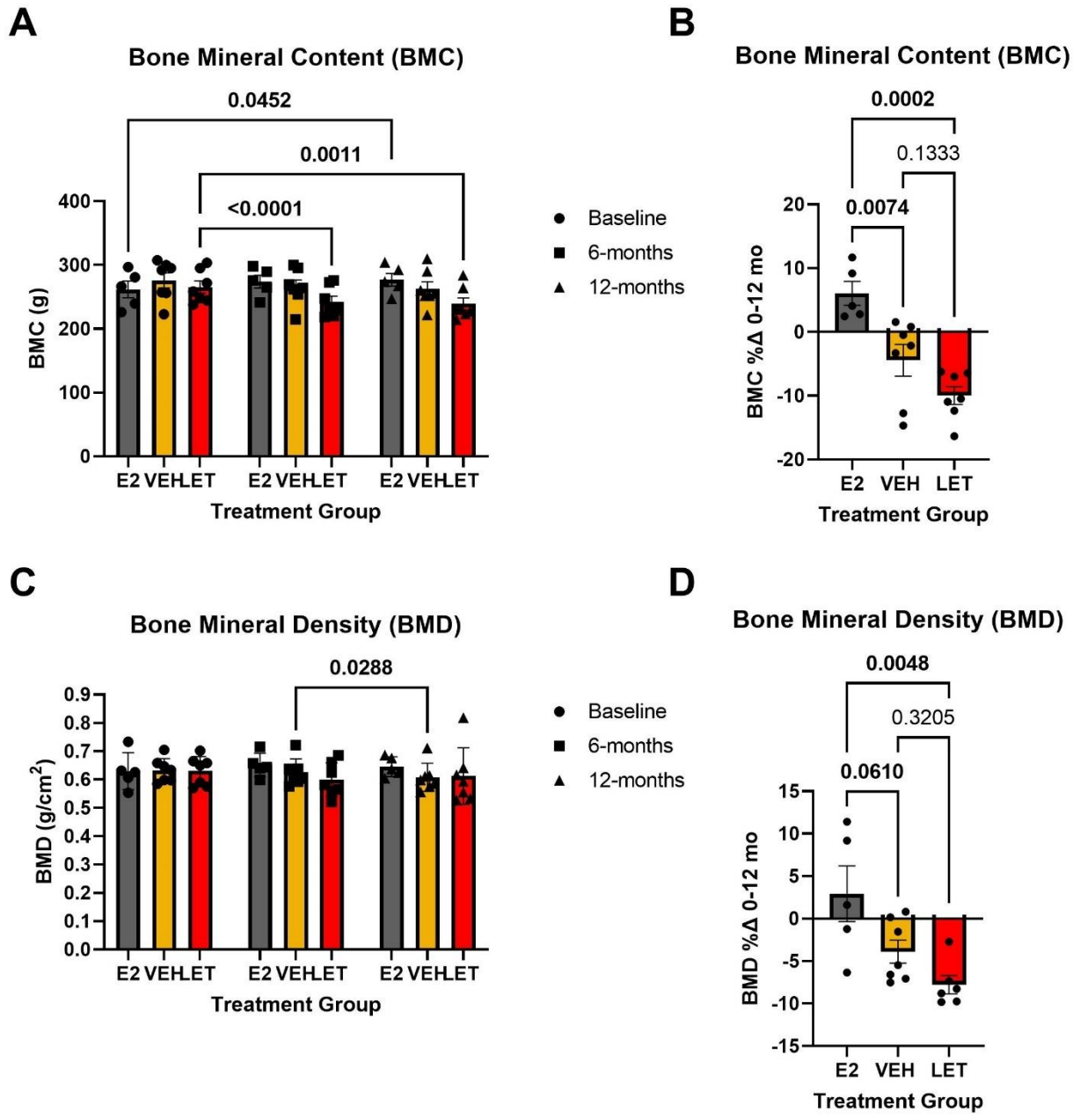

Figure 8: Bone mineral content (A) and bone mineral density (C) at baseline, 6-months, and 12-months post-OVX DXA scans and percent change BMC (B) and BMD (D) from baseline to 12-months post-OVX. Plots expressed as mean ± SEM. Significance assessed via RM-ANOVA and ordinary one-way ANOVA. E2 (grey, n=5), VEH (yellow, n=7) and LET (red, n=7).

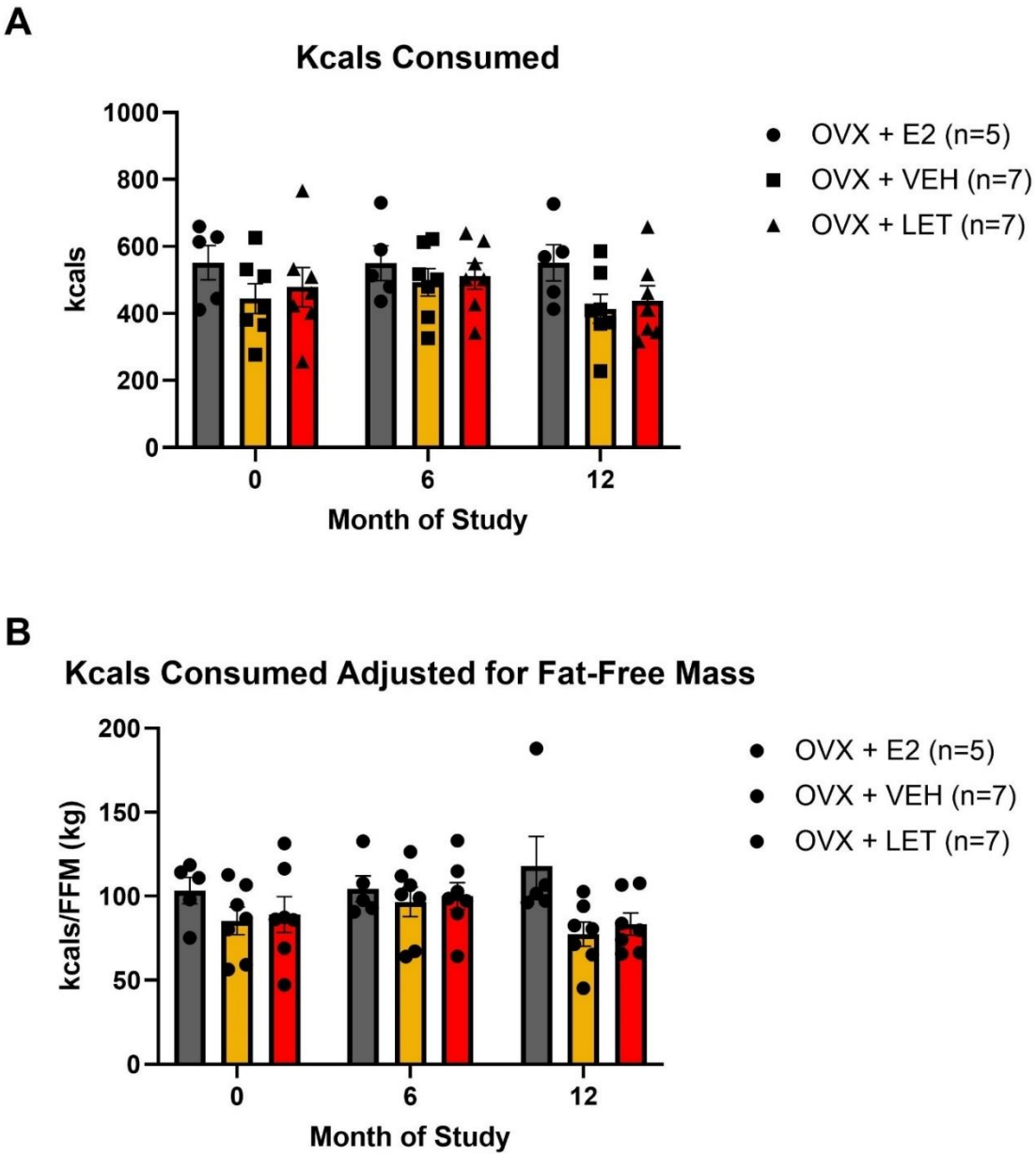

Figure 9: Calories (kcals) consumed (A) and Calories (kcals) consumed adjusted for fat-free mass (kg) averaged over the food assessment at baseline, 6-months, and 12-months post-OVX. Plots expressed as mean ± SEM. Significance assessed via RM-ANOVA. E2 (grey, n=5), VEH (yellow, n=7) and LET (red, n=7).

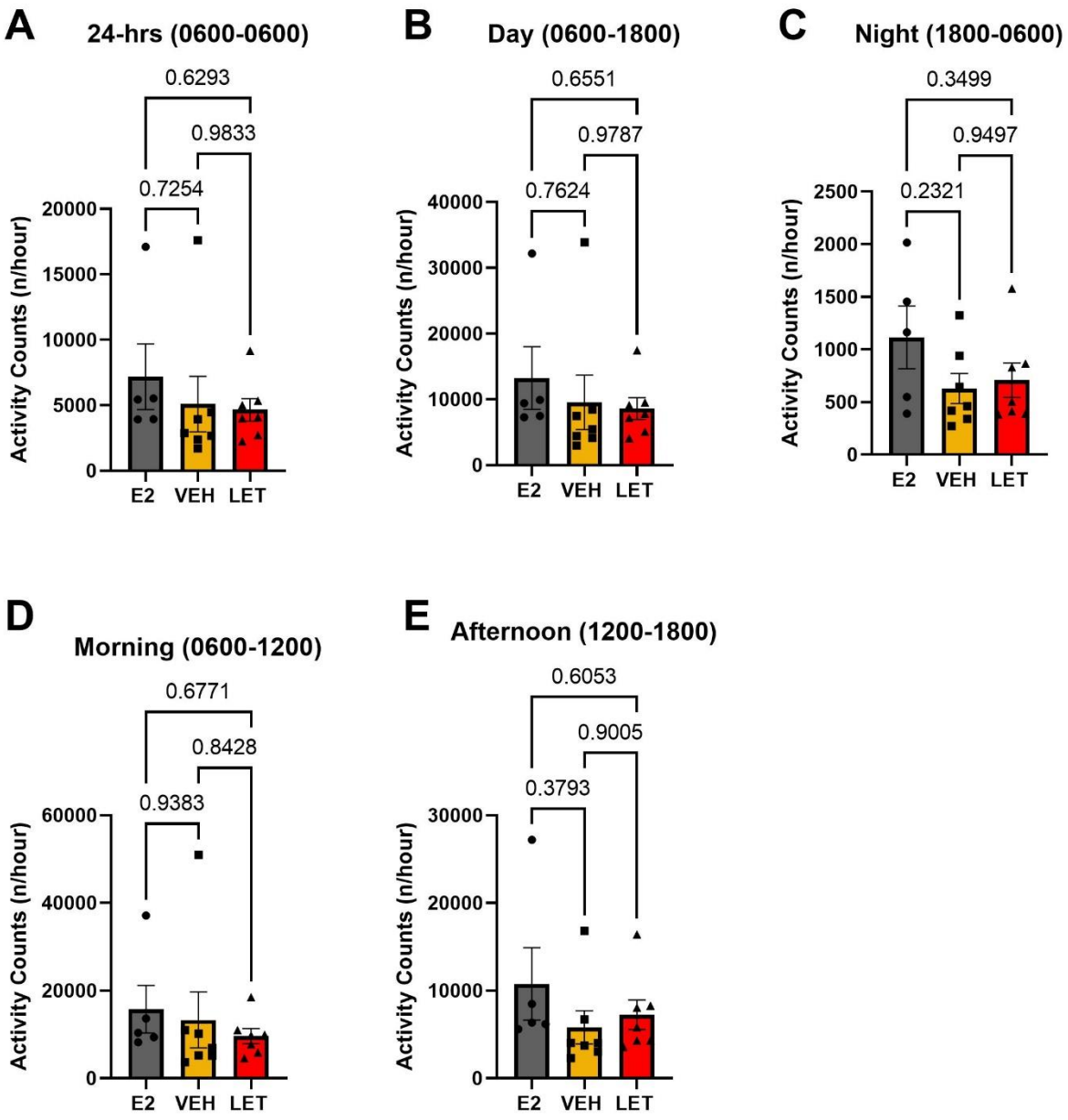

Figure 10: Activity counts averaged over 24-hrs (A), Day (B), Night (C), Morning (D) and Afternoon (E) at baseline. Plots expressed as mean ± SEM. Significance assessed ordinary one-way ANOVA. E2 (grey, n=5), VEH (yellow, n=7) and LET (red, n=7).

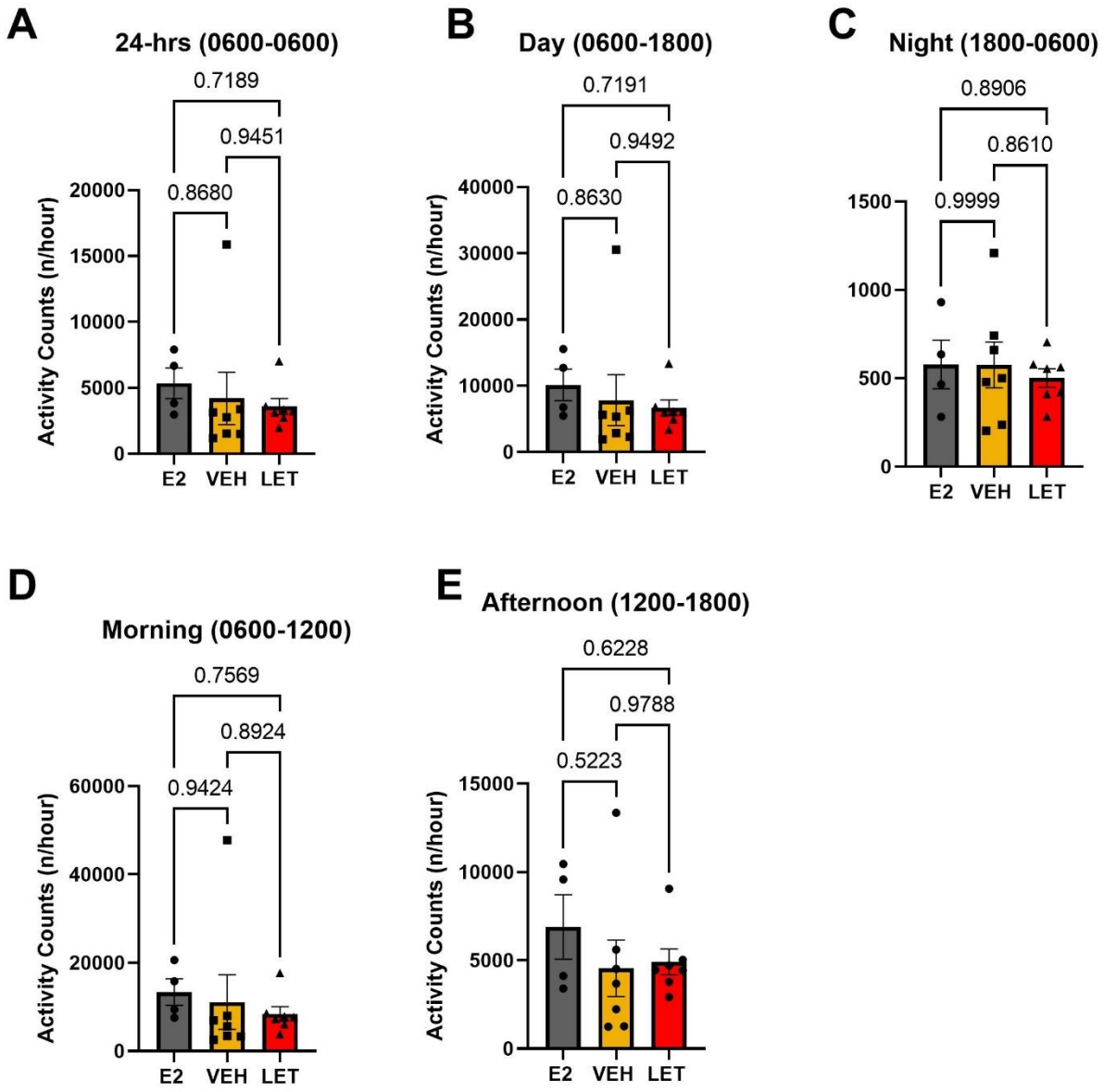

Figure 11: Activity counts averaged over 24-hrs (A), Day (B), Night (C), Morning (D) and Afternoon (E) at 12-months post-OVX. Plots expressed as mean ± SEM. Significance assessed ordinary one-way ANOVA. E2 (grey, n=5), VEH (yellow, n=7) and LET (red, n=7).

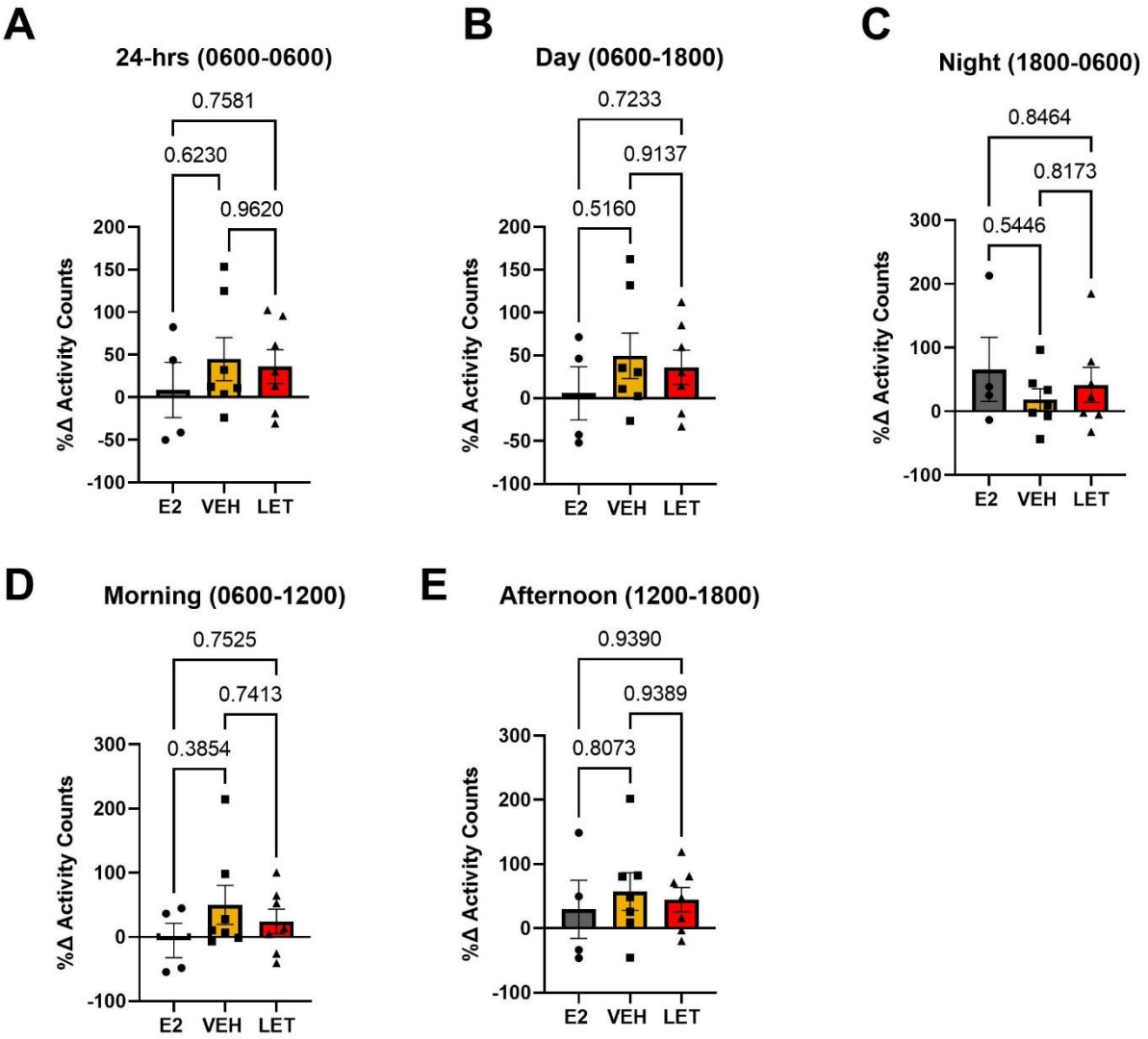

Figure 12: Percent change in activity over 24-hrs (A), Day (B), Night (C), Morning (D) and Afternoon (E) between baseline and 12-months post-OVX. Plots expressed as mean ± SEM. Significance assessed ordinary one-way ANOVA. E2 (grey, n=5), VEH (yellow, n=7) and LET (red, n=7).

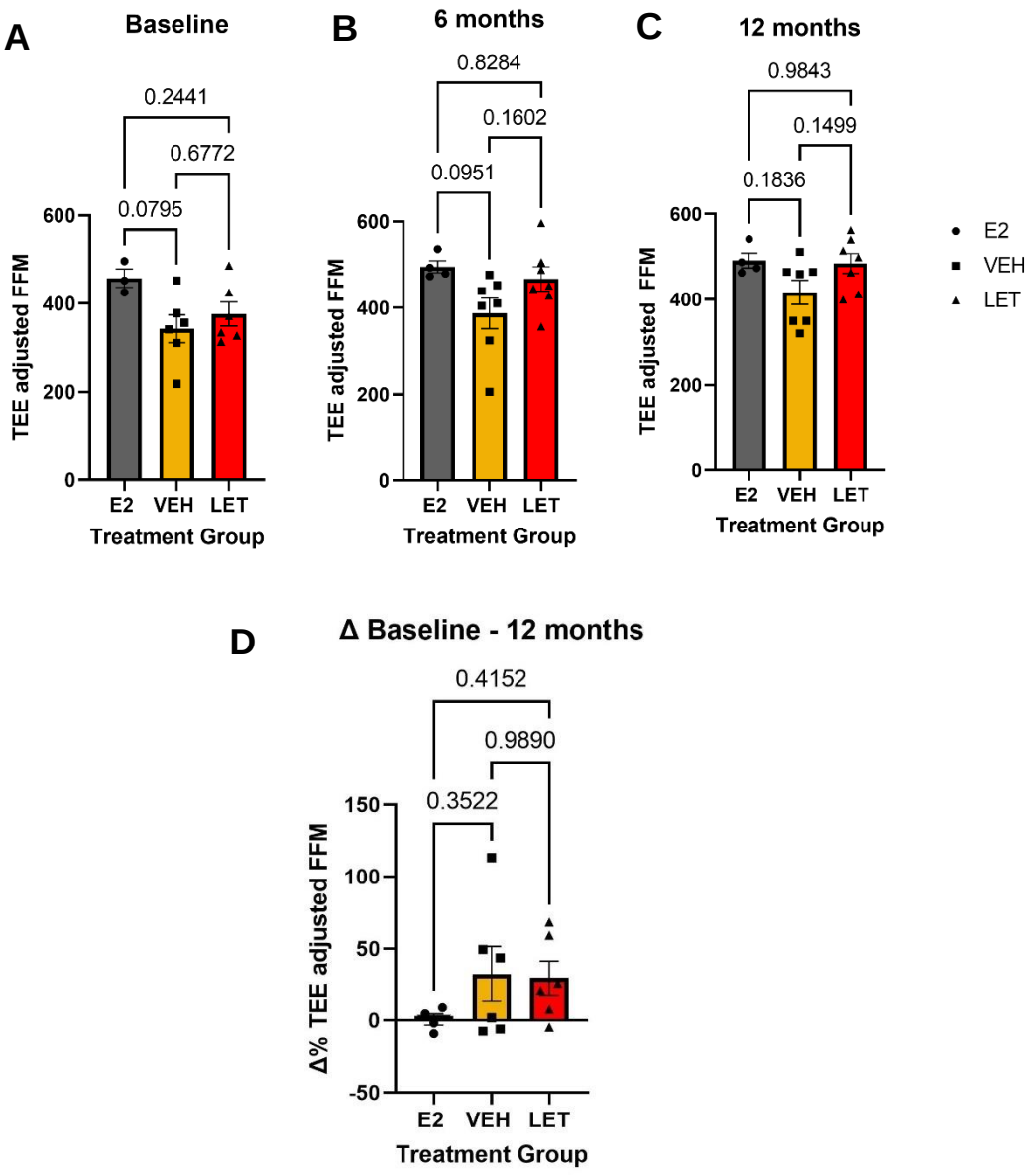

Figure 13: Total energy expenditure (TEE) adjusted for fat-free mass (kg) at baseline (A), 6-months (B) and 12-months (C). Percent change of TEE adjusted for FFM between baseline and 12 months (D). Plots expressed as mean ± SEM. Significance assessed ordinary one-way ANOVA. E2 (grey, n=5), VEH (yellow, n=7) and LET (red, n=7).

		Treatment Group			
		E2	**VEH**	**LET**	**p-value**
SI	Baseline	4.95±1.04	7.18±1.21	5.83±0.93	0.38
	12-months	8.16±1.18	5.79±2.52	4.81±0.94	0.46
	% change	114.6±68.2	-11.39±40.8	-8.58±21.2	0.11
AIRg	Baseline	1243±394	1034±235	1103±240	0.88
	12-months	900±352	1300±318	1276±311	0.67
	% change	-18.73±16.0	62.46±47.3	42.65±31.1	0.34
DI	Baseline	40.83±5.30	44.61±3.08	43.13±5.34	0.86
	12-months	46.39±3.61	36.04±4.67	40.08±5.11	0.34
	% change	26.7±27.15	-13.21±17.16	31.61±47.2	0.59
Sg	Baseline	0.04±0.01	0.03±0.01	0.05±0.01	0.25
	12-months	**0.042±0.003**	**0.031±0.003**	**0.032±0.003**	**0.07**
	% change	40.62±39.3	24.92±37.1	-22.74±17.75	0.37
Ib	Baseline	22.06±5.79	31.36±11.67	18.70±4.73	0.54
	12-months	9.18±1.95	21.56±8.19	12.63±2.27	0.30
	% change	-45.99±15.1	-13.52±19.3	74.87±98.3	0.42
Gb	Baseline	55.92±2.56	58.26±2.61	54.46±3.13	0.62
	12-months	51.02±0.98	51.17±2.00	52.41±1.31	0.79
	% change	-8.34±3.00	-11.49±4.05	-1.62±6.76	0.39

Table 4: Values of glucoregulation calculated via the Bergman Minimal Model program. Values represented as group mean ± SEM. **Bold** indicates trend towards significance, p<0.1.SI=insulin sensitivity, AIRg=acute insulin response to glucose, DI= disposition index, Sg=glucose effectiveness, Ib= basal insulin, Gb=basal glucose, KG=X.

4.7 References

1. Molly C. Carr, The Emergence of the Metabolic Syndrome with Menopause, The Journal of Clinical Endocrinology & Metabolism, Volume 88, Issue 6, 1 June 2003, Pages 2404– 2411, https://doi.org/10.1210/jc.2003-030242
2. Clegg D, Hevener AL, Moreau KL, Morselli E, Criollo A, Van Pelt RE, et al. Sex Hormones and Cardiometabolic Health: Role of Estrogen and Estrogen Receptors. Endocrinology. 2017;158(5):1095– 105.
3. Al-Safi ZA, Polotsky AJ. Obesity and menopause. Best Pract Res Clin Obstet Gynaecol. 2015;29(4):548– 53.
4. Davis SR, Castelo-Branco C, Chedraui P, Lumsden MA, Nappi RE, Shah D, et al. Understanding weight gain at menopause. Climacteric. 2012;15(5):419–29.
5. Sullivan Mitchell E, Fugate Woods N. Midlife women's attributions about perceived memory changes: observations from the Seattle Midlife Women's Health Study. J Womens Health Gend Based Med. 2001;10:351–362.
6. El Khoudary SR, Greendale G, Crawford SL, Avis NE, Brooks MM, Thurston RC, Karvonen-Gutierrez C, Waetjen LE, Matthews K. The menopause transition and women's health at midlife: a progress report from the Study of Women's Health Across the Nation (SWAN) Menopause. 2019;26:1213–1227.
7. Lovejoy, J. C., Champagne, C. M., de Jonge, L., Xie, H. & Smith, S. R. Increased visceral fat and decreased energy expenditure during the menopausal transition. Int J Obes (Lond) 32, 949-958, doi:10.1038/ijo.2008.25 (2008)
8. Chmouliovsky L, Habicht F, James RW, Lehmann T, Campana A, Golay A. Beneficial effect of hormone replacement therapy on weight loss in obese menopausal women. Maturitas. 1999;32(3):147–53.
9. dos Reis CM, de Melo NR, Meirelles ES, Vezozzo DP, Halpern A. Body composition, visceral fat distribution and fat oxidation in postmenopausal women using oral or transdermal oestrogen. Maturitas. 2003;46(1):59–68.
10. Salpeter SR, Walsh JM, Ormiston TM, Greyber E, Buckley NS, Salpeter EE. Meta-analysis: effect of hormone-replacement therapy on components of the metabolic syndrome in postmenopausal women. Diabetes Obes Metab. 2006;8(5):538–54.
11. Duncan AC, Lyall H, Roberts RN, Petrie JR, Perera MJ, Monaghan S, Hart DM, Connell JM, Lumsden MA. The effect of estradiol and a combined estradiol/progestagen preparation on insulin sensitivity in healthy postmenopausal women. J Clin Endocrinol Metab. 1999 Jul;84(7):2402-7. doi: 10.1210/jcem.84.7.5836. PMID: 10404811.
12. Sites CK, L'Hommedieu GD, Toth MJ, Brochu M, Cooper BC, Fairhurst PA. The effect of hormone replacement therapy on body composition, body fat distribution, and insulin sensitivity in menopausal women: a randomized, double-blind, placebo-controlled trial. J Clin Endocrinol Metab. 2005;90(5):2701–7.
13. Cardiovascular disease and use of oral and injectable progestogen-only contraceptives and combined injectable contraceptives. Results of an

international, multicenter, case-control study. World Health Organization Collaborative Study of Cardiovascular Disease and Steroid Hormone Contraception. Contraception. 1998 May;57(5):315-24. PMID: 9673838.

14. Coughlan GT, Betthauser TJ, Boyle R, Koscik RL, Klinger HM, Chibnik LB, Jonaitis EM, Yau WW, Wenzel A, Christian BT, Gleason CE, Saelzler UG, Properzi MJ, Schultz AP, Hanseeuw BJ, Manson JE, Rentz DM, Johnson KA, Sperling R, Johnson SC, Buckley RF. Association of Age at Menopause and Hormone Therapy Use With Tau and β-Amyloid Positron Emission Tomography. JAMA Neurol. 2023 Apr 3:e230455. doi: 10.1001/jamaneurol.2023.0455. Epub ahead of print. PMID: 37010830; PMCID: PMC10071399.
15. Yonezawa R, Wada T, Matsumoto N, Morita M, Sawakawa K, Ishii Y, Sasahara M, Tsuneki H, Saito S, Sasaoka T. Central versus peripheral impact of estradiol on the impaired glucose metabolism in ovariectomized mice on a high-fat diet. Am J Physiol Endocrinol Metab. 2012 Aug 15;303(4):E445-56. doi: 10.1152/ajpendo.00638.2011. Epub 2012 May 1. PMID: 22550066.
16. Hong, J., Stubbins, R. E., Smith, R. R., Harvey, A. E. & Nunez, N. P. Differential susceptibility to obesity between male, female and ovariectomized female mice. Nutr J 8, 11, doi:10.1186/1475-2891-8-11 (2009)
17. Boldarine VT, Pedroso AP, Brandão-Teles C, LoTurco EG, Nascimento CMO, Oyama LM, Bueno AA, Martins-de-Souza D, Ribeiro EB. Ovariectomy modifies lipid metabolism of retroperitoneal white fat in rats: a proteomic approach. Am J Physiol Endocrinol Metab. 2020 Aug 1;319(2):E427-E437. doi: 10.1152/ajpendo.00094.2020. Epub 2020 Jul 14. PMID: 32663100.
18. Musatov S, Chen W, Pfaff DW, Mobbs CV, Yang XJ, Clegg DJ, Kaplitt MG, Ogawa S. Silencing of estrogen receptor alpha in the ventromedial nucleus of hypothalamus leads to metabolic syndrome. Proc Natl Acad Sci U S A. 2007 Feb 13;104(7):2501-6. doi: 10.1073/pnas.0610787104. Epub 2007 Feb 6. PMID: 17284595; PMCID: PMC1892990
19. Sandoval-Guzman, T., Stalcup, S. T., Krajewski, S. J., Voytko, M. L. & Rance, N. E. Effects of ovariectomy on the neuroendocrine axes regulating reproduction and energy balance in young cynomolgus macaques. J Neuroendocrinol 16, 146-153 (2004).
20. Cefalu WT, Wagner JD, Bell-Farrow AD, Wang ZQ, Adams MR, Toffolo G, Cobelli C. The effects of hormonal replacement therapy on insulin sensitivity in surgically postmenopausal cynomolgus monkeys (Macaca fascicularis). Am J Obstet Gynecol. 1994 Aug;171(2):440-5. doi: 10.1016/0002-9378(94)90280-1. PMID: 8059824.
21. Dumesic DA, Abbott DH, Eisner JR, Goy RW. Prenatal exposure of female rhesus monkeys to testosterone propionate increases serum luteinizing hormone levels in adulthood. Fertil Steril. 1997 Jan;67(1):155-63.
22. Kenealy, B.P., Kapoor, A., Guerriero, K.A., Keen, K.L., Garcia, J.P., Kurian, J.R., Ziegler, T.E., and Terasawa, E. (2013). Neuroestradiol in the Hypothalamus

Contributes to the Regulation of Gonadotropin Releasing Hormone Release. Journal of Neuroscience 33, 19051–19059.

23. Kenealy, B.P., Keen, K.L., Garcia, J.P., Kohlenberg, L.K., and Terasawa, E. (2017). Obligatory role of hypothalamic neuroestradiol during the estrogen-induced LH surge in female ovariectomized rhesus monkeys. Proc. Natl. Acad. Sci. U.S.A. 114, 13804–13809.
24. Bertin, J., Dury, A.Y., Ke, Y., Ouellet, J., and Labrie, F. (2015). Accurate and sensitive liquid chromatography/tandem mass spectrometry simultaneous assay of seven steroids in monkey brain. Steroids 98, 37–48. 10.1016/j.steroids.2015.02.013.
25. Raman A, Colman RJ, Cheng Y, Kemnitz JW, Baum ST, Weindruch R, Schoeller DA. Reference body composition in adult rhesus monkeys: glucoregulatory and anthropometric indices. J Gerontol A Biol Sci Med Sci. 2005 Dec;60(12):1518-24. doi: 10.1093/gerona/60.12.1518. PMID: 16424283.
26. Kushner RF, Schoeller DA. Estimation of total body water by bioelectrical impedance analysis. Am J Clin Nutr. 1986 Sep;44(3):417-24. doi: 10.1093/ajcn/44.3.417. PMID: 3529918.
27. Zhou R, Bruns CM, Bird IM, Kemnitz JW, Goodfriend TL, Dumesic DA, Abbott DH. Pioglitazone improves insulin action and normalizes menstrual cycles in a majority of prenatally androgenized female rhesus monkeys. Reprod Toxicol. 2007 Apr-May;23(3):438-48. doi: 10.1016/j.reprotox.2006.12.009. Epub 2007 Jan 14. PMID: 17306503; PMCID: PMC2705750.
28. Kenealy BP, Keen KL, Kapoor A, Terasawa E. Neuroestradiol in the stalk median eminence of female rhesus macaques decreases in association with puberty onset. Endocrinology. 2016;157(1):70-6.
29. Schlinger BA, Remage-Healey L. Neurosteroidogenesis: insights from studies of songbirds. J Neuroendocrinol. 2012 Jan;24(1):16-21. doi: 10.1111/j.1365-2826.2011.02150.x. PMID: 21535249; PMCID: PMC3197953.
30. Hamadeh IS, Patel JN, Rusin S, Tan AR. Personalizing aromatase inhibitor therapy in patients with breast cancer. Cancer Treat Rev. 2018 Nov;70:47-55. doi: 10.1016/j.ctrv.2018.07.014. Epub 2018 Jul 23. PMID: 30086432.
31. Ji MX, Yu Q. Primary osteoporosis in postmenopausal women. Chronic Dis Transl Med. 2015 Mar 21;1(1):9-13. doi: 10.1016/j.cdtm.2015.02.006. PMID: 29062981; PMCID: PMC5643776.
32. Bassatne A, Bou Khalil A, Chakhtoura M, Arabi A, Van Poznak C, El-Hajj Fuleihan G. Effect of antiresorptive therapy on aromatase inhibitor induced bone loss in postmenopausal women with early-stage breast cancer: A systematic review and meta-analysis of randomized controlled trials. Metabolism. 2022 Mar;128:154962. doi: 10.1016/j.metabol.2021.154962. Epub 2021 Dec 24. PMID: 34958816.
33. Mann DR, Gould KG, Collins DC. A potential primate model for bone loss resulting from medical oophorectomy or menopause. J Clin Endocrinol Metab. 1990 Jul;71(1):105-10. doi: 10.1210/jcem-71-1-105. PMID: 2196277.

5. CHAPTER FIVE: Future Directions

Willging MM, Levine JE, and Abbott DH

5.1 Menopausal and ovarian estrogen depletion and implications for female metabolic health

Menopause is characterized by a cessation of menstrual cycles and a reduction in circulating levels of estradiol, E_2. Individuals experiencing personally distressing symptoms of menopause, including hot flashes and night sweats, are typically prescribed hormonal replacement therapy (HRT, usually including synthetic or naturally occurring estrogens with or without accompanying progestins or progesterone) to alleviate symptoms and help reduce osteoporosis induced by declining circulating E_2 levels. Although protection of bone integrity is a clear benefit of HRT[1], increased risks of cancer of the breast and endometrium, blood clots, stroke, heart disease and dementia are consequences of considerable concern[2]. Therefore, it is incredibly important to elucidate the mechanisms by which E_2 regulates energy homeostasis and how these mechanisms are altered in a menopausal environment.

Ovariectomy (OVX) during a female's reproductive years, while mimicking the ovarian E_2 depletion of menopause, occurs within a less aged bodily environment and may not completely represent the E_2 depletion of menopause in the context of aging. While OVX in rodents induces weight gain, adiposity, reduced energy expenditure and glucose intolerance, in female NHP, OVX-mediated E_2 depletion inconsistently increases body weight[3,4]. Despite the lack of a robust E_2-associated metabolic phenotype following OVX in NHPs, selective estrogen receptor modifiers (SERMs) can induce modest weight loss in OVX rhesus monkeys[5]. Interestingly, in OVX cynomolgus macaques, E_2 replacement therapy has no effect on body weight gain and ovarian estrogen depletion fails to diminish insulin sensitivity[4]. In addition to ovarian E_2, E_2

synthesized in the brain (neuro-E_2) can stimulate top-down neuronal signaling cascades. Such neuro-E_2 is proposed to act as a neurotransmitter and neuromodulator[6,7]. Aromatase, the enzyme responsible for converting testosterone to E_2 as well as the conversion of androstenedione to estrone, before its onward enzymatic conversion to E_2, has been documented as present in rhesus macaque brain regions, including the hypothalamus[8]. Therefore, it is a plausible hypothesis that the failure for OVX to increase female NHP body weight is due to the residual actions of neuro-E_2 orchestrating energy balance in the hypothalamus of OVX NHPs, and likely women.

5.2 Neural Regulation of Female Metabolic Function in Adult Marmoset and Rhesus Monkeys

The studies included in this thesis identify ERα as the predominate hypothalamic estrogen receptor governing E_2-regulated energy homeostasis in adult female marmoset and female rhesus monkeys. Adult female marmosets with reduced ERα protein expression in the MBH exhibited reduced locomotor activity and trended towards glucose intolerance, while ERαKD adult female rhesus monkeys exhibited body weight percent increase and reduced morning locomotor activity. Although these metabolic findings are less severe and less timely than those exhibited by ERαKD rodents[9,10], they highlight the importance of hypothalamic ERα in regulating certain aspects of female metabolism. In both of our ERαKD NHP studies, we identified disruption of locomotor activity with reduced hypothalamic ERα protein expression, but in neither study was knockdown complete or uniformly achieved within and between individual female monkeys. It has been well established in rodent studies that reduced hypothalamic ERα contributes to reduced locomotor activity, specifically, estrogens acting via ERα in the

mPOA[11,12]. Therefore, it is possible that the less robust locomotor activity phenotype we observed in female marmosets and female rhesus monkeys is due to (1) less than complete ERα knockdown, especially since the extent of ERα knockdown negatively correlated with aspects of induced metabolic phenotype, and (2) contributions of modest off-target knockdown of ERα protein expression, such as within mPOA incurred the inability of our current MRI-guided viral vector neuro-infusion inducing gene knockdown within the brain to be localized within a single hypothalamic nucleus, alone. Further, ERα expressing neurons within specific hypothalamic nuclei and sub-regions therein such as the ventral VMN (VMNv) may mediate specific metabolic processes.

5.3 Estrogen Regulation of Female Bone Density in Adult Female Marmoset and Rhesus Monkeys

In adult female marmoset monkeys, we demonstrated that OVX + aromatase inhibition did not exaggerate body weight gain beyond that demonstrated by ovarian E_2 depletion, alone. Additionally, neither OVX nor aromatase inhibition contributed to discernable skeletal bone loss. In almost all female mammals with regular, frequent estrous, ovarian, or menstrual cycles, a reduction in circulating E_2 concentrations, either spontaneous or experimentally induced, leads to a reduction in bone mass[13-17]. This has been demonstrated in NHP species and occurs in as little as 3 months in rhesus monkeys[13-17]. It is therefore surprising that we found no deficit in bone mass or bone density of either the total body or lumbar spine associated with systemic or systemic and hypothalamic E_2 deficiency in female marmosets after 7 months on study, though, importantly, estrogen and aromatase activity within the bone microenvironment[18] were not assessed. It is possible that marmoset monkeys evolved metabolic control systems

regulated by extra-ovarian E_2 or that are generally less subject to E_2 regulation. A conclusion arising from Chapter 2 suggested that brain derived E_2 may be enough to maintain bone mass even in the context of circulating E_2 deficiency. Bone in marmosets may therefore have evolved to be less subject to estrogen regulation when, in the wild and captivity, adult females can spend two years or more exhibiting intermittent or absent ovarian cycles, and thus low E_2, while they help raise the offspring their social group's dominant female[18.]

In contrast to our marmoset study (Chapter 2), we found in adult rhesus monkeys that OVX + aromatase inhibition induced greater skeletal bone loss compared to E2 females than OVX alone. These macaque findings are consistent with human studies and the association of bone loss and osteoporosis with the menopausal transition[19]. Osteoblasts are cells of the bone responsible for osteogenesis or "bone growth"[27]. Human osteoblasts have all necessary biological components to synthesize estrogens[26]. Although the mechanisms by which estrogens influence bone metabolism have not been fully elucidated, it is evident that diminished circulating E_2 during menopause contributes to bone loss. In addition, post-menopausal cancer patient aromatase inhibitor use exaggerates bone loss[25-28]. Since menopause typically begins in the later half of life, it can be difficult to tease apart menopause associated metabolic effects from the effects of aging. Studies investigating bone integrity in young women (~20-40 years old) with amenorrhea have identified that estrogen deficiency at these ages is sufficient to significantly reduce bone mineral density and the age correlated with demineralization[32]. This highlights that although age is an important variable to consider when investigating menopause associated phenotypes, bone integrity seems

to be strongly reliant on E_2. It is therefore possible that E_2 synthesized within osteoclasts, and thus a component of extra-ovarian E_2, may contribute independently towards maintenance of bone density, independent of ovarian produced E_2. Our evidence suggests that when bone synthesized E_2 is reduced via aromatase inhibition, bone loss accelerates compared to OVX, alone. Molecular and hormonal assessments within bone and homeostatic endocrine regulation of bone density were not performed. Such assessments may provide insight into how letrozole alters bone steroidogenesis and turnover. Additionally, our findings confirm the previously published promptness during which bone loss occurs following systemic E_2 depletion in rhesus monkeys[13-17] and humans[1]. Further, our identification of E_2-mediated bone loss in adult female rhesus monkeys suggests that bone is regulated by E_2 in female Old World monkeys, as found in women, and unlike marmoset monkeys, and possibly other New World primates.

5.4 Potential importance of high calorie diets or DIO to experimental designs exploring estrogen depletion altering female weight gain in NHPs, and likely women

In regard to body weight and energy expenditure, we did not observe OVX or OVX + aromatase inhibition altered metabolic function in rhesus monkeys. In marmosets, however, we identified OVX and OVX + aromatase inhibition induced body weight gain. Importantly, the marmoset study was performed in context of DIO. It is possible that we did not observe body weight differences in rhesus monkeys because their metabolic processes were not challenged by an experimentally induced positive energy balance and thus did not have to accommodate a greater potential for positive dysfunctional onset. Previous research has shown rhesus monkeys fed a high fat diet demonstrated body weight increase[20], hyperinsulinemia and hyperglycemia[21] within 6-

months. Moreover, a sedentary lifestyle is another load on regulatory mechanisms and in humans, has been shown to be associated with severe symptoms of menopause and obesity[22], together with an increased likelihood of positive energy balance. In this regard, the subtle difference in reduced glucose effectiveness observed between E_2 depleted and E_2 replete female rhesus monkeys may be highlighting early indications of disruption to glucoregulation, and ultimately energy balance, unless compensated for effectively by increased pancreatic islet beta cell insulin production and release during meal-typical immediately post-prandial hyperglycemia. This hint of a trend towards hyperglycemia was nevertheless achieved without requiring DIO in the experimental design and challenging the E_2 depleted monkeys with a prevailing positive energy balance environment. Therefore, it is plausible that reduced E_2 is accommodated metabolically by alternate energy balance mechanisms for a limited duration, or until caloric intake increases, such as from DIO or higher calorie diet, or diminished locomotory activity level occurs. Figure 1 provides a diagrammatic representation of this newly acquired understanding of mechanism in female NHPs that may have application to clinical management of women experiencing E_2-depleted environments.

5.5 Potential hypothalamic metabolically regulatory mechanism in parallel to E_2 regulation

One potential mechanism for maintaining energy balance in a diminished E_2 environment is the leptin-melanocortin pathway. Like leptin, E_2 is a strong anorexigenic signal regulating energy balance by stimulating hypothalamic preopiomelanocortin (POMC) and cocaine-and amphetamine-regulated transcript (CART) neurons and inhibiting neuropeptide Y (NPY) and agouti-related peptide (AgRP) neurons. It had been

assumed that E_2's effect on energy balance acts in tandem with leptin's role via co-expression of leptin receptor (LepRb) and ERα in the mediobasal hypothalamus[23], but recent research in female rodents has shown co-expression is more pronounced in the preoptic area (POA) and is limited in the mediobasal hypothalamus, including the VMN and ARC. Quantification of LepRb and ERα colocalization throughout the murine hypothalamus has shown the absence of reliable colocalization in all areas aside from the POA. In addition, one month after OVX, co-expression of LepRb and ERα tend to decline[24]. E_2 mediation of energy homeostasis may therefore not be dependent on activation of LepRb on co-expressing cells and circulating levels of E_2 may act indirectly on the leptin-melanocortin pathway. It might therefore be speculated that in the absence of circulating levels of E_2, circulating levels of leptin maintain the hypothalamic leptin-melanocortin pathway and energy balance. In this latter regard, our adult female rhesus monkey study (Chapter 4) indicated no between female group differences in circulating levels of leptin, but hypothalamic leptin expression was not assessed, as illustrated diagrammatically in Figure 1. Analysis of gene expression in the hypothalamus of these monkeys could provide insight into upregulated and thus, compensatory mechanisms in an E_2 depleted environment.

Another potential mechanism for maintaining female energy balance may involve a ligand-independent mechanism. We found reduced hypothalamic ERα expression in adult female rhesus monkeys exhibiting body weight percent increase and decreased morning activity. OVX and OVX + extra-ovarian E_2 depletion in adult female rhesus monkeys, however, failed to induce alterations to body weight or energy expenditure. Mouse and in vitro studies have demonstrated that estrogen receptors, in particular,

ERα, can be activated in the absence of E_2[29-31]. For example, in the absence of E_2, IGF-1 and activators of the protein kinase A can activate ERα and induce otherwise E_2-dependent gene transcription[29-31]. Therefore, it is plausible that ERα activation is necessary for female energy balance even when its ligand, E_2, is diminished in concentration or absent, as in a post-menopausal environment or due to aromatase inhibitor use. In such E_2 depleted instances, ERα is activated by other factors. Further investigation into the specific ligand-dependent and ligand independent mechanisms of energy balance may elucidate how female metabolism is maintained in an E_2 depleted environment with hypothalamic ERα expression intact.

5.6 Applications of this study to Understanding and Treating Metabolic Dysfunction in Post-menopausal Women and Female Cancer Survivors

Our recently completed marmoset and rhesus macaque studies sought to investigate whether or not failure of ovarian E_2 depletion (OVX or VEH) to reliably increase female NHP body weight is due to residual actions of extra-ovarian E_2, including neuro-E_2 via estrogen receptor alpha (ERα) orchestrating energy balance in the hypothalamus. We demonstrated that NHP ERα expression may indeed be the predominate estrogen receptor governing female NHP metabolism and that there is a component of extra-ovarian E_2 involved in metabolic regulation, but the latter can be highly NHP species specific.

The studies in this thesis identified how organs or sub-regions therein, including the brain and its hypothalamus, may sense and adjust to changes in systemic hormone levels to maintain energy homeostasis. It is of utmost importance that future research aims to identify tissue-specific mechanisms of E_2-mediated and E_2-independent

metabolic regulation. Specifically, how organ specific hormonal mechanisms may change during systemic reduction of E_2. Understanding the roles of endocrine organs such as adipose, liver and brain, to maintain energy homeostasis during the menopausal transition or following cancer survival will enable discovery of novel therapeutic targets to improve negative symptoms of menopause and cancer survival while reducing harmful off target effects of current HRTs or the inability to administer HRT because of the increased risk of recurring E_2-associated cancer.

5.7 Figures

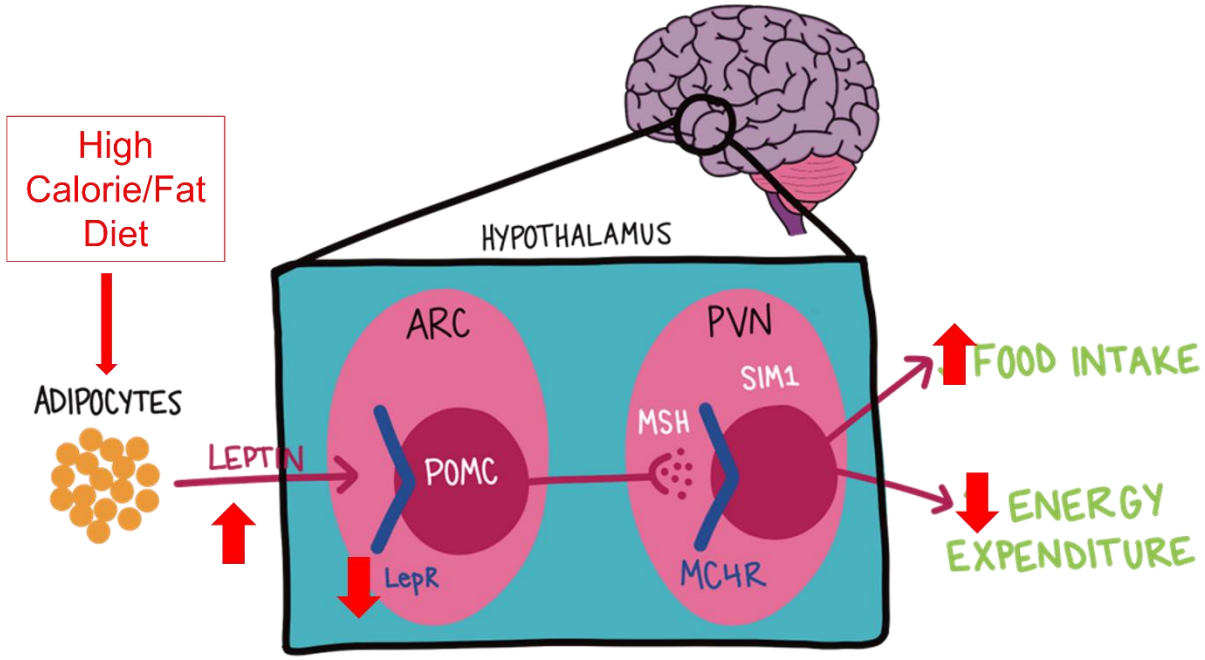

Figure 1: A high calorie/fat diet or diet induced obesity (DIO), increases adipose tissue via fat accumulation, resulting in increased levels of circulating leptin. The heightened levels of circulating leptin reduce the sensitivity of leptin receptors and reduce downstream connections, resulting in increased food intake and decreased energy expenditure.

5.8 References

1. Gambacciani M, Levancini M. Management of postmenopausal osteoporosis and the prevention of fractures. *Panminerva Med*. 2014 Jun;56(2):115-31. Epub 2014 Jun 19. PMID: 24942322.
2. Vinogradova Y, Coupland C, Hippisley-Cox J. Use of hormone replacement therapy and risk of breast cancer: nested case-control studies using the QResearch and CPRD databases*. BMJ*. 2020 Oct 28;371:m3873. doi: 1 0.1136/bmj.m3873. PMID: 33115755; PMCID: PMC7592147.
3. Sandoval-Guzman, T., Stalcup, S. T., Krajewski, S. J., Voytko, M. L. & Rance, N. E. Effects of ovariectomy on the neuroendocrine axes regulating reproduction and energy balance in young cynomolgus macaques. *J Neuroendocrinol* 16, 146-153 (2004).
4. Cefalu WT, Wagner JD, Bell-Farrow AD, Wang ZQ, Adams MR, Toffolo G, Cobelli C. The effects of hormonal replacement therapy on insulin sensitivity in surgically postmenopausal cynomolgus monkeys (Macaca fascicularis). *Am J Obstet Gynecol*. 1994 Aug;171(2):440-5. doi: 10.1016/0002-9378(94)90280-1. PMID: 8059824.
5. Sullivan EL, Shearin J, Koegler FH, Cameron JL. Selective estrogen receptor modulator promotes weight loss in ovariectomized female rhesus monkeys (Macaca mulatta) by decreasing food intake and increasing activity. *Am J Physiol Endocrinol Metab*. 2012 Apr 1;302(7):E759-67. doi: 10.1152/ajpendo.00327.2011. Epub 2012 Jan 17. PMID: 22252940.
6. Ellinwood WE, Hess DL, Roselli CE, Spies HG, Resko JA, 1984. Inhibition of aromatization stimulates luteinizing hormone and testosterone secretion in adult male rhesus monkeys. *J. Clin. Endocrinol. Metab* 59, 1088–1096
7. Terasawa E. Neuroestradiol in regulation of GnRH release. Horm Behav. 2018 Aug;104:138-145. doi: 10.1016/j.yhbeh.2018.04.003. Epub 2018 Apr 19. PMID: 29626484; PMCID: PMC6941749.
8. Roselli CE, Klosterman S, Resko JA, 2001. Anatomic relationships between aromatase and androgen receptor mRNA expression in the hypothalamus and amygdala of adult male cynomolgus monkeys. *J. Comp. Neurol* 439, 208–223.
9. Yonezawa R, Wada T, Matsumoto N, Morita M, Sawakawa K, Ishii Y, Sasahara M, Tsuneki H, Saito S, Sasaoka T. Central versus peripheral impact of estradiol on the impaired glucose metabolism in ovariectomized mice on a high-fat diet. *Am J Physiol Endocrinol Metab.* 2012 Aug 15;303(4):E445-56. doi: 10.1152/ajpendo.00638.2011. Epub 2012 May 1. PMID: 22550066.
10. Hong, J., Stubbins, R. E., Smith, R. R., Harvey, A. E. & Nunez, N. P. Differential susceptibility to obesity between male, female and ovariectomized female mice. *Nutr J* 8, 11, doi:10.1186/1475-2891-8-11 (2009).
11. Ogawa S, Eng V, Taylor J, Lubahn DB, Korach KS, Pfaff DW. Roles of estrogen receptor-alpha gene expression in reproduction-related behaviors in female mice.

Endocrinology. 1998 Dec;139(12):5070-81. doi: 10.1210/endo.139.12.6357. PMID: 9832446

12. Ogawa S, Chan J, Gustafsson JA, Korach KS, Pfaff DW. Estrogen increases locomotor activity in mice through estrogen receptor alpha: specificity for the type of activity. *Endocrinology.* 2003 Jan;144(1):230-9. doi: 10.1210/en.2002-220519. PMID: 12488349.
13. Binkley N, Kimmel D, Bruner J, et al.. Zoledronate prevents the development of absolute osteopenia following ovariectomy in adult rhesus monkeys. *J Bone Miner Res.* 1998;13(11):1775-1782.
14. Fox J, Miller MA, Newman MK, Turner CH, Recker RR, Smith SY. Treatment of skeletally mature ovariectomized rhesus monkeys with PTH(1-84) for 16 months increases bone formation and density and improves trabecular architecture and biomechanical properties at the lumbar spine. *J Bone Miner Res.* 2007;22(2):260-273.
15. Colman RJ, Kemnitz JW, Lane MA, Abbott DH, Binkley N. Skeletal effects of aging and menopausal status in female rhesus macaques. *J Clin Endocrinol Metab.* 1999;84(11):4144-4148.
16. Florio M, Gunasekaran K, Stolina M, et al.. A bispecific antibody targeting sclerostin and DKK-1 promotes bone mass accrual and fracture repair. *Nat Commun.* 2016;7:11505.
17. Havill LM, Levine SM, Newman DE, Mahaney MC. Osteopenia and osteoporosis in adult baboons (Papio hamadryas). *J Med Primatol.* 2008;37(3):146-153.
18. Amanatullah DF, Tamaresis JS, Chu P, et al.. Local estrogen axis in the human bone microenvironment regulates estrogen receptor-positive breast cancer cells. *Breast Cancer Res.* 2017;19(1):121.
19. Deroo BJ, Korach KS. Estrogen receptors and human disease. *J Clin Invest.* 2006;116(3):561-70.
20. Christopher-Hennings J, Kurzman ID, Haffa AL, Kemnitz JW, Macewen EG. The effect of high fat diet and dehydroepiandrosterone (DHEA) administration in the rhesus monkey. *In Vivo.* 1995 Sep-Oct;9(5):415-20. PMID: 8900917.
21. Lu SY, Qi SD, Zhao Y, Li YY, Yang FM, Yu WH, Jin M, Chen LX, Wang JB, He ZL, Li HJ. Type 2 diabetes mellitus non-genetic Rhesus monkey model induced by high fat and high sucrose diet. *Exp Clin Endocrinol Diabetes*. 2015 Jan;123(1):19-26. doi: 10.1055/s-0034-1385923. Epub 2014 Oct 14. PMID: 25314651.
22. Blümel JE, Fica J, Chedraui P, Mezones-Holguín E, Zuñiga MC, Witis S, Vallejo MS, Tserotas K, Sánchez H, Onatra W, Ojeda E, Mostajo D, Monterrosa A, Lima S, Martino M, Hernández-Bueno JA, Gómez G, Espinoza MT, Flores D, Calle A, Bravo LM, Benítez Z, Bencosme A, Barón G, Aedo S; Collaborative Group for Research of the Climacteric in Latin America. Sedentary lifestyle in middle-aged women is associated with severe menopausal symptoms and obesity. *Menopause.* 2016 May;23(5):488-93. doi: 10.1097/GME.0000000000000575. PMID: 26818013.

23. Diano S, Kalra SP, Sakamoto H, Horvath TL. Leptin receptors in estrogen receptor-containing neurons of the female rat hypothalamus. *Brain Res.* 1998 Nov 23;812(1-2):256-9. doi: 10.1016/s0006-8993(98)00936-6. PMID: 9813356.
24. Del Bianco-Borges B, Cabral FJ, Franci CR. Co-expression of leptin and oestrogen receptors in the preoptic-hypothalamic area. *J Neuroendocrinol.* 2010 Sep;22(9):996-1003. doi: 10.1111/j.1365-2826.2010.02046.x. Epub 2010 Jun 24. PMID: 20584107.
25. Christensen Holz, S. Aromatase Inhibitor Musculoskeletal Syndrome and Bone Loss: a Review of the Current Literature. *Curr Oncol Rep* (2023).
26. Janssen JM, Bland R, Hewison M, Coughtrie MW, Sharp S, Arts J, Pols HA, van Leeuwen JP. Estradiol formation by human osteoblasts via multiple pathways: r elation with osteoblast function. *J Cell Biochem*. 1999 Dec 1;75(3):528-37. doi: 10.1002/(sici)1097-4644(19991201)75:3<528::aid-jcb16>3.3.co;2-v. PMID: 10536374.
27. Henry JP, Bordoni B. Histology, Osteoblasts. [Updated 2022 May 8]. In: StatPearls [Internet]. Treasure Island (FL): *StatPearls Publishing*; 2023 Jan-. Available from: https://www.ncbi.nlm.nih.gov/books/NBK557792/
28. Watanabe M, Simpson ER, Pathirage N, Nakajin S, Clyne CD. Aromatase expression in the human fetal osteoblastic cell line SV-HFO*. J Mol Endocrinol.* 2004 Apr;32(2):533-45. doi: 10.1677/jme.0.0320533. PMID: 15072557.
29. Klotz DM, Hewitt SC, Ciana P, Raviscioni M, Lindzey JK, Foley J, Maggi A, DiAugustine RP, Korach KS. Requirement of estrogen receptor-alpha in insulin-like growth factor-1 (IGF-1)-induced uterine responses and in vivo evidence for IGF-1/estrogen receptor cross-talk. *J Biol Chem*. 2002 Mar 8;277(10):8531-7. doi: 10.1074/jbc.M109592200. Epub 2001 Dec 21. PMID: 11751931.
30. Cho H, Katzenellenbogen BS 1993 Synergistic activation of estrogen receptor-mediated transcription by estradiol and protein kinase activators. Mol Endocrinol 7:441–452
31. Olesen KM, Jessen HM, Auger CJ, Auger AP. Dopaminergic activation of estrogen receptors in neonatal brain alters progestin receptor expression and juvenile social play behavior. Endocrinology. 2005 Sep;146(9):3705-12. doi: 10.1210/en.2005-0498. Epub 2005 May 26. PMID: 15919740.
32. Choktanasiri W, Rojanasakul A, Rajatanavin R. Bone mineral density in primary and secondary amenorrhea*. J Med Assoc Thai.* 2000 Mar;83(3):243-8. PMID: 10808678.